


For Reference

NOT TO BE TAKEN FROM THIS ROOM

Ex LIBRIS
UNIVERSITATIS
ALBERTAEASIS





Digitized by the Internet Archive
in 2022 with funding from
University of Alberta Library

<https://archive.org/details/Khoo1984>

T H E U N I V E R S I T Y O F A L B E R T A

R E L E A S E F O R M

N A M E O F A U T H O R S . B . K H O O

T I T L E O F T H E S I S I N T E R A C T I O N S O F O R G A N I C N E G A T I V E
I O N S W I T H C A T I O N S .

D E G R E E F O R W H I C H T H E S I S W A S P R E S E N T E D P H . D .

Y E A R T H I S D E G R E E G R A N T E D 1 9 8 4

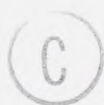
Permission is hereby granted to THE UNIVERSITY OF ALBERTA LIBRARY to reproduce single copies of this thesis and to lend or sell such copies for private, scholarly, or research purposes only.

The author reserves other publication rights, and neither the thesis nor extensive abstracts from it may be printed or otherwise reproduced without the author's written permission.

THE UNIVERSITY OF ALBERTA

INTERACTIONS OF ORGANIC NEGATIVE IONS WITH CATIONS

by



S. B. KHOO

A THESIS

SUBMITTED TO THE FACULTY OF GRADUATE STUDIES AND RESEARCH
IN PARTIAL FULFILMENT OF THE REQUIREMENTS FOR THE DEGREE
DOCTOR OF PHILOSOPHY

DEPARTMENT OF CHEMISTRY

EDMONTON, ALBERTA

FALL, 1984

THE UNIVERSITY OF ALBERTA
FACULTY OF GRADUATE STUDIES AND RESEARCH

The undersigned certify that they have read, and recommend
to the Faculty of Graduate Studies and Research, for
acceptance, a thesis entitled

INTERACTIONS OF ORGANIC NEGATIVE IONS WITH CATIONS

submitted by S. B. KHOO

in partial fulfilment of the requirements for the degree of
DOCTOR OF PHILOSOPHY.

To my wife, Judy

ABSTRACT

The electroreduction of the polycyclic aromatic hydrocarbons anthracene, fluoranthene, and the π -acids tetracyanoethylene and 7,7,8,8-tetracyanoquinodimethane in non-aqueous aprotic media was examined. In particular, the interactions between the electrogenerated organic negative ions with countercations were investigated. It was found that in general, the dianions formed ion pairs with alkali metal cations but the dianion radicals did not.

Polarographic reduction waves for mixtures of aromatic hydrocarbon-alkali metal cations showed unusual current depressions. It was found that these current depressions were not due to adsorption or film formation processes but to the effect of the interactions between the organic dianions with metal cations. A model was proposed to account for the current depressions and the stoichiometries of the dianion-metal cation complexes were determined. However, the formation constants for the complexes could not be calculated due to the unstable nature of the dianions. Kinetic studies showed that the rate of ion-pair complex formation was very fast, close to the calculated diffusion controlled rate. The experimental rate constants were determined based on the competition between metal cations and water for the dianions.

In the case of the π -acids, cyclic voltammetric studies

showed that the electrochemical reduction of the anion radicals to the dianions was highly dependent on the countercations of the supporting electrolyte. The reduction of the tetracyanoethylene anion radicals to the dianions was found to be either quasi-reversible or irreversible depending on the electrolyte used. Heterogeneous rate constants were determined from the variation of $\Delta E(p)$ values with scan rate. Large shifts in E_h values for the second reduction waves of tetracyanoethylene and 7,7,8,8-tetracyanoquinodimethane were found when different supporting electrolytes were used, pointing to the existence of strong ion pairing of the dianions. For tetracyanoethylene the use of mixed electrolytes gave rise to strong adsorption effects. Thus ion pairing constants could not be determined. However, for 7,7,8,8-tetracyanoquinodimethane, two types of ion pairs were found with stoichiometries of 1:1 and 1:2 (dianion:cation). The formation constants for these ion pair complexes were calculated. Further evidence for the existence of dianion--cation interactions was provided by the shifts in IR adsorption bands with different supporting electrolytes.

ACKNOWLEDGEMENTS

I would like to thank my supervisor, Dr. S. Pons, for the constant help and advice he has given me throughout the course of my studies. His support has very often gone beyond just that of a supervisor. Without him, the present thesis would not have been possible. I would also like to thank my wife, Judy, for her moral support. For her patience and understanding, I am grateful. Thanks is also due to my friend, Dr. M. Shamim, who although far away, has never ceased to give encouragement over the years. Last, but not least, I thank my colleagues for our many discussions, and especially Jack Cassidy, one of the most unselfish persons I know.

TABLE OF CONTENTS

Chapter 1.	INTRODUCTION	PAGE
1.1	Objective	1
1.2	Historical Background	3
1.2.1	Electrochemical Reduction of Aromatic Hydrocarbons in Non-aqueous Media	3
1.2.2	Electrochemical Reduction of Alkali Metal Cations in Nonaqueous Media	10
1.2.3	The Interaction between Aromatic Hydrocarbon Negative Ions and Alkali Metal Cations. . . .	16
1.2.4	Tetracyanoethylene (TCNE)	24
1.2.5	7,7,8,8-Tetracyanoquinodimethane (TCNQ) . . .	30
Chapter 2.	ELECTROCHEMICAL TECHNIQUES	
2.1	Introduction.	37
2.2	General Considerations.	37
2.3	Chronoamperometry	44
2.4	Cyclic Voltammetry.	46
2.5	Normal Pulse Polarography	54
2.6	Modulated Specular Reflectance Spectroscopy .	61

Chapter 3. THE ELECTROCHEMICAL REDUCTION OF ALKALI
METAL CATIONS, ANTHRACENE AND FLUORANTHENE
IN ACETONITRILE AND DIMETHYLFORMAMIDE:
INTERACTIONS BETWEEN THE ALKALI METAL CATIONS
AND HYDROCARBON NEGATIVE IONS

3.1	Introduction.	69
3.2	Experimental.	73
3.2.1	Instrumentation	73
3.2.2	Purification of Chemicals	76
3.2.3	Procedure	78
3.3	Results	81
3.4	Discussion.	132

Chapter 4. THE EFFECT OF WATER ON THE INTERACTIONS
BETWEEN AROMATIC NEGATIVE IONS AND ALKALI
METAL CATIONS

4.1	Introduction.	164
4.2	Experimental.	166
4.2.1	Instrumentation	166
4.2.2	Purification of Chemicals	166
4.2.3	Procedure	166
4.3	Results	169
4.4	Discussion.	192

Chapter 5. ELECTROCHEMICAL STUDIES OF TETRACYANOETHYLENE
(TCNE) AND 7,7,8,8-TETRACYANOQUINODIMETHANE
(TCNQ).THE EFFECT OF COUNTERCATIONS.

5.1	Introduction.	221
5.2	Experimental.	227
5.2.1	Instrumentation	227
5.2.2	Purification of Chemicals	233
5.2.3	Procedure	234
5.3	Results	235
5.4	Discussion.	288
Literature References.		309

LIST OF TABLES

	PAGE
Table 1. Polarographic Parameters	85
Table 2. Summary of the behavior of the various limiting currents.	121
Table 3. Estimated Rate Constants.	211
Table 4. Peak Potentials for the First Reduction of TCNE.	240
Table 5. Peak Potentials for Second Reduction Wave of TCNE.	246
Table 6. Variation of $i(pa)/i(pc)$ for Second Reduction of TCNE with LiClO ₄ Supporting Electrolyte at a Glassy Carbon Electrode	247
Table 7. Apparent Heterogeneous Rate Constants for TCNE Second Reduction at a Glassy Carbon Electrode With TBAF Supporting Electrolyte	249
Table 8. Apparent Heterogeneous Rate Constants for TCNE Second Reduction at a Glassy Carbon Electrode With TEAP Supporting Electrolyte	251
Table 9. Apparent Heterogeneous Rate Constants for TCNE Second Reduction at a Platinum Electrode With TEAP Supporting Electrolyte	251
Table 10. Apparent Heterogeneous Rate Constants for the Reduction of TCNE ⁺ to TCNE ⁼ at a Platinum Electrode.	254

Table 11. Determination of α for TCNE $^{\cdot-}$ Reduction at a Platinum Electrode using Equation (5.13)	256
Table 12. Peak Potentials for the First Reduction of TCNQ	257
Table 13. Peak Potentials for the Second Reduction of TCNQ	257
Table 14. Peak Potentials for TCNQ Reduction as a Function of TBAF Concentration	267
Table 15. Half Wave Potential Shifts and Calculated Junction Potentials for TCNQ Reductions as a Function of TBAF Concentration	268
Table 16. Conductance Data for Ions of TBAF in ACN	270
Table 17. Formation Constants of TCNQ Ion Pairs.	276
Table 18. Apparent First Order Rate Constants for Decay of TCNE and TCNQ Anion Radicals.	284
Table 19. Comparison of Eh Values for the First Reduction Wave of TCNE and TCNQ in Acetonitrile	290
Table 20. Vibrational Absorption ($C\equiv N$ stretch) for TCNQ $^{\cdot-}$ and TCNQ= with Different Supporting Electrolytes	305

LIST OF FIGURES

PAGE

Figure 1.	Normal pulse polarographic potential program .	59
Figure 2.	The coordinate system used in modulated specular reflectance spectroscopy.	67
Figure 3.	Polarographic cell arrangement	75
Figure 4.	Polarographic background current	83
Figure 5a.	Plots of E vs $\log (i(d)-i)/i$	88
Figure 5.	Alkali metal cations calibration plots in DMF at 25°C.	89
Figure 6.	Alkali metal cation calibration plots in ACN at 25°C.	90
Figure 7.	Alkali metal cation calibration plots in ACN at 25°C.	91
Figure 8.	Anthracene and flouranthene calibration plots in DMF at 25°C	94
Figure 9.	Anthracene and fluoranthene calibration plots in ACN at 25°C	95
Figure 10.	Polarograms of anthracene-lithium cation mixtures in DMF at 25°C.	96
Figure 11.	Polarograms of anthracene-sodium cation mixtures in DMF at 25°C.	97
Figure 12.	Polarograms of anthracene-potassium cation mixtures in DMF at 25°C.	98
Figure 13.	Polarograms of anthracene-rubidium cation mixtures in DMF at 25°C.	99
Figure 14.	Polarograms of fluoranthene-lithium cation mixtures in DMF at 25°C.	100
Figure 15.	Polarograms of fluoranthene-sodium cation mixtures in DMF at 25°C.	101
Figure 16.	Polarograms of fluoranthene-potassium cation mixtures in DMF at 25°C.	102

Figure 17.	Polarograms of fluoranthene-rubidium cation mixtures in DMF at 25°C.	103
Figure 18.	Polarograms of anthracene-lithium cation mixtures in ACN at 25°C.	104
Figure 19.	Polarograms of anthracene-sodium cation mixtures in ACN at 25°C.	105
Figure 20.	Polarograms of fluoranthene-lithium cation mixtures in ACN at 25°C.	106
Figure 21.	Polarograms of fluoranthene-sodium cation mixtures in ACN at 25°C.	107
Figure 22.	A. Polarogram of a solution mixture containing 1.00 mM anthracene and 3.53 mM lithium cation in ACN (0.10 M TBAF) at 25°C. B. Current-time transients for the same solution at 25°C	111
Figure 23.	Normal pulse (NP) and reverse pulse (RP) polarograms of a solution mixture containing 1.00 mM anthracene and 3.83 mM lithium cation in DMF (0.10 M TBAF) at 25°C.	112
Figure 24.	Plots of limiting currents versus concentration of metal cations for anthracene-metal cation mixtures in DMF at 25°C	116
Figure 25.	Plots of limiting currents versus concentration of metal cations for fluoranthene-metal cation mixtures in DMF at 25°C	117
Figure 26.	Plots of limiting currents versus concentration of metal cations for anthracene-metal cation and fluoranthene-metal cation mixtures at 25°C	118
Figure 27.	Plot of the amount of metal cation reacted versus cation concentration for the anthracene-metal cation system in DMF at 25°C. . . .	124
Figure 28.	Plot of the amount of metal cation reacted versus cation concentration for the fluoranthene-metal cation system in DMF at 25°C	125
Figure 29.	Plot of the amount of metal cation reacted versus cation concentration for the anthracene-metal cation system in ACN at 25°C. . . .	126

Figure 30.	Plot of the amount of metal cation reacted versus cation concentration for the fluoranthene-metal cation system in ACN at 25°C	127
Figure 31.	Plots of limiting currents and amount of lithium cation reacted versus anthracene concentration in DMF at 25°C	129
Figure 32.	Plots of limiting currents and amount of sodium cation reacted versus anthracene concentration in DMF at 25°C	131
Figure 33.	Dilution experiments: polarograms showing the effect of dilution on mixtures of anthracene: lithium cation in the concentration ratio 1:1.5 in DMF at 25°C	170
Figure 34.	Dilution experiment: plots of limiting currents and percentage of lithium cation reacted versus lithium cation concentration in DMF at 25°C.	172
Figure 35.	A. Effect of water on the limiting current of a 3.83 mM lithium cation solution in DMF at 25°C B. Effect of water on the limiting currents of a 1.00 mM solution of anthracene in DMF at 25°C	175
Figure 36.	Polarograms showing the effect of water addition on a mixture of 1.00 mM anthracene and 3.83 mM lithium cation in DMF at 25°C. . .	176
Figure 37.	Effect of water addition on the limiting currents and amount of lithium cation reacted for a mixture of 1.00 mM anthracene and 3.83 mM lithium cation in DMF at 25°C	178
Figure 38.	Plots of limiting currents and the amount of lithium cation reacted versus lithium cation concentration for mixtures of anthracene and lithium cations containing 2.14 M water in DMF at 25°C.	180
Figure 39.	Effect of water addition on the limiting currents and the amount of sodium cation reacted for a mixture of 1.00 mM anthracene and 3.92 mM sodium cation in DMF at 25°C . . .	182

Figure 40.	Plots of limiting currents and amount of sodium cation reacted versus sodium cation concentration for mixtures of anthracene and sodium cation containing 0.22 M water in DMF at 25°C	184
Figure 41.	Effect of water addition on the limiting currents of a 1.00 mM fluoranthene solution in DMF at 25°C	185
Figure 42.	Effect of water addition on the limiting currents and amount of lithium cation reacted for a mixture of 1.00 mM fluoranthene and 1.02 mM lithium cation concentration in DMF at 25°C.	187
Figure 43.	A. Plots of limiting currents and amount of lithium cation reacted versus lithium cation concentration for mixtures of fluoranthene and lithium cations containing 1.72 M water in DMF at 25°C B. Calibration plots for lithium cation in DMF solutions containing 1.72 M water. . .	189
Figure 44.	A. Effect of water addition on the amount of sodium cation reacted for a mixture of 1.00 mM fluoranthene and 2.45 M sodium cation in DMF at 25°C. B. Effect of water on the limiting currents for the same mixture above	191
Figure 45.	Plot of Y versus lithium cation concentration for mixtures of anthracene and lithium cation.	207
Figure 46.	Plot of Y versus sodium cation concentration for mixtures of anthracene and sodium cations containing 0.22 M water in DMF at 25°C	208
Figure 47.	Plot of Y versus lithium cation concentration for mixture of fluoranthene and lithium cation containing 1.72 M water in DMF at 25°C	209
Figure 48.	Instrumentation for MSRS	228
Figure 49.	Optical cell for MSRS experiment	230
Figure 50.	Cell configuration for the voltammetric and chronoamperometric experiments	231

Figure 51.	A. Cyclic voltammogram showing the reduction of anthracene B. Chronoamperograms for (i) 0.943 mM anthracene in ACN	238
Figure 52.	Cyclic voltammograms showing the first and second reduction of TCNE	241
Figure 53.	A. Plots of $i(pc)/v$ versus v for the first reduction wave of TCNE B. Cyclic voltammogram of TCNE recorded in y-t mode	243
Figure 54.	Plot of Δ function versus $\Delta E(p)$ Assume $\alpha = 0.5$	250
Figure 55.	Cyclic voltammograms for reduction of TCNQ at glassy carbon with different supporting electrolytes	258
Figure 56.	Cyclic voltammogram for reduction of TCNQ at platinum electrode recorded in the y-t mode	260
Figure 57.	Plot of $\log i$ versus $E-E_i$ for the reduction of TCNE anion radical at platinum.	255
Figure 58.	Plot of half-wave potential (E_h) versus ionic radii of counteranions for TCNE second reduction wave at platinum and glassy carbon	263
Figure 58a.	Cyclic voltammetry of TCNE with mixtures of supporting electrolytes	264
Figure 59.	Plot of half-wave potential change (ΔE_h) versus the negative logarithm of metal ion concentration ($-\log(m)$).	275
Figure 60.	Electronic Absorption Spectra of TCNE and TCNQ in ACN.	278
Figure 61.	MSRS Spectra of anion radicals and dianions of TCNE and TCNQ in ACN	280
Figure 62.	Normalized reflectance-time profile for TCNE: and TCNQ:, with and without water addition	285
Figure 63.	Plot of normalized reflectance versus square root of time for 1.00 mM solutions of anion radicals of TCNE and TCNQ	286
Figure 64.	Plots of normalized reflectance versus square root of time for TCNE and TCNQ anion radical in ACN with water addition	287

Chapter 1 Introduction

1.1 Objective

The main goal of this thesis research is to investigate the interactions of the electrochemically generated negative ions of polycyclic aromatic hydrocarbons, and the π -acids tetracyanoethylene and 7,7,8,8-tetracyanoquinodimethane with cations present in solution. The electrochemistry is investigated in nonaqueous, aprotic media (N,N-dimethylformamide (DMF) and acetonitrile (ACN)). It is envisioned that through these studies the electrochemical behavior of the organic substrates could be established, as well as the dependence of this behavior on various counter-cations and also the role played by the solvent medium. In particular, the manner of interactions of electrogenerated organic negative ions with cations,

their stoichiometries and the mechanism of these interactions are examined. Although many polycyclic aromatic hydrocarbons are studied, a detailed report is confined to two of them; namely, anthracene and fluoranthene. The cations considered are alkali metal and tetraalkylammonium. The justification for these types of studies is well-established. Electrochemical characteristics can give insight into the molecular structure of reactants and products (1-3). Reduction potentials can be correlated to electron affinities and molecular orbital energy (4-8). Electrochemical behavior can be dependent on the nature of electrolyte cation (9-11). The anions of organic molecules are known to be reactive species. The reactivity of these species is greatly affected by the presence and type of ionic interactions in solution (12-16). In some cases the reaction pathway can be altered (17,18).

Solvation plays a major role in all these processes and must be considered. It is intended that the results of these investigations add to the knowledge of these areas of chemistry.

1.2 Historical Background

In the following sections, a historical survey of the areas pertaining to the present research will be summarized.

1.2.1 Electrochemical Reduction of Aromatic Hydrocarbons In Non-aqueous Media

The earliest studies on the electroreduction of aromatic hydrocarbons were done by Laitinen and Wawzonek (19-20), and Wawzonek and Fan (21). These investigations were not carried out in fully non-aqueous media but rather in 75% dioxane-water mixture. Polycyclic

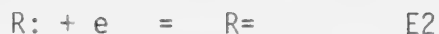
aromatic hydrocarbons e.g. anthracene were found to give a two-electron polarographic wave. Anthracene gave a small second wave in this medium but it was ignored. A mechanism involving the transfer of one electron from the electrode to the organic molecule to form an anion radical was postulated. This was an important step at this time and Austen et al (31) later proved that the intermediate in the first reduction step was indeed a free radical ion by electron spin resonance (esr) studies. Chopard-dit-Jean and Heilbronner (22), from their studies of reduction of azulenes, deduced the general rule that alternant hydrocarbons always give a two-electron polarographic wave whereas non-alternant hydrocarbons may give either a one- or two-electron wave. Hoijtink et al (23) recognized that the mechanism proposed earlier (19-20) was inconsistent

with the results; namely, the existence of the second wave. They found that in 96% dioxane-water mixture (a "more aprotic" solvent than 75% dioxane-water), anthracene exhibited two successive one-electron waves of approximately equal height. If the water content was increased, the first wave changed from a one-electron to an overall two-electron wave with the disappearance of the second wave. The same effect could be brought about by the addition of hydrogen iodide as a proton source instead of water. Thus, the general rule derived by Chopard-dit-Jean and Heilbronner was shown to be incorrect. Subsequently, the reduction of aromatic hydrocarbons was carried out in acetonitrile and dimethylformamide (24) and similar results were obtained. Hoijtink et al extended their studies to dimethylformamide solvent and found that for all

the aromatic hydrocarbons studied, the rate constants for the first electron transfer were practically the same and had the value 0.1 cm/s. However, it is now known that rate constants for electron transfer to aromatic hydrocarbons are very much faster (28). Aten et al (29) determined a value of 5 cm/s for the first electron transfer and about one order lower for the second step. Kojima and Bard (30) found a value of 5 cm/s for the first electron transfer of anthracene and perylene in DMF. Further, it was found that addition of water up to 5% did not affect the processes in the first wave.

The mechanism currently accepted for the electro-reduction of aromatic hydrocarbons, as was established by Hoijtink et al and later confirmed by Given and Peover (26,27), is discussed below. In a totally aprotic environment, the reduction of the aromatic hydrocarbon R

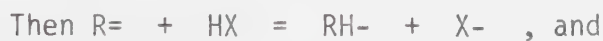
occurs in two successive one-electron steps



where E2 is more negative than E1.

Since the rate constants for electron transfer of both processes are large, the Nernst equation will be obeyed and the processes are reversible. However, a totally aprotic environment is difficult to achieve for even the most carefully purified solvent contains traces of water.

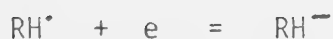
The dinegative ion is more reactive than the anion radical, and while small amounts of proton donors may not react with the anion radical, they could cause the protonation of the dianion.





The rate of protonation is dependent on the proton affinity of the dianion and on the strength and amount of the proton donor. The product of protonation, RH_2 , could further be reduced to give rise to additional wave(s) at more negative potentials. It has been reported that dianion protonation could be prevented by adding neutral alumina to the solution to remove the last traces of proton donors (32).

If sufficient proton donors are present, the stability of the anion radical could be affected:





In the case of alternant hydrocarbons, the radical $RH^{\cdot-}$ is always reduced at a potential less negative than the parent R and therefore will be reduced as soon as it is formed (23). In this case only one wave will be observed involving the overall transfer of two electrons. In the intermediate case where the rate of protonation of $R^{\cdot-}$ is not too fast, two waves will be observed, the first of which (involving more than one electron) will be greater in height than the second. Detailed discussions regarding this mechanism are discussed in the references cited. A review was given by Hoijtink in 1970 (4).

1.2.2 Electrochemical Reduction of Alkali Metal Cations in Nonaqueous Media.

The first reported electrodeposition of alkali metal in nonaqueous solvent was in 1895 by Laszczynski (33). Up to the 1920's a number of studies on the electrochemistry of alkali metal cations had been made, most of which were rather qualitative in nature. A review was made by Brenner in 1967 (34). Observations of the electrochemical reduction of alkali metal cations in nonaqueous solvents are important in the understanding of solute-solvent and solute-solute interaction in solution. Also they have a direct impact on the field of high energy density batteries (35,36).

The electrochemical deposition of alkali metals on electrodes of the same metal or on inert materials such as vitreous carbon or pyrolitic graphite (37), platinum, etc. in nonaqueous solvents is complicated by the extreme

reactivity of these metals. The deposited metal could react with the solvent or with trace impurities (water, oxygen) present. Such reactions lead to highly irreproducible results (38-40) and possibly, in the extreme case, to the passivation of the electrode towards further electrolysis. Further, where the electrode material is different from the deposited metal, implantation of the deposited metal into the electrode often occurs (41-43).

Such problems are essentially absent where mercury is the electrode material since the alkali metal is dissolved in mercury and forms an amalgam which greatly lowers the reactivity of the metal. Thus, at the mercury cathode, reduction of the alkali metal cations can conveniently be performed even in aqueous media (44-48). The d.c. polarographic behavior of alkali metal cations has been studied in such nonaqueous solvents as acetic acid anhydride (49), propionitrile, benzonitrile,

phenylacetonitrile (50), isobutyronitrile (51), dimethylsulfoxide (52,53) and a host of other solvents (54-57).

Alkali metal cations, in general, give well-defined, diffusion-controlled polarographic waves in nonaqueous solvents. In acetonitrile (58) the reduction of sodium, potassium and rubidium iodides, with tetraalkylammonium salts as supporting electrolyte, show reversible character. Similar behavior was obtained in dimethylformamide (59). However, the nature of the reduction of lithium cation is somewhat more contradictory, as can be seen from literature results. For example, Brown and Urfali (59) found lithium reduction to be d.c. reversible in dimethylformamide whereas McMasters et al (60) observed irreversible behavior in the same solvent. Diggle et al (61) pointed out the results obtained by the above workers are not comparable because Brown and Urfali used iodide salts whereas McMasters et al used

perchlorate salts. They determined values of standard heterogeneous rate constants k_s for the cations at the hanging mercury drop electrode, in dimethylformamide, by cyclic voltammetry. It was found that k_s increased in the order Li^+ ($1.2 \times 10^{-3} \text{ cm/s}$) $<$ K^+ ($4.3 \times 10^{-3} \text{ cm/s}$) $<$ Na^+ ($7.2 \times 10^{-3} \text{ cm/s}$) $<$ Cs^+ ($9.4 \times 10^{-3} \text{ cm/s}$) .

Although the authors found that lithium reduction was d.c. reversible, they reported that in general, lithium reduction is less reversible than the other alkali metal cations.

The ease of alkali cation reduction has been correlated to their solvation energies, where more negative values of solvation energies are associated with smaller values of k_s . The trend above is in agreement with this since lithium is the most strongly solvated and caesium the least. This type of argument has frequently been used to explain trends in k_s values for alkali metal cations (61,62).

In dimethylacetamide, d.c. polarographic and oscillopolarographic studies again showed that sodium, potassium, rubidium and caesium cations are reduced reversibly (63). However, lithium was not reduced in strictly anhydrous dimethylacetamide in the potential range available. With the addition of water, a wave appeared which shifted more positive with increasing water content. Also, the wave height increased with increasing water content up to 3% water, then remaining constant up to 7% water. Logarithmic analysis showed that the wave (3% water) was partially irreversible with a 66 mV slope. However, oscillopolarographic results indicated that the reduction was reversible. The above results were explained in terms of strong solvation of the lithium ions forming a stable symmetrical complex with a high polarographic overvoltage. Addition of water distorted the symmetry of the complex and decreased this

overvoltage. Also, the d.c. irreversibility was attributed to slow deactivation of the primary reduction product which under oscillopolarographic conditions was not given enough time to occur, thus explaining the reversibility under these conditions. Besette and Harwood (64) studied the same system using cyclic voltammetry. They found agreement with the above results. A series of periodic oxidation waves was obtained on the reverse scan in cyclic voltammetry. These oscillations were attributed to reaction of the lithium amalgam with water, giving rise to a film of lithium hydroxide and hydrogen gas evolution.

More recently, Fawcett and co-workers, in a series of studies (65-67), investigated the effect of solvents, solution composition and electrode composition on the electroreduction of alkali metal cations. They found that the kinetic parameters, namely, k_s and α , the apparent transfer coefficient, depend strongly on the above factors.

Changes in solvation of reactants and products and the electrostatic environment were considered to be the main contributing factors.

1.2.3. The Interaction between Aromatic Hydrocarbon Negative Ions and Alkali Metal Cations

No account of the interactions between aromatic hydrocarbon negative ions and alkali metal cations is complete without mentioning the early attempts in trying to react hydrocarbons with alkali metals. Berthelot (68), in 1867, reacted potassium directly with naphthalene at elevated temperature and obtained the dipotassium product. More intensive studies were made by Schlenk et al in diethyl ether as solvent (69,70). The reaction of sodium with anthracene was observed and lithium reacted with naphthalene to give the dilithium product, though only to a limited extent. A solution of sodium in liquid ammonia was reported to bring about the addition of sodium to

It appears that this is the first instance where some sort of anion radical intermediate was proposed. However, the authors erroneously thought that the green color of the solution was due to the dianion which was also thought to be the major product. From these pioneering studies, it was realized that the soluble alkali metal-hydrocarbon complexes are highly colored, very reactive and ionic in nature (as evidenced by the electrical conductivity of the solutions (74)).

However, the mechanism of the reactions and the type of products formed was not well understood. For example, it was thought that the reaction of naphthalene with sodium involved the transfer of one or two electrons from sodium atoms to one naphthalene molecule and a complex of the form $\text{NaC}_{10}\text{H}_8\text{Na}$ was proposed (74). Also, stoichiometries such as 1:1, 2:1, 4:1 for alkali metal-hydrocarbon complexes have been proposed (see previous references).

The next important step was made by Lipkin et al (75) who first established the free radical nature of the product of these reactions. They reacted sodium with naphthalene, anthracene, phenanthrene etc. in 1,2-dimethoxyethane and tetrahydrofuran and found that the product exhibited intense paramagnetic absorptions and all products were found to have a free electron value of one. They deduced that the reactions involved the transfer of one electron from sodium to the hydrocarbons to form free radical ions. However, it was not thought that dianions could be formed as well. The equilibrium nature of alkali metal-hydrocarbon reactions was known (72) and these authors suggested that the principal factor which determines the ability of high oxygen content ethers such as dimethyl ether and 1,2-dimethoxyethane to promote reaction was due to the favorable energy of solvation of the metal ion (and possibly the hydrocarbon anion) thus shifting the

equilibrium to the anion side. They also suggested that the solvation of the metal ion involves chelate structures with unhindered ethers as was proposed earlier (37). At about the same time, Weissman et al (89) reported the first published hyperfine splittings in the paramagnetic resonance spectrum of the naphthalene anion radical in tetrahydrofuran which exhibited nineteen components. Chu and Yu (76) studied the magnetic susceptibilities of sodium with anthracene, biphenyl, naphthalene, phenanthrene, and m-terphenyl in tetrahydrofuran. They reported that in the case of anthracene and phenanthrene, dianions are formed as well as anion radicals.

Further studies in this area were made by Hoijtink (77,78, 81-87) and co-workers. Comparison was made between chemical and electrochemical reductions, both of which yielded the same products, namely, the anion radicals and dianions. However, in the case of chemical reduction,

whether or not the dianions are formed depends on the electron affinities of the hydrocarbons. Potentiometric (77,78) and spectrophotometric (80) techniques were used to establish a relative electron affinity scale for the hydrocarbons. In the potentiometric studies, standard reduction potentials referenced to the reduction potential of biphenyl were in good agreement with polarographic values. However the results obtained from the two techniques did not agree. Jagur-Gradzinski et al (88) made careful studies in tetrahydrofuran using both techniques in order to resolve the differences obtained in the two studies above. They assumed that the ions are mainly undissociated in tetrahydrofuran, and compared the two techniques. Their results were in qualitative agreement with those of Hoijtink et al (78).

In most of these studies, it was implicitly assumed that the hydrocarbon negative ions exist as free ions in

solution. The role played by the counterions in solvent was not well understood. However, the pioneering work of Winstein et al (90) and Grunwald (91) has established the existence of different types of ion associates. Szwarc and his school established the presence of an equilibrium between contact and solvent-separated ion pairs (92).

There has been tremendous interest in the reactivities of organic anions since they take part in numerous important processes. For example, radical anions act as initiators in anionic polymerization (93). These reactivities are greatly affected by counter cations, solvent, and temperature. It is interesting to note that early interest in alkali metal-hydrocarbon reactions led naturally to later studies of ionic interactions and discovery that these reactions occur so well in solvents of low dielectric constant such as tetrahydrofuran, 2-methyltetrahydrofuran, 1,2-dimethoxyethane and dioxane. It follows that chemical

reduction is the predominant method of generation of hydrocarbon anions in later studies. More attention has been paid to anion radicals than dianions. There are several reasons for this. First, chemical reductions do not produce dianions in all aromatic hydrocarbons. Second, the dianions, even if they are produced, are much more reactive than anions, and require special techniques for their preservation. Third, one of the most powerful methods for studying ion associates is electron spin resonance which can only be applied to free radical ions. Electrochemical generation of anions has been employed in numerous such studies (31, 94, 95).

Many techniques have been used in the study of ion pairing. Conductance methods were used to detect the presence of ion pairs of polycyclic aromatic hydrocarbon anions with alkali metal cations (96). Spectroscopic methods include UV-VIS (93,96-98), and infrared (99-101).

However, by far the most powerful and popular techniques employed are magnetic resonance, both nuclear and electron spin. These methods yield detailed information about the structural and dynamic properties of the various ion pairs. Several reviews have been written concerning the development of the concept of ion pairing and its importance in different fields of chemical research (14,15,102).

1.2.4. Tetracyanoethylene (TCNE)

There is tremendous interest in tetracyanoethylene and its related family members due to their unusual properties. TCNE was the first of a new class of compounds (known as percyano olefins) to be synthesized (103). Prior to this, the only known cyanocarbons were dicyanoacetylene and dicyanobutadiene (104). TCNE is exceptionally reactive and undergoes addition and substitution readily. These reactions have been

discussed (105-109).

The physical and electronic properties of TCNE have been extensively studied. Relative electron affinities were obtained from studies of molecular charge transfer complexes (110-112). The absolute electron affinity was found to be $2.3(\pm 0.3)$ eV by the technique of photo-detachment of electrons from negative ions (113) which is about 0.5 eV less than the value obtained by the magnetron surface ionization technique (114). The theoretically calculated value is 3.06 eV (115). Vibrational spectra of TCNE has been studied in detail. Raman and iR spectra, both in the solid state and in solution have been published (116-122). Electronic absorption spectra in solvents such as 2-methyltetrahydrofuran (123) and acetonitrile (124) are available. Theoretical absorption energies (125) and simulated spectra (126) have been calculated.

The most widely studied property of TCNE results from the presence of its four cyano groups. These four electron withdrawing groups make TCNE a very strong π -acid. It forms molecular π -complexes with π -bases such as aromatic hydrocarbons. The formation constants of these complexes have been obtained from spectroscopic (127) and polarographic studies (128,129). Molecular orbital calculations of these complexes have been made (130).

TCNE can be easily reduced in a number of different ways. Chemically, it can be reduced by iodides, thiols, mercaptans and hydrogen on palladium (106), and even cyanide ion (124). TCNE is found to react with metals such as K, Na, Al, Mg, Cu, Pb etc. at room temperature to give the corresponding metal salts (124,131). The existence of these metal tetracyanoethylenides was first recognized by Weissman (132). These metal salts are

very stable in the solid state. For example, $K+TCNE=$ has been known to remain unchanged even after heating for three hours at $150^{\circ}C$ in an inert atmosphere, and also after exposure to the atmosphere for one month (124).

The anion radical of TCNE ($TCNE^{\dot{-}}$) can also be produced by irradiation with a light pulse from an Argon flash lamp (133). In solution, the anion radical, in contrast to the solid salt, is sensitive to oxygen and less so, to water (124). It has been reported that $TCNE^{\dot{-}}$ is produced spontaneously in solvents such as dimethylsulfoxide, dimethylformamide and dimethylacetamide, the rate of production being accelerated in the presence of light. The anion radical production was explained in terms of the thermal ionic dissociation of the electron donor-acceptor complexes (EDA) formed with these solvents (134-137). However, Butler et al studied the dimethylsulfoxide-TCNE system and came to the conclusion that the presence of $TCNE^{\dot{-}}$

was the result of complex chemical reactions taking place between the components of the system and not due to thermal dissociation of the EDA complex (137).

$\text{TCNE}^{\cdot-}$ has been studied by IR and Raman spectroscopy (121,138-141) and UV-VIS spectroscopy (123,142).

Electron spin resonance studies were undertaken (143-145) to study the effect of counterions on the reactions of $\text{TCNE}^{\cdot-}$. Theoretical studies on the electron spin distribution of $\text{TCNE}^{\cdot-}$ have also been made (146).

The anion radical and dianion of TCNE can also be prepared by electrochemical methods. Peover studied the polarographic reduction of TCNE to $\text{TCNE}^{\cdot-}$ in acetonitrile, dimethylformamide, chloroform and methylene chloride.

In acetonitrile and dimethylformamide using tetraethylammonium perchlorate, the reduction was found to be reversible and involved the transfer of one electron. Further reduction was not carried out. In chloroform,

using tetrabutylammonium perchlorate (0.5M), similar results were obtained. However, in methylene chloride, reduction to the dianion was carried out (0.5M tetrabutylammonium perchlorate). Both waves involved one electron transfer and were reversible. Van Duyne et al (138) reduced TCNE at platinum electrode in acetonitrile using tetrabutylammonium perchlorate as solvent. Employing cyclic voltammetry they found the first wave to be a reversible one-electron wave and the anion radical was found to be stable over at least 40 minutes. However the second wave was irreversible. The irreversibility of the second reduction was attributed to the change in geometry in going from $\text{TCNE}^{\cdot-}$ to TCNE^{2-} . Pons et al (139) obtained similar results, but showed that the irreversibility was due to other causes. Kaplan et al plotted the reduction potentials against the calculated energy of the lowest unoccupied molecular orbitals for a series of

cyanocarbons but could find no correlation (147). Heterogeneous rate constants for the first electron transfer have been determined by cyclic voltammetry at different electrode materials and in different solvents. The diffusion coefficients were also obtained (148,149).

1.2.5 7,7,8,8-Tetracyanoquinodimethane (TCNQ)

Since the discovery of TCNE, and the demonstration of its exceptional properties, there was increased effort to explore new members of the percyano class of compounds. Particular interest was paid to structures where the ethylene bond was replaced by a conjugated system. One outstanding member which surfaced was 7,7,8,8-tetracyanoquinodimethane (TCNQ).

TCNQ was prepared for the first time in 1961 (150) but details of its preparation were only published in 1962 (151). Although many properties of TCNQ parallel

those of TCNE, there are also some important differences.

For example, TCNQ undergoes displacement of its cyano group on the same carbon atom as does TCNE. However, TCNQ does not form the Diels-Alder adduct with dienes and addition occurs at the 1,6-positions in contrast to the 1,4-positions for TCNE.

TCNQ, like TCNE, is a strong π -acid. It has been reported (152), based on polarographic half-wave potentials, that TCNE has the stronger acidity of the two. The E_h values, obtained in acetonitrile, are TCNQ = +0.127 V (vs SCE) and TCNE = +0.152 V (vs SCE). However, experimental (115) and theoretical (113) determinations both showed that TCNQ has slightly higher absolute electron affinity. The experimental values were 2.4 and 2.3 eV for TCNQ and TCNE respectively and the theoretical values were 3.42 and 3.06 eV respectively.

Like TCNE, TCNQ forms 1:1 π -complexes with many

organic donors. These complexes can be isolated in the solid form. Many of them are electrically conductive and have been the subject of intensive research. The electrical properties of the most famous of them, the tetrathiofulvalene-tetracyanoquinodimethane (TTF-TCNQ) complex was first discovered by Heeger et al (153). It was found that, at room temperature, TTF-TCNQ has an electrical conductivity comparable to that of graphite (about $1000/\Omega \text{ cm}$). The conductivity increased dramatically at lower temperatures, reaching a maximum value of slightly over $11000/\Omega \text{ cm}$ at 60 K before decreasing again. Due to this high conductivity and its chain-like structure, it has been referred to as a quasi-one-dimensional metal (154,155).

The duPont group, who discovered TCNQ (as well as TCNE) (147), has published an extensive series of studies of the chemical and physical properties of TCNQ and its derivatives (151,152,156). TCNQ can be easily reduced to

its anion radical by iodides and metals such as copper, silver, etc. to form simple salts. With tetraalkylammonium cations, complex salts of formula $M^+:(TCNQ^{\dot{-}})TCNQ$ are obtained. Peover (128,129) has studied TCNQ-aromatic hydrocarbon complexes polarographically and has determined their stability constants. Heats of formation and electron affinities have also been derived from thermochemical studies. As for TCNE, relative electron affinities have been determined (110-112) and absolute electron affinities obtained both experimentally and theoretically (113-115). Various spectroscopic methods have been employed to study TCNQ and its anions.

Jeanmaire and Van Duyne obtained the electronic and Raman resonance spectra of TCNQ and its anion radical in acetonitrile. The anion radical, $TCNQ^{\dot{-}}$, was generated electrochemically (157). Infrared spectroscopy has been applied to the study of its anion radical in solution

(158,159) and in the solid state (160,161). Khatkale and Devlin studied the vibrational and electronic spectra of the mono-, di-, and trianion salts of TCNQ using a vapor deposition method (162). The resonance Raman spectroelectrochemistry of the dianion and its oxygen decay product was studied by Suchanski and Van Duyne (163). Theoretical calculations of the spectroscopic properties of TCNQ, $\text{TCNQ}^{\cdot-}$, and TCNQ^{2-} have been performed. The ionization and reduction potentials and dipole moment has also been calculated theoretically (126). Electron spin resonance has been applied to the study of $\text{TCNQ}^{\cdot-}$ and its reactions (165-167). Theoretical spin density distribution calculations have also been made (146,147).

Electrochemical studies have shown that the reduction of TCNQ in homogeneous solvents involve two well-defined one-electron steps, with the formation of the

anion radical and then the dianion. Peover found that both steps were polarographically reversible in chloroform and methylene chloride. In acetonitrile and DMF, where only the first reduction step was studied, the same result was obtained (128,129). Suchanski and Van Duyne also found reversibility for both electron transfers in acetonitrile on a voltammetric time scale (0.2 to 2.0s (163)). Sharp obtained the heterogeneous rate constants for the first reduction steps in various dipolar aprotic solvents and at different electrode materials. Diffusion coefficient values were also obtained (148,149).

Due to its additional conjugation, the anions of TCNQ are expected to be more stable than those of TCNE (148). However the stability of the anion radical and dianion are still affected by oxygen and water. In deaerated acetonitrile, $\text{TCNQ}^{\cdot -}$ is reported to be stable for 3 hours whereas

TCNQ⁻ at least for 40 m. The oxygen decay of TCNQ⁻ has also been studied (163). The rate of protonation of TCNQ⁻ in methanol, ethanol, acetonitrile and water has also been determined (169,170). TCNQ⁻ is known also to dimerize in water (171).

Chapter 2 Electrochemical Techniques

2.1 Introduction

In this chapter the electrochemical techniques employed in this reasearch are described. As far as possible, detailed mathematical derivations are avoided. Since most of them are established techniques, the details are presented in most textbooks and review series (172-176). However, pertinent equations will be given here.

2.2 General Considerations

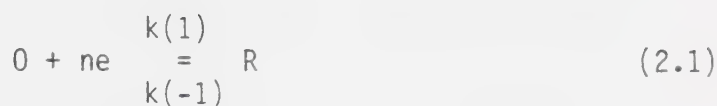
The modern electrochemical experiment employs a three electrode system. This consists of the working electrode, where the electrode reaction of interest is monitored, the counter electrode which completes the

current path through the solution, and the reference electrode. The reference electrode draws extremely small currents and its potential remains essentially constant. The applied potential is controlled with respect to the reference electrode by a potentiostat. Also, depending upon the technique used, a potential program (e.g. ramp, pulse etc.) can be applied from some source such as a waveform generator.

In earlier two electrode systems, problems of voltage loss (iR loss) due to high solution resistance (especially in nonaqueous media) arose. However, with the use of the potentiostat employing operational amplifier circuitry in a three electrode configuration, the iR loss can be reduced to very small values by employing a positive feedback circuitry and proper placement of the reference electrode close to the working

electrode.

Consider the electrode reduction process



where n is the number of electrons transferred, O and R are the oxidized and reduced species of the redox couple, and $k(1)$ and $k(-1)$ are the forward and reverse heterogeneous rate constants respectively. At equilibrium where no net current is flowing the Nernst equation applies

$$E(\text{eq}) = E(0) + \frac{RT}{nF} \ln(a(O)/a(R)) \quad (2.2)$$

where $E(\text{eq})$ is the equilibrium potential, $E(0)$ is the standard potential, $a(O)$ is the bulk activity of O , $a(R)$ is the bulk activity of R . All the activity coefficients can be incorporated into $E(0)$ to give the formal potential $E(0)'$

$$E(\text{eq}) = E(0)' + RT/nF \ln(C(0)/C(R)) \quad (2.3)$$

where the C's refer to concentration. Also, if the electrode kinetics are very fast (i.e. the standard heterogeneous rate constant k_s is large), equation (2.3) can be applied to concentrations at the surface of the electrode and the reaction is said to be electrochemically reversible

$$E = E(0)' + RT/nF \ln(C(0)'/C(R)') \quad (2.4)$$

where $C(0)'$ and $C(R)'$ are concentrations of O and R respectively at the surface of the electrode.

The total current i , which flows in the electrochemical experiment comes primarily from two sources

$$i = i(c) + i(f) \quad (2.5)$$

The charging current $i(c)$, is the current required to charge the electrical double layer at the electrode-solution interphase. The faradaic current $i(f)$, is the current which flows as a result of the system's response to an applied potential, in order that equation (2.4) could be obeyed. If the response of the system is slow with respect to a changing potential (i.e. small k_s) then equation (2.3) cannot be established at the electrode surface and the reaction is said to be electrochemically irreversible. (It is assumed that species O and R are otherwise stable so that homogeneous kinetics do not have to be considered.) If the electrode kinetics are fast, the current is only governed by the rate at which O can be transported to the electrode. The electrode reaction is then said to be mass-transfer controlled.

There are three methods of mass transport, namely, convection, migration and diffusion. Therefore

$$i(f) = i(\text{conv}) + i(m) + i(d) \quad (2.6)$$

where $i(\text{conv})$ is the convection current, $i(m)$ the migration and $i(d)$ the diffusion current. In electrochemical experiments, the migration current is suppressed by using a large excess (ca 100 times substrate) of the supporting electrolyte which conducts the current through the bulk solution as well. Then, depending upon the electrochemical technique, either convection or diffusion could be the method of choice for mass transport. In the case of diffusion control, Fick's laws of diffusion apply and for linear diffusion to a plane electrode

$$-J(0)(x,t) = i/nFA = D(0)(\delta C(0)(x,t)/\delta x) \quad (2.7)$$

$$\Delta C(0)(x,t)/\delta t = D(0)\Delta^2 C(0)(x,t)/\delta x^2 \quad (2.8)$$

At this point, one or two words should be said about

"electrochemical reversibility or irreversibility." Any process is said to be thermodynamically reversible if an infinitesimal change in the direction of the driving force changes the direction of the process. However, all electrode processes occur at a finite rate and therefore cannot be thermodynamically reversible. The definition of electrochemical reversibility is thus one of practical value rather than thermodynamic rigor. In the practical sense, therefore, an electrochemical process is reversible if the deviations from the Nernst equation are too small to be measured. Also, reversibility would depend on the technique used. If the time scale of the experiment is short, and the kinetics of electron transfer are not fast enough so that the Nernst equation cannot be established at the electrode surface, the process will be irreversible.

2.3 Chronoamperometry

Chronoamperometry, as the name implies, is a technique whereby the current is monitored as a function of time. In common practice, the potential of the working electrode, which is initially set at a value where no electrode reaction is occurring, is stepped to a value large enough so that the electrode process is limited only by the diffusive transport of material to the electrode surface. Since the experiment is carried out in a conductive quiescent solution, this is the only mode of mass transport. Therefore, assuming semi-infinite linear diffusion to a plane, Fick's laws can be applied (equations (2.7) and 2.8)) together with some initial and boundary conditions:

$$C(0)(x,0) = C^* \quad (2.9)$$

$$C(0)(\text{large } x,t) = C^* \quad (2.10)$$

$$C(0)(0,t) = 0 \quad (2.11)$$

Equations (2.7) and (2.8) together with the conditions above, can be solved by making use of the Laplace transformation. The current time function is given by

$$i = nFA D(0)^{\frac{1}{2}} C^* / (\pi t)^{\frac{1}{2}} \quad (2.12)$$

where i = current (μA)

D = diffusion coefficient cm^2/s)

C^* = bulk concentration (mM)

A = area of electrode , cm^2

n = number of electrons transferred

t = time (s)

F = 96487 coulombs.

Equation (2.12) is known as the Cottrell equation (177).

It should be noted that in the Cottrell equation the current is independent of potential since the potential is stepped to a value large enough so that the rate of the electrode process is essentially infinite. Therefore, if there are no coupled chemical reactions, the Cottrell equation will hold whether or not the electrochemical process is reversible or irreversible.

2.4 Cyclic Voltammetry

Linear sweep cyclic voltammetry is one of the most popular electrochemical techniques used today. It has been employed in many applications such as determination of reversibility and standard heterogeneous rate constants, elucidation of reaction mechanisms, determination of homogeneous kinetic parameters, etc. It is almost always used in initial investigations of new systems. For the electrode process without coupled chemical reactions, the

theories for the reversible (178-183), quasi-reversible (180,183,184) and the irreversible cases (186) have been given. Many cases of charge transfer coupled with chemical reactions have also been studied (187-190). Later, Nicholson and Shain (191), in a classic paper, reported the analytical derivations for the theory for various cases, both with and without coupled chemical reactions.

Although spherical, cylindrical and planar electrodes have all been used in cyclic voltammetry, the following discussion assumes planar diffusion. In the cyclic voltammetric experiment, if we consider the reduction process as given by equation (2.1), the potential of the working electrode is varied linearly in time from an initial value where no electrode reaction is occurring to a more negative value where the electrode reaction is governed by diffusion. On reaching this value, known as the switching potential, the linear potential sweep is reversed. The

sweep rate is usually the same for the forward and reverse scans but need not be so. It can vary widely from a few mV/s to over 1000 V/s. To describe the process occurring at the electrode we consider the forward scan. As the potential is scanned negative from the initial potential, faradaic current will begin to flow as prescribed by the Butler-Volmer equation. The surface concentration of the substrate O will thus begin to decrease. The current increases exponentially with the potential, and the concentration of O is inevitably driven to zero at the surface. At this point it is impossible for the flux to continue increasing at such a rate. As a result, the concentration of O near the electrode continues to fall causing a decrease in the gradient of O in the vicinity of the electrode. Since the current is simply related to this gradient by Fick's first law, it is observed that the current begins to fall,

causing a peak to appear in the current-voltage characteristic. At more negative potentials, the current is still diffusion limited, and the characteristic is the same as that of a chronoamperogram, i.e. the current falls as root t . Simultaneously, the concentration profile of the electrogenerated species R has been increasing near the surface of the electrode. It is found, that if the potential sweep is now reversed, a similar inverted response is observed. A peak in the opposite signed direction is formed which corresponds to the oxidation of R . Similar arguments are in effect for the observed behavior.

For the reversible case the current is given by

$$i = nFAC(0) * (\pi a D(0))^{\frac{1}{2}} X(at) \quad (2.13)$$

where $a = (nFv / RT) \quad (2.14)$

$$v = \text{scan rate (V/s)}$$

and $\chi(at)$ is the current function which can be numerically calculated (191). The peak current is given by $\chi(at) = 0.4463$.

$$i(p) = 0.4463 nFAC(0)^*(nFvD(0)/RT)^{\frac{1}{2}} \quad (2.15)$$

At 25°C

$$i(p) = (269000)n^{\frac{3}{2}} A (D(0)v)^{\frac{1}{2}} C(0)^* \quad (2.16)$$

where $i(p)$ = amperes, A = cm², $D(0)$ = cm²/s,

$C(0)^*$ = mol/cm³ and v = V/s. Equation (2.16) is known as the Randles- Sevcik equation.

For the reversible case the peak potential $E(p)$ is related to the polarographic half-wave potential E_h by

$$E(p) - E_h = -1.109(RT/nF) \quad (2.17)$$

Also the potential at $1/2 i(p)$, $E(p/2)$ is

$$E(p/2) - E_h = 1.09 (RT/nF) = (28.0/n) \text{ mV} \quad (2.18)$$

at 25°C

and
$$E(p) - E(p/2) = 2.20 (RT/nF) = (56.5/n) \text{ mV} \quad (2.19)$$

at 25°C .

Considering both the forward and reverse waves

(cyclic voltammogram), for a Nernstian wave with stable R

$$(i(p_a)/i(p_c)) = 1 \text{ if the switching potential} \quad (2.20)$$

E_λ is at least $35/n$ mV past

the peak

where $i(p_a)$ = peak anodic current measured from the

asymptotic limit of the decaying cathodic

current as baseline

$i(p_c)$ = peak cathodic current.

Also $\Delta E(p) = |E(p)(ox) - E(red)| = (59/n)mV$ at $25^\circ C$ (2.21)

For the totally irreversible case

$$i = nFAC(0) \cdot (\alpha n' F D(0) v \pi / RT) \cdot X(bt) \quad (2.22)$$

where $b = (\alpha n' F v / RT)$

and n' is the number of electrons transferred up to and including the rate determining step.

$$i(p) = (299000) n(\alpha n') AC(0) \cdot (D(0)v) \quad (2.23)$$

where n is the total number of electrons transferred.

When the current is at its peak

$$E(p) = E(0)' - (RT/\alpha n' F) [0.780 + \ln(D(0)/k_s) + \ln(\alpha n' F v / RT)] \quad (2.24)$$

$$\text{and } |E(p) - E(p/2)| = (1.857RT/\alpha n'F) = (47.7/\alpha n') \text{ mV} \quad (2.25)$$

at 25°C.

Thus, for the reversible case, $E(p)$ is independent of scan rate whereas for the irreversible case $E(p)$ shifts

$(1.15 RT/\alpha n'F) = (30/\alpha n') \text{ mV}$ more negative at 25°C for each

decade increase in scan rate. Also it is noticed that

for the Nernstian case, no kinetic information can be

obtained, whereas the kinetic parameters, namely the

transfer coefficient α and the standard heterogeneous

rate constant k_s , appear in the equations describing the

irreversible electron transfer.

Nicholson (184), has also derived the cyclic voltammetric behavior for the quasi-reversible case. It was

found that, if $E(\lambda)$ is at least $(90/n) \text{ mV}$ past

the cathodic peak, the current-potential curves are

dependent on the dimensionless parameter α and Δ where

$$\Delta = ((D(0)/D(R))^{1/2} k_s) / [(D(0)\pi v(nF/RT)]^{1/2} \quad (2.26)$$

Also for $0.3 < \alpha < 0.7$, $\text{del}E(p)$ values are essentially independent of α and depend only on Δ . $\text{Del}E(p)$ values together with their corresponding Δ values have been calculated (assuming $\alpha = 0.5$). From these values, a working curve can be plotted from which k_s values for quasi-reversible electrode reactions can be obtained by observing the variation of $\text{del}E(p)$ with sweep rate v .

For more details concerning the equations introduced in this section references (172, 191) should be consulted.

2.5 Normal Pulse Polarography

The dropping mercury electrode (dme) was initially introduced by Heyrovsky (206). The technique which its use generated is called polarography, and has since gained widespread use. (The term polarography used

here is distinguished from voltammetry in that the former applies solely to the use of the dropping mercury electrode.) Over the years, the polarographic technique has undergone so much transformation and improvement that the classical method commonly called d.c. polarography is nowadays seldom used. This is because related techniques which arose such as a.c. polarography, normal pulse polarography, differential pulse polarography, current-sampled polarography, etc. offer large advantages in terms of diagnostics, sensitivity, resolution, recording etc.

Although normal pulse polarography is the method of choice in this work, the general polarographic theory must be briefly described with reference to the closely related d.c. polarography. In the polarographic experiment, the mercury issues from a capillary and grows as spherical drops until the weight exceeds the surface tension, when it drops. A new drop then emerges. Mean-

while the potential applied to the electrode is linearly varied (slowly) so that the potential change per drop is not more than 5 mV (174). This is required to satisfy the condition of essentially constant potential and thus electrochemical equilibrium. During the growth of each drop, a current flows and the electroactive species in the vicinity of the drop will be depleted. As the drop falls, it stirs the solution and carries most of the diffusion layer away so that each new drop is again born into an essentially (not completely) fresh solution. The periodic growth and fall of the mercury drops is reflected in d.c. polarograms (current vs voltage plots) which exhibit current oscillations.

For the reversible d.c. polarographic process as given by equation (2.1), equations (2.3) and (2.4) hold. The instantaneous current at the diffusion limit has been derived by Ilkovic (207,208)

$$i(d) = 708 \, n \, C(0) \cdot (D(0))^{\frac{1}{2}} m^{2/3} t^{1/6} \quad (2.27)$$

where m = mass flow rate of mercury in mg/sec

All the other terms have their usual meaning.

At the end of drop life $t = t(\max)$, and

$$i(d \max) = 708 \, n \, C(0) \cdot D(0)^{\frac{1}{2}} (t \max)^{1/6} m^{2/3} \quad (2.28)$$

Also, it can be easily shown that the current-potential

curve is given by (174)

$$E = E(0)' + (RT/nF) \ln((i(d) - i)/i)(D(R)/D(0))^{\frac{1}{2}} \quad (2.29)$$

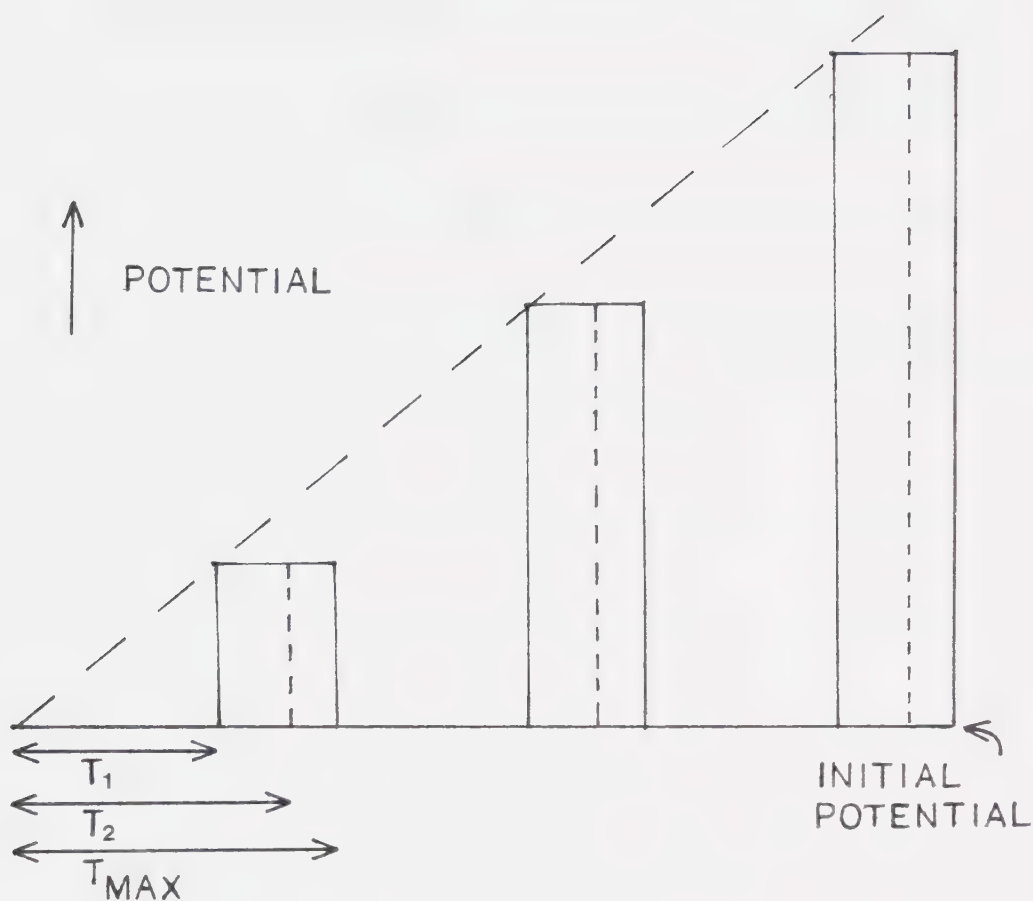
$$E = E(0)' + (RT/nF) \ln (D(R)/D(0))^{\frac{1}{2}} +$$

$$(RT/nF) \ln (i(d) - i)/i \quad (2.30)$$

In the pulse polarographic experiment, the potential program is different from the continuous linear change of d.c. polarography. Here, the potential is always kept at an initial value where the reduction process does not occur. Towards the end of each drop life, a potential pulse is applied, the amplitude of which increases monotonically with each application. This program is illustrated in Figure 1. Thus, if the potential is at the diffusion controlled limit the current is given by the Cottrell equation

$$i = (nFA(D(O))^{1/2} C(O)^*) / (\pi(t(2)-t(1)))^{1/2} \quad (2.31)$$

Equation (2.31) is based on the same assumptions of linear diffusion as the Ilkovic equation (equation (2.27)) except that in the latter, the expansion of the mercury drop is taken into account. Since in pulse polarography the potential pulse is applied at the end of drop life,



AT T_1 PULSE APPLIED

AT T_2 CURRENT MEASURED

T_{MAX} = DROP LIFE, 0.5S

$T_{MAX} - T_1 = 57 \text{ MS}$

$T_{MAX} - T_2 = 16.7 \text{ MS}$

Figure 1. Normal pulse polarographic potential program.

the drop area is not changing very much. Thus the form of the pulse polarogram consists of steps rather than the current oscillations encountered in d.c. polarograms.

The current potential curve can also be shown to have the same form as equation (2.30) i.e.

$$E = E(0)' + (RT/nF)\ln (D(R)/D(0))^{1/2} + (RT/nF)\ln((i(d)-i)/i) \quad (2.32)$$

At $i = i(d)/2$

$$E_h = E(0)' + (RT/nF)\ln (D(R)/D(0))^{1/2} \quad (2.33)$$

where E_h is the half-wave potential. In many cases $D(R) =$

$D(0)$ so that E_h is usually taken to be the same as $E(0)'$.

Therefore for a reversible reaction, a plot of E vs $\log (i(d)-i/i)$ should give an intercept equal to E_h and a

slope equal to $(2.303 RT)/(nF)$ which has the value 59/n mV at 25°C. The above equations apply equally well to d.c. polarography. Also, it can be shown that under the usual operating conditions, normal pulse polarography is about 6 to 7 times more sensitive than d.c. polarography (see reference (174), p. 244).

2.6 Modulated Specular Reflectance Spectroscopy (MSRS)

Spectroscopy was successfully combined to electrochemistry in the 1960's (192,193). With this combination, an extra selectivity dimension was added to the electrochemical experiment. Thus wavelength and potential became the controllable experimental variables. This new addition to the electrochemical arsenal is aptly called spectroelectrochemistry.

Spectroelectrochemistry has been applied to the studies of adsorption (194,195), double layer structure

(196,197), identification of intermediates and elucidation of reaction mechanisms (198-200). The spectral regions used have included IR and Raman (139,157,201), and UV-VIS (198,202). Recently, the spectroscopic response to the a.c. voltammetric experiment has been studied (203). It has been noted that the spectroelectrochemical techniques have the advantage in that the deleterious effects of charging current which affect current measuring methods have been eliminated.

In the spectroelectrochemical experiment both transmission (192,203,204) and reflectance (198,202,205) methods have been used. However, reflectance has some advantages over transmission in that due to its setup, the counter electrode in the transmission method cannot be positioned in such a way that every point in the working electrode is equidistant from it. Thus uneven current distribution arises. Also, the fact that the

optically transparent electrode is a thin conductive film deposited on a transparent insulating material gives rise to high resistance. Further discussion will be restricted to the modulated specular reflectance technique (MSRS) although the equations which arise are, in principle, applicable to the transmission technique.

As used in the author's laboratory, the UV-VIS MSRS experiment can be attained in two ways. For the electrode process given in equation (2.1), the potential is modulated such that, periodically, either O or R is present in the diffusion layer. Meanwhile, the wavelength of the incident radiation is scanned. Light passing through the solution hits the electrode at an angle and is reflected. In doing so, it passes twice through the layer where the absorbing species are present with the periodic formation and removal of R in the diffusion layer. The resulting light signal is a difference spectrum of R since

the background condition is that with 0 initially present.

The light signal is detected by a photomultiplier and extracted out of background noise using a lock-in amplifier referenced to the same frequency as the modulation.

In obtaining the spectrum, the signal is fed into a lock-in amplifier. In doing so, time information is complicated. To obtain kinetic information after obtaining the spectrum, the wavelength of the incident radiation is fixed, usually at the absorption maximum. This time, the modulated light signal after detection at the photomultiplier is processed by a signal averager. Here, the signals for the formation and disappearance of R for a single cycle are signal averaged over a chosen number of cycles to increase the signal-to-noise ratio. The result is a reflectance-time transient from which kinetic information is available.

In the single beam MSRS experiments discussed above,

the parameter which is actually measured is the normalized reflectance

$$(\text{del}R/R) = [R(t)-R(0)]/R(0) \quad (2.34)$$

where $R(0)$ = reflectance at time $t=0$

$R(t)$ = reflectance at time t

$$\text{del}R/R = [R(t)/R(0)]-1 \quad (2.35)$$

$$R(t)/R(0) = 1+[\text{del}R/R] \quad (2.36)$$

It has been shown that for any electrode process where only R may absorb, the time-dependent absorbance for the optical transmission electrode (OTE) experiment is given by (199)

$$A(t) = (\epsilon(R)/nFA) \int_0^t i(t)dt \quad (2.37)$$

where $\epsilon(R)$ is the absorptivity of R and all the other symbols have the usual meaning. The integral of the

current with respect to time is related to the number of absorbing species in the light path length. For the MSRS experiment, as mentioned earlier, light passes through the path length twice at an angle θ as shown in Figure 2. In the figure,

$$q/2 = x/\cos(\theta)$$

$$q = 2x/\cos(\theta)$$

Therefore, the path length in the MSRS experiment is enhanced by $2/\cos(\theta)$ times that in the transmission experiment.

$$A(t) = (2\ell(R)/nFA \cos(\theta)) \int_0^t i(t) dt \quad (2.38)$$

But the absorbance

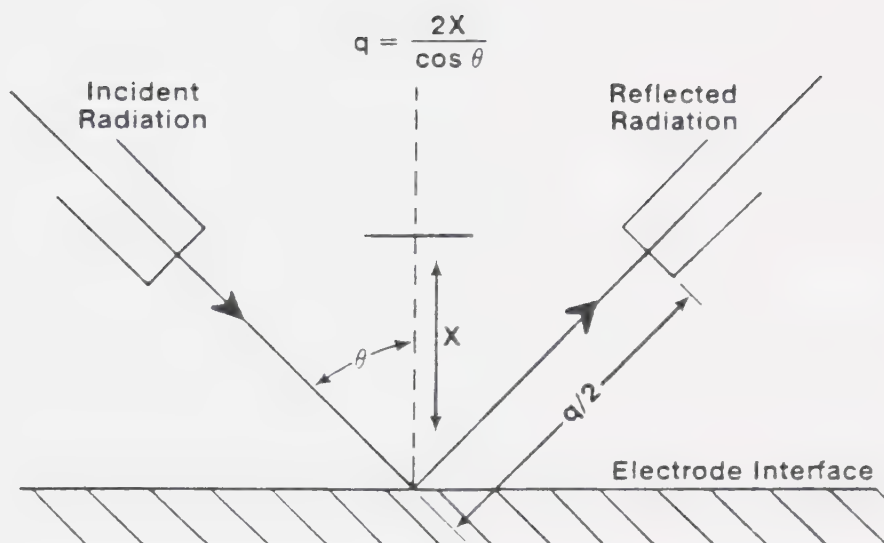


Figure 2. The coordinate system used in modulated specular reflectance spectroscopy.
 q is the pathlength of light beam
 θ is the angle of incidence
 x is the solution layer containing absorbing species of interest

$$A(t) = \log(I(0)/I(t)) \quad (2.39)$$

$$A(t) = \log(R(0)/R(t)) \text{ or}$$

$$A(t) = -\log(R(t)/R(0)) \quad (2.40)$$

Thus

$$\log(R(t)/R(0)) = \log(1 + \Delta R/R) \quad (2.41)$$

$$\log(1 + (\Delta R/R)) = (-2\ell(R)/nFA \cos(\theta)) \int_0^t i(t) dt \quad (2.42)$$

$$\text{and } \ln(1 + (\Delta R/R)) = (-4.606\ell(R)/nFA \cos(\theta)) \int_0^t i(t) dt \quad (2.43)$$

For small $\Delta R/R$ (experimental values of $\Delta R/R$ are seldom greater than 1.0×10^{-3} equation (2.43) can be approximated by

$$-\Delta R/R = 4.6\ell(R)/nFA \cos(\theta) \int_0^t i(t) dt \quad (2.44)$$

Chapter 3 The Electrochemical Reduction of Alkali Metal Cations, Anthracene and Fluoranthene in Acetonitrile and Dimethylformamide.

3.1 Introduction

In this thesis research, I have undertaken to observe the electrochemical behavior of alkali metal cations, anthracene (An), and fluoranthene (Fa) in aprotic solvents acetonitrile and dimethylformamide at the mercury electrode. The electroreduction of anthracene and fluoranthene was also carried out in the presence of alkali metal cations. Observations were focussed on the effect of the cations on the anion radicals and dianions of the polycyclic aromatic hydrocarbons.

As was mentioned in Chapter 1, in most of the previous studies of aromatic hydrocarbon negative ions-alkali metal cation interactions, the reaction was a chemical

reduction with alkali metals in ethereal solvents of low dielectric constants. The powerful esr technique has been frequently applied to the study of the anion radicals. The fact that the dianions are very reactive means that these species are difficult to study without extreme experimental precautions. Buschow et al (96) measured the electrical conductance of solutions of alkali-aromatic hydrocarbon salts in 2-methyltetrahydrofuran, tetrahydrofuran and 1,2-dimethoxyethane. Information was obtained for conditions under which the hydrocarbon negative ions are free or associated with alkali counter ions. It was found that at room temperature a 0.1 mM solution of the monolithium salts of anthracene, tetracene, pentacene in 2-methyltetrahydrofuran are completely dissociated whereas sodium and potassium salts are associated. The dinegative ions showed much stronger association and two counteranions were thought to be involved. The tendency of hydrocarbon

ion to associate with cations was found to increase with

(i) smaller size of the hydrocarbon ion, (ii) larger

radius of the cation, and (iii) increasing temperature.

Solvation was thought to play a very important role.

Disproportionation of solution phase radical anions is

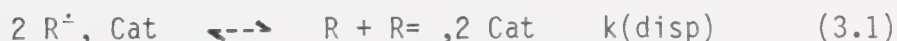
affected by countercations as well as solvents. The

presence of ion pairing substantially increased the

equilibrium constants for the disproportionation espec-

ially if contact ion pairs are formed between the dianions

and the cations.



There have been many studies of the disproportionation

reactions of aromatic hydrocarbon anion radicals (223-225).

However, the $k(\text{disp})$ values have been found to be small,

ranging from $1.0\text{e-}7$ to $1.0\text{e-}12$.

Electrochemical techniques such as polarography and cyclic voltammetry have been applied to the studies of ion pairing of negative ions of organic molecules with alkali metal cations. In the cases where ion pairing occurs, shifts in half-wave potentials or peak potentials toward more positive values are observed. In the study of polycyclic aromatic hydrocarbon dianion-alkali metal cation interactions by electrochemical means, one problem arises. This is because in most cases, the reductions of the alkali cations are in the same potential region as those of the aromatic hydrocarbon dianions. Therefore, if solid electrodes of inert materials such as platinum, carbon, gold etc. are used, deposition of alkali metals occurs. Various complications could then arise due to the reactivity of these alkali metals, as mentioned in Chapter 1. Therefore, if solid electrodes are to be used, the reduction potentials of the dianions

of the organic species under investigation have to be positive to those of the alkali cations. However, this problem could be easily solved, as noted earlier, with the use of the mercury electrode. This material also has the advantage of high surface reproducibility. Also the use of electrochemical methods affords a very important advantage over chemical reduction. The production of the desired anions to be studied can be easily controlled by controlling the potential. In chemical reduction, species control is not easily accomplished.

3.2 Experimental

3.2.1. Instrumentation

The instrument used in the polarographic analyses was the PAR 174A Polarographic Analyser which was operated in the normal pulse mode. For this particular instrument in

the normal pulse mode, the duration of each pulse was 57 ms, the pulse being applied towards the end of drop life. However, the current was only sampled during the last 16.7 ms of the pulse length in order to minimize the contribution of charging current to the total current. Figure 1 illustrates the potential program and the current sampling time interval. The scan rate used in all experiments was 10 mV/s. Polarograms were recorded, without smoothing, with a Houston Instruments Omnigraphic 2000 X-Y recorder. The capillary used for the dropping mercury electrode was of length 18.4 cm and internal diameter 0.03 mm. The mercury drop time was controlled by an electromechanical drop timer set at 0.5 s. The use of the drop timer avoids the problem of the variation of surface tension and therefore drop time with potential. The polarographic cell was a single compartment type with an outer jacket for temperature control purposes. (Figure 3).

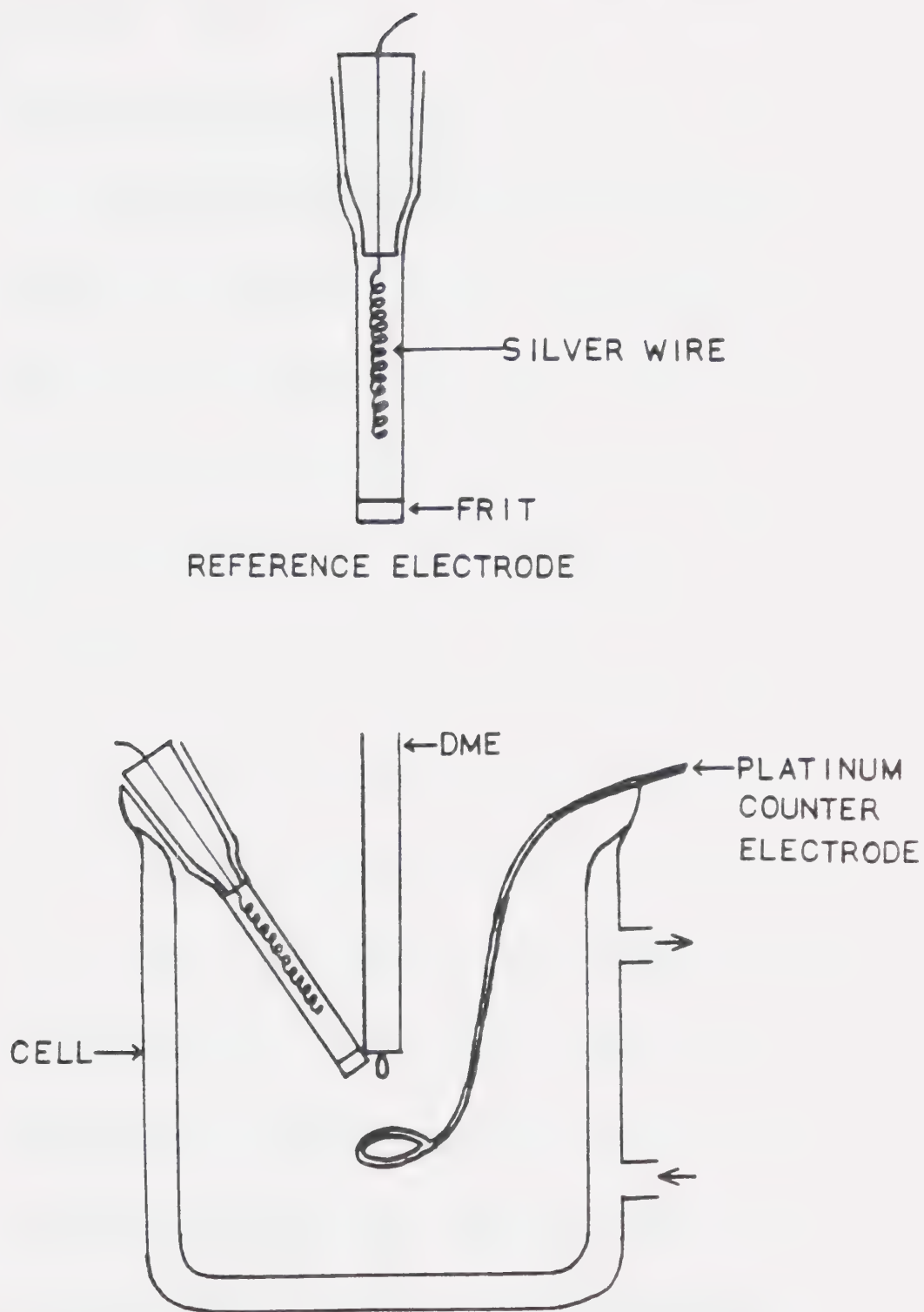


Figure 3. Polarographic cell arrangement.

3.2.2 Purification of Chemicals

The mercury used was triply distilled and filtered through a pin hole made in a filter paper to remove any particulates or surface oxides. Reagent grade lithium, sodium, potassium and rubidium perchlorates were recrystallized twice from triply distilled water. The purified products were dried in vacuo at 110°C for a minimum of 48 hours and stored in a vacuum dessicator over calcium chloride. Anthracene (Aldrich Gold Label 99.9%) was used as received. Fluoranthene (Aldrich 98%) was recrystallized once from ethanol. Tetra-n-butylammonium tetrafluoroborate (TBAF) was prepared according to a method similar to that of Lund and Iverson (213). This was done as follows: equal numbers of moles of tetra-n-butylammonium hydrogen sulfate and sodium tetrafluoroborate were dissolved separately in a minimum amount of distilled water. The solutions were mixed in a separating

funnel whereby the TBAF precipitated out. Methylene chloride was added to the separating funnel to dissolve the TBAF. After shaking, the methylene chloride layer was allowed to settle and drained out. It was then added to ice-cooled anhydrous ether with stirring, whereupon the TBAF crystallized and was recovered.

The product was redissolved in methylene chloride, mixed with distilled water in the separating funnel and the crystallization step repeated. The final product was dried in vacuo at 80°C for a minimum of 48 hours and then stored in a vacuum dessicator over calcium chloride.

Dimethylformamide (Fisher reagent grade) was allowed to stand over anhydrous barium oxide for 24 hours with occasional shaking. It was then distilled from the barium oxide under reduced pressure (trapped aspirator) through a 1 m Vigreux column (214). The freshly distilled solvent was always used immediately since

dimethylformamide decomposes to form dimethylamine on standing. Purification of acetonitrile has been described elsewhere (202). However, it was found that Caldeon HPLC grade acetonitrile (water content nominally 0.005%) after drying over Woelm neutral alumina (Super-grade I) gave excellent results and was used in the present work.

3.2.3. Procedure

In all experiments the supporting electrolyte used was tetra-*n*-butylammonium tetrafluoroborate at a concentration of 0.10 M. The counter electrode was a large piece of platinum wire and the reference electrode (see Figure 3) employed was Ag/Ag⁺ (0.01 M Ag⁺, 0.10 M TBAF, acetonitrile or dimethylformamide) dissolved in the same solvent as that for the experiment. In the case of dimethylformamide the reference solution was also always

prepared fresh for each experiment. The cell temperature was controlled by circulating water through the outer jacket from a temperature regulated bath controlled at $25.0 \pm 0.1^{\circ}\text{C}$. The cell setup is shown in Figure 3. The mercury head was set at either 57.0 cm or 40.0 cm from the tip of the electrode. The mercury mass flow rate in air at 57.0 cm was 1.29 mg/s and at 40.0 cm was 0.91 mg/s.

Calibration curves were set up for anthracene (An) and fluoranthene (Fa) in dimethylformamide and acetonitrile. This was also done for the alkali cations lithium (Li^+), sodium (Na^+), potassium (K^+) and rubidium (Rb^+) in dimethylformamide. However, in acetonitrile, only Li^+ and Na^+ were studied due to low solubilities of potassium and rubidium perchlorates in this solvent. The calibration curves were obtained by employing the method of standard addition. 25 ml of the background

solution (i.e. solvent containing only TBAF at 0.10 M) which had been pre-equilibrated at 25°C was pipetted into the polarographic cell. Portions of a stock solution (usually about 9-13 mM, 0.10 M TBAF) of the electroactive species of interest which also had been equilibrated at 25°C was then added to the cell using a micropipette. Solvent saturated argon was bubbled through the cell solution. An argon atmosphere was kept above the solution at all times. This deaeration procedure was used in all experiments.

To investigate the effect of alkali metal cations on the reduction of anthracene and fluoranthene, the standard addition method was again used. 25 ml of a solution containing 1.00 mM of the hydrocarbon (0.10 M TBAF) kept at 25°C was pipetted into the cell. After each polarographic run, a known volume of a stock solution of the alkali metal cation (10 mM, 0.10 M TBAF) which was also 1.00 mM in the hydrocarbon and which has been controlled

at 25°C was added to the cell with a micropipette.

For the anthracene:lithium and the anthracene:sodium systems in DMF, experiments were also performed where the metal cation concentration was kept constant and the hydrocarbon concentration varied. In the case of An:Li⁺, the Li⁺ concentration was fixed at 1.50 mM whereas for the An:Na⁺ system, the Na⁺ concentration was fixed at 2.00 mM. The procedure used in these instances was the same as that above, the only changes being that the additions involved the hydrocarbon and not the metal cations.

3.3 Results

The background solution containing only the solvent and supporting electrolyte was always obtained for a new batch of solvent or supporting electrolyte to check for purity. If the background breakdown occurred

more positive than -3.10V for ACN or -3.20 V (vs the respective reference electrodes) for DMF, the solvent was redistilled or the electrolyte recrystallized. Also, the current should be less than $1\text{ }\mu\text{A}$ at these potentials for the polarographic conditions used. Figure 4 shows typical background polarograms for the two solvents.

It was mentioned earlier in the procedure section that the mercury head used was either 57.0 cm or 40.0 cm . In all experiments in DMF the mercury height used was 57.0 cm . However, it was found that, especially in acetonitrile at high negative potentials, instability of the mercury due to low surface tension at the electrode/solution interface (66,67) gave rise to "missed drops." This problem was largely alleviated by lowering the height of mercury to increase the natural drop life of the dme. Therefore in some experiments with ACN, the mercury head was lowered to 40.0 cm .

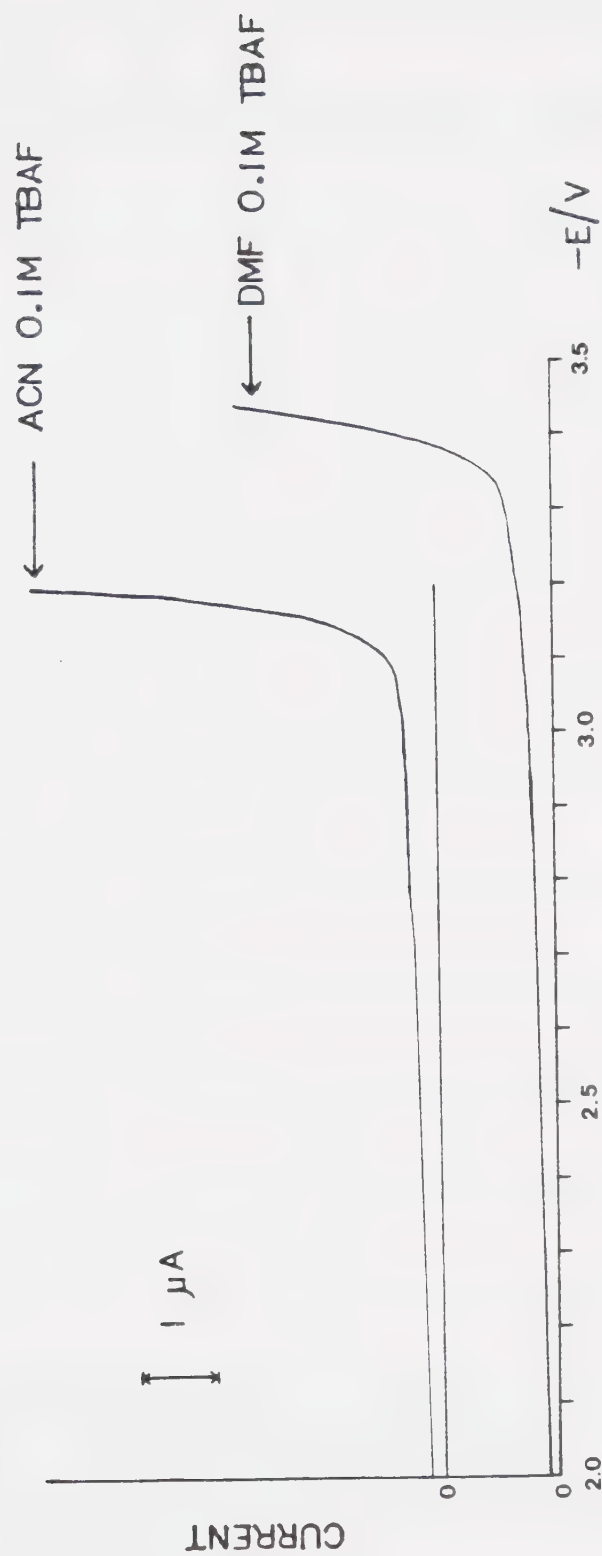


Figure 4. Polarographic background current.

The alkali metal cations showed single well-defined polarographic waves in both solvents. Logarithmic analysis revealed that, except for Li cation, all the cations gave slopes for plots of E vs $\log ((i(d)-i)/i)$ of 59 mV (± 2 mV) for a one-electron reversible wave in both solvents. However, in the case of Li^+ , slopes of 66 mV (± 2 mV) were obtained in both solvents, indicating quasi-reversible behavior. Some examples of plots of E vs $\log (i(d)-i)/i)$ are given in Figure 5a. In DMF, the E_h value for Li^+ was markedly more negative, by about 300 mV than the others. The others were closely grouped, with only about 30 mV separating them. The E_h value for Li^+ in DMF was 506 mV more negative than in ACN whereas for Na^+ , this value was only 304 mV. Again, in ACN, Li^+ has an E_h value negative of Na^+ , this time only by 104 mV compared to 308 mV in DMF. These E_h values are tabulated in Table 1.

Linear calibration plots were obtained for the alkali

Table 1. Polarographic Parameters **

Reaction	Eh/-V vs Ag/Ag+	DMF	
		i(d)/uA/mM	
		h=57.0 cm	h=40.0 cm*
An \rightleftharpoons An:	2.381	5.8	-
An: \rightleftharpoons An=	2.989	6.1	-
Fa \rightleftharpoons Fa:	2.193	5.4	-
Fa: \rightleftharpoons Fa=	2.819	5.7	-
Li+ \rightleftharpoons Li(Hg)	2.771	4.0	-
Na+ \rightleftharpoons Na(Hg)	2.463	4.9	-
K+ \rightleftharpoons K(Hg)	2.492	5.0	-
Rb+ \rightleftharpoons Rb(Hg)	2.481	5.2	-

*At high negative potentials, especially in ACN solutions, the instability of the mercury drop gave rise to "missed" drops. After normal precautions were made, it was found that increasing the natural drop time alleviated most of the problem.

**Continued next page.

Table 1 Continued

ACN			
Reaction	Eh/-V vs Ag/Ag+	i(d)/uA/mM	
		h=57.0 cm	h=40.0 cm*
An ⇌ An:	2.319	8.8	6.7
An: ⇌ An=	2.904	8.9	7.2
Fa ⇌ Fa:	2.130	-	6.3
Fa: ⇌ Fa=	2.689	-	6.6
Li+ ⇌ Li(Hg)	2.265	7.1	5.4
Na+ ⇌ Na(Hg)	2.159	7.8	5.9
K+ ⇌ K(Hg)	-	-	-
Rb+ ⇌ Rb(Hg)	-	-	-
		.	

cations for concentrations up to about 4.00 mM in both DMF and ACN. These plots are shown in Figures 5-7. It can be seen that in DMF, the slope of the Li^+ is significantly smaller than the others having a value of 4.0 $\mu\text{A}/\text{mM}$. In acetonitrile, where only Li^+ and Na^+ were studied, Li^+ has a smaller slope than Na^+ . The values of these slopes are given in Table 1. At concentrations about 3.00 mM, it was observed that polarograms for the alkali metal cations, especially Rb^+ , showed polarographic maxima. These maxima were not reproducible and did not always appear, even for the same conditions. They did not pose any serious problems in these investigations.

Anthracene and fluoranthene both gave two well-defined waves in ACN and DMF. The first wave in all cases showed one-electron reversible behavior, giving slopes of 59 mV ($\pm 2\text{mV}$) for E vs $\log ((i(d)-i)/i)$ plots. In DMF, both hydrocarbons gave second waves close to

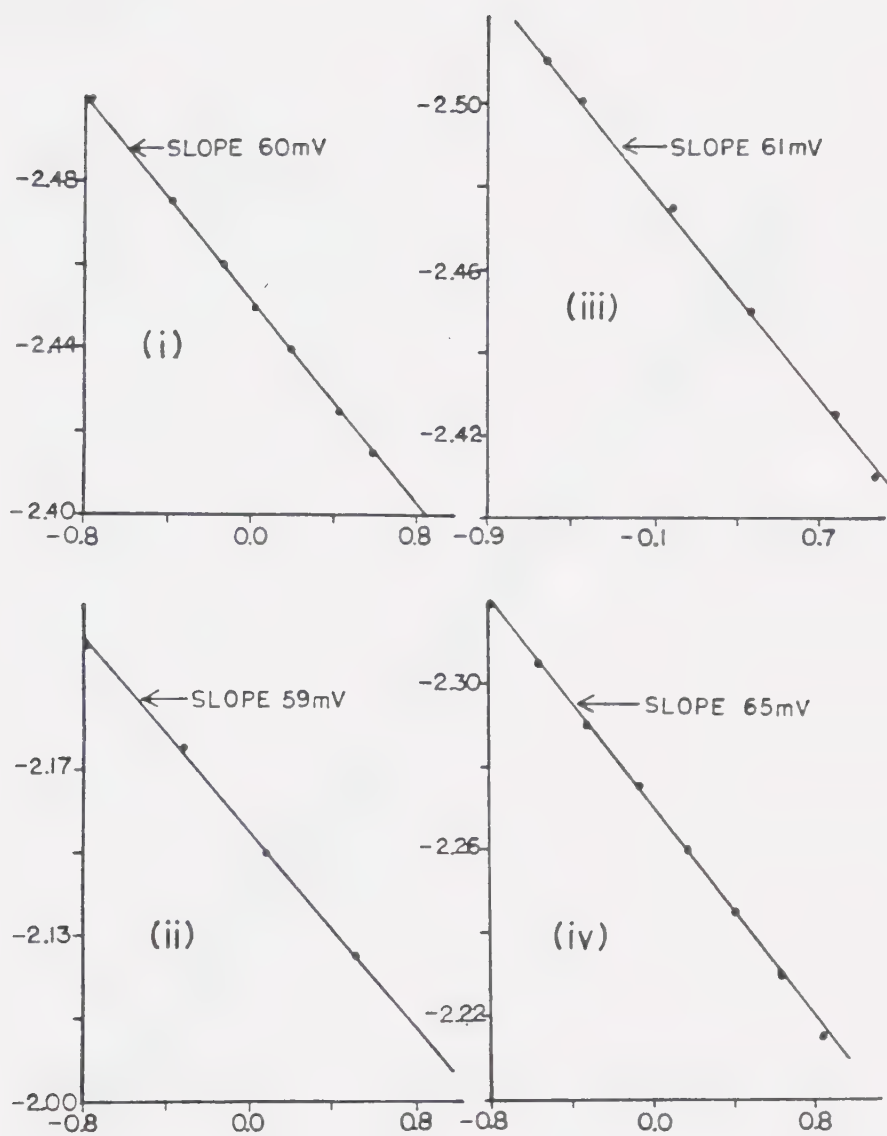


Figure 5a. Plots of E vs $\log \frac{i_d - i}{i}$

(i) Na^+ in DMF

(ii) Na^+ in ACN

(iii) Li^+ in DMF

(iv) Li^+ in ACN

Mercury column 57.0 cm. 25 C.

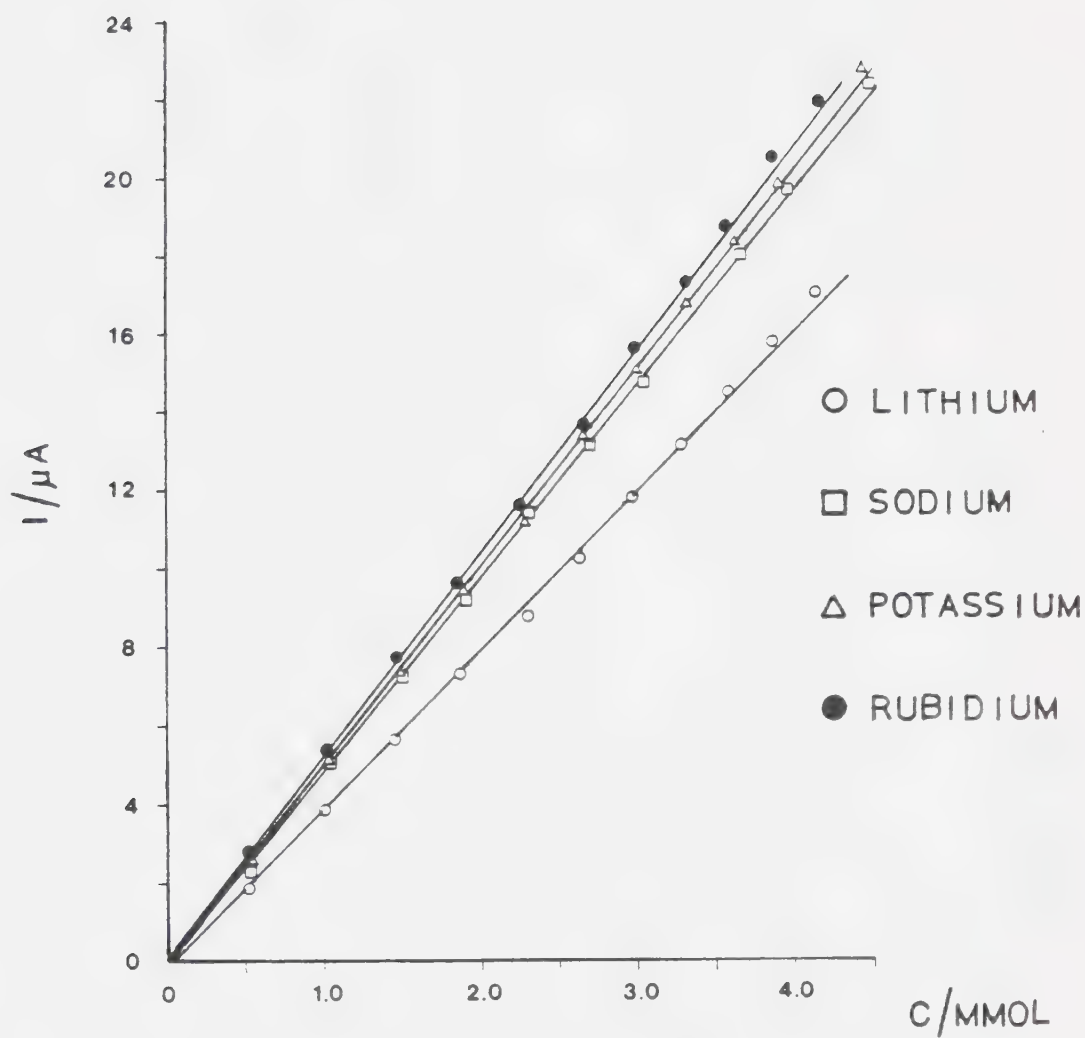


Figure 5. Alkali metal cations calibration plots in DMF at 25°C.
Mercury column 57.0 cm.

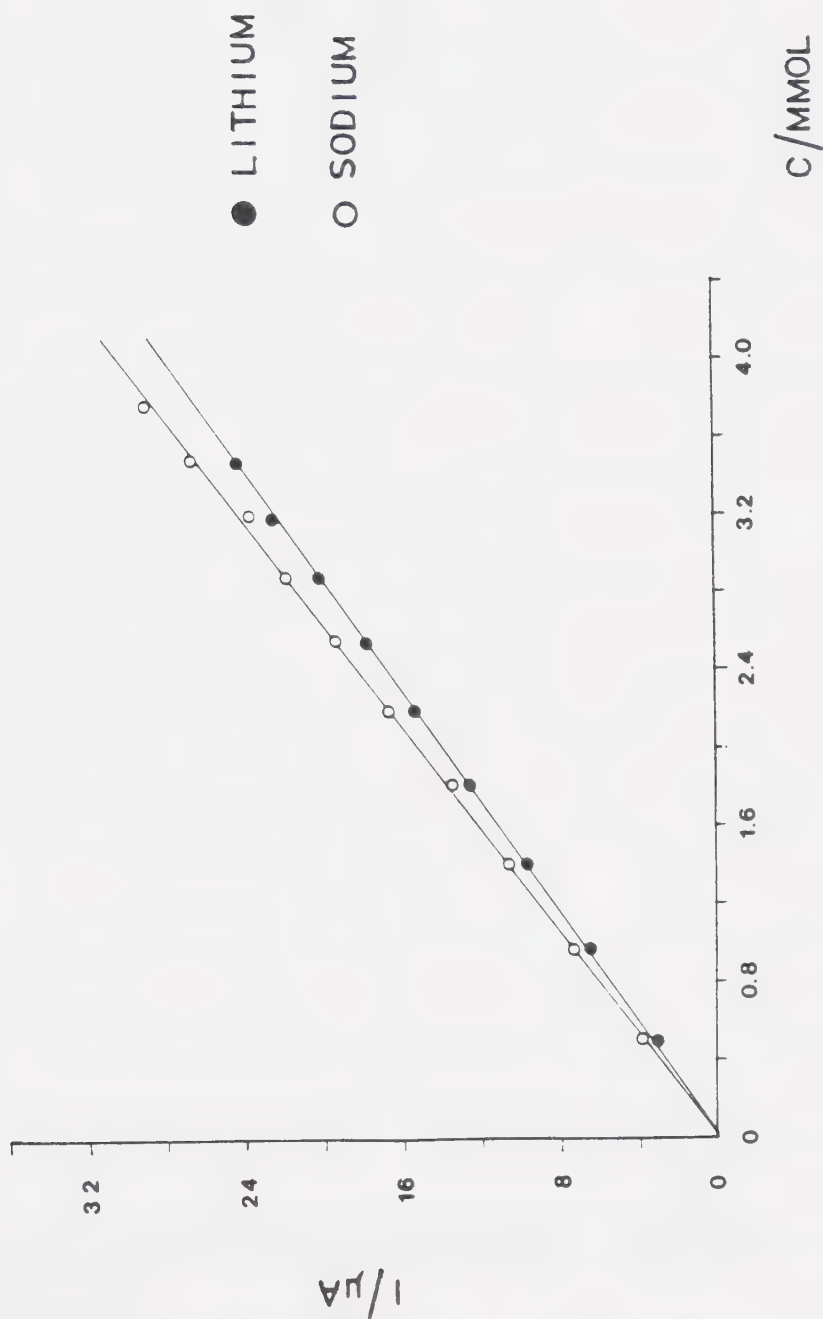


Figure 6. Alkali metal cation calibration plots in
ACN at 25°C.
Mercury column 57.0 cm.

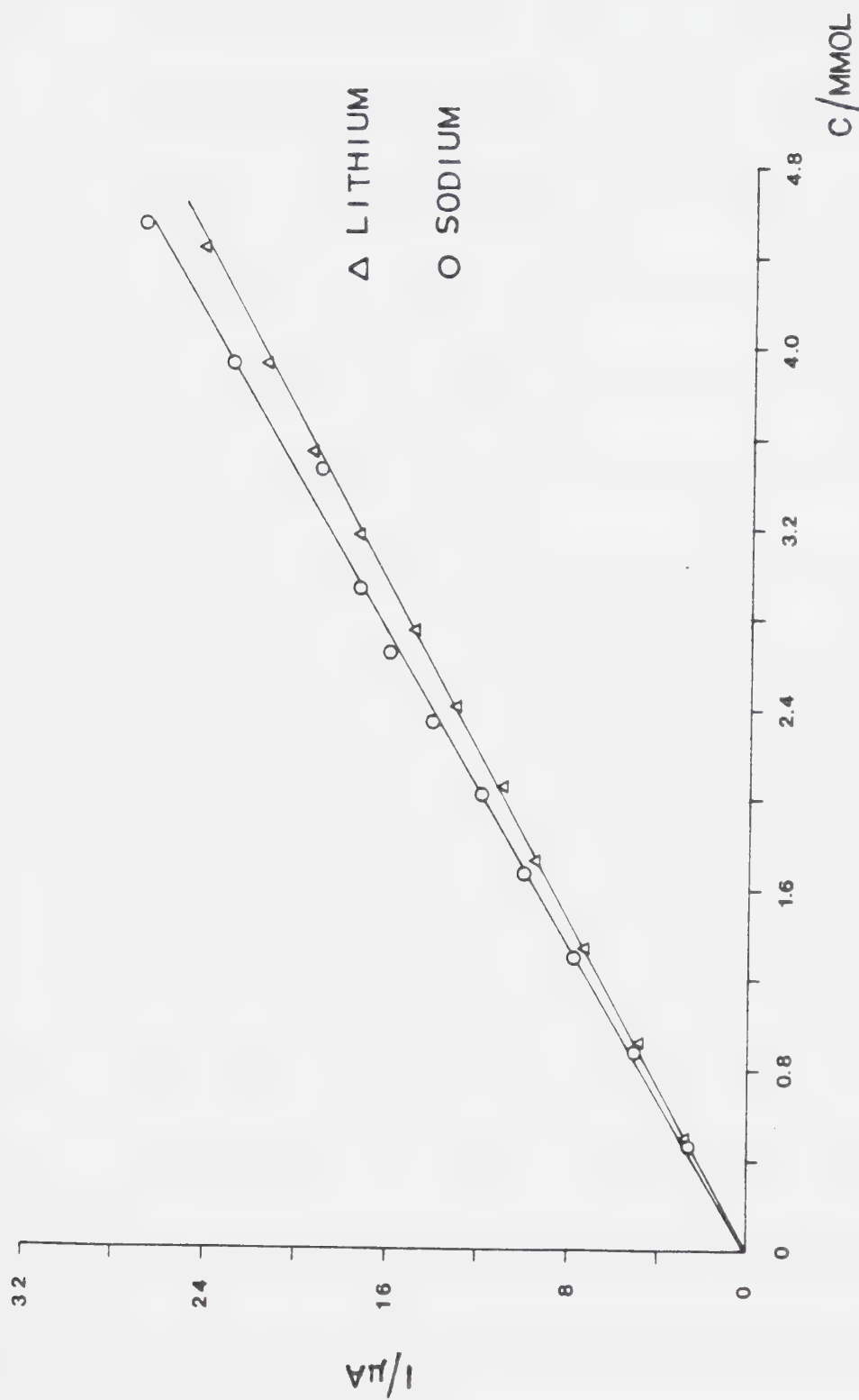


Figure 7. Alkali metal cation calibration plots in ACN at 25°C.
Mercury column 40.0 cm.

reversible behavior. For example, from these determinations, anthracene gave slopes of 63, 61 and 64 mV.

However, in ACN, these slopes have much larger values with an average of 76 mV for anthracene and 67 mV for fluoranthene. Cyclic voltammetric data showed that the first waves of anthracene and fluoranthene were reversible but the second waves did not show any oxidation current on the reverse scan for the second waves in both solvents.

The scan rate used was 100 mV/s. For both anthracene and fluoranthene, the first and second polarographic waves were approximately equal in height. Further, linear calibration curves of approximately equal slopes were obtained in both waves for concentrations up to about 4.00 mM. The values of these slopes are given in Table 1. It was observed that at concentrations greater than about 2.00 mM, both anthracene and fluoranthene gave polarographic maxima in their second wave. There were no

maxima in the first waves. The calibration plots are given in Figures 8 and 9. For the second waves, currents measured at the top of the maxima and also at the plateau are given. The half-wave potentials are listed in Table 1. These E_h 's are again more positive in acetonitrile than in dimethylformamide and further, fluoranthene is reduced more positive of anthracene by about 190 mV.

Figures 10-21 show polarograms of mixtures of An and Fa with alkali metal cations. In DMF, An:Li⁺ (Figure 10) exhibited three well-defined waves corresponding to anthracene reduction, Li⁺ reduction and the anthracene anion radical reduction respectively. On the other hand, An:Na⁺, An:K⁺ and An:Rb⁺ solutions exhibited only two waves (Figures 11-13) since the reduction of anthracene and the alkali metal cations were not polarographically resolved. With fluoranthene, the converse is true: Fa:Li⁺ solutions have two waves (Figure 14), this time

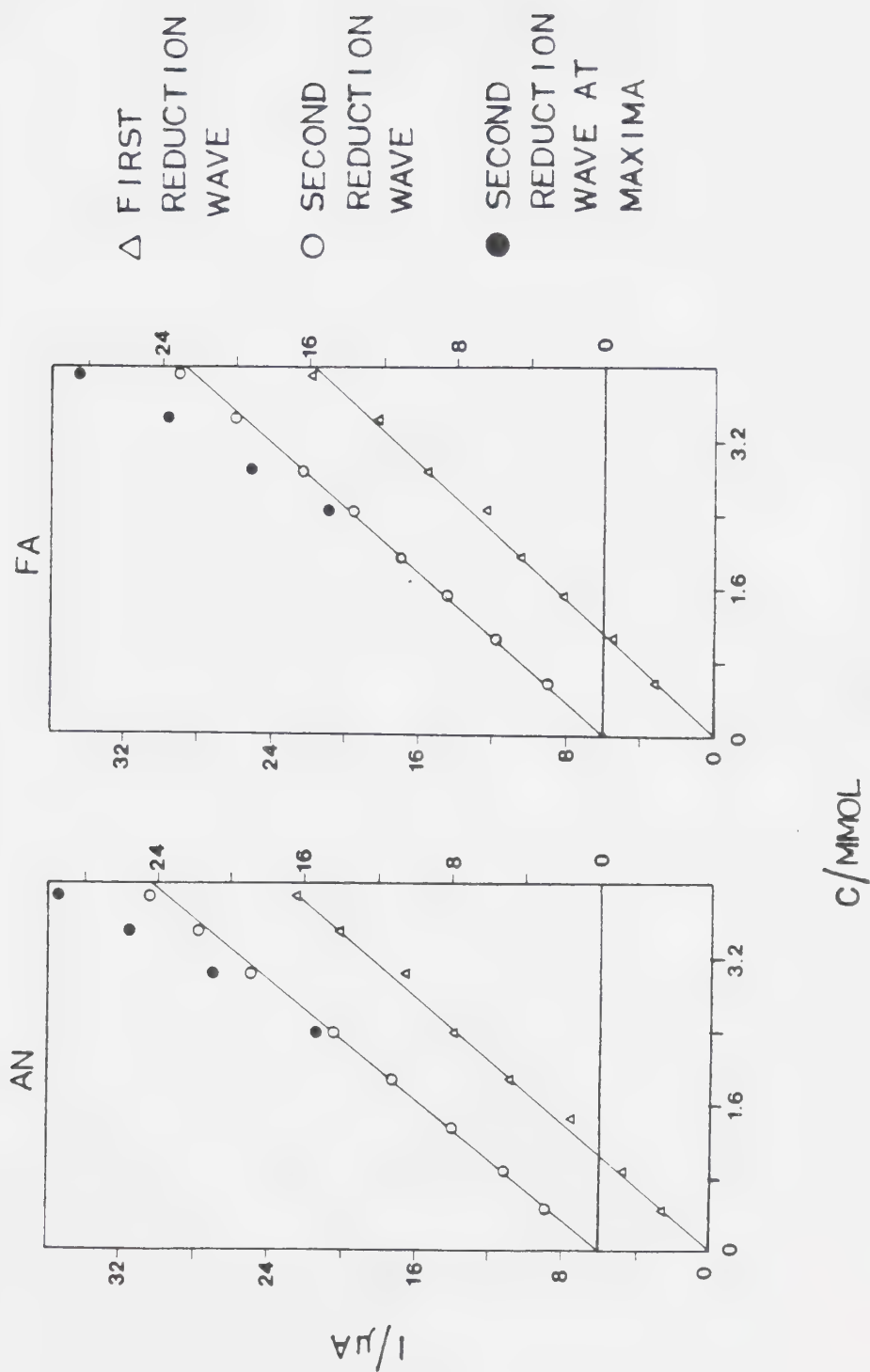


Figure 8. Anthracene and flouanthene calibration plots in DMF at 25°C.
Mercury column 57.0 cm.

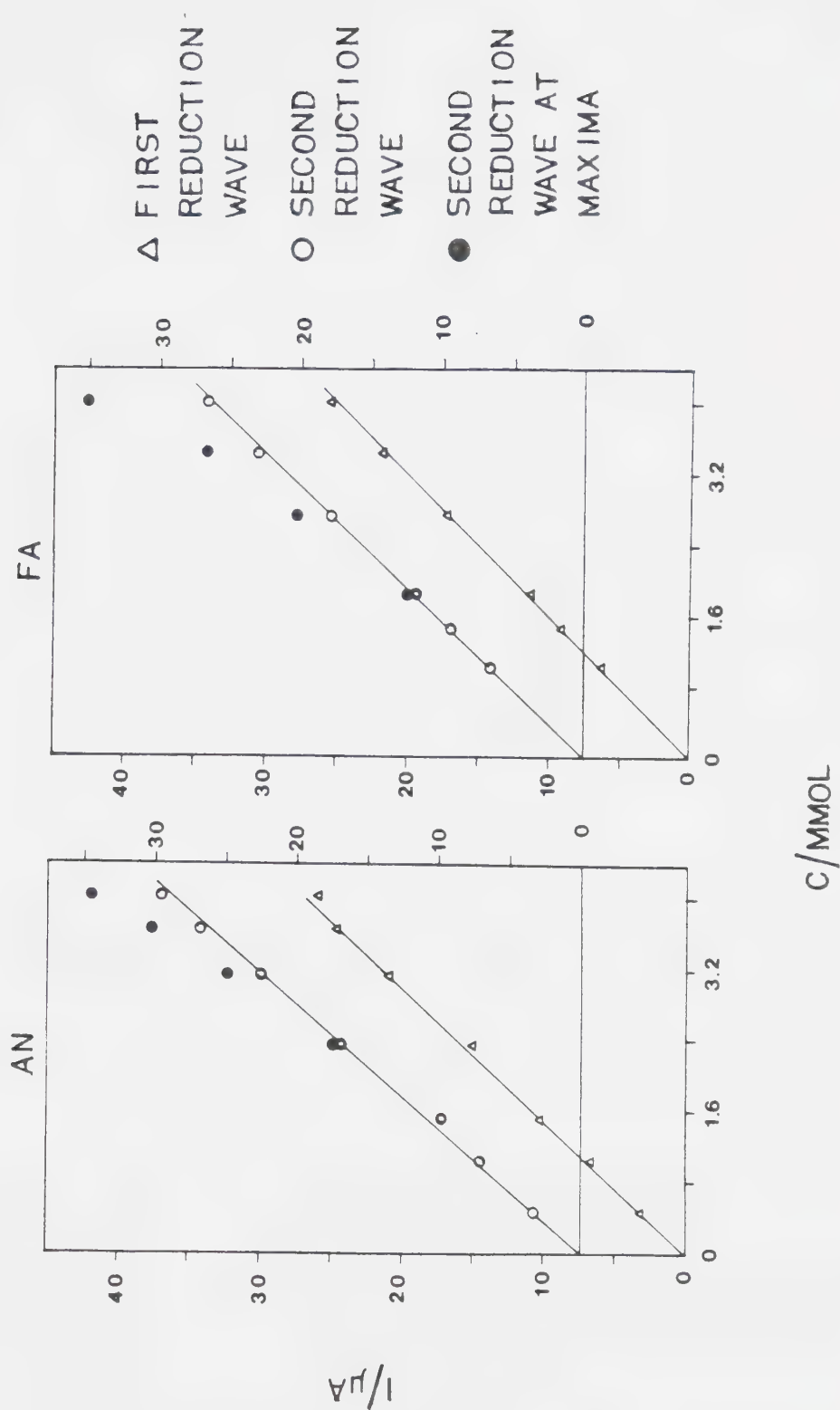


Figure 9. Anthracene and fluoranthene calibration plots in ACN at 25°C. Mercury column 40.0 cm.

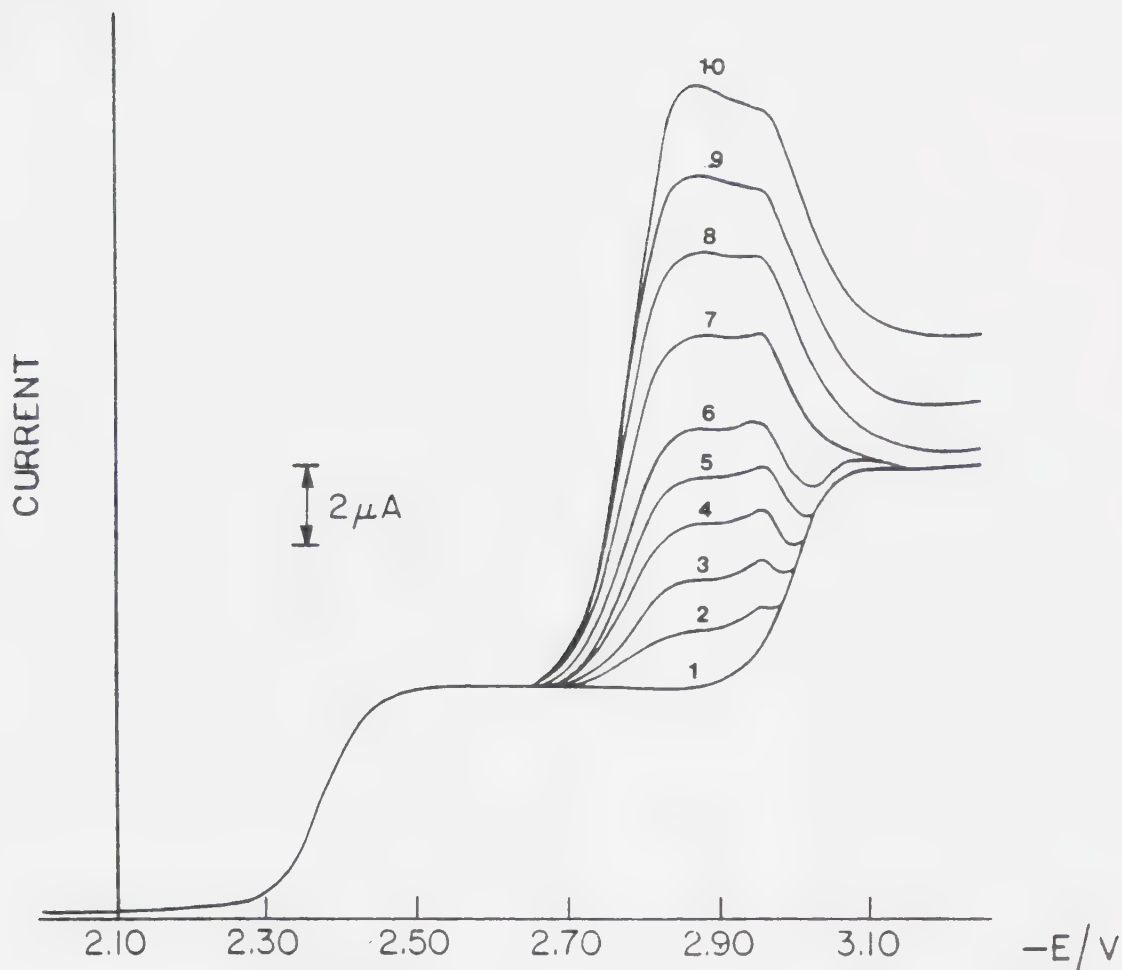


Figure 10. Polarograms of anthracene-lithium cation mixtures in DMF at 25°C. Anthracene concentration is fixed at 1.00 mM. Lithium cation concentrations are (in mM): (1) 0.00, (2) 0.38, (3) 0.73, (4) 1.06, (5) 1.36, (6) 1.65, (7) 2.16, (8) 2.54, (9) 3.02, (10) 3.47. Mercury column 57.0 cm.

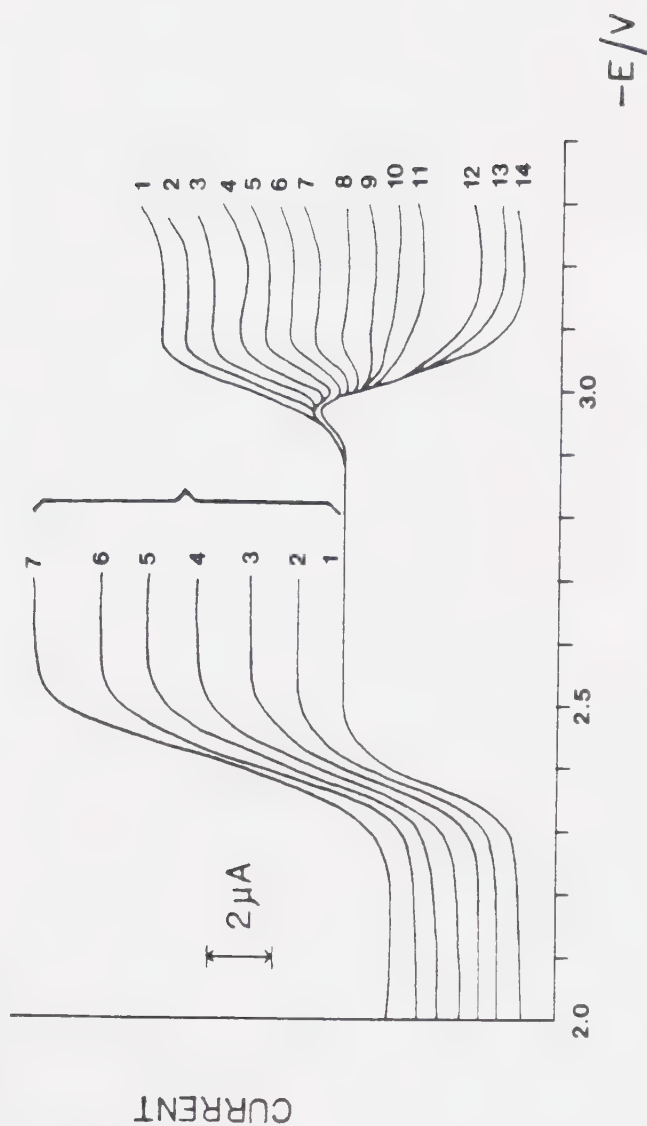


Figure 11. Polarograms of anthracene-sodium cation mixtures in DMF at 25°C.
 Anthracene concentration is fixed at 1.00 mM.
 Sodium cation concentrations are (in mM):
 (1) 0.00, (2) 0.21, (3) 0.41, (4) 0.60,
 (5) 0.79, (6) 0.97, (7) 1.14, (8) 1.31,
 (9) 1.47, (10) 1.62, (11) 1.78, (12) 2.32,
 (13) 3.04, (14) 3.82.
 Mercury column 57.0 cm.

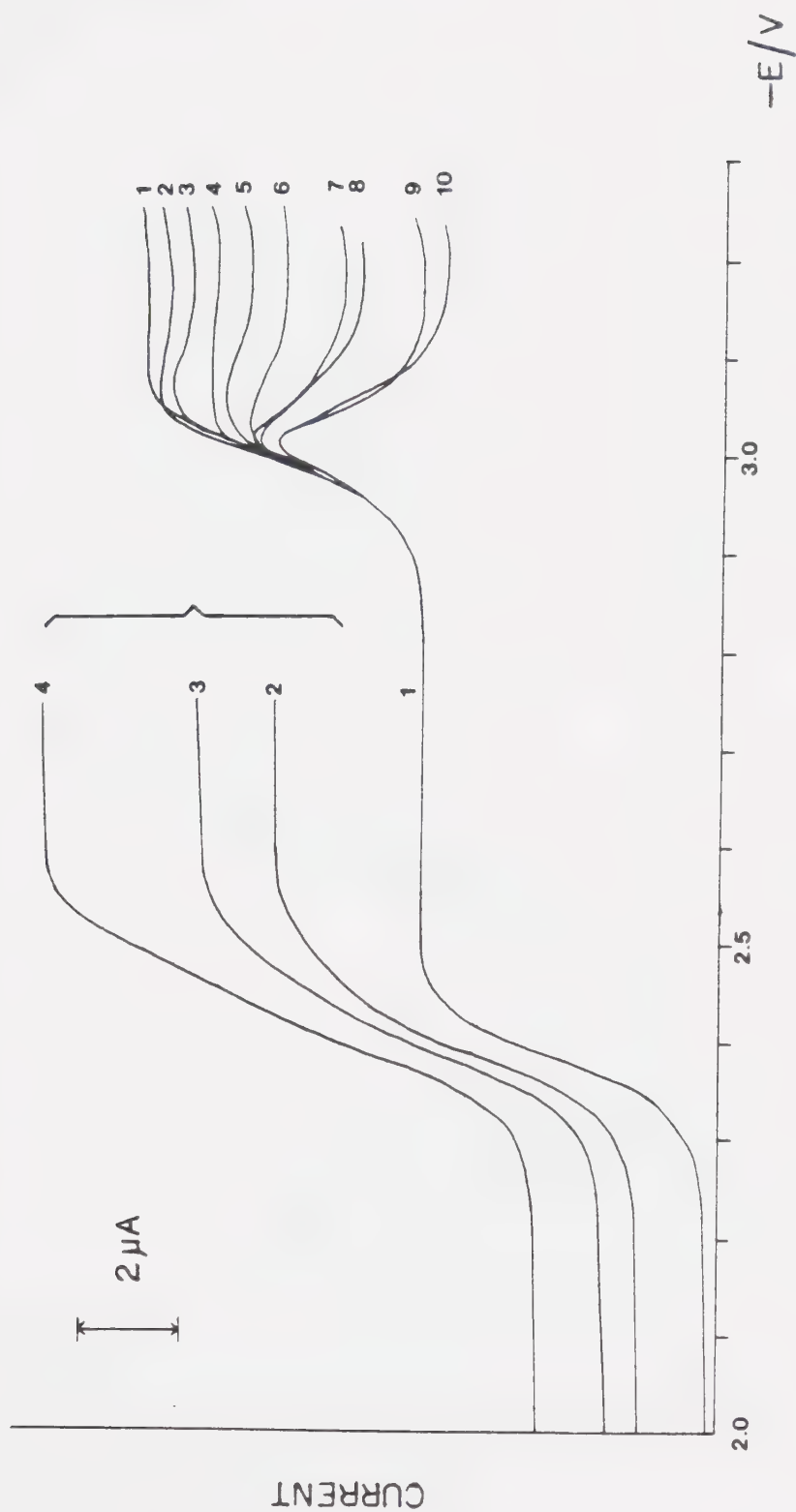


Figure 12. Polarograms of anthracene-potassium cation mixtures in DMF at 25°C. Anthracene concentration fixed at 1.00 mM. Potassium cation concentrations are (in mM): (1) 0.00, (2) 0.39, (3) 0.57, (4) 1.08, (5) 1.24, (6) 1.54, (7) 2.20, (8) 2.67, (9) 3.45, (10) 3.93.

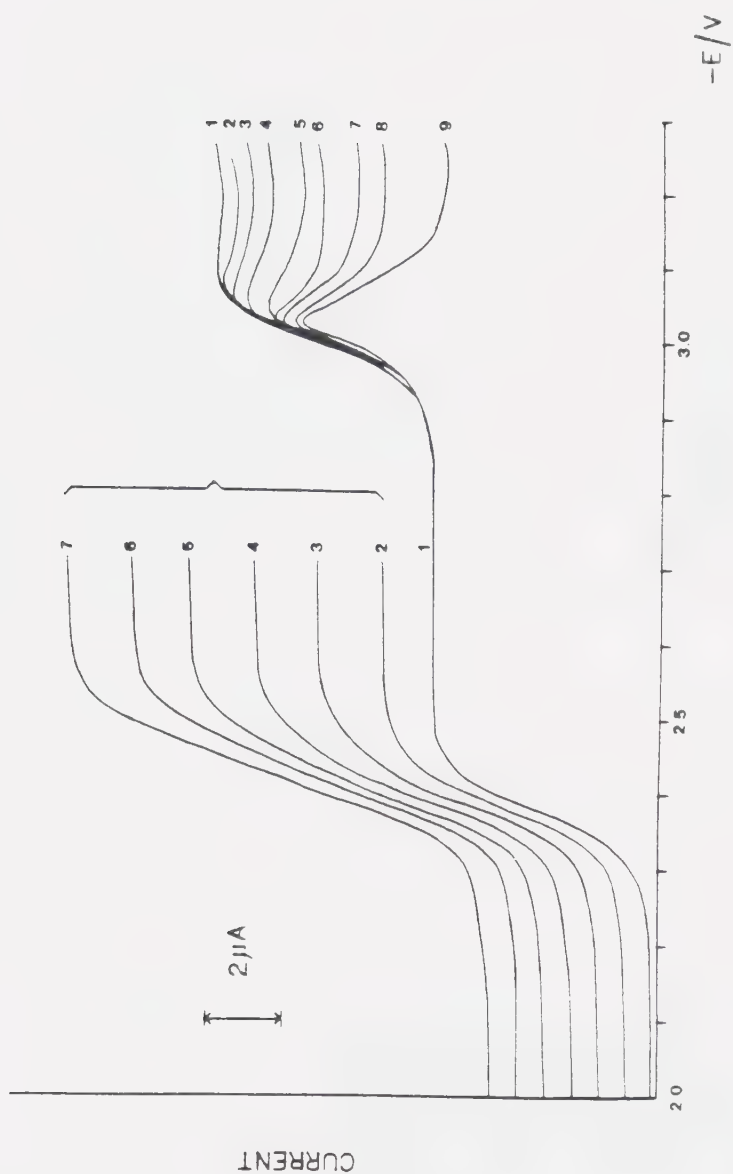


Figure 13. Polarograms of anthracene-rubidium cation mixtures in DMF at 25°C.
 Anthracene concentration fixed at 1.00 mM.
 Rubidium cation concentrations are (in mM):
 (1) 0.00, (2) 0.56, (3) 0.74, (4) 0.90,
 (5) 1.22, (6) 1.52, (7) 1.93, (8) 2.84,
 (9) 3.13.
 Mercury column 57.0 cm.

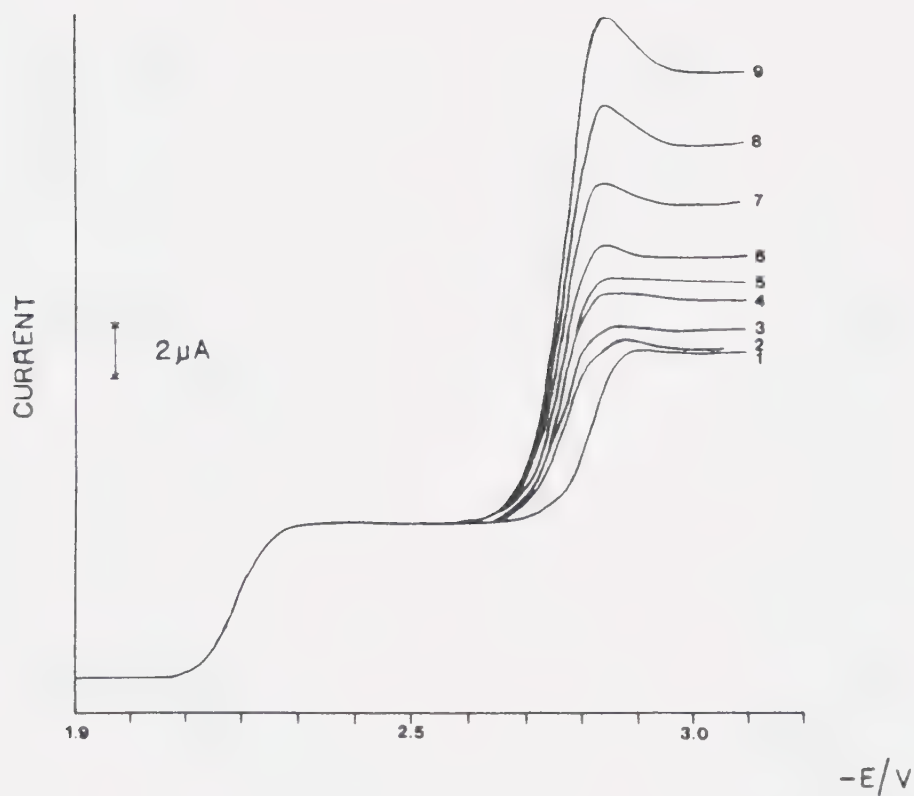


Figure 14. Polarograms of fluoranthene-lithium cation mixtures in DMF at $25^{\circ}C$. Fluoranthene concentration fixed at 1.00 mM. Lithium cation concentrations are (in mM): (1) 0.00, (2) 1.36, (3) 1.50, (4) 1.78, (5) 1.91, (6) 2.05, (7) 2.61, (8) 3.10, (9) 3.69. Mercury column 57.0 cm.

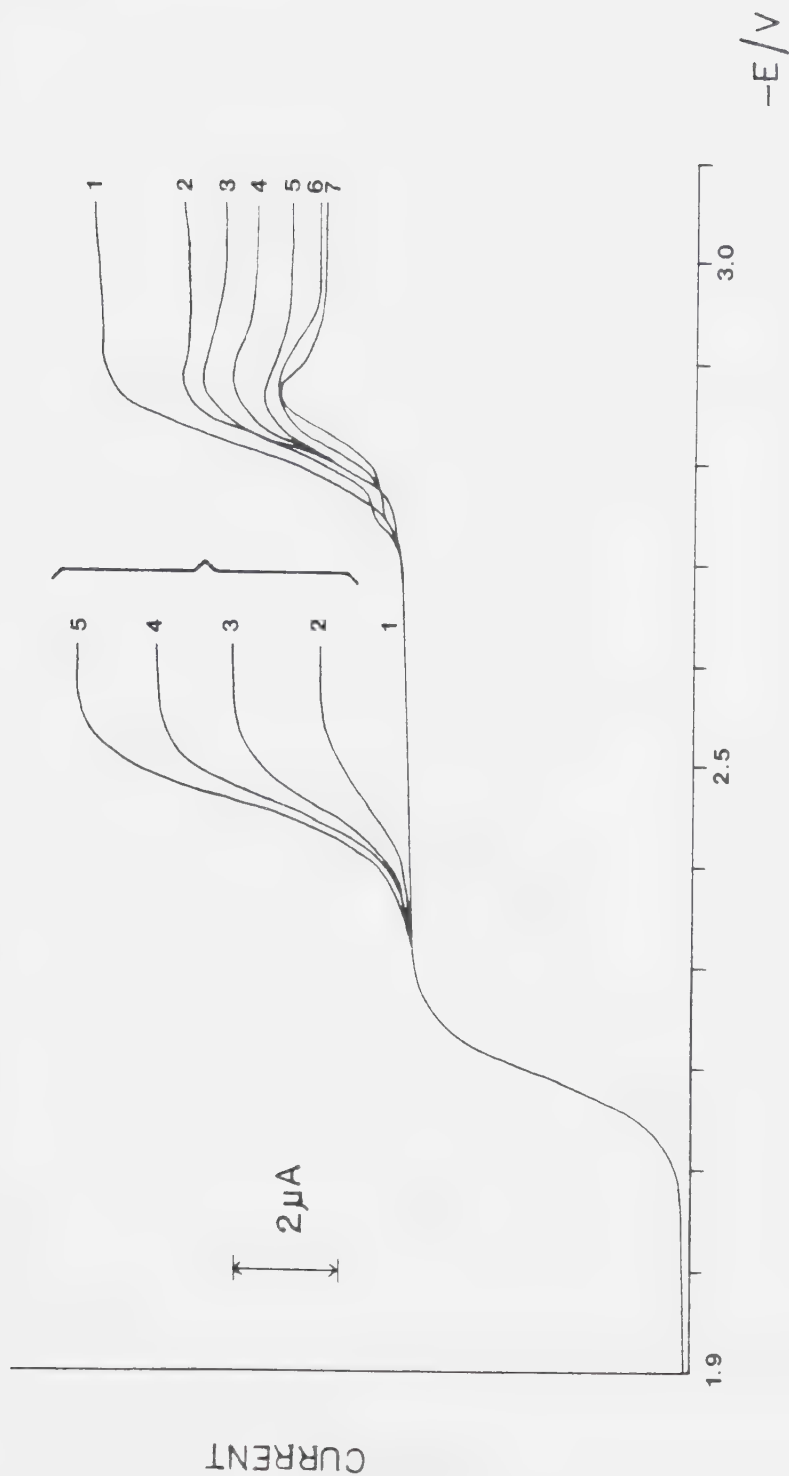


Figure 15. Polarograms of fluorethane-sodium cation mixtures in DMF at 25°C.
 Fluorethane concentration is fixed at 1.00 mM.
 Sodium cation concentrations are (in mM):
 (1) 0.00, (2) 0.38, (3) 0.73, (4) 1.06,
 (5) 1.37, (6) 2.17, (7) 4.14.
 Mercury column 57.0 cm.

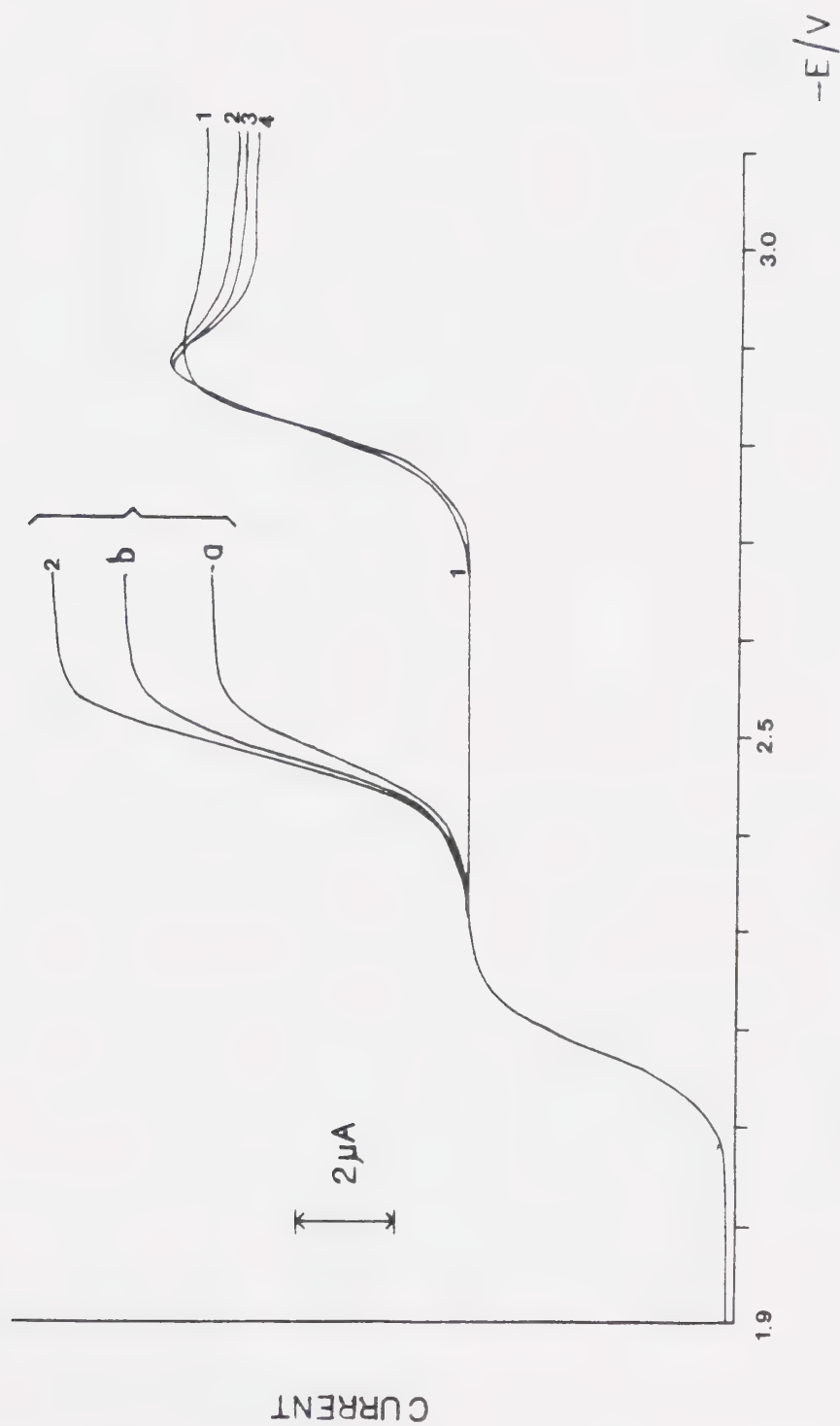


Figure 16. Polarograms of fluoranthene-potassium cation mixtures in DMF at 25°C.
 Fluoranthene concentration fixed at 1.00 mM.
 Sodium cation concentrations are (in mM):
 (1) 0.00, (a) 1.09, (b), 1.40, (2) 1.69,
 (3) 2.69, (4) 3.65.



Figure 17. Polarograms of fluoranthene-rubidium cation mixtures in DMF at 25°C. Fluoranthene concentration fixed at 1.00 mM. Rubidium cation concentrations are (in mM): (1) 0.00, (2) 0.39, (3) 1.40, (4) 1.70, (5) 3.97. Mercury column 57.0 cm.

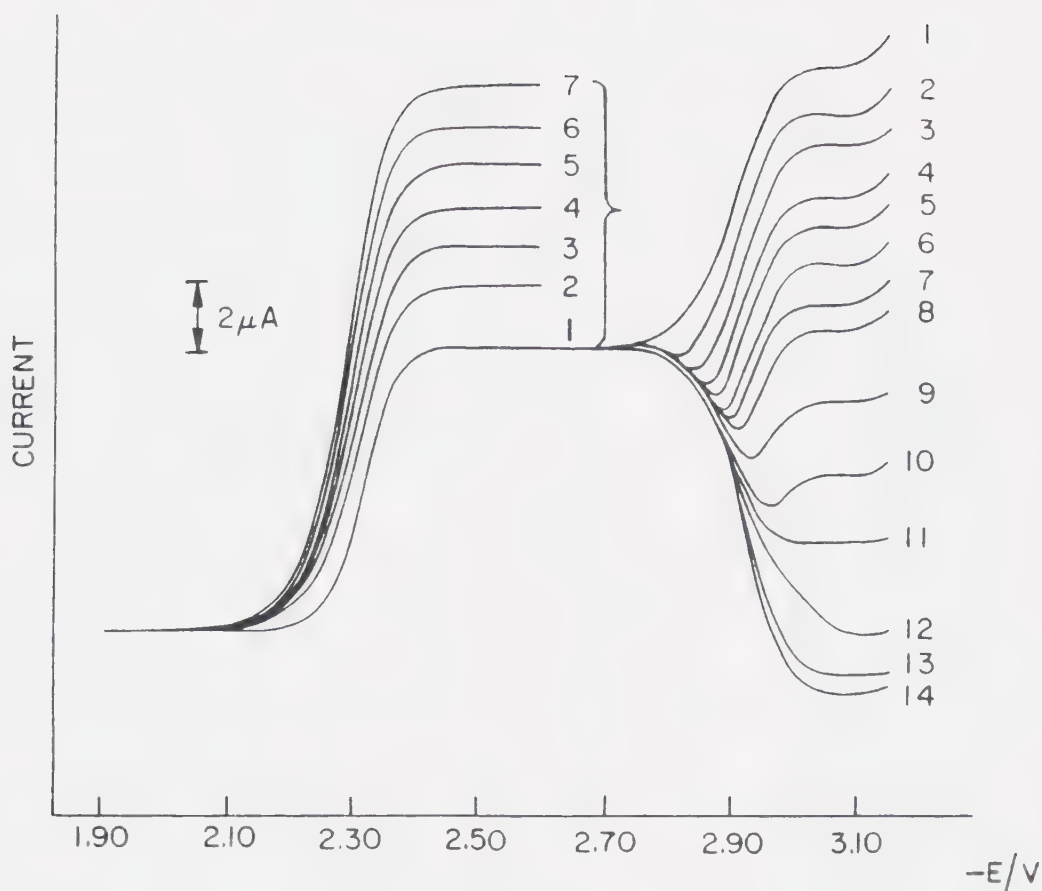


Figure 18. Polarograms of anthracene-lithium cation mixtures in ACN at 25°C. Anthracene concentration fixed at 1.00 mM. Lithium cation concentrations are (in mM): (1) 0.00, (2) 0.38, (3) 0.57, (4) 0.74, (5) 0.91, (6) 1.07, (7) 1.23, (8) 1.38, (9) 1.67, (10) 1.94, (11) 2.19, (12) 2.65, (13) 3.59, (14) 3.90. Mercury column 57.0 cm.

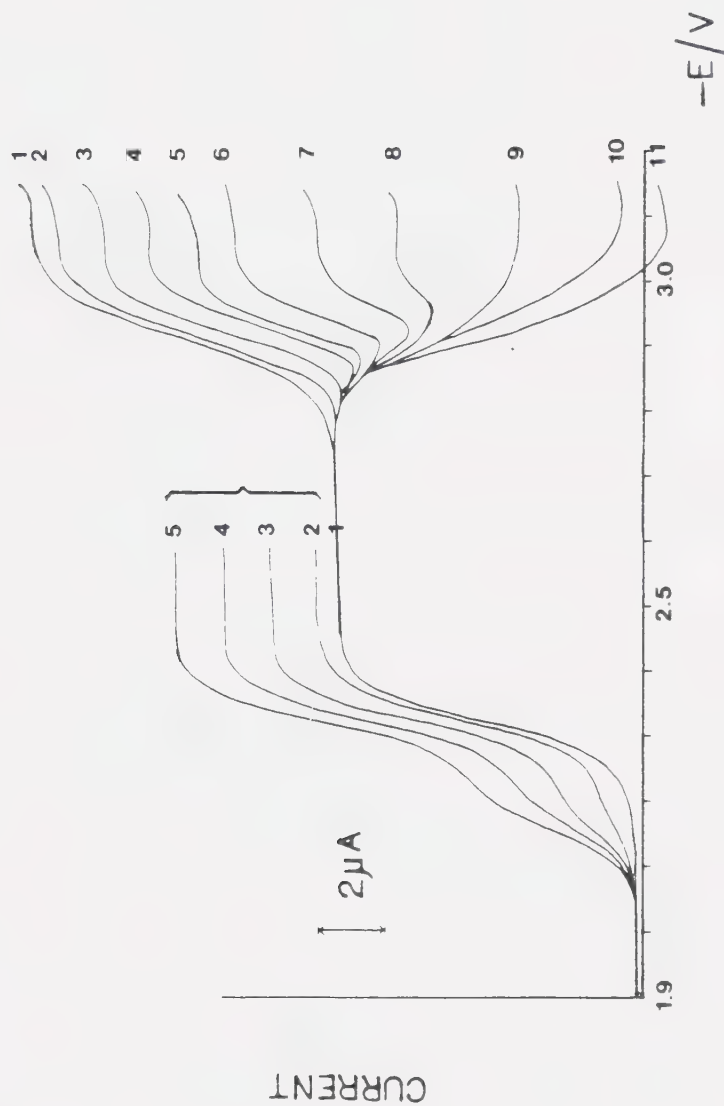


Figure 19. Polarograms of anthracene-sodium cation mixtures in ACN at 25°C.
 Anthracene concentration fixed at 1.00 mM.
 Sodium cation concentrations are (in mM):
 (1) 0.00, (2) 0.20, (3) 0.39, (4) 0.57,
 (5) 0.74, (6) 0.91, (7) 1.23, (8) 1.53,
 (9) 1.94, (10) 2.54, (11) 3.43.
 Mercury column 57.0 cm.

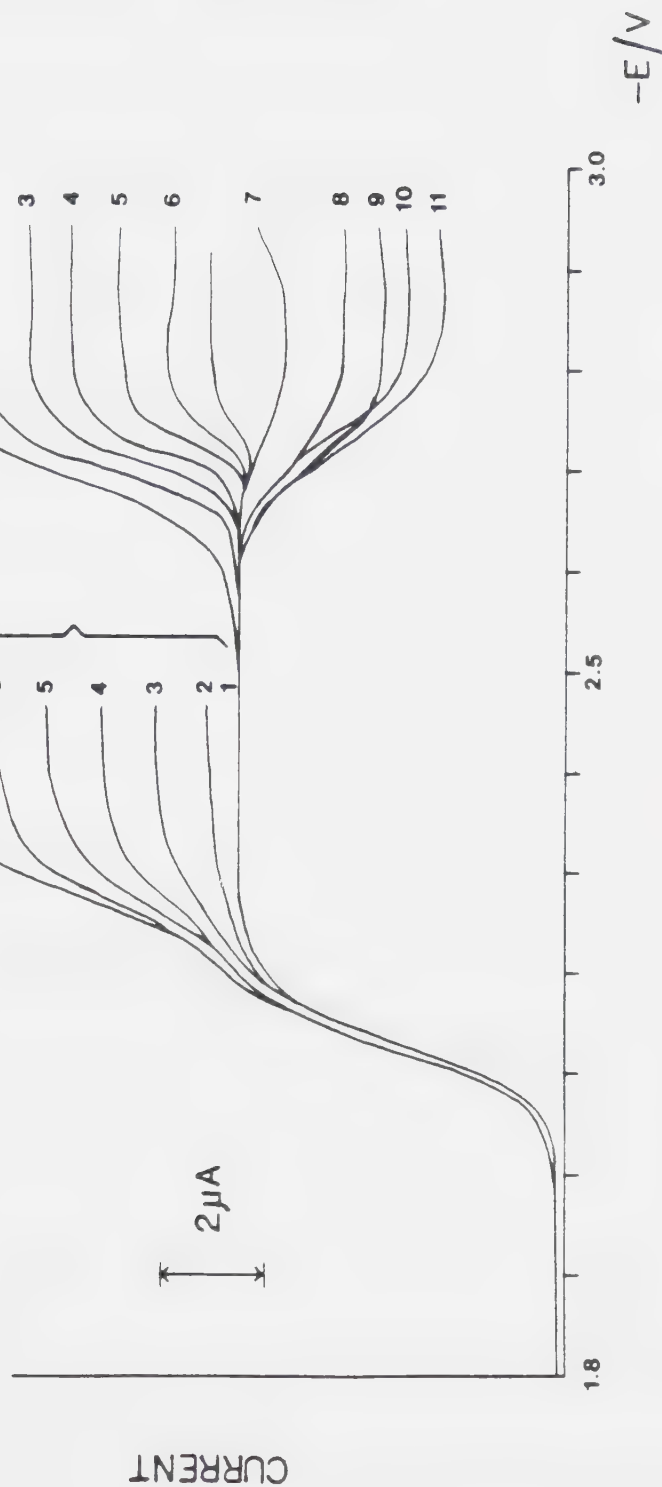


Figure 20. Polarograms of fluoranthene-lithium cation mixtures in ACN at 25°C.
 Fluoranthene concentration fixed at 1.00 mM.
 Lithium cation concentrations are (in mM):
 (1) 0.00, (2) 0.39, (3) 0.57, (4) 0.75,
 (5) 0.92, (6) 1.08, (7) 1.24, (8) 1.68,
 (9) 2.20, (10) 2.56, (11) 3.17.
 Mercury column 40.0 cm.

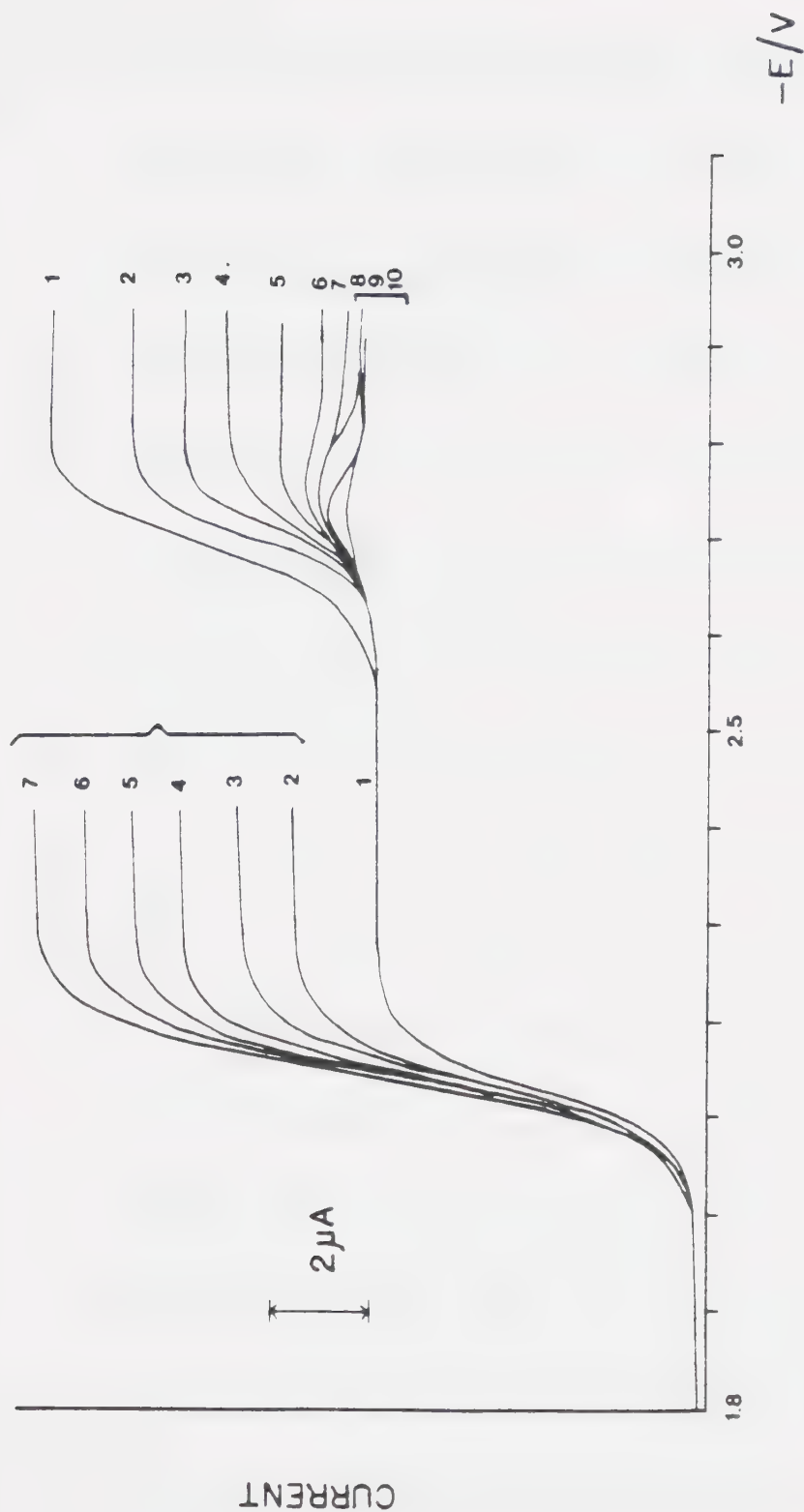


Figure 21. Polarograms of fluoranthene-sodium cation mixtures in ACN at 25°C.
 Fluoranthene concentrations fixed at 1.00 mM.
 Sodium cation concentrations are (in mM):
 (1) 0.00, (2) 0.39, (3) 0.58, (4) 0.75,
 (5) 0.93, (6) 1.09, (7) 1.25, (8) 1.41,
 (9) 1.97, (10) 2.47.
 Mercury column 40.0 cm.

since the Li^+ and the anion radical reduction occurred concomitantly. Fa solutions with the other three cations exhibited three resolved waves (Figure 15-17).

As mentioned earlier, in acetonitrile, studies were limited to Li^+ and Na^+ , since the solubilities of K^+ and Rb^+ were too low. In acetonitrile, in all cases, the hydrocarbon reduction wave and that of the metal cation were not resolved (Figures 18-21).

It is obvious from Figures 10-21, except in the case of Fa: Li^+ in DMF (Figure 14), that the addition of alkali metal cations caused the reduction wave of the anion radical of the hydrocarbon to dianion to decrease in height. The amount of height reduction is a function of metal cation concentration, generally increasing with increasing concentration. In some instances, especially where Li^+ and Na^+ were concerned, the current depressions were so severe that the polarographic wave was reversed (i.e. the

current as measured from the plateau of the previous wave is negative). It is believed these are the first reported examples of "inverted" diffusion controlled polarograms.

There have been examples of current depression in polarographic waves due to adsorption processes. Two such reports involved the polarographic reduction of hexamine cobalt (III) ion (215) and copper (II) acetate (216) in the presence of alkali metal cations in ACN. In the first case, a decrease in the current was noted as the hexamine cobalt (III) concentration was increased to 5 mM and above. The decrease was attributed to the formation of a film of cobaltous hydroxide at the mercury surface. The intensity of the current decrease was independent of depolarizer concentration. In the second case, a decrease in the amount of the second polarographic wave of copper (II) in the presence of Li^+ and Na^+ was attributed to the formation of an insoluble film of alkali metal acetate at the

electrode surface. Film formation was also implicated by the abnormal behavior of the current time transients in the potential region exhibiting the decrease.

However, in this work, the current-time transients exhibited normal diffusion control characteristics at potentials on the diffusion plateau and the current depression region. For example, in the case of anthracene in the presence of Li^+ in ACN, (Figure 22), current-time transients at the diffusion plateau (potentials -2.500 and -2.800 V) and at the current depression (potential -3.100 V) showed diffusion controlled behavior (Figure 22). Further, by employing reverse pulse polarography, (i.e. setting the initial potential at negative potentials (-3.200 V) and scanning to more positive potentials) on a solution of 1.00 mM anthracene and 3.83 mM Li^+ in DMF, it was noted that no desorption or film destruction currents were observed. What was observed was the interesting fact

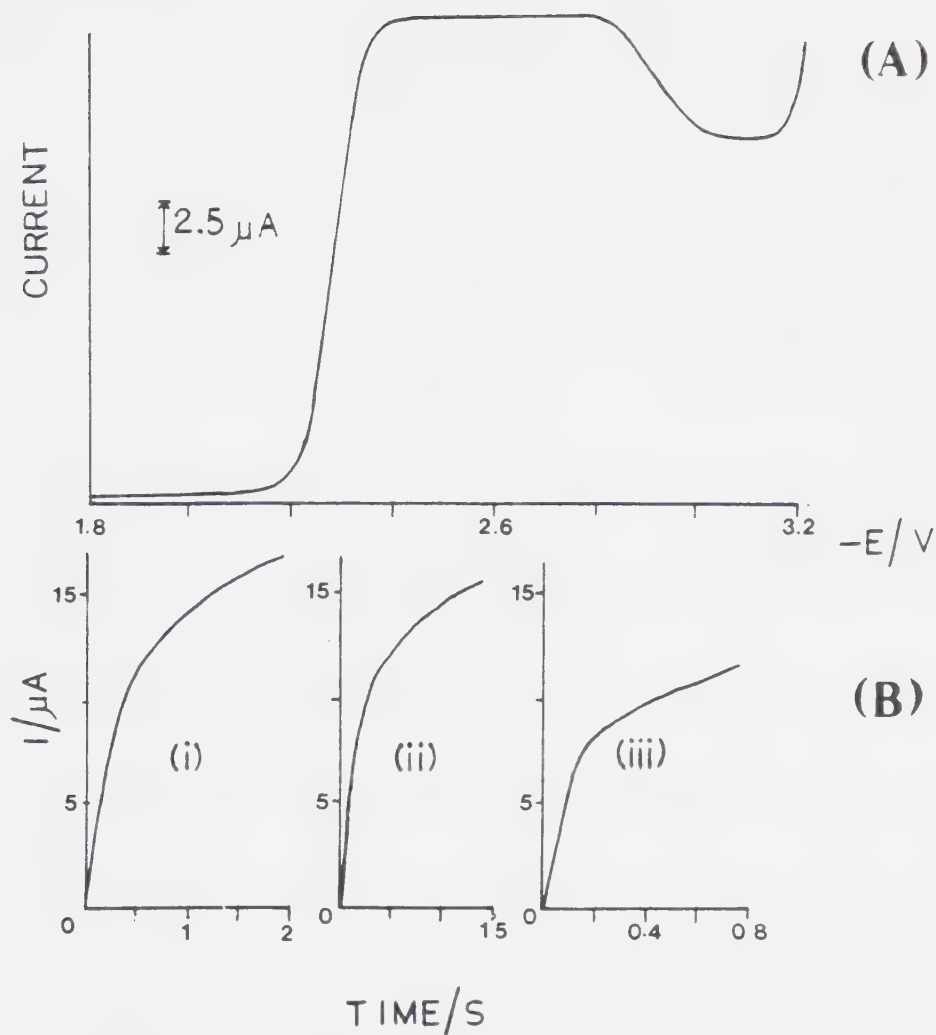


Figure 22. A. Polarogram of a solution mixture containing 1.00 mM anthracene and 3.53 mM lithium cation in ACN (0.10 M TBAF) at 25°C. B. Current-time transients for the same solution at 25°C: (i) -2.5 V, (ii) -2.8 V, (iii) -3.10 V. In both cases, the mercury column was 40.0 cm.

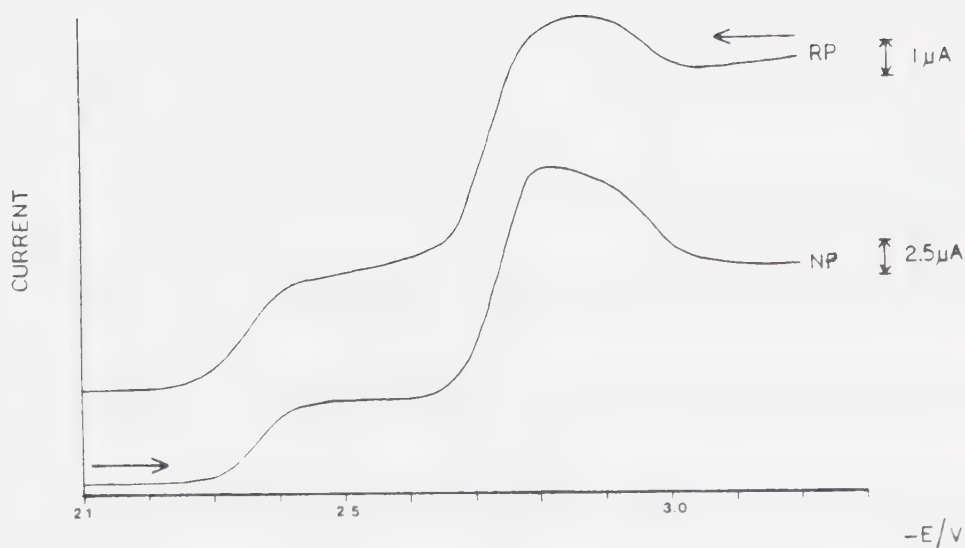


Figure 23. Normal pulse (NP) and reverse pulse (RP) polarograms of a solution mixture containing 1.00 mM anthracene and 3.83 mM lithium cation in DMF (0.10 M TBAF) at 25°C. For NP, the initial potential was -2.1 V whereas for RP the initial potential was -3.2 V. Mercury column was 57.0 cm.

that the current, in the potential region of the Li^+ reduction plateau just positive of the second reduction wave of anthracene, moved to cathodic values; thus a cathodic current was observed on a positive potential scan (Figure 23).

The case of $\text{Fa}:\text{Li}^+$ in DMF was a rather special one in that this was the only system studied where the reduction wave of Li^+ and the fluoranthene anion radical (Fa^\cdot) to the dianion (Fa^{2-}) were not resolved. Therefore only two reduction waves were observed for this system. Here there was no change in the height of the second wave with addition of Li^+ up to a concentration of 1.36 mM, after which the wave increased in height with further Li^+ addition (Figure 14). It was noted in Figures 10 and 11 ($\text{An}:\text{Li}^+$, Nat^+ systems) that a small peak appeared at the beginning of the wave corresponding to the reduction of the anion radical of anthracene (An^\cdot), prior to current depression. This peak

was absent in ACN (Figures 18-19).

The magnitude of the decrease of the anion radical reduction waves of the hydrocarbons in the presence of alkali cations is a direct measure of the strength of the interaction between metal cations and aromatic hydrocarbon dianions ($\text{Fa}^=$, $\text{An}^=$). To facilitate further discussions, the following notation will be used: in systems where there were three resolved waves ($\text{An}:\text{Li}^+$ in DMF, $\text{Fa}:\text{Na}^+$, K^+ , Rb^+ in DMF), the limiting currents due to the aromatic hydrocarbons reduction are denoted by i_1 and i_2 while that of the metal cations reduction by i_m ($m=\text{Li}^+$, Na^+ , K^+ , Rb^+). Where the reductions of the hydrocarbon and that cations were not well resolved ($\text{An}:\text{Na}^+$, K^+ , Rb^+ in DMF, $\text{An}:\text{Li}^+$, Na^+ , $\text{Fa}:\text{Li}^+$, Na^+ in ACN), the limiting currents are combined as $i_1 + i_m$. Finally, in the case of $\text{Fa}:\text{Li}^+$ in DMF, where only two waves were observed, the limiting current of the combined Li^+ reduction and $\text{An}^{\cdot-}$ reduction was denoted

by $i_m + i_2$. The plots of these currents for the various systems are given in Figures 24-26.

For the system An:Li^+ in DMF (Figures 24-25), the value of i_1 was unaffected by the addition of metal cations. The E_h values for these reduction waves of the hydrocarbons were also unchanged in the presence of cations. In addition, the i_m vs metal ion concentration plots are linear and the slopes (Figures 24-25) are virtually identical to those of the calibration curves for the metal cations (compare values in Figures 24-25 with those in Table 1). The E_h values for the metal cation waves were also unchanged. In all the other systems, where there were only two measurable limiting currents, linear plots of $i_1 + i_m$ vs metal cation concentrations were observed, the slopes of which agree well with the calibration curves for the metal cations. Further, the intercepts of these plots with the current

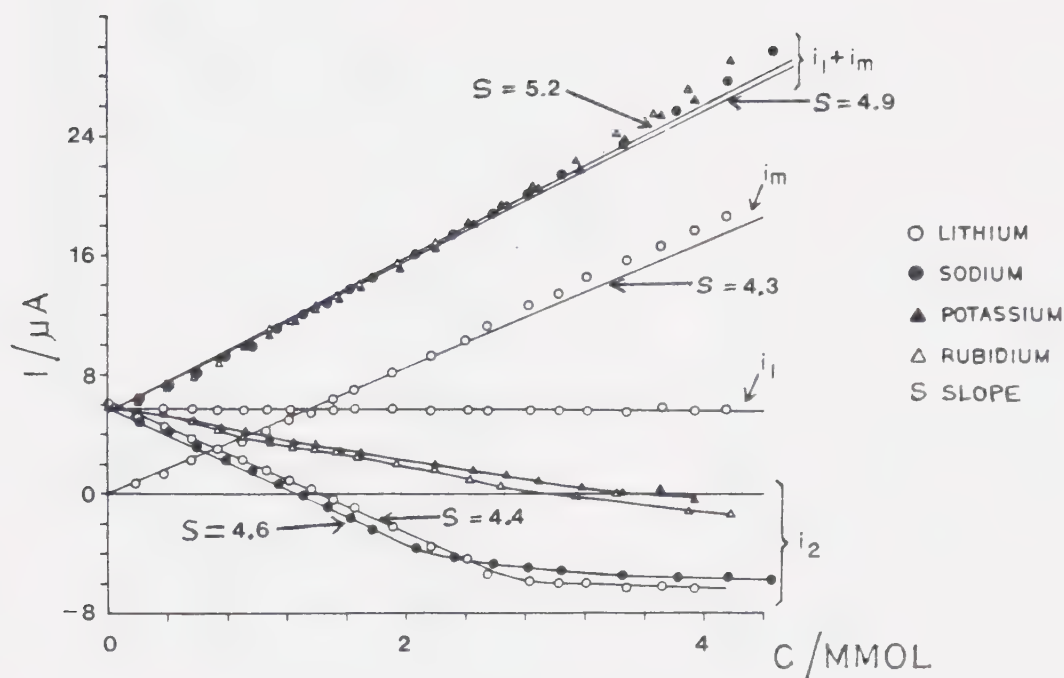


Figure 24. Plots of limiting currents versus concentration of metal cations for anthracene-metal cation mixtures in DMF at 25°C.

The anthracene concentration was fixed at 1.00 mM. Mercury column 57.0 cm.

i_1 : limiting current of anthracene reduction

i_2 : limiting current of anthracene anion radical reduction

i_m : limiting current of cation reduction

$i_1 + i_m$: combined limiting current of anthracene and cation reductions

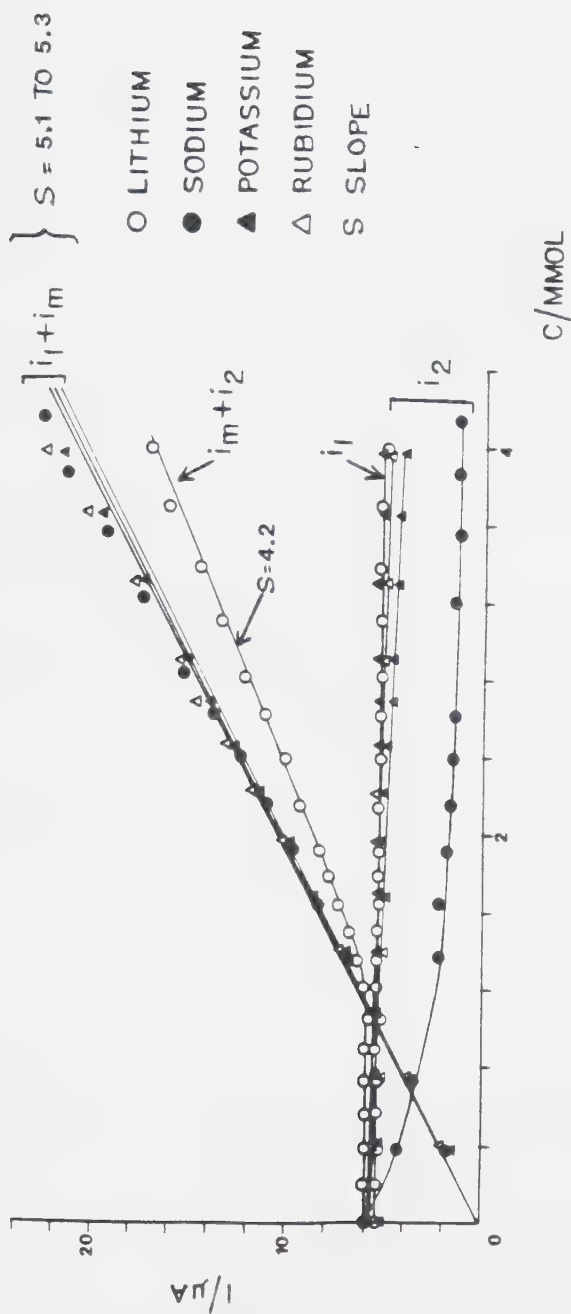


Figure 25. Plots of limiting currents versus concentration of metal cations for fluoranthene-metal cation mixtures in DMF at 25°C. The fluoranthene concentration was fixed at 1.00 mM. Mercury column 57.0 cm.
 i_1 : limiting current of fluoranthene reduction
 i_2 : limiting current of fluoranthene anion radical reduction
 $i_1 + i_m$: combined limiting current of fluoranthene and cation reductions
 $i_m + i_2$: combined limiting current of metal cation and fluoranthene anion radical reductions

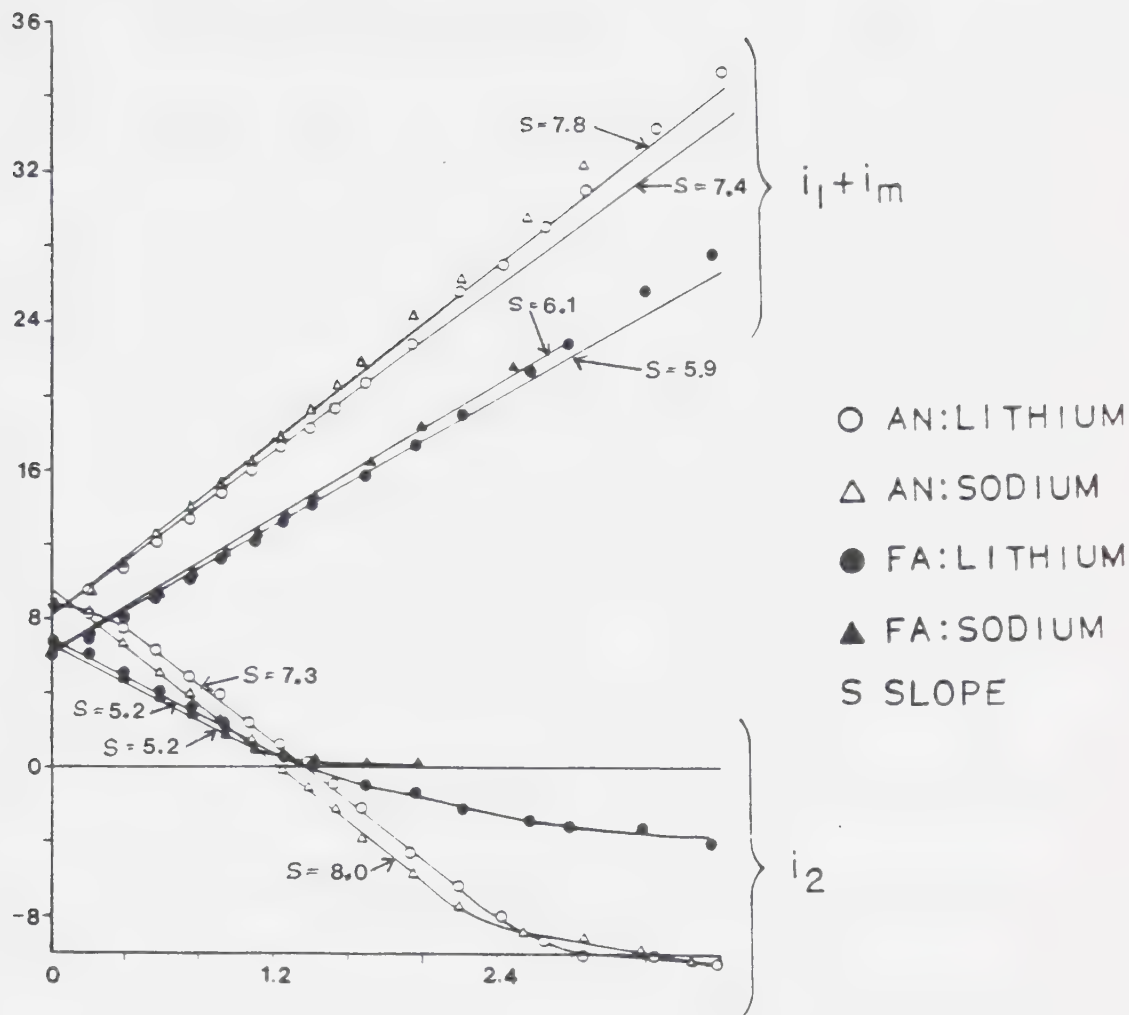


Figure 26. Plots of limiting currents versus concentration of metal cations for anthracene-metal cations and fluoranthene-metal cations mixtures in ACN at 25°C.

The anthracene and fluoranthene concentrations were fixed at 1.00 mM. The mercury column for anthracene-cation systems was 57.0 cm while that for the fluoranthene-cation systems was 40.0 cm.

$i_1 + i_m$ is the combined limiting current for the first reduction wave of the hydrocarbon and the cations. i_2 is the limiting current for the second reduction wave.

axis corresponded closely with the limiting current value for the reduction of the hydrocarbon for the particular system. However, it should be noted that both the i_m and i_1+i_m plots gave significant positive deviations of the points from linearity at the high end of the metal concentration range. In the special case of Fa:Li⁺ in DMF system i_1 was again independent of Li⁺ concentration and the E_h values remained constant (Figure 25). Further, $i_m + i_2$ remained constant at a value equal to that of i_2 for fluoranthene in the absence of Li⁺, for Li⁺ concentrations up to about 1.31 mM. At higher concentrations of Li⁺, $i_m + i_2$ increased and the slope of this increase was 4.2 $\mu\text{A}/\text{mM}$, close to that for Li⁺ calibration (4.0 $\mu\text{A}/\text{mM}$, see Table 1).

Figures 24-26 also showed that the value of i_2 is a function of the system considered. For the Fa:K⁺, Rb⁺ in DMF systems, only a slight decrease in the value of i_2 was

observed even at high metal cation concentrations. At the other extreme, large negative values of i_2 were observed for the An:Li⁺, Na⁺ systems in DMF and ACN, indicating strong interactions of the dianion with Li⁺ and Na⁺ to form species which were not reducible at these potentials. In these latter systems, the slopes of the i_2 vs metal concentration plots correspond closely to those of the i_m or $i_1 + i_m$ plots for the respective systems. These results are summarized in Table 2.

A clear way to graphically demonstrate the extent of interaction dianion with metal cation M⁺ is to plot the number of mmol of M⁺ reacted as a function of the concentration of M⁺. The ordinate for such a plot may be obtained for each polarogram (which represents one point) from the relation

Table 2. Summary of the behavior of the various limiting currents (μA)**

System	Number of waves	DMF	
		i_1 , i_m or $i_1 + i_m$	i_2
An:Li+	3	i_2 constant at 5.6. i_m linear with slope 4.3	i_2 decreasing to negative values with slope -4.4
An:Na+	2	$i_1 + i_m$ linear with slope 5.0	i_2 decreased to negative values with slope -4.6
An:K+	2	$i_1 + i_m$ linear with slope 5.2	slow decrease did not reach negative values
An:Rb+	2	$i_1 + i_m$ linear with slope 5.3	slow decrease did not reach negative values until high Rb+ concentration
Fa:Li+	2	i_1 constant at 5.4 * $i_m + i_2$ constant until [Li+]=1.20 mM, then linear increase with slope 4.2	---
Fa:Na+	3	i_1 constant at 5.4. i_m linear with slope 5.1	decreased but did not reach negative values
Fa:K+	3	i_1 constant at 5.4. i_m linear with slope 5.2	very small decrease
Fa:Rb+	3	i_1 constant at 5.4. i_m linear with slope 5.3	very small decrease

**Continued next page.

Table 2 Continued

ACN			
System	Number of waves	i1, im or i1 + im	i2
An:Li	2	i1 + im linear with slope 7.4	decreased to negative values with slope -7.3
An:Na+	2	i1 + im linear with slope 7.8	decrease to negative values with slope -8.0
An:K+	---	---	---
An:Rb+	---	---	---
Fa:Li+	2	i1 + im linear with slope 5.9	decreased to negative values with slope -5.2
Fa:Na+	2	i1 + im linear with slope 6.1	decreased to negative values with slope -5.2
Fa:K+	---	---	---
Fa:Rb+	---	---	---

$$\text{mmol } M^+ \text{ reacted} = [(i(\text{absence of interaction}) - i(\text{observed}))](M^+ \text{ mmol})/i_m \quad (3.2)$$

These results are shown in Figures 27-30. It is observed that in DMF that the plots for the An:Li⁺ and An:Na⁺ (Figure 27) have slopes of unity on the linear portions of the plots. For the An:Na⁺ system, the curve has a plateau at 2 mM metal ion concentration whereas An:Li⁺ has a plateau close to 3 mM Li⁺. In the An:K⁺ and An:Li⁺ solutions, the curves increase continuously up to the highest concentration used.

Figure 28 shows the results for the Fa:M⁺ solutions in DMF. Like the anthracene systems, the Fa:Li⁺ and Fa:Na⁺ plots show an initial slope of 1 but the Fa:Na⁺ curve levels at 1 mM whereas the Fa:Li⁺ curve levels at less than 2 mM. Similar trends are observed in the acetonitrile solutions of both An:M⁺ and Fa:M⁺ (Figure 29



Figure 27. Plot of the amount of metal cation reacted versus cation concentration for the anthracene-metal cation system in DMF at 25°C. The concentration of anthracene is fixed at 1.00 mM. Mercury column 57.0 cm.

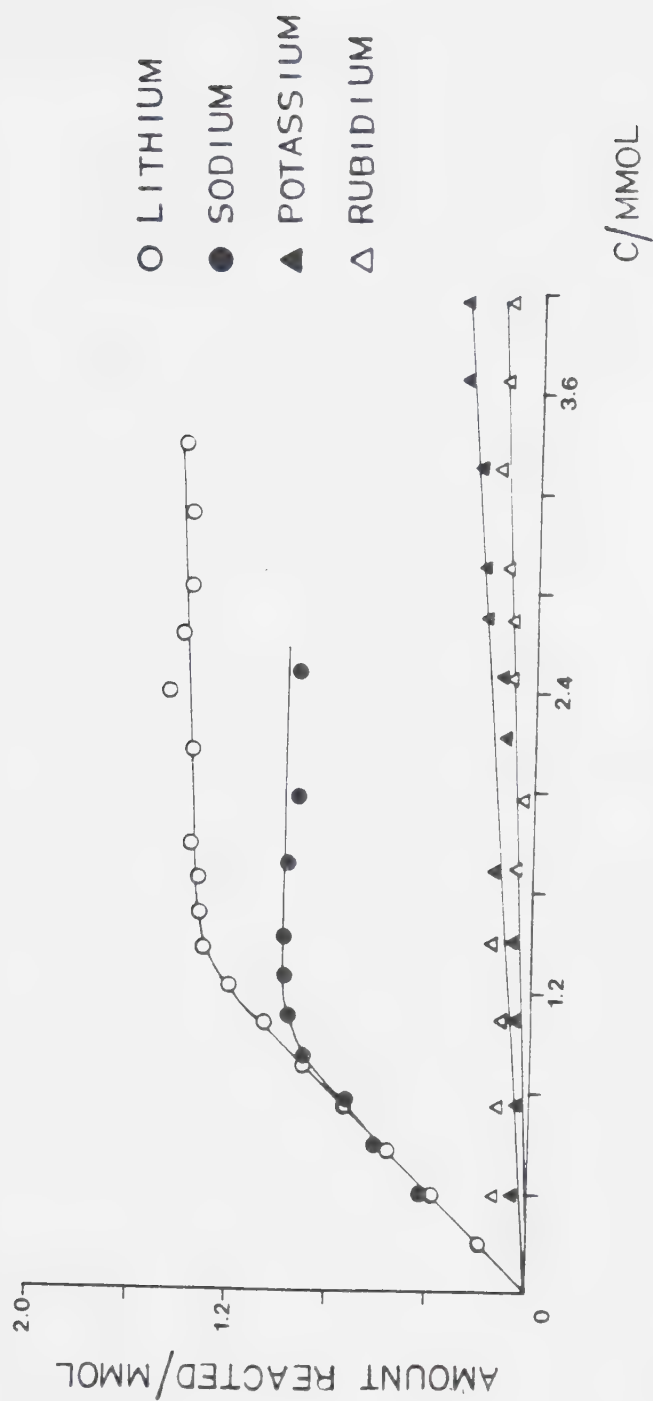


Figure 28. Plot of the amount of metal cation reacted versus cation concentration for the fluorene-metall cation system in DMF at 25°C.
The concentration of fluorene is fixed at 1.00 mM.
Mercury column 57.0 cm.

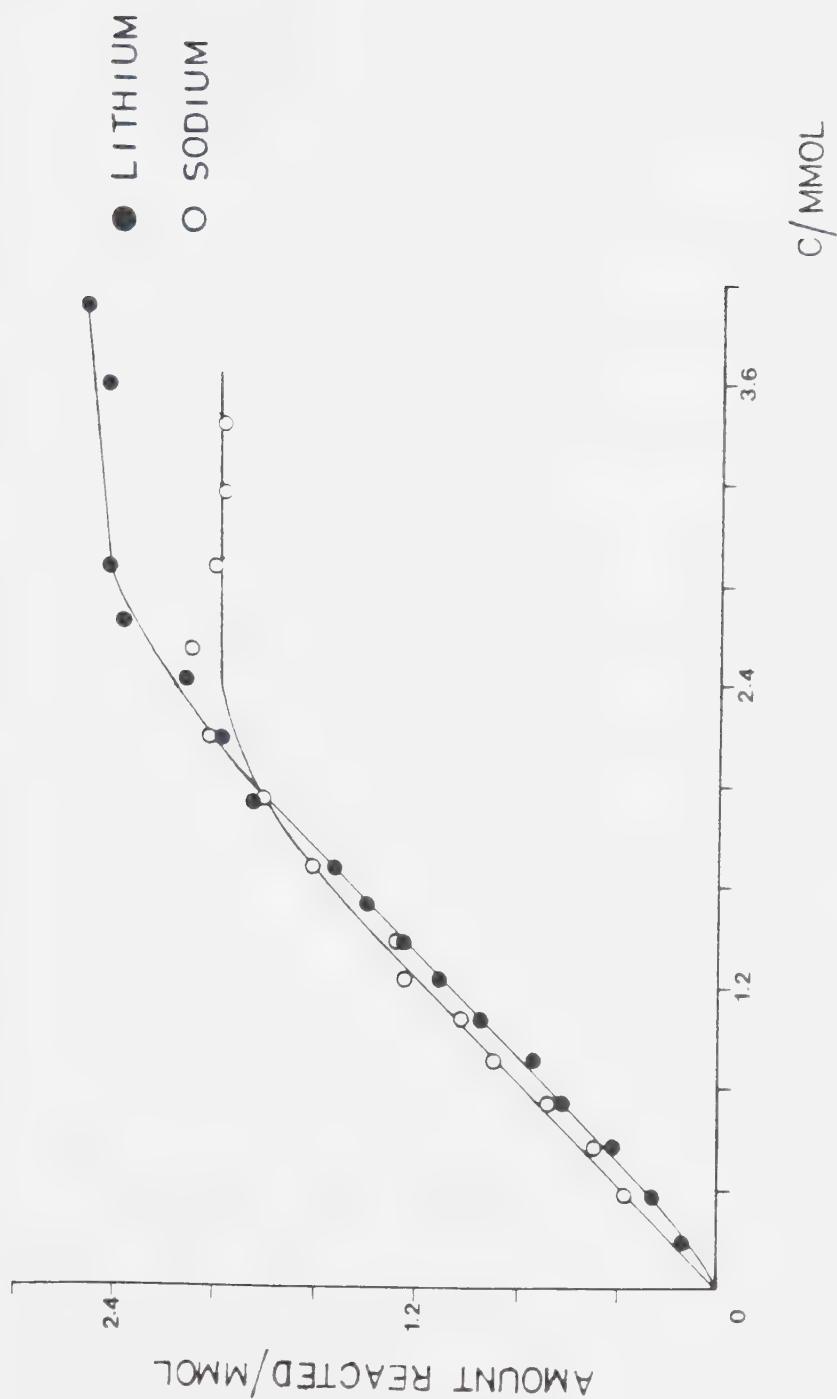


Figure 29. Plot of the amount of metal cation reacted versus cation concentration for the anthracene-metal cation system in ACN at 25°C. The concentration of anthracene is fixed at 1.00 mM. Mercury column 57.0 cm.



Figure 30. Plot of the amount of metal cation reacted versus cation concentration for the fluoranthene-metal cation system in ACN at 25°C.
 The concentration of fluoranthene is fixed at 1.00 mM.
 Mercury column 40.0 cm.

and 30).

Experiments were also carried out where the hydrocarbon concentration was varied while that of the cation remained fixed. This was done as a further check to ensure that the current depression observed was indeed due to the interaction between the metal cation and the dianion. If this was so, a similar behavior should be observed by performing the experiments in reverse, i.e. varying the concentrations of the hydrocarbon. Figure 31 shows the result of the experiment where the Li^+ concentration was kept fixed at 1.50 mM and the anthracene concentration was varied in DMF. As can be seen, at low concentrations of An, i_2 was negative but this was increased linearly with increased An concentration. The slope of this increase was approximately equal to that for i_1 . Here, the Li^+ reduction wave (i_m) remained constant in height. Figure 31 also shows the plot of mmol Li^+ reacted vs An concen-

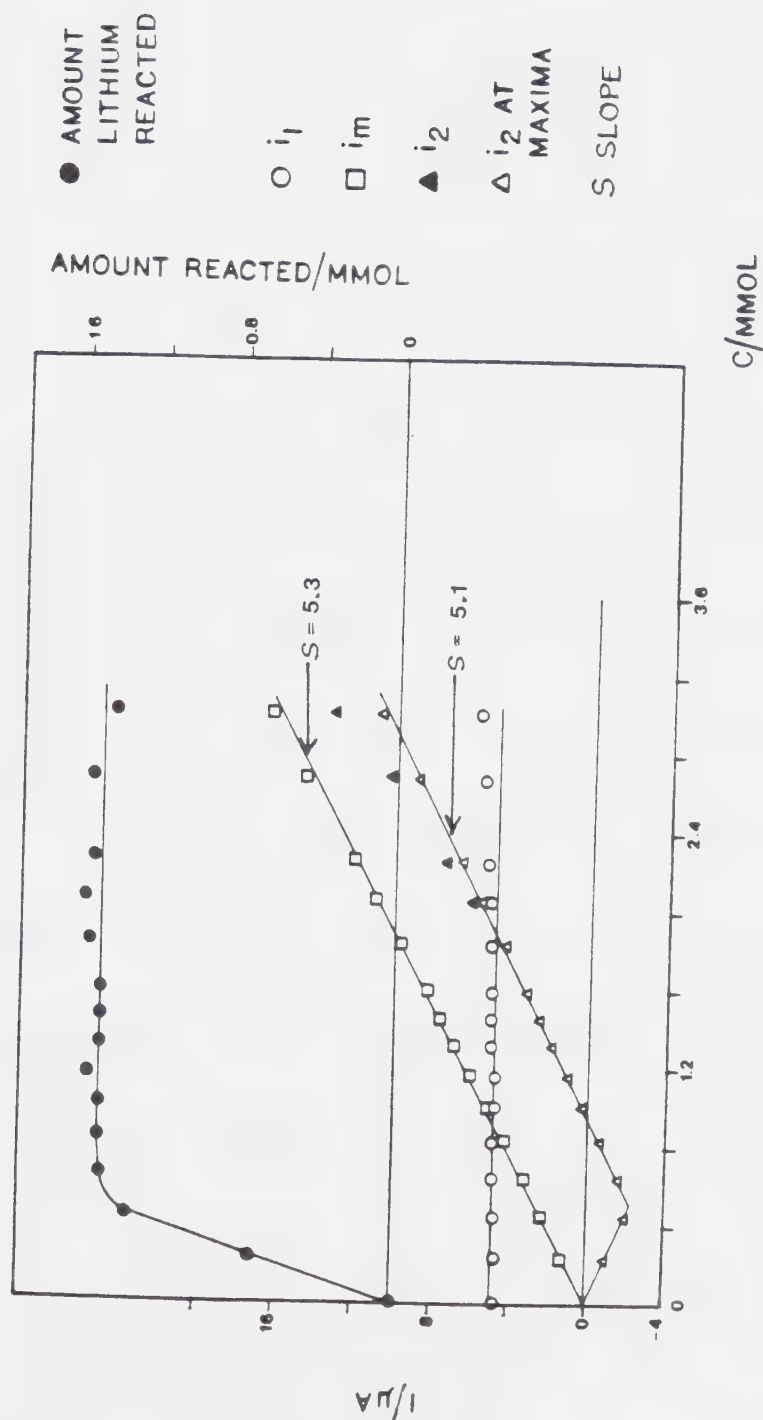


Figure 31. Plots of limiting currents and amount of lithium cation reacted versus anthracene concentration in DMF at 25°C. Lithium cation concentration was fixed at 1.50 mM. Mercury column 50.0 cm.

i_1 : limiting current for anthracene reduction
 i_m : limiting current for lithium cation reduction
 i_2 : limiting current for anthracene anion radical reduction

tration. It can be seen that, at low concentration of An, a linear portion with a slope of 3.0 was obtained and the plot leveled out at 1.50 mM Li⁺. It should also be pointed out that the curve begins to level out when the concentration of An is about 0.50 mM.

Figure 32 shows a similar experiment where the Na⁺ concentration was kept constant at 2.00 mM and the anthracene concentration varied in DMF. As mentioned earlier, in the system only two waves were observed corresponding to $i_1 + i_m$ and i_2 . Again, i_2 was negative at low concentrations of An and starts to increase linearly with a slope equal to that for the $i_1 + i_m$ plot. It is significant that the intercept for the $i_1 + i_m$ cuts the current axis at the current value for 2.00 mM Na⁺ in the absence of any anthracene. Again the mmol Na⁺ vs An concentration plot starts with a linear portion with a slope of 1.9 and then starts to level at about 1.00 mM An. The leveling

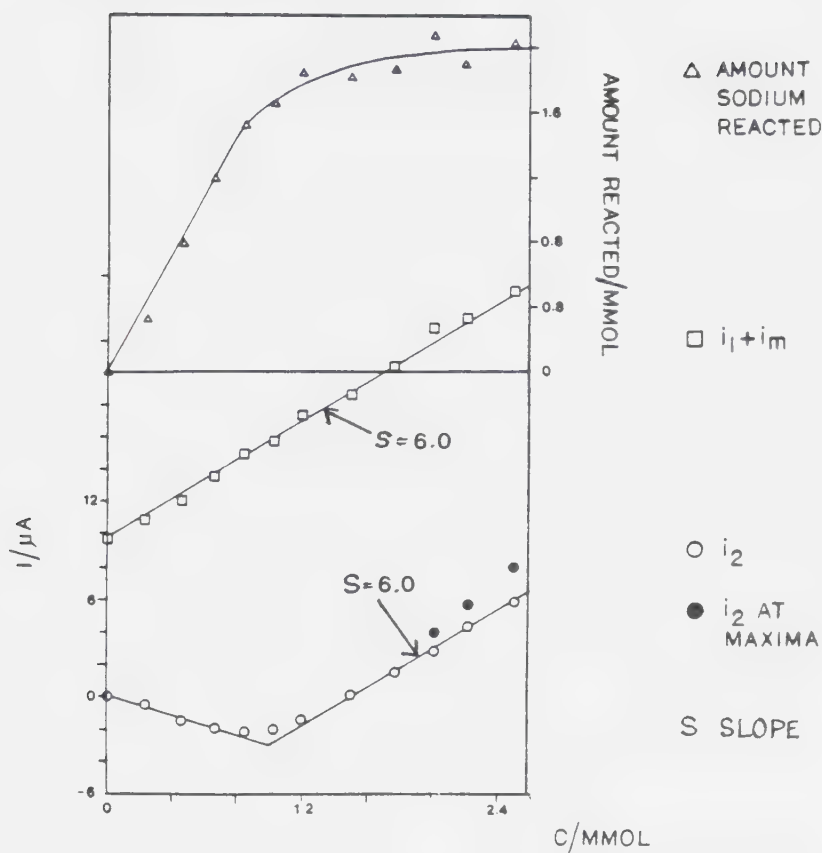


Figure 32. Plots of limiting currents and amount of sodium cation reacted versus anthracene concentration in DMF at 25°C.

Sodium cation concentration was fixed at 2.00 mM.

Mercury column 57.0 cm.

$i_1 + i_m$: combined limiting current of anthracene and sodium cation reduction

i_2 : limiting current of anthracene anion radical reduction

occurs at Na^+ concentration of 2.00 mM.

It was observed in Figures 31 and 32 that for the second wave of the hydrocarbon, i2, that polarographic maxima were obtained. It was stated earlier that for anthracene and fluoranthene, maxima appeared at concentrations of the hydrocarbon above about 2.00 mM.

However, as can be observed in Figures 31 and 32, current measured at the diffusion plateau following the maxima gave good results.

3.4 Discussion

The electrochemical behavior of the alkali metal cations observed in aprotic solvents such as acetonitrile and dimethylformamide were found to be in agreement with those of many previous workers. Previous studies have found that Na^+ , K^+ , and Rb^+ were polarographically reversible (59,60,63). Polarographic maxima have also

been observed previously (59) for Li^+ and Na^+ at concentrations greater than 3 mM and for Rb^+ at even lower concentrations. However in this work, only small maxima were observed at higher concentrations for all cations (greater than 3 mM) and did not pose any serious problems. From the slopes of the calibration plots (Table 1), it can be seen that Li^+ has a much lower value than the other cations. This is due to the higher solvation of Li^+ . For example, Li^+ has higher solvation numbers than those of the other cations in DMF:

Cation	Solvation number in DMF (217)	Slope of calibration plot ($\mu\text{A}/\text{mmol}$) in DMF
Li^+	5.0	4.0
Na^+	3.0	4.9
K^+	2.6	5.0
Rb^+	2.5	5.2

Also, it has been found that the Stokes radii of the alkali metal cations in most solvents follows the order

$\text{Li}^+ > \text{Na}^+ > \text{K}^+ > \text{Rb}^+$ (217). Brown and Urfali (59) have found that diffusion current constants for the alkali metal cations in DMF are 60% to 70% of the values obtained in acetonitrile. Table 1 shows that this can also be said for the present study. The diffusion coefficients of the ions are affected mainly by two factors; namely, solvation and viscosity. Within the same solvent, it can be seen that solvation determined the size of the ions and therefore the diffusion coefficients. However comparison in different solvents has to involve viscosities. Certainly, the solvation of the cations in DMF (Gutmann donor number 26.6) is higher than that in ACN (Gutmann donor number 14.1). However, the viscosity of DMF (0.802, 25°C) is also larger than that of ACN (0.345 25°C). Therefore, these two factors contribute to the much smaller diffusion currents observed in DMF than in ACN. E_h values in Table 1 also reflect the greater solvation of Li^+ compared to the

other alkali metal cations and also the more basic character of DMF as compared to ACN. Although comparisons of Eh values cannot be absolute where different reference electrodes are used, relative inferences can be drawn. Therefore, the relative ease of reduction of the alkali cations in this work was in accord with the results of Brown and Urfali in DMF.

Cation	This work V vs Ag/Ag ⁺	Brown and Urfali(59) V vs Hg pool
Li ⁺	-2.771	-1.81
Na ⁺	-2.463	-1.53
K ⁺	-2.492	-1.55
Rb ⁺	-2.481	-1.52

The electroreduction of anthracene and fluoranthene gave two waves of approximately equal height. This implies that the diffusion coefficients for the hydrocarbon and its anion radical are not greatly different. In tetrahydrofuran, it was found that the diffusion coefficients of the

anion radicals of biphenyl and anthracene are equal to those of the uncharged hydrocarbons (218). These results are expected since the single negative charge in these conjugated systems is well dispersed and solvation does not increase. The reversibility of the first reduction waves of anthracene and fluoranthene, in both aprotic solvents are in agreement with results obtained for aromatic hydrocarbons as discussed in the introduction of Chapter 1. Also cyclic voltammetric data (not given here) have shown that the anion radicals of both hydrocarbons are stable in DMF and ACN for at least the time scale of the cyclic voltammetric experiments (about 10 s). Cyclic voltammetry also showed the dianions to be unstable since no reoxidation current was observed on the reversed scan. Therefore the polarographic irreversibility as evidenced by the slope of the E vs $\log((i(d)-i)/i)$ plots results from chemical instability rather than slow rate of electron

transfer. The rate constant for electron transfer to the anion radical of anthracene has been estimated to be 0.5 cm/s, which is fast and therefore electrochemical reversibility should result if there were no chemical complications (29). In DMF, the slopes for the second waves of anthracene and fluoranthene were close to reversibility (61-64 mV). Although the cyclic voltammetric data showed no reoxidation current, the pulse polarographic time scale is much shorter, 57 ms compared to several seconds. Therefore, protonation of the dianions in DMF possibly was only partial. Further, DMF is a more "aprotic" solvent than ACN with respect to the presence of small amounts of water. This arises out of the ability of amide type solvents to form complexes with water (219). As will be discussed later, the present work, and previous investigations have shown that addition of water (< 5% volume/volume) to DMF did not seem to affect the stability

of the anion radicals of the hydrocarbons (25). In contrast, the slope of E vs $\log((i(d)-i)/i)$ plots for the second waves in acetonitrile showed a higher degree of irreversibility; 67 mV for fluoranthene and 76 for anthracene. Acetonitrile does not have as good an ability as DMF to complex water and therefore water activity is much higher in the solvent. Also since the wave heights were approximately equal for both waves of the hydrocarbons, the protonation products of the dianion are not reducible at the potentials of the second wave.

The E_h values showed that fluoranthene is more easily reduced than anthracene. This is expected because the electron affinity of fluoranthene is 0.840 eV whereas that for anthracene is 0.653 eV but the energies of solvation of the hydrocarbon anion radical are not much different (4,220). This argument follows from the relation between the half-wave potential and electron

affinity as given by

$$E_h = EA + i^* - \Delta G_{\text{solv}} (m^{\cdot-}) \quad (3.3)$$

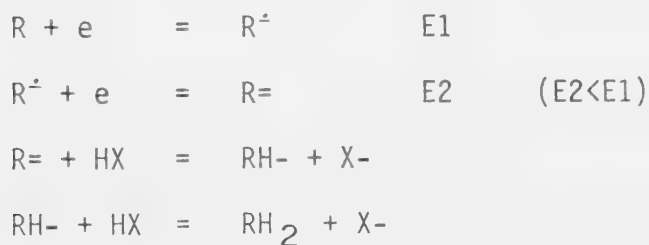
where EA = electron affinity

i^* = electric work function of the mercury

electrode

$\Delta G_{\text{solv}} (m^{\cdot-})$ = free energy of solvation of the anion
radical.

From the experimental evidence presented so far in this work, the mechanism for the electroreduction of aromatic hydrocarbons in aprotic media follows that of Hoijtink et al (23). Therefore, if R is the hydrocarbon



In the case of anthracene and fluoranthene in DMF and ACN, it appears that RH_2 is not reducible at the potentials investigated.

Before starting the actual investigations into the interactions of the anions of anthracene and fluoranthene with alkali metal cations, it was decided to check whether the addition of Woelm supergrade neutral alumina to the solutions could improve the stability of the dianions by removing the trace water. However, it was found that addition of alumina affected the reduction of the alkali metal cations. For example, Li^+ reduction waves were found to be drastically reduced in the presence of alumina, and even disappeared completely if enough alumina was added. It is conjectured that Li^+ ions are adsorbed onto the active alumina surface sites although no further work was done to confirm this.

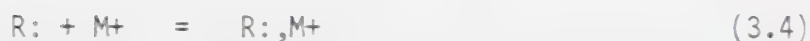
Also, in the early phase of these studies, the results

were found to be irreproducible and seem to vary with the deaeration time. This was attributed to the presence of oxygen due to insufficient deaeration time. At the negative potentials used, oxygen is reduced to the superoxide anion radical in aprotic media (221). The superoxide has been reported to tie up alkali metal ions, causing low results for the electrolysis of these ions (222). However, this problem was simply overcome by longer deaeration times (at least 15 minutes) to reduce the oxygen concentration to negligible values.

Prior studies in solvents of low dielectric constants (223-225) have shown that ion pairs were formed between anion radicals of polycyclic aromatic hydrocarbons and alkali metal cations. The anion radicals could disproportionate to give the dianions which were also paired with the cations. In this work no evidence of any ion pairing interactions between $An^{\bullet-}$, $Fa^{\bullet-}$, and the alkali metal cations

was observed. This is not surprising since the dielectric constants of acetonitrile (36.0) and dimethylformamide (37.0) (226) are much higher than those of ethereal solvents and also, the single negative charge in the conjugated hydrocarbons is well dispersed.

Thus, the equilibrium



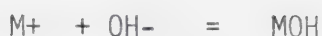
lies far to the left. The constancy of E_h values for the first hydrocarbon wave with increasing cation concentration provides the evidence for the lack of any significant ion pairing. Further, i_1 values were unchanged by cations in all systems studied as opposed to i_2 where clearly dianion-cation interaction occurs. The linearity of the i_m vs cation concentration plots is further proof that no complications arise from any reaction between the

anion radicals and the cations. The slopes of these lines coincided well with the calibration plots for the individual metal cations. Where the wave of the metal cation is not resolved from that of the hydrocarbon, the linearity, slopes and intercepts of the $i_l + i_m$ vs metal concentration plots imply that these combined waves are simply additive with no chemical complications. The fact that the slopes agree well with those for the calibration plots of the metal cations and the intercepts are close to the wave height of the hydrocarbon reduction strongly support this deduction. Positive deviations from linearity of the i_l and $i_l + i_m$ plots at high metal concentrations are probably due to maxima observed at these high concentrations. However, these deviations are small and do not detract from the results.

It is proposed that the current depression of the dianion waves, i_2 , is due to the interaction between the

dianion and the metal cations. All the results observed point in this direction. Adsorption and film formation effects have been ruled out from the normal diffusion controlled behavior of the current-time transients at the potentials where current depression occurs. These effects do not normally show the concentration dependence which has been observed in these experiments. Reverse pulse polarography does not show any desorption or film destruction currents which will support the presence of adsorption or film formation. Another possible explanation for the current depression could be due to the presence of trace water. Under the careful purification procedure used in this work, the water concentration is probably much less than 5 mM. However, in the presence of water, the following reactions could conceivably occur:





If this were the case, the addition of water should increase the magnitude of the current depression. This could happen if the presence of OH^- results in the removal of metal cations. However, alkali metal hydroxides are relatively soluble in these solvents, and it is doubtful that at such low concentration the solubility products could be exceeded. However, what is more important is that further experiments involving the addition of water, which will be discussed in a later chapter, lifted the depression of current i_2 rather than reinforcing it.

Therefore, from the above discussion, the only possible explanation for depression of current i_2 is the interaction of dianions with metal cations. The course of events leading to the decrease in the magnitude of i_2 is

viewed as follows: at the diffusion current plateau for the metal ion reduction, the concentration of the metal ion at the surface of the electrode is zero and a virtually linear metal concentration gradient has been established in the diffusion layer. As the potential scan proceeds to more negative values, reduction of the hydrocarbon anion radical to the dianion begins. The dianions which are formed start to diffuse through the diffusion layer out into solution. In this layer, encounters between the dianions and the metal cations result in interaction between the two. Interaction with the cations effects their removal and thus reduces the number of cations which can arrive at the electrode to be reduced. This means that the diffusion current of the metal cation which has been established prior to the formation of the dianions can no longer be maintained. Since this phenomenon occurs at the potential region of the reduction of the

anion radicals, it manifests itself as a drop in i_2 . The reason for the observed cathodic current on an anodic scan for the An:Li^+ in DMF system is now clear (Figure 23). As the potential is scanned positive, a potential is reached where dianions are no longer formed and Li^+ is no longer being removed in the diffusion layer. Thus the arrival of the Li^+ to the electrode surface results in a cathodic current.

It is therefore logical that the strength of interaction between the dianions and the metal cations is reflected in the magnitude of the current depression. Li^+ and Na^+ react strongly with $\text{An}^=$ in both ACN and DMF. In Figures 24 and 26, the slopes for the i_2 plots are essentially equal to the slopes for the i_1 and $i_1 + i_m$ plots. This means that almost complete removal of Li^+ and Na^+ is effected. It is interesting to note, in the An:Li^+ system in DMF for example, that the point where

the i_2 plot crosses the concentration axis occurs at 1.45 mM. If complete removal of Li^+ is the case, the removal of 1.45 mM of Li^+ would result in a loss in current of $1.45 \times 4.0 = 5.8 \text{ uA}$. Since the current depression occurs at the i_2 wave for anthracene and the diffusion current for this wave for 1.00 mM An is 6.1 uA, this would mean that the actual observed i_2 is only $6.1 - 5.8 = 0.3 \text{ uA}$ which is very close to zero. The very strong interaction of Li^+ and Na^+ with $\text{An}^{\cdot-}$ is obvious if Figure 27 is considered. It can be seen that up to a concentration of 2.00 mM of Li^+ added, the amount of Li^+ reacted is also 2.00 mM, resulting in a slope of 1 for the curve given in Figure 27. The same can be said for Na^+ up to 1.00 mM. With Na^+ , the curve levels off at 2.00 mM whereas with Li^+ it approaches 3 mM. The interpretation is therefore that a 1:3 stoichiometry of $\text{An}:\text{Li}^+$ is obtained in DMF whereas $\text{An}:\text{Na}^+$ gives a 1:2 stoichiometry.

The same result is true for An⁻ with Li⁺ and Na⁺ in ACN.

The formation of the 1:3 complex An⁻,3Li⁺ is very interesting from charge considerations since it gives rise to an overall positive charge. However, this is not without precedent since the same stoichiometry was found for the interaction of anthraquinone dianion with Li⁺ (227).

In the case of K⁺ and Rb⁺, i_2 did not reach large negative values as can be seen from Figure 24. Figure 27 also shows that reactions between An⁻ and these cations are not as strong as for Li⁺ and Na⁺. The plots in Figure 27 show continuous increase in the mmol of cation reacted with increasing metal concentration. Reaction for Rb⁺ appears to be slightly greater than K⁺. It is proposed that for these two cations, both 1:1 and 1:2 complexes are present and these have small formation constants.

Li⁺ with Fa⁻ reacts strongly on a 1:1 basis in DMF.

There is some 1:2 complex formed but this does not appear to be strong. This can be observed from Figure 25 where the $i_l + i_m$ plot remains constant up to about 1.2 mM Li^+ and then increases linearly with a slope of 4.2 which is approximately equal to that for Li^+ calibration of 4.0 $\mu\text{A}/\text{mM}$. This is supported by Figure 28 where a slope of 1 was obtained and the mmol Li^+ reacted starts to level out at 1.2 mM Li^+ . In acetonitrile, similar results are obtained (Figure 26) except that more of the 1:2 complex $\text{Fa}^-, 2\text{Li}^+$ is formed and the mmol Li^+ reacted approaches 2.0 mM (Figure 30).

Na^+ reacts very strongly with Fa^- both in DMF and ACN as can be seen from Figures 28 and 30 where slopes of 1 were obtained. However, only a 1:1 complex (Fa^-, Na^+) appears. The reaction did not proceed to the 1:2 complex $\text{Fa}^-, 2\text{Na}^+$ since the curves leveled off exactly at 1 mM of Na^+ . K^+ and Rb^+ reacted only very weakly with Fa^- and from what

has been said for Li^+ and Na^+ with Fa^- , it can be deduced that only 1:1 complexes are formed with very small formation constants (Figure 28).

The results obtained from the experiments where the hydrocarbon concentrations were varied confirm the conclusions which were reached in the above discussion. In the $\text{An}:\text{Li}^+$ in DMF system (Figure 31), where the Li^+ concentration was fixed at 1.50 mM, the constancy of the Li^+ reduction current with added anthracene concentration and the fact that E_h values for the first anthracene wave and the Li^+ waves did not change significantly imply that no interaction occurs between $\text{An}^{\cdot-}$ and Li^+ . The i_1 vs An concentration plot was linear. The i_2 plot which was linearly increasing beyond a concentration of 0.51 mM for An , has the same slope as the i_1 plot. This means that no further reduction in the i_2 current occurred after 0.51 mM of anthracene had been added. The mmol Li^+

reacted vs An concentration plots is most informative.

The initial linear portion has a slope of 3.0 and it starts to level off at an anthracene concentration of 0.5. In the level portion the mmol Li⁺ reacted was 1.50 mM. All this supports the argument that Li⁺ reacts very strongly with An= to form the 1:3 complex An=,3Li⁺. (Note: Current values in this experiment (Figure 31) should not be compared with calibration plots of other experiments because for this particular experiment the Hg head was changed to 50.0 cm instead of the usual 57.0 cm in DMF throughout this work.)

The results for the experiment where the Na⁺ concentration was fixed at 2.00 mM (Figure 32) again confirmed earlier conclusions for this system. The $i_1 + i_m$ plot has a slope of 6.0 which agrees with the calibration plots for An in DMF. The i_2 plot increased linearly with An concentration beyond 1.00 mM and has a slope of 6.0.

The mmol Na⁺ reacted vs An concentration has a slope of 1.9 and levels at 2.00 mM Na⁺. Therefore Na⁺ forms a strong 1:2 complex with An⁼ in DMF.

From the above discussion, it is clear that interaction of dianions with alkali metal cations increases

- 1) with decreasing size of the cation;
- 2) with decreasing size of the hydrocarbon; and
- 3) from dimethylformamide to acetonitrile.

The nature of the interaction between the dianion and the alkali metal cation needs to be discussed. In the chemical reduction of aromatic hydrocarbons with alkali metals in ethereal solvents it is assumed that the dianions form ion pairs with the alkali metal cations. Here, the dianion-alkali metal cation interactions are also believed to be ion pairing. Since the extent of ion pairing increases with decreasing radius of the cations, contact ion pairs are formed. This is reason-

able since the larger the charge/radius ratio for the cations ($\text{Li}^+ > \text{Na}^+ > \text{K}^+ > \text{Rb}^+$), the greater the strength of interaction. The ionic radii of Li^+ , Na^+ , K^+ , and Rb^+ are 0.68, 0.97, 1.33 and 1.47 Å respectively. Contact ion pairs have also been found in interactions of ketone anions with alkali metal cations (227). This trend is observed in this work except for K^+ and Rb^+ with An in DMF where the two are reversed (Figure 27). For these two cations, solvent separated ion pairs may exist since stabilization by contact ion pair formation may not be large enough to compensate for the destabilization arising from desolvation. It is known that increase in radius of countercation favors the solvent separated ion pair because the gain in coulombic energy on collapse to the contact ion pair is decreased (reference 217, p. 356). The situation can arise, where both the solvent separated and contact ion pair exist in equilibrium. For the K^+ and Rb^+ case then, the solvent separated ion pair should

be more favored resulting in the reversal in trend as observed above. This study however, does not provide enough information to test this situation.

The dianions of the aromatic hydrocarbons had half-wave potentials more negative than the alkali metal cations (Table 1). (Note: The hydrocarbon anion radicals reductions to the dianions were not reversible, therefore the Eh values do not have any thermodynamic significance. However, for the sake of argument here, they will be assumed to be reversible Eh values.) Examination of Table 1 shows that in DMF, the second reduction wave of anthracene has the most negative Eh, this value being -2.989 V and Na⁺ the most positive Eh, with value -2.463 V. The difference between these two values is 526 mV. In acetonitrile, where K⁺ and Rb⁺ were not studied, again the most negative and positive Eh values belong to anthracene second wave (-2.904 V) and sodium cation (-2.159 V) respectively, the difference being 745 mV. In

general, solvation effects in going from DMF to ACN are much larger for the cations than for the hydrocarbons and therefore, in terms of electron transfer, the cations are more acidic in acetonitrile. Therefore considering the anthracene-cation systems in ACN, it seems that the $An=$ is a much stronger base compared to the cations. As mentioned above, the difference in E_h between the $An^{\dot{-}}/An=$ couple and Na^+ is 745 mV. The difference between the same couple and Li^+ is 639 mV. From these views therefore, the argument can be made that the current depression observed is due to electron transfer from $An=$ to the metal cations in the diffusion layer which would prevent these cations from reaching the electrode.

However, careful examination shows that the above argument cannot be true. This is because polarographic half-wave potentials obtained for alkali metal cations are not applicable since reduction at the mercury electrode results in amalgam formation whereas reduction by $An=$, if it were to

occur, would result in formation of the alkali metal in the solution. This means that $E(0)$ values for the alkali metal cations must be used. The standard reduction potentials for Na^+ and Li^+ in ACN are given below (see reference 172, p.400).

Cation	$E(0)$ (vs Standard Hydrogen Electrode (SHE))
Li^+	-2.645 V
Na^+	-2.421 V

Since the E_h value for the $\text{An}^{\dot{+}}/\text{An}^-$ couple was obtained with reference to the Ag/Ag^+ (0.01 M) reference electrode, this can be converted to the hydrogen scale. The Ag/Ag^+ electrode is +0.3 vs aqueous SCE which in turn is +0.246 vs SHE and therefore the E_h value for $\text{An}^{\dot{+}}/\text{An}^-$ is -2.358 V vs SHE which means that the solution reduction of the cations without amalgam formation is negative of the $\text{An}^{\dot{+}}/\text{An}^-$ couple. Charge-transfer complexes (EDA type) have been observed for contact ion pairs in solvents of low dielectric constant (reference 217, p. 410). However, in view of the

above discussion and from the fact that no colored species were observed at the surface of a hanging mercury drop electrode, this type of complex is not thought to occur to any extent in this case.

The increase in ion pairing in going from anthracene to fluoranthene can be explained in terms of the larger size of the fluoranthene molecule due to more fused rings. Therefore, the two negative charges in fluoranthene dianion are more diffuse compared to anthracene. This is evident from the more positive reduction potential of fluoranthene.

It is obvious that solvation must play an important part in the dianion-cation interactions. The results of the An:Li^+ system in ACN and DMF serve to demonstrate this point. A distinct peak appears at the beginning of the dianion wave before depression occurs in DMF (Figure 10). This peak is absent in ACN (Figure 18). It is well known

that Li^+ is much more strongly solvated in DMF than in ACN.

It is expected that both the kinetics and the equilibrium of ion pair formation is more favorable in ACN than in DMF.

The appearance of the peaks in DMF could mean that a small amount of dianion has to be present before interaction becomes favorable. The slopes of the calibration plots for Na^+ , K^+ and Rb^+ are closely grouped in DMF. This means that the solvated radii of these ions in DMF are not very much different. However, Na^+ interacts much more strongly than K^+ or Rb^+ with dianions. This is another indication of contact type of ion pairing in the case of Na^+ . Unfortunately, no studies could be made for K^+ and Rb^+ in ACN so that no comparison could be made for these two ions in different solvents.

The observation of different stoichiometries for different systems in this study is very interesting. In many previous studies in ethereal solvents, not much

attention has been paid to these variations in stoichiometries. In most cases, it has been implicitly assumed that anion radicals pair with one cation whereas dianions pair with two cations. However, electrochemical studies of ion pairs of negative ions of ketones with alkali metal cations in DMF and ACN have revealed that these different stoichiometries exist (209-212). It is not very clear to the author at this point why these different stoichiometries occur for the aromatic hydrocarbons. Clearly charge considerations alone are not enough since Li^+ and An^- forms a 1:3 complex $\text{An},3\text{Li}^+$. Obviously, structural factors and solvation of the ion pairs play important roles in these interactions. Fast spectroscopic techniques could provide valuable information on these aspects. Spectroelectrochemical methods would be relevant in these areas. However, difficulties arise in electrode fabrication. Mercury thin film electrodes have so far not been

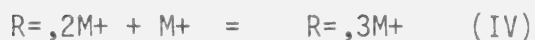
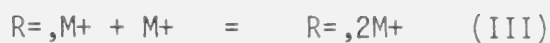
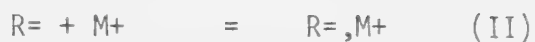
very successful. Further research in this area in these laboratories is in progress.

Temperature studies have also been made. Experiments were carried out at 5°C and 45°C besides 25°C. However, over this temperature range, no measurable changes in the interactions were detected. So far, the discussion has been qualitative in nature. It is necessary to perform some calculations to obtain the equilibrium constants for the ion pairs. However, the value of these calculations would be very doubtful due to the unstable nature of the dianions. However, it is felt that this present study provides an important starting point for further investigation. To the best of the author's knowledge, this is one of the few, if not the only, study of the interactions between aromatic hydrocarbon dianions and alkali metal cations in dipolar aprotic solvents. From the results and discussion presented so far,

the following summary concerning the interaction of the negative ions of anthracene and fluoranthene with alkali metal cations in ACN and DMF can be made:

- i) No interaction of the anion radicals with alkali metal cations occurs in either solvent.
- ii) Ion pairs are formed between the dianions and alkali metal cations. These ion pairs are of the contact type except for K^+ and Rb^+ with $An^=$ in DMF where solvent separated ion pairs may exist.
- iii) The strength of interaction follows the trend
 $Li^+ > Na^+ > K^+ > Rb^+.$
- iv) Interactions are stronger in ACN compared to DMF.
- v) The stoichiometries of interactions do not depend on charge considerations alone.

The following scheme for the reactions are postulated where R represents the aromatic hydrocarbon and M^+ the alkali metal cation:



Step II occurs very strongly for An:Li⁺, Na⁺, and

Fa:Li⁺, Na⁺ in both solvents, but only weakly for

An:K⁺, Rb⁺ and Fa:K⁺, Rb⁺ in DMF. Step III occurs very

strongly for An:Li⁺ in both solvents, An:Na⁺ in ACN but not

quite as strong for An:Na⁺ in DMF. It is of moderate

strength for Fa:Li⁺ in ACN but weak for Fa:Li⁺ in DMF

and An:K⁺, Rb⁺ in DMF. Step IV occurs strongly in An:Li⁺

in both solvents.

Chapter 4. The Effect of Water on the Interactions between Aromatic Negative Ions and Alkali Metal Cations

4.1 Introduction

In Chapter 3, it was found that the second reduction wave of anthracene and fluoranthene was irreversible due to the reactive nature of the dianion with respect to protonation by proton donors (such as water) present in the solvents even after purification. However, it has been established that Li^+ and Na^+ interact strongly with the dianions. Hence, under the experimental conditions described earlier, the dianions-cation interactions take precedence over protonation in the diffusion layer. Also, the possible presence of the hydroxide ions was not thought to be the cause for the observed current depression of the dianion wave. In this chapter, evidence will be presented that shows this is indeed so.

From what has been discussed, it is reasonable to expect that there is a competition between the metal cations and the proton donors for the available dianions close to the electrode surface. If this is true, then conditions could be altered so that the protonation reaction proceeds faster compared to the dianion-cation reaction. One such alteration is then to drastically reduce the concentrations of the electroactive species and determine the effect on the limiting currents. Another is to have controlled addition of water to the system. The addition of water would also substantiate the proposal that hydroxyl ions are not the cause of current depression since if this were so, current depression will be increased or in the limit remain constant.

The following sections describe the experiments performed to test the above assumption.

4.2 Experimental

4.2.1 Instrumentation

The equipment used is exactly the same as that described in Chapter 3.

4.2.2 Purification of Chemicals

The purification of anthracene, fluoranthene, alkali metal perchlorates and the solvents acetonitrile and dimethylformamide has already been described. The water used here was tap distilled water which had been deionized. It was then made alkaline by adding sodium hydroxide. Potassium permanganate was then added. This mixture was distilled and the distillate was taken through another distillation stage.

4.2.3 Procedure

In all experiments, the supporting electrolyte used

was tetra-*n*-butylammonium tetrafluoroborate (TBAF) at 0.10 M. The deaeration procedure was the same as that described in Chapter 3. Temperature was controlled at $25.0 \pm 0.1^{\circ}\text{C}$.

In the dilution experiment, 25 ml of a solution containing 2.00 mM anthracene and 3.00 mM lithium perchlorate in DMF was pipetted into the polarographic cell. Into each solution, measured volumes of the background solution (solvent at 0.10 M TBAF) equilibrated at 25°C was transferred .

In water addition experiments, water was added to separate solutions of the metal cations and the hydrocarbons in DMF. Then water was added to mixtures of solutions of the metal cations and the hydrocarbon. For example, in the first case water was added separately to 1.00 mM anthracene and also to 3.83 mM Li^{+} solutions in DMF. Then a mixture containing 1.00 mM anthracene and

3.83 mM Li^+ was used to which water addition was performed.

Finally, a water concentration was chosen to be used in kinetic studies. In the case of the An: Li^+ system this concentration was 2.14 M in water. 25 ml of a 1.00 mM solution of anthracene in DMF (0.10 M TBAF) which was also 2.14 M in water was pipetted into the polarographic cell. After each run a known volume of a stock solution of Li^+ which was also 1.00 mM in anthracene and 2.14 M in water was transferred into the cell.

Similar experiments were also carried out for the An: Na^+ system in DMF. In this case water was added to a mixture containing 1.00 mM anthracene and 3.92 mM Na^+ in DMF. From this experiment a water concentration of 0.22 M was chosen for further studies.

For fluoranthene, water was also added, using a micro-syringe, to a 1.00 mM solution of fluoranthene in DMF.

Similar experiments as for anthracene were carried out with

water addition to Fa:Li⁺ and Fa:Na⁺ solution mixtures in DMF. In the case of Li⁺, the concentration of fluoranthene was 1.00 mM and Li⁺ was 1.02 mM whereas for Na⁺, the concentration of fluoranthene was 1.00 mM and Na⁺ was 2.45 mM. From these experiments a fixed water concentration of 1.72 M was chosen for kinetic studies of the Fa:Li⁺ system. The limiting currents were corrected for dilution effects due to the addition of water.

4.3 Results

Figure 33 shows the effect of dilution on a mixture of 2.00 mM anthracene and 3.00 mM Li⁺ in DMF. It can be seen that at the high concentration end, current depression of the third wave is obvious. As the solution was made more and more dilute, the magnitude of the depression became less until at a concentration of 0.09 mM anthracene and 0.15 mM Li⁺, the current depression was completely

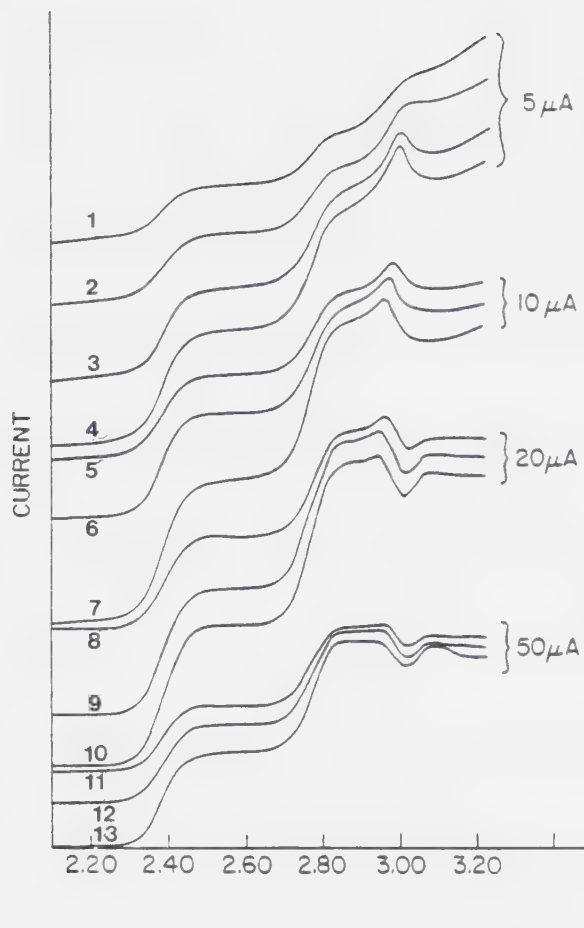


Figure 33. Dilution experiments: polarograms showing the effect of dilution on mixtures of anthracene: lithium cation in the concentration ratio 1:1.5 in DMF at 25°C.

Anthracene:Li⁺ concentrations are (in mM):

(1) 0.07:0.11, (2) 0.09:0.15, (3) 0.13:0.21,
 (4) 0.24:0.37, (5) 0.34:0.52, (6) 0.44:0.66,
 (7) 0.62:0.93, (8) 0.79:1.19, (9) 1.11:1.67,
 (10) 1.25:1.88, (11) 1.43:2.14, (12) 1.67:2.50,
 (13) 2.00:3.00.

Mercury column 57.0 cm.

lifted. At this concentration, the height of the third wave which was due to the reduction of the anthracene anion radical to the dianion, was equal to that of the first wave, which is the expected result in the total absence of any interaction between the dianion and Li^+ . Figure 34 shows the plots of the heights of the anthracene and lithium reduction waves against concentration. It can be seen that these plots are linear and the slopes agree well with those of the calibration plots given in Table 1. Further, the plot of percentage of Li^+ reacted vs concentration of Li^+ shows that below about 0.90 mM Li^+ , the An: Li^+ interaction begins to be affected as the percentage of Li^+ reacted starts to decrease sharply from 100%. It should also be pointed out that polarographic behavior remained essentially unchanged with dilution within the limits of experimental error. For example, the Eh values of the anthracene and Li^+ reduction waves remained con-

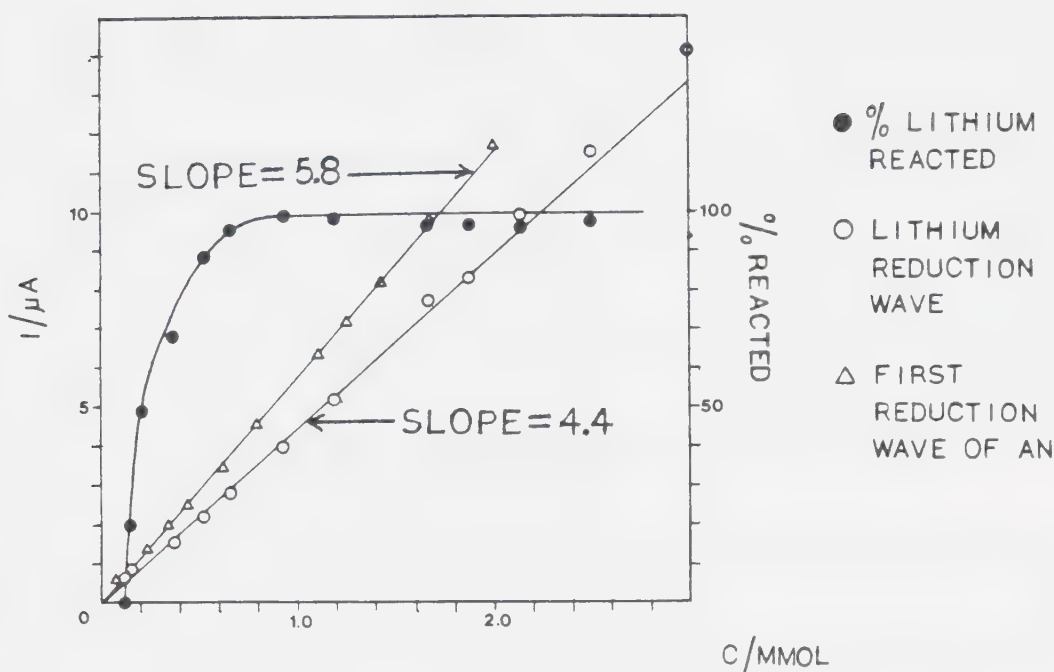


Figure 34. Dilution experiment: plots of limiting currents and percentage of lithium cation reacted versus lithium cation concentration in DMF at 25°C. An:Li⁺ concentration ratios kept at 1:1.5. Mercury column 57.0 cm.

stant.

Before the effect of water on mixtures of anthracene and Li^+ solution was examined, it was decided to investigate the effect of water on separate solutions of anthracene and Li^+ in DMF. Figure 35 shows the effect of water, up to 5.00 M, on the limiting currents of a 1.00 mM solution of anthracene and a 3.83 mM solution of Li^+ in DMF. In the case of anthracene, both the limiting currents of the first (i_1) and second (i_2) reduction waves decreased linearly with water concentration. The limiting currents were corrected for dilution effects due to the addition of water. The decreases were approximately equal for both waves and amounted to about 17% at a water concentration of 5.20 M. The E_h values for the first wave were shifted negative by about 20 mV, but those for the second wave were shifted positive by about 55 mV at 5.05 M water as compared to the dry solution.

Plots of E vs $\log((i_l - i)/i)$ showed that for the first wave the slope was 60 mV for a reversible one-electron transfer. This behavior did not change even up to addition of about 4.31 M water. For the second wave, the slope was 66 mV in the absence of water but increased to 71 mV at 4.31 M water.

In the case of the 3.83 mM Li^+ solution in DMF, the limiting current decreases from 15.2 μA in the absence of water to 12.6 μA in the presence of 5.05 M water, again a decrease of 17% (see Figure 35). The E_h values remained essentially constant(within 10 mV). Plots of E vs $\log ((i_A - i)/i)$ showed that the slopes did not change very much, decreasing slightly from 65 mV with no water to 63 mV at 4.31 M water.

The results of the addition of water to a mixture of 1.00 mM anthracene and 3.83 mM Li^+ in DMF are shown in Figure 36. It can be seen that at low water concentra-

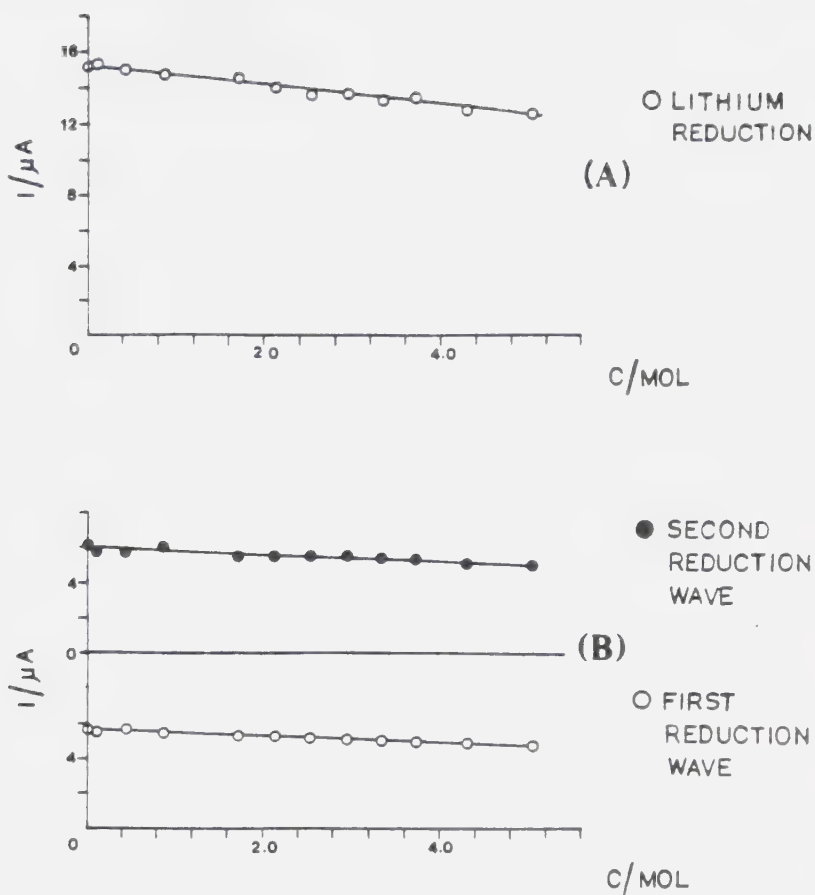


Figure 35. A. Effect of water on the limiting current of a 3.83 mM lithium cation solution in DMF at 25°C.
 B. Effect of water on the limiting currents of a 1.00 mM solution of anthracene in DMF at 25°C.
 Horizontal axis show concentration of water.
 Mercury column 57.0 cm.

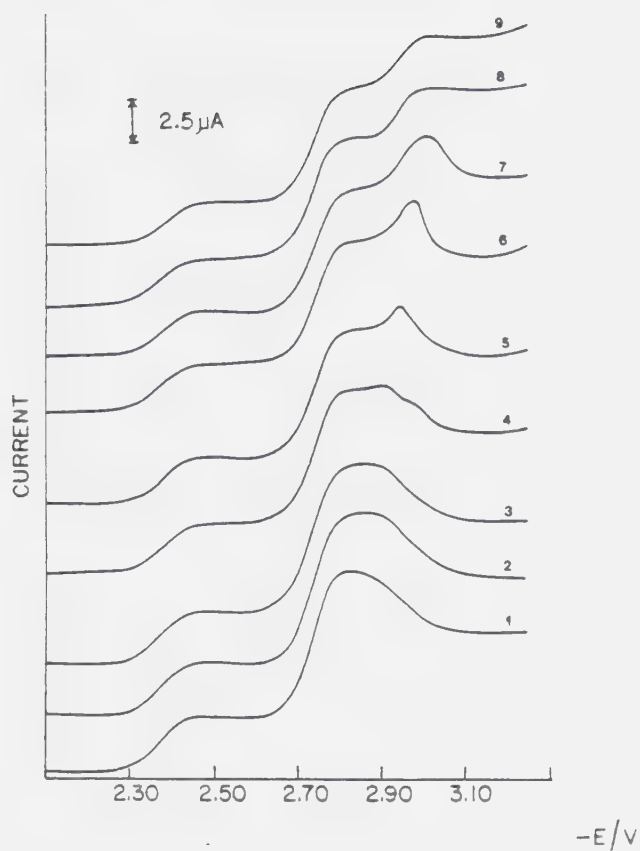


Figure 36. Polarograms showing the effect of water addition on a mixture of 1.00 mM anthracene and 3.83 mM lithium cation in DMF at 25 C. Water concentrations are (in M): (1) 0.00, (2) 0.11, (3) 0.44, (4) 1.72, (5) 2.34, (6) 2.75, (7) 3.14, (8) 3.73, (9) 4.31. Mercury column 57.0 cm.

tions (up to about 0.11 M), there was not much effect on the current depression of the third wave. As the concentration of water was increased, the magnitude of the current depression decreased until at about 3.73 M water, there was no depression and the height of the third wave became equal to the first. Figure 37 shows the plots of the limiting currents vs water concentration. The currents have been corrected for the dilution effects due to water addition. The plots of anthracene (i_l) and Li^+ (i_m) reduction currents vs water concentration show the same trend as those of Figure 35. They decreased linearly with increasing water concentration. However, the limiting current for Li^+ appeared to be slightly higher here. For the anthracene and Li^+ reduction waves, the same results were obtained here concerning the E_h values and the E vs $\log ((i_l - i)/i)$ as for the separate solutions with respect to water addition. The current due to the reduction of

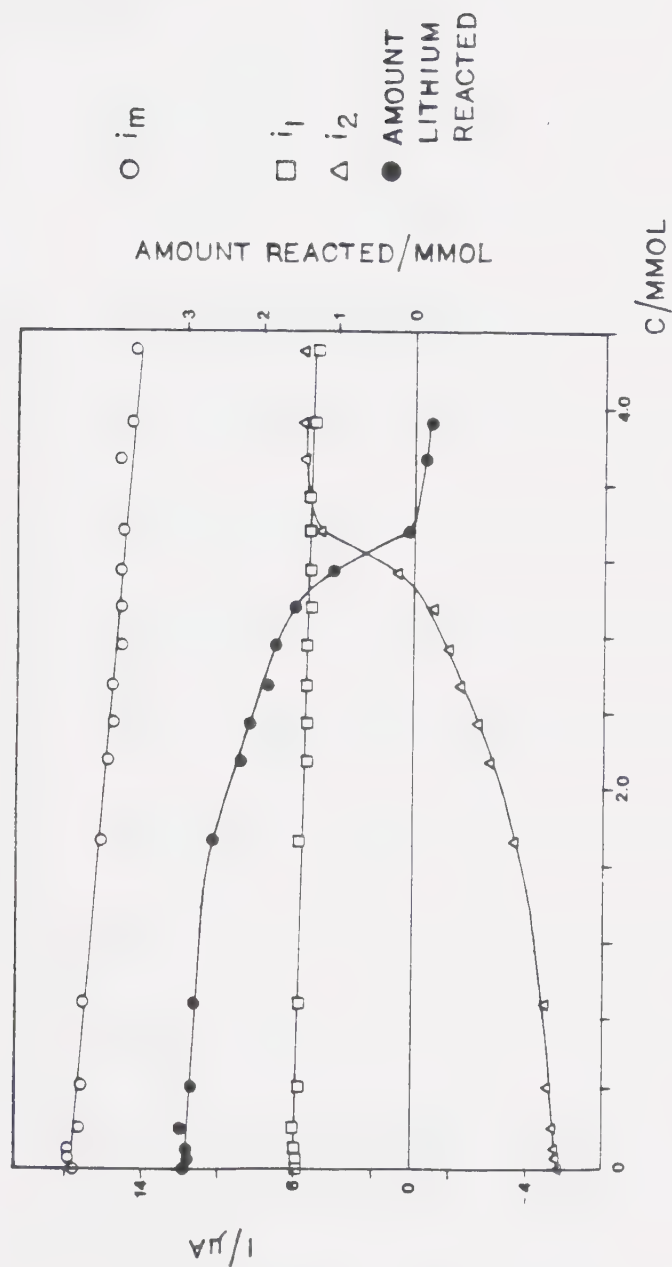


Figure 37. Effect of water addition on the limiting currents and amount of lithium cation reacted for a mixture of 1.00 mM anthracene and 3.83 mM lithium cation in DMF at 25°C. Horizontal axis show water concentrations. Mercury column 57.0 cm.
 i_1 : limiting current for anthracene reduction
 i_m : limiting current for lithium cation reduction
 i_2 : limiting current for anthracene anion radical reduction

the anthracene anion radical (i_2) remained approximately constant at its depressed value up to about 1.0 M water and then increased at higher water concentrations. Above 3.4 M water, the height of the dianion wave became equal to that for the first wave. The plot of mM Li^+ reacted vs water concentration is also shown in Figure 37.

When no water was added, the amount of Li^+ reacted was exactly 3.00 mM. Increasing the water concentration up to about 1.70 M did not change this value much. However, at higher water concentrations, the amount of Li^+ reacted decreased and approached zero at 3.35 M water. Figure 38 shows the results of the experiment where the water concentration was fixed at 2.14 M and the concentration of Li^+ in a 1.00 mM anthracene solution was increased. As expected the limiting current of the first wave (i_1) remained constant while the Li^+ wave (i_m) showed a linear increase with slope of 3.9 $\mu\text{A}/\text{mM}$, slightly lower

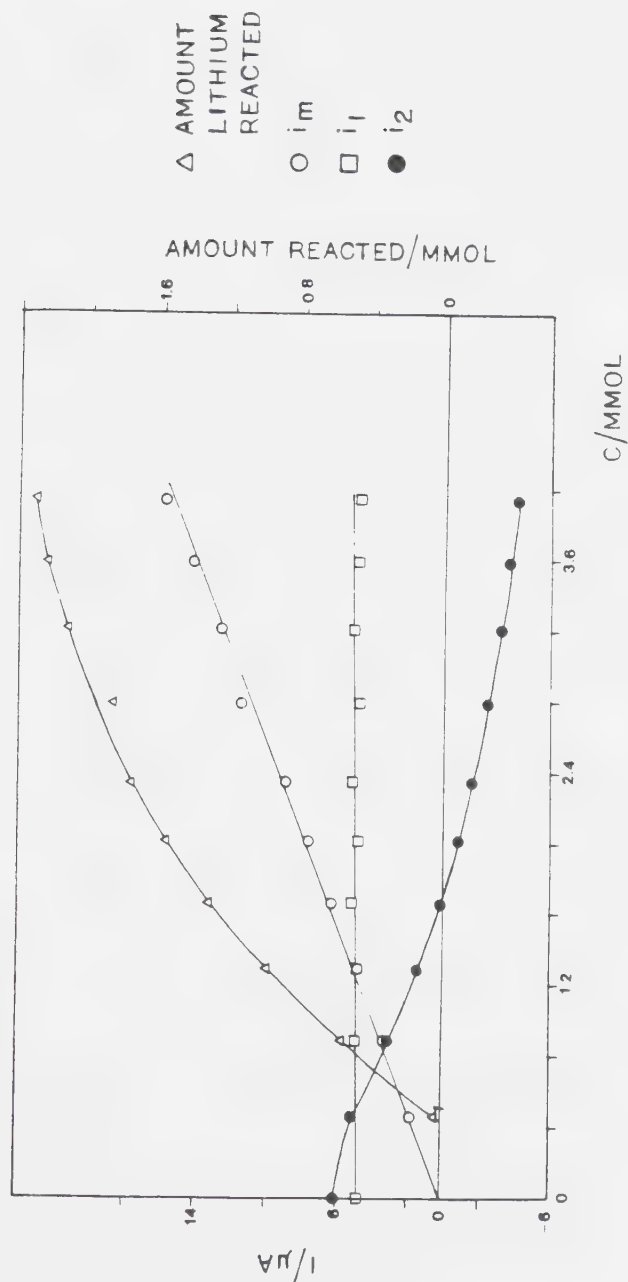


Figure 38. Plots of limiting currents and the amount of lithium cation reacted versus lithium cation concentration for mixtures of anthracene and lithium cations containing 2.14 M water in DMF at 25°C.

Anthracene concentration fixed at 1.00 mM.

Mercury column 57.0 cm.

i_1 : limiting current for anthracene

i_m : limiting current for lithium cation reduction

i_2 : limiting current for anthracene anion radical reduction.

to that of the Li^+ calibration slope of 4.0 uA/mm . The depression of the third wave (i_2), as can be seen from Figure 38, was very much less as compared to that in the absence of water. The plot of mM Li^+ reacted showed an induction region corresponding to about 0.40 mM Li^+ before any reaction occurred between An^- and Li^+ .

Figure 39 shows the effect of water addition on a solution containing 3.92 mM Na^+ and 1.00 mM anthracene in DMF. The first wave corresponding to the unresolved reduction of anthracene and sodium (i_1+i_m) decreased linearly with increased water concentration. The magnitude of the current depression (i_2) decreased until at concentrations of water above about 1.0 M , the value of i_2 was approximately equal to the first reduction of anthracene. Figure 39 shows that initially when no water was added the mM Na^+ reacted was exactly 2.00 mM , and decreased quite sharply with water addition as

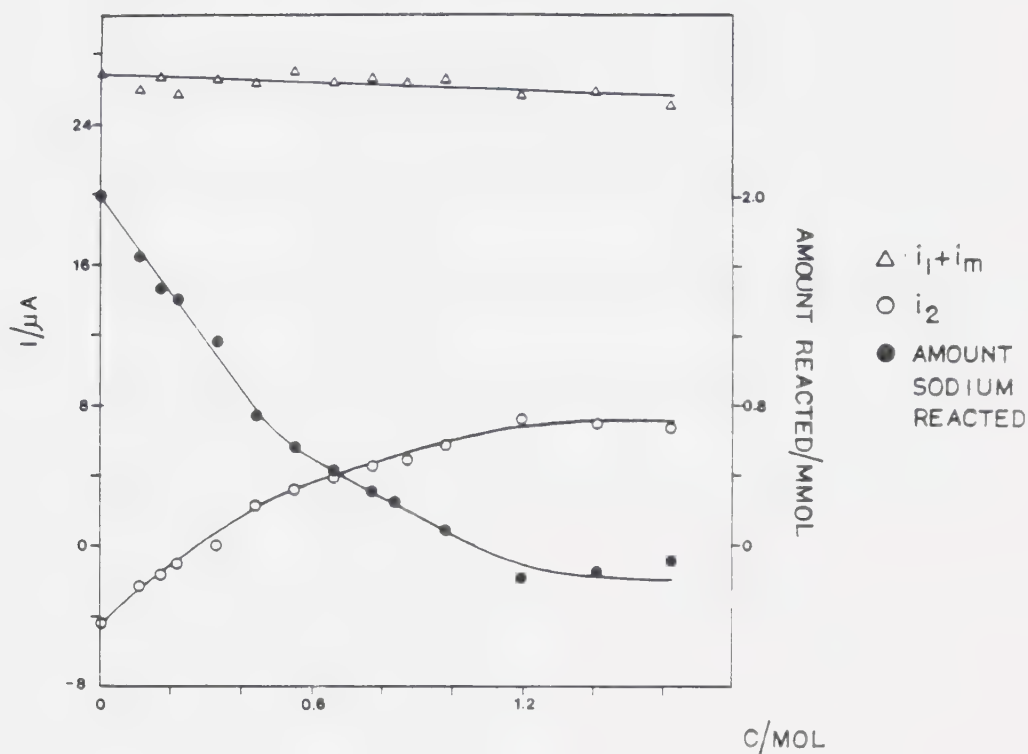


Figure 39. Effect of water addition on the limiting currents and the amount of sodium cation reacted for a mixture of 1.00 mM anthracene and 3.92 mM sodium cation in DMF at 25°C. Horizontal axis show water concentration. Mercury column 57.0 cm.
 $i_1 + i_m$: combined limiting current for anthracene and sodium cation reductions
 i_2 : limiting current for anthracene anion radical reduction

compared to the case of Li^+ (Figure 37) and approached zero at 1.0 M water concentration. Figure 40 shows the results of the experiment where the water concentration was fixed at 0.22 M and the Na^+ concentration in a 1.00 mM anthracene solution in DMF was increased. The i_1 vs i_2 plot was linear with slope of 5.1 $\mu\text{A}/\text{mM}$ and intercept of 5.7 μA . These values are in accord with the calibration slopes of Na^+ and the wave height for 1.00 mM anthracene.

Again, the current depression of the i_2 wave was much less as compared to that in the absence of water. As in the case of An, Li^+ system, the i_1 vs i_2 plot showed an initial induction region, this time up to about 0.20 mM Na^+ .

Figure 41 shows the effect of water on the first (i_1) and second (i_2) reduction waves of fluoranthene. Similar results were obtained for fluoranthene as for anthracene. The limiting currents for both waves decreased linearly

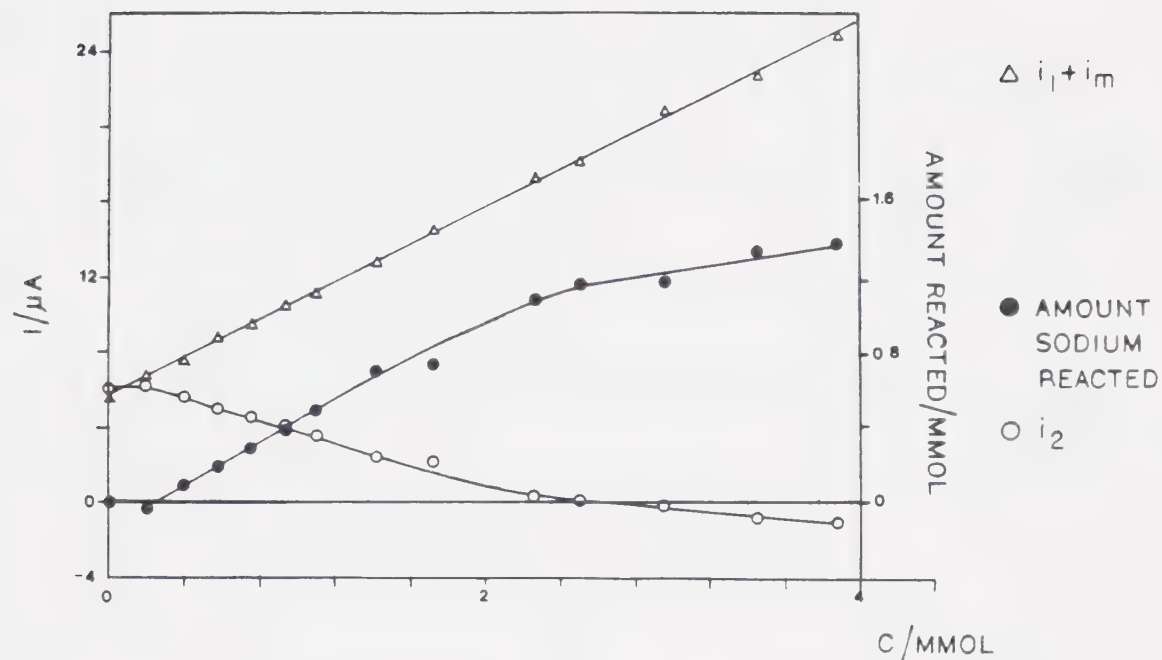


Figure 40. Plots of limiting currents and amount of sodium cation reacted versus sodium cation concentration for mixtures of anthracene and sodium cation containing 0.22 M water in DMF at 25°C. Anthracene concentration fixed at 1.00 mM. Mercury column 57.0 cm.

$i_l + i_m$: combined limiting current for anthracene and sodium cation reductions

i_2 : limiting current for anthracene anion radical reduction

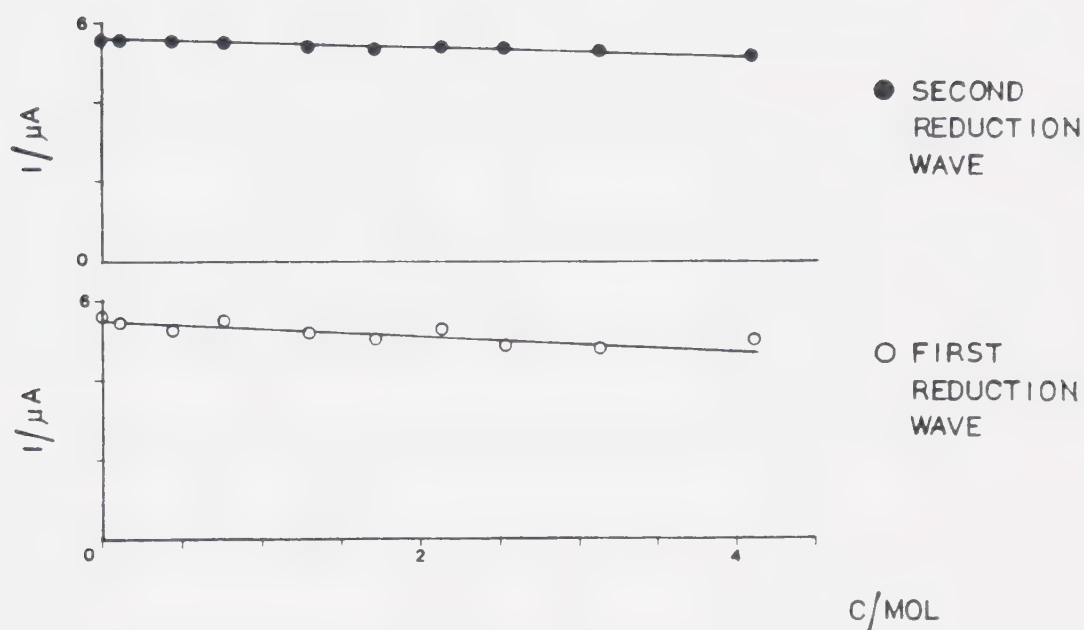


Figure 41. Effect of water addition on the limiting currents of a 1.00 mM fluoranthene solution in DMF at 25°C. Horizontal axis show water concentration. Mercury column 57.0 cm.

by about 10% at 4.1 M water. Eh values for the first wave were approximately constant shifting in magnitude by about 18 mV for the water concentration range studied whereas the Eh values for the second wave shifted positive by about 90 mV. Slope of the E vs $\log ((i_d-i)/i)$ plots for the first wave was unchanged and corresponded to 60 mV for a one-electron reversible wave whereas for the second wave the slope increased slightly from 63 mV to 68 mV for the highest concentration of water used.

The results of water addition to a solution containing 1.00 mM fluoranthene and 1.02 mM Li^+ in DMF are presented in Figure 42. The limiting current for the first wave (i_1), as expected, decreased linearly with water concentration increase as was observed for the addition of water to fluoranthene. The second wave corresponding to $i_m + i_2$, which was not resolved, remained approximately constant until about 1.0 M water

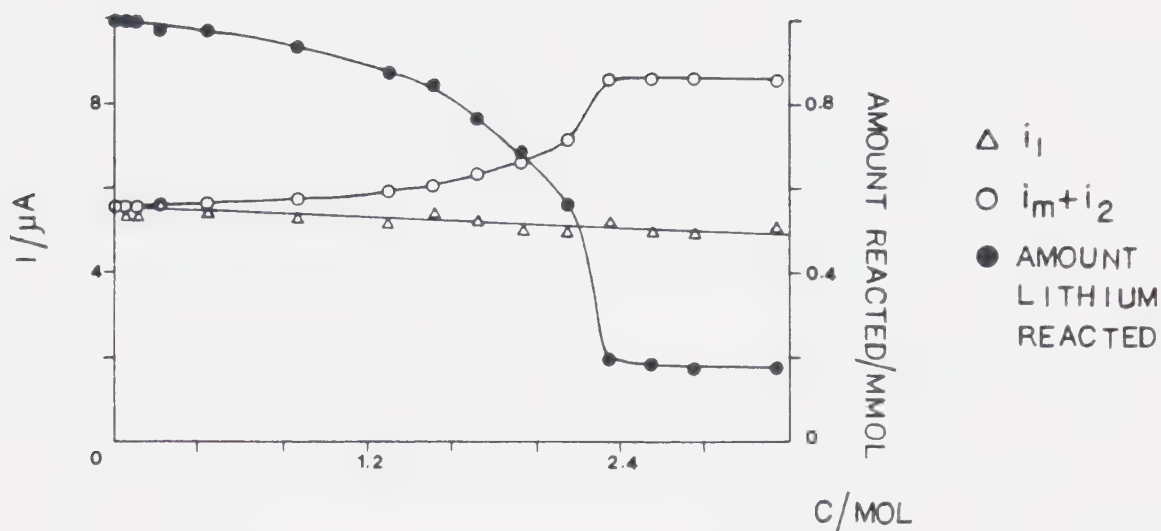


Figure 42. Effect of water addition on the limiting currents and amount of lithium cation reacted for a mixture of 1.00 mM fluoranthene and 1.02 mM lithium cation concentration in DMF at 25°C. Horizontal axis show water concentration. Mercury column 57.0 cm.
 i_1 : limiting current for fluoranthene reduction
 $i_m + i_2$: combined limiting current for lithium cation and fluoranthene anion radical reduction

and then increased before leveling out at a water concentration of 2.34 M. The value of $i_m + i_2$ at the final water concentration of 3.14 M was 8.6 μA . From Figure 41, the limiting current i_2 for the second wave of fluoranthene at 3.14 M water was 5.3 μA . Also, from Figure 35, it can be calculated that at 3.14 M water, the limiting current for 1.02 mM Li^+ is 3.6 μA . The sum of these two waves at 3.14 M water therefore is 8.8 μA which is close to the value of 8.6 μA for the mixture. The mM Li^+ reacted plot (Figure 42) shows that in the absence of water, a value of 1.0 was obtained which decreased and approached zero at high water concentrations.

Figure 43 shows the result for the experiment where the water concentration was fixed at 1.72 M and Li^+ was added to a solution of 1.00 mM fluoranthene in DMF. The value of the first wave (i_1) was constant whereas the $i_m + i_2$ limiting current showed more complex behavior.

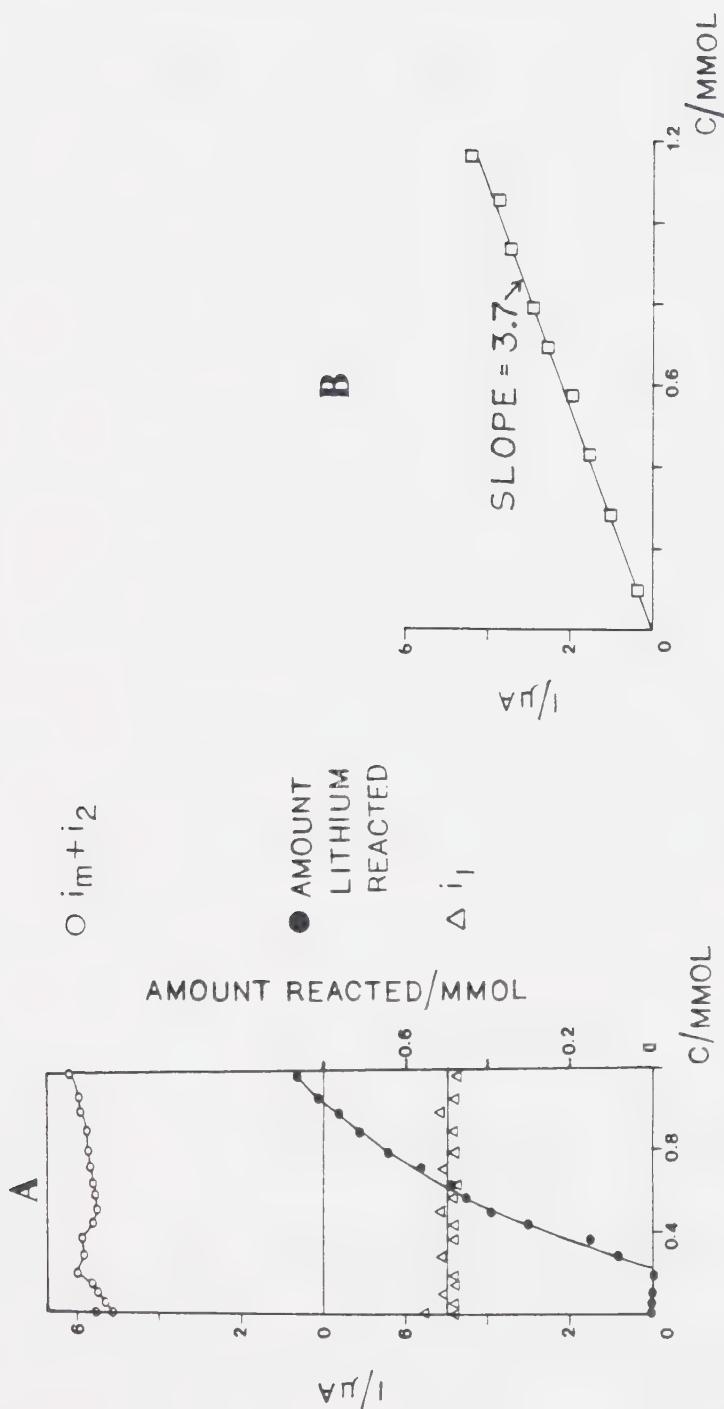


Figure 43. A. Plots of limiting currents and amount of lithium cation reacted versus lithium cation concentration for mixtures of fluoranthene and lithium cations containing 1.72 M water in DMF at 25°C.
 B. Calibration plots for lithium cation in DMF solutions containing 1.72 M water. Mercury column 57.0 cm.
 i_l : limiting current for fluoranthene reduction
 $i_l + i_2$: combined limiting current for lithium cation and fluoranthene anion radical reductions

This result is best presented as the plot of mM Li⁺ reacted vs Li⁺ concentration. Since the Li⁺ reduction wave and the dianion wave were not resolved, to perform the calculations on the mM Li⁺ reacted, a calibration plot for Li⁺ reduction at 1.72 mM water was obtained. The limiting currents from this plot (Figure 43) were then used in subsequent calculations. As in all the other cases, there was an initial induction region corresponding to about 0.20 mM Li⁺, before there was any reaction between the fluoranthene dianion and Li⁺. After the induction region, the mM Li⁺ reacted increased as can be observed from Figure 43.

In Figure 44, the results of water addition to a solution containing 1.00 mM fluoranthene and 2.45 mM Na⁺ are presented. The limiting currents for the first (i₁) and second (i_m) waves again show small decreases due to water addition. In the absence of water, the

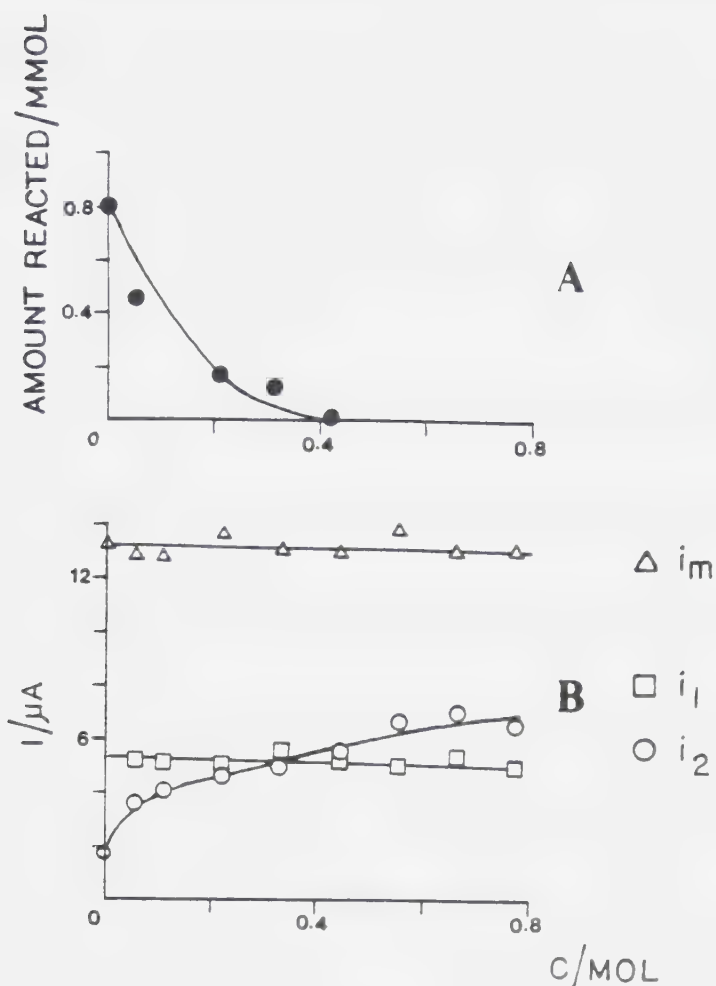


Figure 44. A. Effect of water addition on the amount of sodium cation reacted for a mixture of 1.00 mM fluoranthene and 2.45 M sodium cation in DMF at 25°C.
 B. Effect of water on the limiting currents for the same mixture above.
 Horizontal axis show water concentration.
 Mercury column 57.0 cm.
 i_1 : limiting current for fluoranthene reduction
 i_m : limiting current for sodium cation reduction
 i_2 : limiting current for fluoranthene anion radical reduction

dianion wave gave a depressed current corresponding to only 0.8 mM Na^+ reacted. This is slightly lower than the value of 1.0 mM expected with addition of water. Current depression was again lifted with water addition.

4.4 Discussion

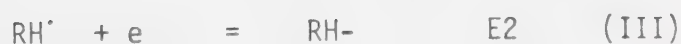
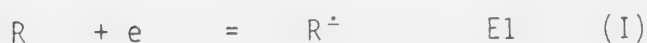
For the An, Li^+ system in DMF at 2.00 mM anthracene and 3.00 mM Li^+ (Figure 34), it is again confirmed that there is a strong interaction between An^- and Li^+ . The data show that at concentrations above 0.60 mM An^- and 0.90 mM Li^+ the amount of Li^+ reacted with An^- is 100%. A 100% reaction is expected since it has been shown that An, Li^+ reacts in the ratio 1:3 whereas in this case the An, Li^+ ratio is only 1:1.5. The proposal that there is a competition between trace proton donors and metal cations for An^- was verified by the results obtained at low concentrations in the dilution experiment. Obviously, at concentrations below

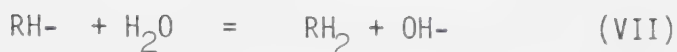
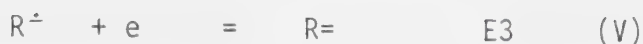
0.09 mM anthracene and 0.15 mM Li^+ , the rate of protonation of An^- is faster than An, Li^+ interaction so that the former predominates. At concentrations in between those mentioned, both processes occur to a varying degree.

The addition of water does not seem to affect the electrochemical behavior of the aromatic hydrocarbons and the alkali metal cations very much. The stability of the anion radicals is evidenced by the slopes of the E vs $\log ((i_d - i)/i)$ plots. These plots show that there is no deviation from one-electron reversible reduction behavior. The small changes in E_h values of the first reduction wave of the hydrocarbons and the decrease in the limiting currents are attributed to changes in dielectric properties of the solvent and diffusion constants of the species. The limiting current of the second wave is affected to the same extent as the first wave and approximate equality of the wave heights at all water concentrations used are main-

tained. However, the Eh values are affected more, shifting positive by about 50 mV for anthracene and 90 mV for fluoranthene. Further, the slopes of the E vs $\log((i_d-i)/i)$ plots tend to increase in the presence of water, indicating the increasing irreversibility of the second wave arising from increasing proton addition to the dianions. These effects have been discussed in previous studies (4,25). At concentrations of water in DMF in the region of 5% or less, water is effectively solvated and is thus unable to react with the anion radicals of both anthracene and fluoranthene. Similar results have been obtained for aromatic hydrocarbons in DMF and dioxane (4,25). Therefore, in the concentration range used, the addition of water does not affect the mechanism of reduction of anthracene and fluoranthene in DMF which involve two successive one-electron transfers, the first of which forms a stable anion radical and the second the unstable dianion.

The same can not be said of acetonitrile. Results obtained for the reduction of anthracene and fluoranthene in the presence of water in acetonitrile have indicated that there is a change in the mechanism of hydrocarbon reduction. As a result no further studies were conducted in this solvent and the results were not presented in the previous section. However, it was observed that in the presence of water, the stability of the anion radicals is affected. The first wave was observed to increase in height at the expense of the second wave which suffers a reduction in wave height. The same results have been observed in dioxane-water mixtures with increasing water concentration (23). Therefore the mechanism now becomes





For alternant hydrocarbons e.g. anthracene, it is known that E2 is positive of E1. At sufficiently high water concentrations, the second wave is nonexistent and the first wave doubled in height corresponding to a two-electron wave. It is apparent that the ability of DMF to complex water causes the water activity to be lower in DMF than in acetonitrile, which has very low acidic and basic properties.

The results obtained for the addition of water to the An:Li⁺,Na⁺ and Fa:Li⁺,Na⁺ systems in DMF further substantiates the conclusion made in Chapter 3 and the discussion at the beginning of this chapter. For the solution mixture

studied, namely 1.00 mM An and 3.83 mM Li⁺, 1.00 mM An and 3.92 mM Na⁺, 1.00 mM Fa and 1.02 mM Li⁺, and 1.00 mM Fa and 2.45 mM Na⁺, the results (Figures 37, 39, 42, 44) in the initial absence of water confirmed the stoichiometries of the dianion-cation interaction obtained in Chapter 3. It is important to note that in all the experiments with so many variations in mixing, the stoichiometries have always remained the same. Here, the An,Li⁺ stoichiometry was again found to be 1:3, the An,Na⁺ gave 1:2 and both the Fa,Li⁺ and Fa,Na⁺ systems gave 1:1 stoichiometry.

The limiting currents of the dianion wave in all cases behaved as expected in the presence of water. The highly depressed values for An:Li⁺ and An,Na⁺ in the absence of water began to increase on addition of water, this indicative of decreased dianion-cation interaction. At high enough water concentrations, the limiting currents approached a value equal to that for the reduction of 1.00

mM An alone. This means that the protonation reaction dominates the dianion-cation interaction. The same can be said of the Fa,Na^+ system except that the interaction in the absence of water leads to a smaller depressed value for the Fa,Li^+ system. The calculation in the previous section again showed that in the presence of enough water, the $i_{\text{m}} + i_{\text{2}}$ limiting current gave a value expected in the total absence of Fa,Li^+ reaction.

Clearly, the disappearance of current depression in the presence of water gives evidence that hydroxyl ions are not responsible for current depression. Further, the results complement that obtained in the dilution experiment. In the dilution experiment, the concentration of the hydrocarbon and the metal ions are brought down to a level where the trace proton donors can compete favorably for the dianions whereas the addition of water brings the concentration of proton donors up to a level for the same

effect.

For the above cases (Figures 37, 39, 42, 44) little need be said concerning the variations of the i_l , i_l+i_m and i_m limiting currents with the addition of water because the values and the slopes found in all cases were in agreement with what has been said in Chapter 3 except for small differences due to changes in diffusion constants arising from the addition of water. However, the plots of amount of metal cation reacted vs. water concentration show a very interesting difference between Li^+ and Na^+ . From Figures 37, 39, 42 and 44, it can be seen that in the case of Li^+ with both An and Fa, the amount of Li^+ reacted decreased only slowly at lower concentrations of water whereas Na^+ with both the aromatic hydrocarbons decreased sharply with the addition of water. This points strongly to a faster dianion- Li^+ reaction as compared to the dianion- Na^+ reaction.

The establishment of a competitive reaction between water and metal cations for dianions provides the basis for kinetic studies of dianion-cation reaction. This can be done if conditions are controlled so that both interaction and protonation reactions can proceed. These conditions can be fulfilled with the proper choice of water concentration so that the protonation reaction does not far outrun the dianion-cation reactions for the range of metal cation concentrations used (up to 4 mM). Thus, from the results of water addition experiments (Figures 37, 39, 42, 44) the water concentration chosen for the An:Li^+ system was 1.72 M and for the An:Na^+ system was 2.14 M. The results for these experiments where the water concentration is fixed has been reported in the previous section (Figures 38, 40, 43). Again, the variation of the limiting currents i_l , i_l+i_m and i_m with metal concentration shows (except for small decreases in values due to changes in

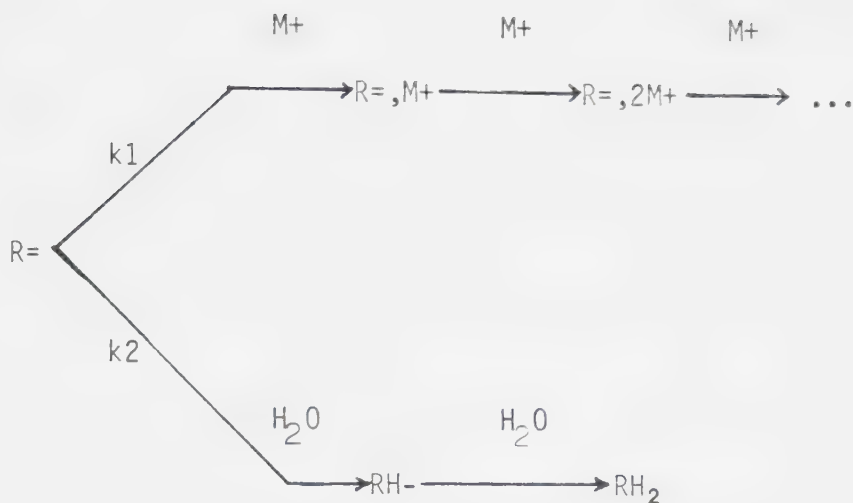
diffusion constants as a result of the presence of water) essentially the same behavior. The depression of the dianion wave for the An,Li⁺ and An,Na⁺ systems, as expected, was smaller as compared to the situation where no water was added (Figures 38, 40). In the An,Li⁺ case, the current had only small negative values at high Li⁺ concentrations. In the An,Na⁺ system, no negative values were obtained at all Na⁺ concentrations. However, the fact that current depression was observed shows that dianion-cation interaction occurred.

Complex behavior was seen for the second wave of the Fa,Li⁺ system in DMF. In the absence of water, this wave, which corresponds to the combined Fa⁺ and Li⁺ reductions, remained constant with the addition of Li⁺ slightly past 1.00 mM Li⁺. However, in the presence of water, at small Li⁺ concentration the $i_m + i_2$ limiting current increased as the protonation reaction is more favorable under these

conditions. At higher concentrations of Li^+ , the current decreased since the Fa, Li^+ reaction became more effective and could compete favorably (Figure 43).

Induction regions were observed in all cases for the amount of cation reaction vs cation concentration plots (Figures 38, 40, 43). The explanation for these is quite simple. Since considerable amounts of water are present initially, protonation of the dianions proceeds very fast. Introduction of small amounts of the metal cations initially have negligible effects. However, with continued addition of metal cations, a concentration of the cations is reached where the dianion-cation reaction is initiated, and at increasing metal cation concentration, the rate increases and becomes competitive with protonation.

The kinetic treatment for the competitive reactions is based on the following model and assumptions:



where $R=$ represents the aromatic hydrocarbon dianions, M^+ the metal cations, and k_1 , k_2 the rate constants for the dianion-cation reaction and the protonation reaction respectively.

It is assumed that the $R=$ which are formed are rapidly and completely destroyed through reaction with M^+ and water. This is reasonable because of the very reactive nature of the dianions and the well known fact that the dianions are rapidly protonated even in aprotic solvents without the addition of water. Further, it is assumed

that the R:M⁺ reactions are strong and follow fixed stoichiometries. These stoichiometries have been established to be 1:3 for An,Li⁺, 1:2 for An,Na⁺, 1:1 for Fa,Li⁺ and Fa,Na⁺. Therefore, even though the R,M⁺ reactions may be stepwise, after the initial reaction of one M⁺, the complexation continues until the stoichiometries are satisfied. For this reason, no kinetic studies have been made for K⁺ and Rb⁺ since results have shown that R:K⁺,Rb⁺ reactions are not strong reactions and therefore the above assumptions will not be true for those cations.

From the above discussion, it follows that

$$[R=]_{\text{total}} = [R=]_{\text{reacted with M}^+} + [R=]_{\text{reacted with water}} \quad (4.1)$$

Also,

$$y = \frac{[R=]_{\text{reacted with M}^+}}{[R=]_{\text{total}}} = \frac{k_1[M^+][R=]}{k_1[M^+][R=] + k_2[H_2O][R=]} \quad (4.2)$$

and

$$x = \frac{[R=]\text{reacted with } H_2O}{[R=]\text{total}} = \frac{k_2[H_2O][R=]}{k_1[M^+][R=] + k_2[H_2O][R^2=]} \quad (4.3)$$

Rearrangement gives

$$y = \frac{[R=]\text{reacted with } M^+}{[R=]\text{total}} = \frac{[M^+]}{[M^+] + (k_2/k_1)[H_2O]} \quad (4.4)$$

and

$$x = \frac{[R=]\text{reacted with } H_2O}{[R=]\text{total}} = \frac{[H_2O]}{(k_1/k_2)[M^+] + [H_2O]} \quad (4.5)$$

The above approach is similar to the common method of determining relative rates of competing reactions from analysis of reaction products. Both the values of x and y are experimentally available. For the present purpose the equation above involving y is used. Thus the parameter of y is calculated from the values of amount of cation reacted which were plotted in Figures 38, 40, and 43. For example, in the

case of An,Li⁺ system, y is obtained by dividing the amount of Li⁺ reacted by 3 and then dividing by the bulk concentration of anthracene, which is 1.00 mM. Similarly, for the An,Na⁺ system, the amount of Na⁺ reacted is divided by 2 and the Fa,Li⁺ system by 1. It should be pointed out that these divisors are merely the stoichiometries of the dianion-cation complexes and follow from the assumptions made earlier. The y values so obtained are plotted against metal concentration in Figures 45-47. From these plots, it can be seen that the initial induction regions occur in all cases. These are expected because the data are calculated from those of Figs 38, 40 and 43 where the induction region exists. From equation (4.4), it can be seen that when $(k_2/k_1)[H_2O] \gg [M^+]$, then equation (4.4) reduces to

$$y = \frac{[M^+]}{(k_2/k_1)[H_2O]} \quad (4.6)$$

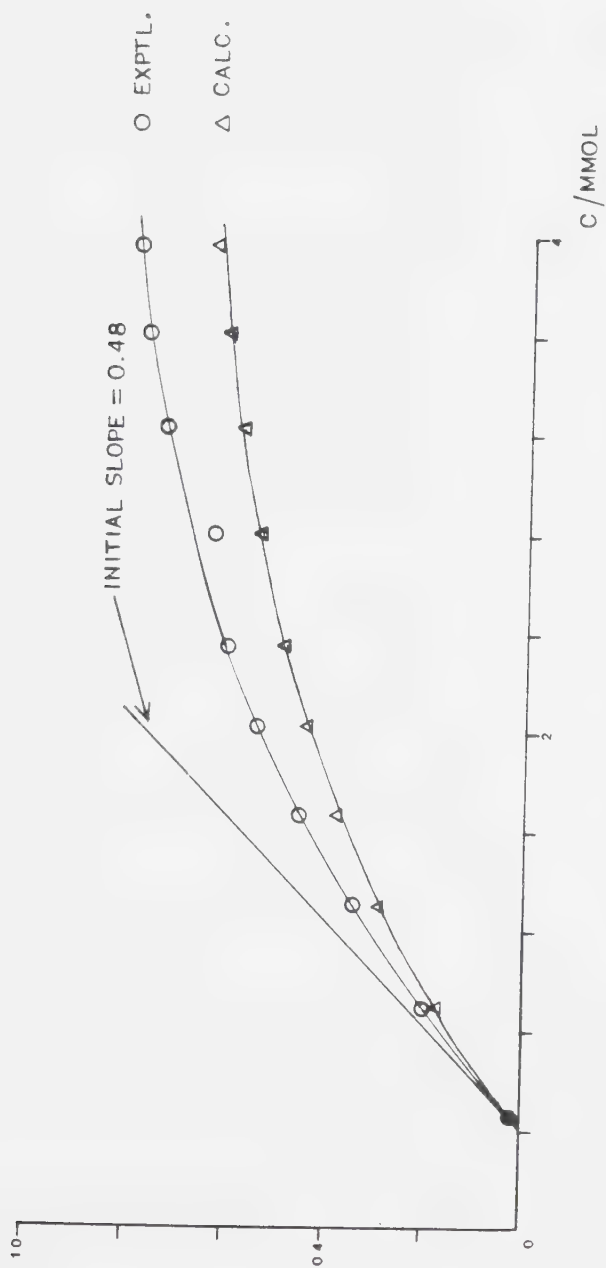


Figure 45. Plot of Y versus lithium cation concentration for mixtures of anthracene and lithium cation containing 2.14 M water in DMF at 25°C. Anthracene concentration fixed at 1.00 mM. Mercury column 57.0 cm. $Y = [\text{An}]_{\text{reacted}}/[\text{An}]_{\text{total}}$

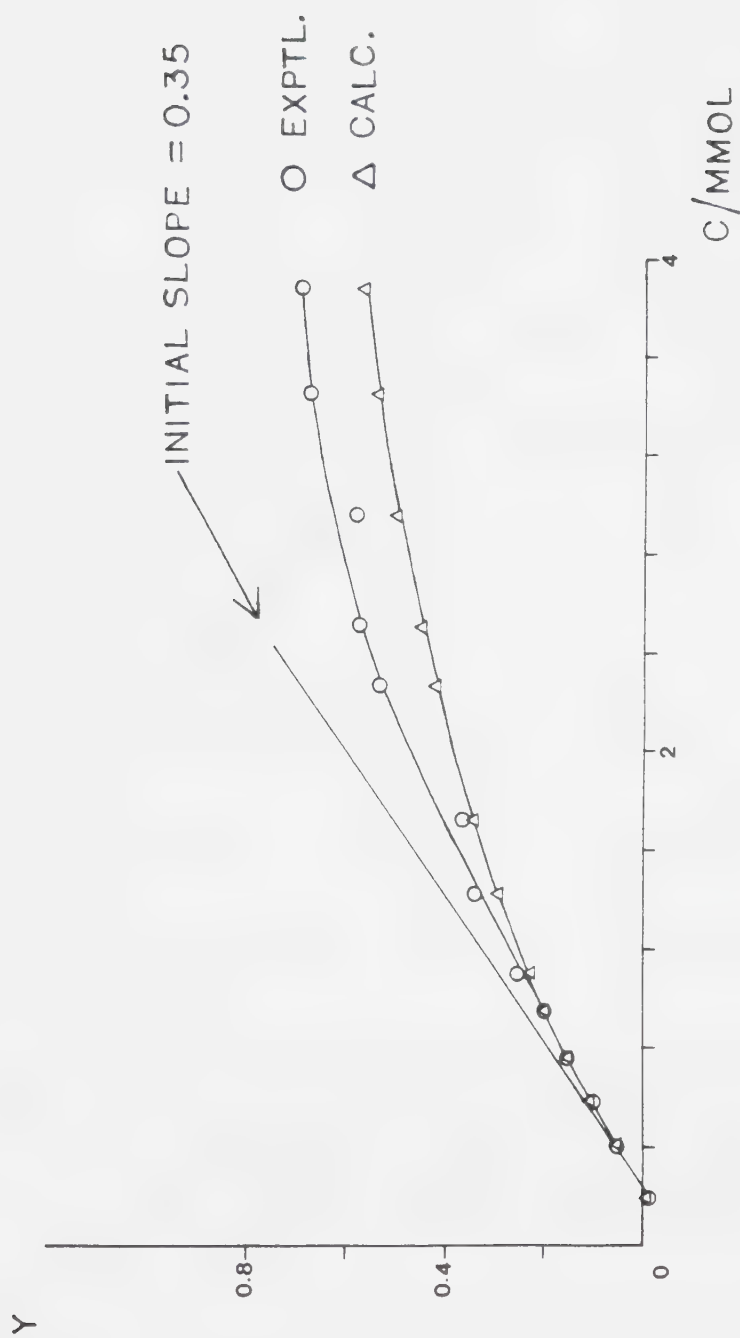


Figure 46. Plot of Y versus sodium cation concentration for mixtures of anthracene and sodium cations containing 0.22 M water in DMF at 25 C. Anthracene fixed at 1.00 mM. Mercury column 57.0 cm. $Y = [\text{An}]_{\text{reacted}}/[\text{An}]_{\text{total}}$

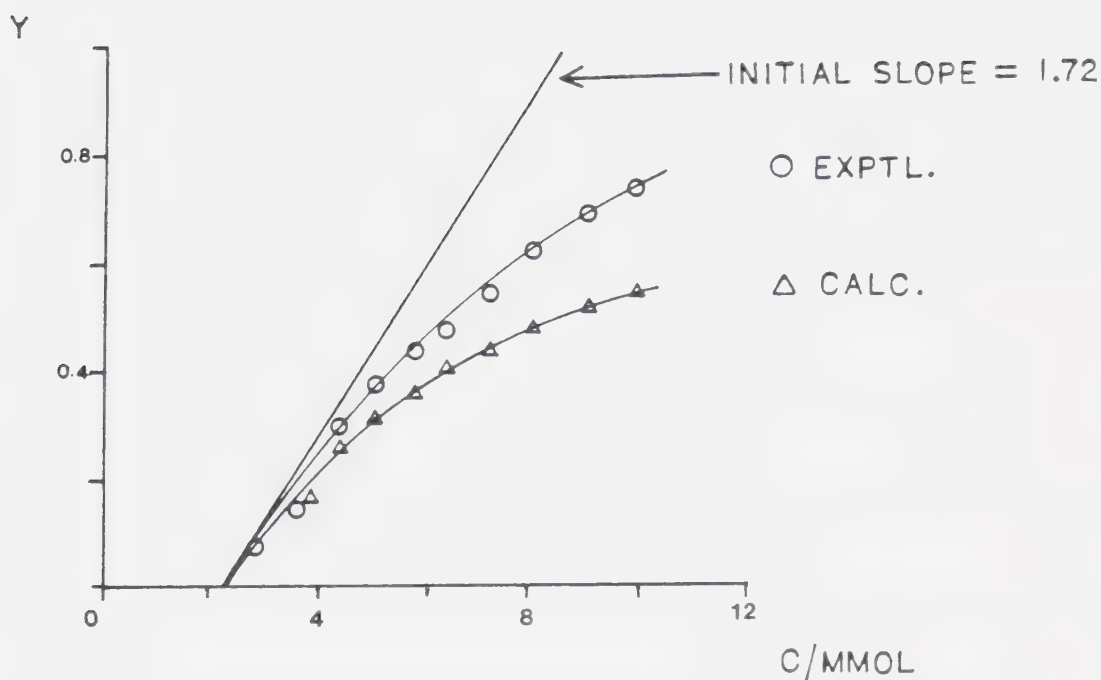


Figure 47. Plot of Y versus lithium cation concentration for mixtures of fluoranthene and lithium cation containing 1.72 M water in DMF at 25°C. Fluoranthene fixed at 1.00 mM. Mercury column 57.0 cm. $Y = [\text{Fa}]_{\text{reacted}} / [\text{Fa}]_{\text{total}}$.

Therefore, at low cation concentrations, the plots should be approximately linear with slope $(k_1/k_2)[H_2O]$. To a first approximation, this is found to be so as can be seen from Figures 45-47. The values of the slopes thus obtained are tabulated in Table 3. From these slopes, the ratios of the rate constants k_1/k_2 are calculated. These ratios are $1.0e3$, 80 and $2.8e3$ for the An,Li⁺, An,Na⁺ and Fa,Li⁺ systems respectively. If the rate constants k_2 for the protonation of the dianions are known then the rate constants k_1 for the dianion-cation interactions can be calculated. There have been many studies of the protonation of the anion radicals of aromatic hydrocarbons by such proton donors as alcohols and water (228-230). However, the protonation of dianions has not been thoroughly studied. Values ranging from $1.0e8$ to $1.0e10$ /M s have been given (231,232). No data for the protonation of fluoranthene dianion is available. Here

Table 3. Estimated Rate Constants**

System	$\frac{[H_2O]}{7M}$	$k_1/k_2[H_2O]$	k_1/k_2	$\frac{k_2}{/M^{-1}s^{-1}}$	$\frac{k_1}{/M^{-1}s^{-1}}$
An:Li+ in DMF	2.14	0.48	1.0e3	1.0e9	1.0e12
An:Na+ in DMF	0.22	0.35	80	1.0e9	0.8e10
Fa:Li+ in DMF	1.72	1.62	2.8e3		-
Fa:Na+ in DMF	-	-	-		

**Continued next page.

Table 3 Continued

System	$\frac{[D_2O]}{M}$	$k_1/k_2[D_2O]$	k_1/k_2	$\frac{k_2}{M^{-1}s^{-1}}$	$\frac{k_1}{M^{-1}s^{-1}}$
An:Li+ in DMF	2.14	0.45	0.9e3	1.1e9	1.0e12
An:Na+ in DMF	0.22	0.38	80	1.0e9	0.8e10
Fa:Li+ in DMF	-	-	-		
Fa:Na+ in DMF	-	-	-		

the rate constant for the protonation of anthracene dianion will be taken to be 1.0×10^9 /M s. The rate constants for the $An^=,M^+$ interaction are 1.0×10^{12} and 8.0×10^{10} /M s for Li^+ and Na^+ respectively.

The rate constants for the diffusion controlled reactions between two ions is given by the Debye extension of the Smoluchowski equation (233,234)

$$k(d) = [(8RT/3000n'')] [0/(e^0 - 1)] \quad (4.7)$$

$$\text{where } 0 = Z(A)Z(B) e^2 / \epsilon kTa \quad (4.8)$$

a =distance of closest approach of ions

ϵ =dielectric constant of solvent

n'' =viscosity

e =electronic charge

$Z(A), Z(B)$ are the charge numbers of the ions.

The other terms have their usual meaning.

For DMF the viscosity is 0.802 c.p.(25°C) and at 25°C the

term $8RT/3000n$ has the value 1.0×10^{10} /M s. Since the dianions and metal cations have charges -2 and +1 respectively and assuming that the distance of closest approach is approximately 2.8 \AA (using 2.1 \AA for the An^- , estimated from covalent bond lengths, and 0.7 \AA for ionic radius of lithium).

Then

$$\phi = \frac{(-2)(+1)(4.8 \times 10^{-10})}{(3.7)(1.38 \times 10^{-16})(296)(2.8 \times 10^{-8})}$$

$$= -109$$

Therefore $k(d) = 1.1 \times 10^{12}$ /M s.

Based on a similar approach, $k(d)$ for Na^+ , K^+ and Rb^+ (ionic radii 1.0 , 1.3 , and 1.5 \AA respectively) can be calculated to be 9.8×10^{11} , 9.0×10^{11} , and 8.5×10^{11} /M s. The experimental value obtained for the $\text{An}:\text{Li}^+$ system in DMF was 1.0×10^{12} /M s which is in very good agreement with the calculated value above.

This value is over an order of magnitude larger than for Na^+ which has an experimentally determined rate of $8.0 \times 10^9/\text{M s}$.

Therefore, the rate of ion pair formation obtained for $\text{An}:\text{Li}^+$ in DMF is very close to the diffusion controlled limit and that for $\text{An}:\text{Na}^+$ about 10 times less than diffusion controlled. These are not too surprising because ion pair formations have been consistently found to be very fast reactions. For example, in tetrahydrofuran, the association of benzophenone anion radical has a rate constant of 1.1×10^{11} and in carbon tetrachloride-nitrobenzene mixture, tetra-*n*-butylammonium bromide has an association rate constant of $1.3 \times 10^{11}/\text{M s}$ (see reference 217, p. 443). It was noted that these rate constants are within a factor of 4 of the computed values for diffusion control.

The experimentally determined rate constants are expected to be a bit high because the actual activity of water in DMF is in all probability lower than the added value. This

is because DMF molecules have the ability to complex water and therefore decrease its activity. Further, very accurate values for the rate constant for protonation of anthracene were not available. The value of $1.0 \times 10^9 \text{ M}^{-1} \text{ s}^{-1}$ used in this study was an estimated figure. Therefore an error range of about half an order of magnitude is to be expected for the determined rate constants, which would occur on the high side from the discussion above. Even so, considering the approximate nature of the reactions, the experimentally determined values are good estimates considering what is known about the rate constants for ion pair formation and taking the other factors into account.

The computed values for the rate constants, based on the distance of closest approach being the sum of the radius of the anthracene molecule and the ionic radius of the cation, shows that the $\text{An}=\text{:Li}^+$ system should be about 10 times faster than the $\text{An}=\text{:Na}^+$ system. However, experimentally,

$\text{An}=\text{Li}^+$ was found to be 100 times faster. For contact ion pair formation, the solvent sheath has first to be removed. The solvation of Li^+ cation by DMF molecules is much stronger than that of Na^+ . The fact that the formation of $\text{An}=\text{Li}^+$ ion pair being 100 times faster than the $\text{An}=\text{Na}^+$ ion pair does not reflect the differences in solvation. The possible explanation is that the initial $\text{An}:\text{M}^+$ reaction involves a solvent separated ion pair which on formation expels the solvent molecules to give the contact ion pair which is the thermodynamically favored species.

Since no data for the rate constant for the protonation of $\text{Fa}=\text{}$ is available, the rate constant for $\text{Fa}:\text{Li}^+$ reaction cannot be calculated. Polarographic data point to the fact that $\text{Fa}=\text{}$ is less basic than $\text{An}=\text{}$ since the E_h value for the $\text{Fa}=\text{}$ wave is positive to that of the $\text{An}=\text{}$ wave by 170 mV. Therefore, it is expected that protonation of $\text{Fa}=\text{}$ is slower. The higher value of 2.8×10^{-3} obtained

for k_1/k_2 for this system as compared to 1.0×10^3 for the An, Li^+ system is likely due, in major part, to this lower basicity.

Figures 45-47 also show the plots of the computed values of the y parameter in equation (4.4). In order to obtain these computed values, the experimental slopes which corresponded to $(k_1/k_2)[\text{H}_2\text{O}]$ are substituted into equation (4.4). This equation is then transformed into

$$y_{\text{calc}} = \frac{([\text{M}^+] - a)}{\text{slope} + ([\text{M}^+] - a)} \quad (4.9)$$

where the constant a refers to the concentration of M^+ corresponding to the induction region. As can be seen from the figures, the agreement at low M^+ concentrations is good but at higher M^+ concentrations the computed values are lower than the experimental values. However, since the other constants are derived from data at the low

concentration end, these deviations are not of too much concern.

As a further check of the model, experiments were also carried out for the An:Li^+ and An:Na^+ systems employing heavy water instead of water. The same concentrations of D_2O as H_2O were used and the results were treated similarly. Table 3 shows that the ratios of k_1/k_2 for the An:Li^+ and An:Na^+ systems are $9.0\text{e}4$ and 80 respectively. Since the rate constants for association of the dianion and cations are independent of whether H_2O or D_2O are used and therefore should remain unchanged, the values of k_2 are calculated to be $1.1\text{e}9/\text{M s}$ for the An:Li^+ system and $1.0\text{e}9$ for the An:Na^+ system. These values are essentially the same as the assumed value of $1.0\text{e}9/\text{M s}$ for the protonation of An^- . Therefore, it is concluded that the protonation of An^- does not show any kinetic isotope effect. Rainis and Szwarc(231) have observed,

that due to the high basicity of An^- , the transition state of its protonation resembles the final state and therefore significant kinetic isotope effect is not expected. The present results support this observation.

Chapter 5 Electrochemical Studies of Tetracyanoethylene (TCNE) and 7,7,8,8-Tetracyanoquinodimethane (TCNQ). The Effect of Countercations.

5.1 Introduction

As already mentioned in Chapter 1, there has been great interest in TCNE and TCNQ since their discovery. These substances have exceptional properties. In particular, intense interest is generated in the organic conducting salts and high conducting charge-transfer complexes formed by those compounds (153,155).

The presence of the four electron-withdrawing cyano groups means that the olefinic and quinoid functionalities of TCNE and TCNQ respectively are electron deficient. The ease with which these molecules are reduced is quite remarkable. For example, they have been reported to undergo a one-electron transfer to form the anion radicals by metals (124,152), by UV light irradiation (133), by CN^- ion (124) and even by certain basic solvents such as

dimethylsulfoxide and dimethylformamide. Formation of anion radicals in these solvents appears to be faster in the presence of light (135-137). The anion radicals are stable in solution in the absence of oxygen and water (124,163).

Relatively few electrochemical studies have been made. The determination of fundamental electrochemical parameters such as the reduction potentials and standard rate constants are useful for testing of theories and in many applications. For example, electrode potentials can be correlated to molecular orbital energies and electron affinities. The conducting salts and complexes formed by TCNE and TCNQ have been employed in batteries (235), photocells (236), electrochromic systems (237) and potentiometric ion selective sensors (238). Knowledge of electrochemical parameters in general is necessary for better understanding of these systems.

In general, the reduction of TCNE and TCNQ to their anion radicals has been found to be electrochemically reversible. Peover (128,129) found this to be so polarographically in dimethylformamide, acetonitrile, chloroform, and methylene chloride. He also found this to be so for the reduction of $\text{TCNE}^{\cdot-}$ to $\text{TCNE}^=$ in methylene chloride and $\text{TCNQ}^{\cdot-}$ to $\text{TCNQ}^=$ in chloroform and methylene chloride. The supporting electrolyte used was tetra-n-butylammonium perchlorate. Sharp studied the first reduction of TCNE and TCNQ at different electrodes and in different solvents (148,149). In acetonitrile, the standard rate constants for TCNE were found to be 0.159 cm/s at platinum, 0.390 cm/s at gold and 0.0019 cm/s at graphite. For TCNQ, the values were 0.260, 0.208 and 0.0035 for platinum, gold and graphite respectively. Rate constants were also determined in dimethylformamide, dimethylsulfoxide and propylene carbonate at platinum and gold electrodes.

Diffusion coefficients for TCNE were found to be 1.91×10^{-5} and 2.8×10^{-6} cm/s in acetonitrile and propylene carbonate respectively. In the case of TCNQ these values were 1.45×10^{-5} cm/s in acetonitrile, 6.7×10^{-6} cm/s in dimethylformamide, 2.7×10^{-6} cm/s in dimethylsulfoxide and 2.8×10^{-6} cm/s in propylene carbonate.

Although these studies invariably found the first reduction to be reversible, there seems to be some inconsistency in the reduction of TCNE^+ to TCNE^{\cdot} . For example, Mulvaney et al (239) reported this reduction to be reversible at 100 mV/s scan rate, using lithium perchlorate as supporting electrolyte in acetonitrile at a platinum electrode. Sharp noted that this wave was irreversible in acetonitrile at a graphite electrode using lithium perchlorate as supporting electrolyte under similar conditions (148). Jeanmaire et al (138) found this wave to be quasireversible in acetonitrile using a platinum elec-

trode. However, the supporting electrolyte used was tetra-
n-butylammonium perchlorate. They proposed a change in
geometry in going from a planar TCNE⁺ to a nonplanar
TCNE= as a possible explanation. Pons et al (139) reported
similar results using a platinum electrode in acetonitrile
with tetra-n-butylammonium tetrafluoroborate as supporting
electrolyte. According to them this behavior could be due
to one of several causes such as complexation of the anion
radical by the electrolyte, distortion of the TCNE⁺ or
adsorption of electrolysis products. FTIR spectroelectro-
chemistry confirmed the existence of adsorption.

The causes of the discrepancies could be the result of
electrode material or supporting electrolyte. To date, no
study of the countercation effect has been undertaken.

In Chapter 3, the electrochemical behavior of aromatic
hydrocarbons has been found to be dependent on the counter-
cations used. It should be interesting to examine these

effects on a different class of compounds. The presence of the four cyano groups in TCNE and TCNQ imparts high electron affinity to these molecules and also higher stability to the negative ions as compared to the hydrocarbons. Therefore, the dianions are not as reactive as their aromatic hydrocarbons counterparts. As a result, they are reduced at more positive potentials which means that the use of solid electrodes does not present any problems.

This chapter describes the use of cyclic voltammetry and chronoamperometry to study the reduction of TCNE and TCNQ to their anion radicals and dianions at glassy carbon and platinum electrodes. The effect of different counter-cations is also studied. The species formed during electrolysis are identified using modulated specular reflectance spectroscopy.

5.2 Experimental

5.2.1 Instrumentation

The modulated specular reflectance (MSRS) technique was described in Chapter 1. A schematic diagram of the instrumentation is given in Figure 48. The lamp source was a 200 watt Hg-Xe arc lamp. Light from the source passed through a GCA MacPherson 201 monochromator. The light reflected from the electrode was detected by means of a RCA 31000M photomultiplier (PMT). The signal from the PMT was taken through a Kronheit filter operated in the band pass mode to pass the modulation frequency of interest. The output was taken into the lock-in-amplifier (LIA, Benthams 223). The output from the LIA, after going through a current-to-voltage conversion and amplification stage, yielded the spectrum of interest.

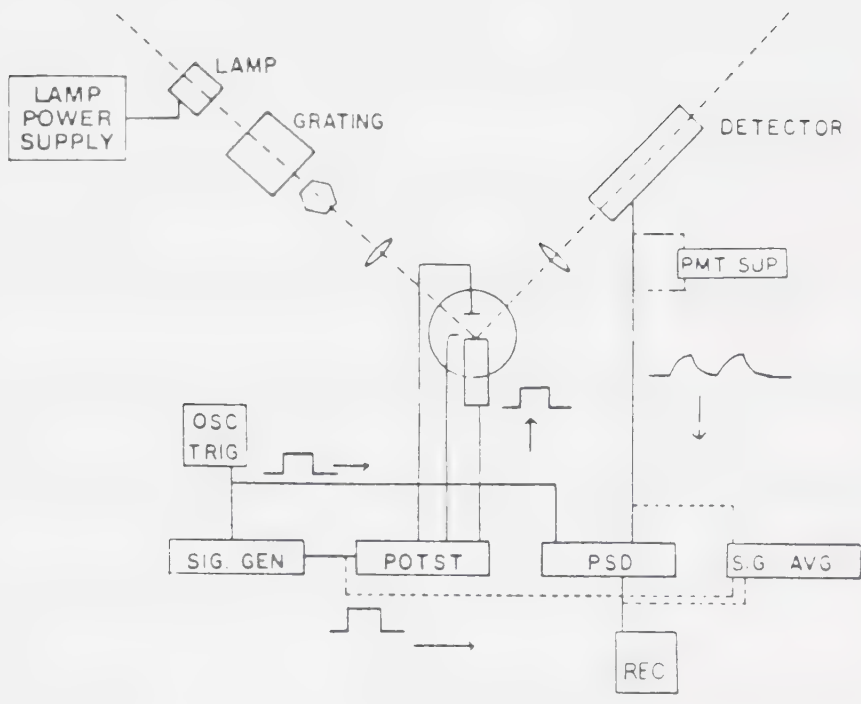
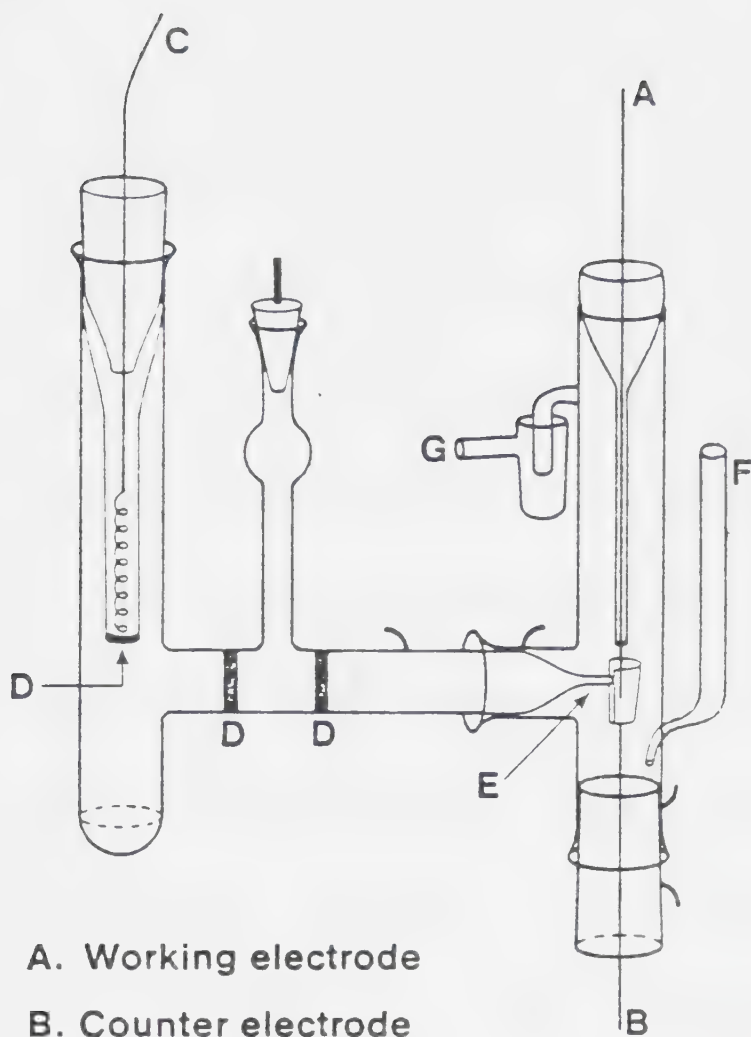


Figure 48. Instrumentation for MSRS.

POTST:	Potentiostat
PSD:	Phase Sensitive Detector
SIG AVG:	Signal Averager
PMT SUP:	Photomultiplier Supply
OSC TRIG:	Oscillator Trigger
SIG GEN:	Signal Generator
REC:	Recorder

The working electrode was a 7 mm diameter polished platinum button attached to the end of a brass rod which had been forced into a heated 9 mm (o.d.) Kel-F tube which shrunk on cooling to give a tight seal. The potential of this electrode was controlled by a HiTek DT 2101 potentiostat. Potential waveform pulses were supplied by a HiTek PPR1 waveform generator which was triggered by square wave pulses from a Global Associates function generator at the required frequency (40Hz). Normalized reflectance-time transients were signal averaged by a signal averager. The cell arrangement used for the MSRS experiment is shown in Figure 49. The quartz windows through which light passed in and out of the cell were positioned at 45 degrees each to the axis along the length of the electrode.

The electrochemical cell used in cyclic voltammetric and chronoamperometric experiments is shown in Figure 50. Two materials for the working electrodes were used. The



- A. Working electrode
- B. Counter electrode
- C. Reference electrode
- D. Frit
- E. Luggin
- F. Gas inlet
- G. Gas Exit

Figure 50. Cell configuration for the voltammetric and chronoamperometric experiments.

platinum working electrode consisted of a platinum wire sealed into glass and connected to the external circuit by a copper lead soldered to the platinum wire. The carbon electrode was made from a piece of glassy carbon rod (3 mm diameter, Tokai) sealed into a glass tubing with epoxy. The end of the carbon rod which was leveled with the end of the glass tubing was polished to a mirror finish with alumina on a polishing cloth. The result was a circular planar glassy carbon electrode. Mercury was then put into the glass tubing to contact the carbon rod. A piece of copper wire was then dipped into the mercury and the external contact was made to this copper wire. The potentiostat used to control the potential of the working electrode with respect to the reference electrode and the waveform generator were the same instruments as those used for the MSRS experiment. The potential ramp for the cyclic voltammetric experiments and the potential steps for the

chronoamperometric experiments were introduced into the adder input of the potentiostat. The reference electrode (Ag/Ag^+) was the same as that used for the polarographic experiments (see Figure 3). The reference solution was 0.01 M AgNO_3 , 0.1 M in the supporting electrolyte in the same solvent as that for the experiments. Recording of experimental curves was made with a Linseis LX1000 recorder which could be operated either in the x-y (voltage-current) or y-t (current-time) mode.

5.2.2 Purification of Chemicals

Purification of lithium and sodium perchlorates, tetra-n-butylammonium tetrafluoroborate and acetonitrile has been described previously (see Chapter 3). Tetra-n-ethyl perchlorate (TEAP) (Eastman, reagent grade) was recrystallized twice from triply distilled water. It was dried in vacuo at 70°C . Commercial reagent grade TCNE

and TCNQ were obtained from Eastman. The TCNE was recrystallized twice from chlorobenzene (148) and TCNQ recrystallized twice from acetonitrile (240). The dried crystals of TCNE melted at 200-201°C while those of TCNQ melted at 294-295°C. These values agreed with those reported in the literature (148).

5.2.3 Procedure

From Figure 50, it can be seen that the cell used for cyclic voltammetric and chronoamperometric experiments consisted of two separated parts. The part which included the Luggin probe was filled with the background solution i.e. the solvent containing 0.10 M of the supporting electrolyte. The other compartment contained a solution of the electroactive species of interest. Concentrations of electroactive species used were in the millimolar range. In all cases, experiments were performed at room tempera-

ture. This temperature was found to be $(23.0 \pm 0.5)^{\circ}\text{C}$ throughout the period in which these experiments were performed. Deaeration of solutions was carried out by bubbling purified nitrogen through the cell.

The Luggin probe was placed as close as possible to the working electrode to reduce iR loss. Further, positive feedback was employed for the same purpose. It was estimated that the iR loss under these circumstances was not more than the error in reading potentials from the recorded voltammograms (± 5 mV). In all cyclic voltammetric experiments, the scan rate used was not more than 800 mV/s. For the chronoamperometric experiments, a pulse time of 2 s was used.

5.3 Results

It is common practice in electrochemistry to use "electrochemical area" rather than the "geometrical area"

of electrodes. This is because electrodes are not perfectly smooth and therefore the actual area is always larger than the geometrical area. One frequently used method in determining electrochemical areas is by utilizing the Cottrell equation (equation 2.12) which is given by

$$i = nFA D(0)^{\frac{1}{2}} C^* / (\pi t)^{\frac{1}{2}}$$

If a compound exhibiting well-behaved electrochemistry and whose diffusion coefficient is known accurately is used, then all the variables in the Cottrell equation can either be measured or are known and therefore the area A can be calculated. One such compound is anthracene. In acetonitrile, the first reduction to the anion radical shows a reversible one-electron wave. The diffusion coefficient in acetonitrile (0.10 M TEAP)) at 25°C has been found to be $2.55 \times 10^{-5} \text{ cm}^2/\text{s}$ (241). Here the

concentration of anthracene used was 0.943 mM in acetonitrile (0.10 M TEAP). Figure 51 shows the cyclic voltammogram for the first reduction of anthracene at a glassy carbon electrode. From this cyclic voltammogram a potential of -2.500 V was chosen for the potential step so that reduction is in the diffusion-controlled limit. The chronoamperograms for the anthracene solution, as well as for the background solution are also shown in Figure 51. From these, the value of $(it)^{\frac{1}{2}}$ can be calculated with correction for background current. Since the literature value for the diffusion coefficients of anthracene was quoted at 25°C and the experiment was conducted at 23°C, a simple correction for this temperature difference can be made by making use of the Stokes-Einstein equation.

$$D = kT/6\pi\eta r \quad (5.1)$$

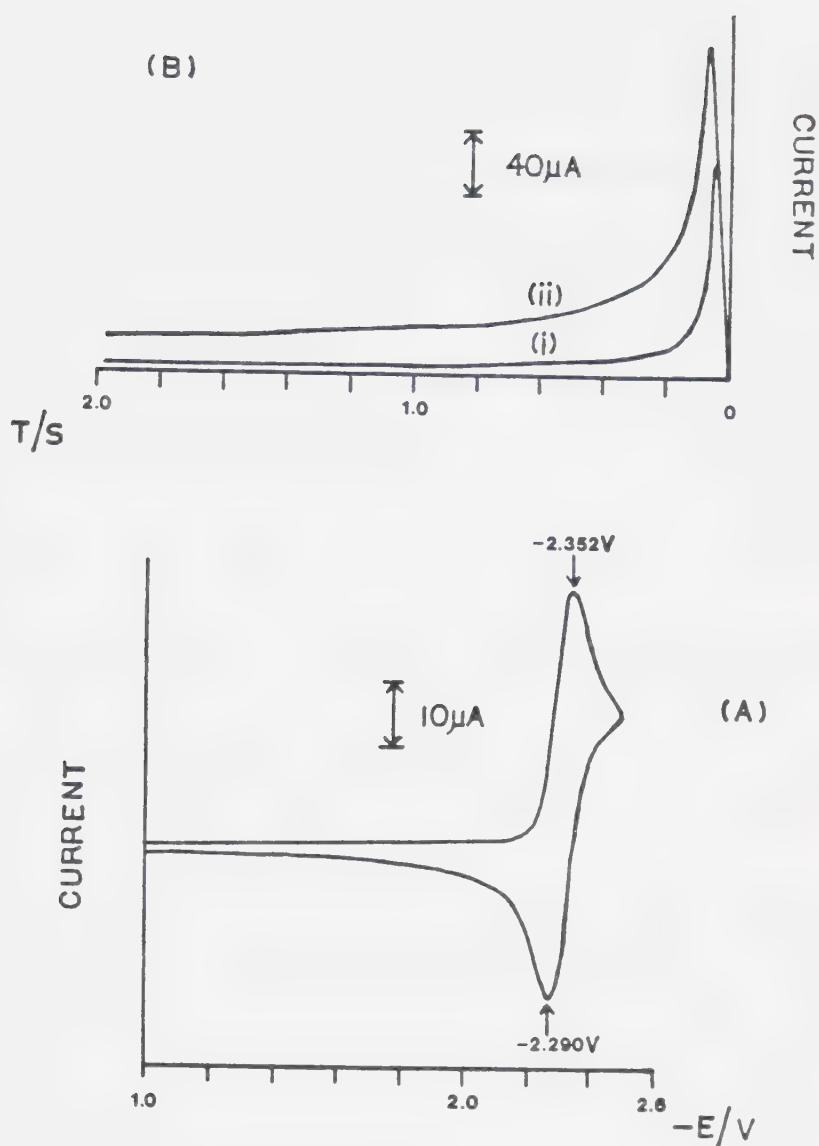


Figure 51. A. Cyclic voltammogram showing the reduction of anthracene (0.943 mM in ACN, 0.1 M TEAP) to its anion radical at platinum electrode. 100 mV/s. Peak reduction current is 38 μA . B. Chronoamperograms for (i) 0.943 mM anthracene in ACN (0.1 M TEAP) (ii) ACN background (0.1 M TEAP). Pulse -1.00 V to -2.500 V for 2 s. Pt electrode. $it_{1/2}^{1/2}$ (corrected for background) = $22.7\text{ }\mu\text{A s}^{1/2}$.

where η = viscosity and r = radius of the molecule and the other symbols have their usual meaning. Assuming that the radius is independent of temperature, then

$$D_1/D_2 = (T_1\eta^2)/(T_2\eta^1) \quad (5.2)$$

where η (25°C) is 3.44 millipoise and η (23°C) is 3.495 millipoise (242). Therefore

$$2.55/D_2 = [298(3.495)]/[296(3.44)]$$

and D_2 is 2.45 cm²/s at 23°C.

From the results of four different experiments, the area of the glassy carbon electrode was found to be 0.095 ± 0.005 cm² and that of the platinum electrode was 0.229 ± 0.016 cm².

Cyclic voltammograms of 1.00 mM solutions of TCNE

using different supporting electrolytes were obtained at sweep rates ranging from 25 mV/s to 600 mV/s at platinum and glassy carbon electrodes. Figure 52 shows some representative cyclic voltammograms. The relevant cyclic voltammetric parameters for the first reduction wave at a scan rate of 100 mV/s are given in Table 4.

Table 4 Peak Potentials for the First Reduction of TCNE (1.00 mM) at 100 mV/s

Glassy Carbon Electrode				Platinum Electrode		
Supporting Electrolyte	$E(p,c)$ (-V)	$E(p,a)$ (-V)	$\Delta E(p)$ mV	$E(p,c)$ (-V)	$E(p,a)$ (-V)	$\Delta E(p)$ mV
TBAF	0.091	0.020	71	0.110	0.038	72
TEAP	0.102	0.040	59	0.105	0.042	63
NaClO ₄	0.102	0.041	61	0.110	0.042	68
LiClO ₄	0.114	0.052	62	0.108	0.045	63

In all cases, $\Delta E(p)$ values did not change significantly from the above values with variation of sweep rates

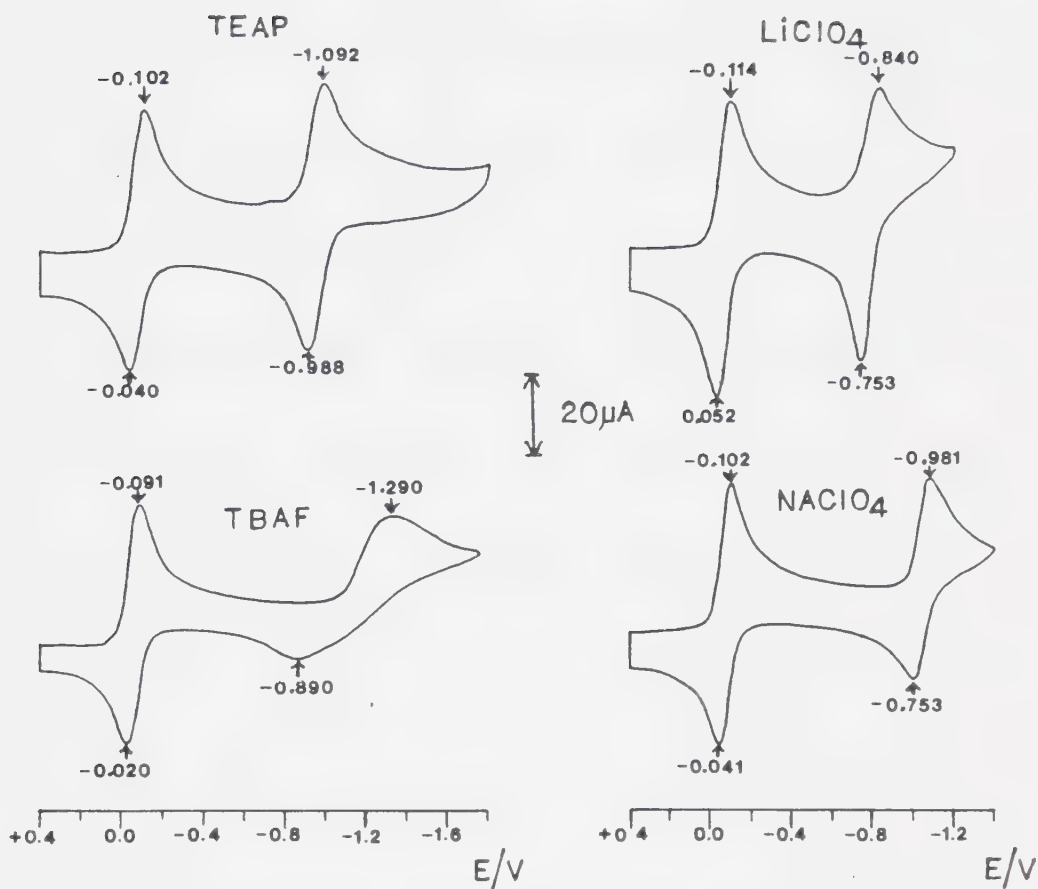


Figure 52. Cyclic voltammograms showing the first and second reduction of TCNE (1.00 mM in ACN, 0.1 M supporting electrolyte) at glassy carbon with different supporting electrolytes at 100 mV/s.

ranging from 25 mV/sec to 600 mV/sec.

Values for the ratio of the anodic peak current to the cathodic peak current $i(\text{pa})/i(\text{pc})$ for the first wave were obtained by recording cyclic voltammograms in the current-time (y-t) mode. For all sweep rates and supporting electrolytes, the observed values were very close to 1.00 (for example see Figure 53). For the planar glassy carbon electrode, the ratio of peak cathodic current to square root of the sweep rate $i(\text{pc})/v^{\frac{1}{2}}$ was constant for all sweep rates studied and had approximately the same values for the different electrolytes. They were 112, 111, 108 and 110 $\mu\text{A}/(\text{v/s})^{\frac{1}{2}}$ for TBAF, TEAP, NaClO_4 and LiClO_4 respectively. However, for the platinum wire electrode, $i(\text{pc})/(v)^{\frac{1}{2}}$ values appeared to be larger at slower sweep rates. Figure 53 shows a plot of $i(\text{pc})/(v)^{\frac{1}{2}}$ for TBAF at glassy carbon and platinum wire electrodes.

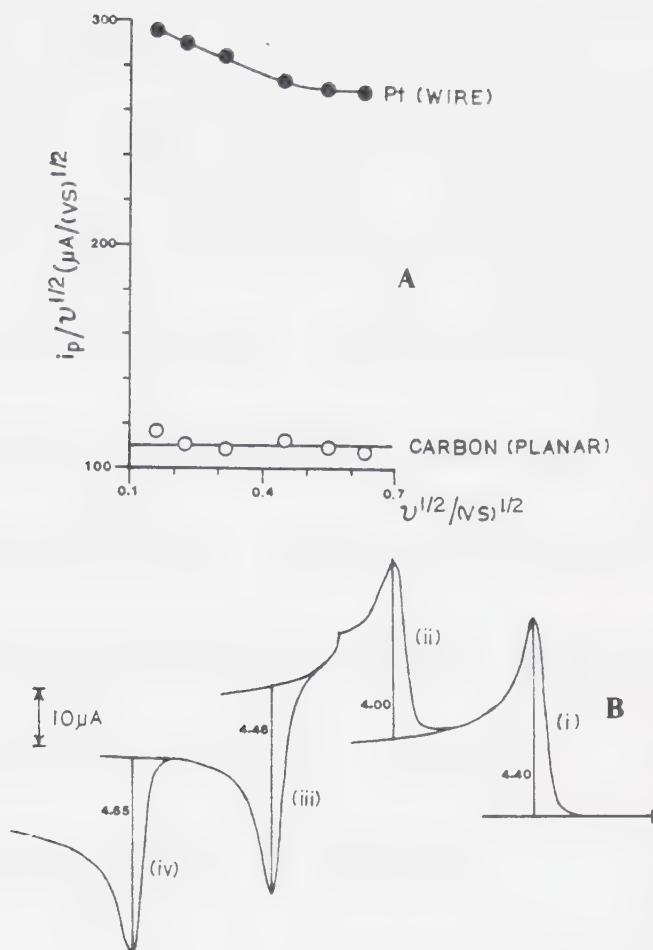


Figure 53. A. Plots of $i(pc)/v^{\frac{1}{2}}$ versus $v^{\frac{1}{2}}$ for the first reduction wave of TCNE (1.00 mM in ACN, 0.1 M TBAF) at glassy carbon and platinum electrodes.
 B. Cyclic voltammogram of TCNE (1.00 mM in ACN, 0.1 M TBAF) at platinum electrode recorded in y-t mode.
 Scan +0.5 V to -1.10 V at 25 mV/s.

$$\frac{i(pa)1}{i(pc)1} = \frac{(iv)}{(i)} = 1.1 \quad \frac{i(pa)2}{i(pc)2} = \frac{(iii)}{(ii)} = 1.1$$

Diffusion coefficients for TCNE, as determined by chronoamperometry, were found to be independent of the counteranions used. The observed value was $(2.20 \pm 0.05) \times 10^{-5} \text{ cm}^2/\text{s}$. For a reversible wave, the peak current from the cyclic voltammograms and the $i t^{1/2}$ values for the chronoamperometric experiment can be combined to give the value for the number of electrons transferred. From the Randles-Sevcik equation (2.16)

$$i_p = 2.69 \times 10^5 (n)^{3/2} A (D(0)v)^{1/2} C(0)$$

and the Cottrell equation (2.12)

$$i t^{1/2} = nFA (D(0))^{1/2} C(0)$$

we obtain

$$i_p / i t^{1/2} = (2.69 \times 10^5 n^{1/2} \pi^{1/2} v^{1/2}) / F \quad (5.3)$$

where i_p is in μA , $i_t^{\frac{1}{2}}$ is in $\mu\text{A s}^{\frac{1}{2}}$ and v is in V/s .

$$\text{Thus } n = [(i_p)F / ((i_t^{\frac{1}{2}}) (2.69 \times 10^5) (\pi^{\frac{1}{2}} v^{\frac{1}{2}}))] \quad (5.4)$$

where n is the number of electrons transferred. This method of obtaining n is known as Malachuk's method (120).

It is very convenient since no prior knowledge of the electrode area is required and the concentration of the solution need not be known as long as it is the same for both techniques. One drawback is that it can only be applied to a reversible electrode reaction with no chemical complications. Malachuk's method was applied to study the number of electrons transferred for the first reduction of TCNE. For both electrodes and all supporting electrodes used, values of n ranging from 0.9 to 1.0 were obtained.

It is observed in Figure 52 that the second reduction wave for TCNE in acetonitrile shows remarkable

differences with different counteranions. Similar behavior was also observed at a platinum electrode. The cyclic voltammetric parameters for this wave at 100 mV/s scan rate are given in Table 5.

Table 5 Peak Potentials for Second Reduction Wave of TCNE (1.00 mM) at 100 mV/s

Glassy Carbon				Platinum Wire		
Supporting Electrolyte	E(p,c) (-V)	E(p,a) (-V)	delE(p) mV	E(p,c) (-V)	E(p,a) (-V)	delE(p) mV
TBAF	1.290	0.890	400	1.625	1.100	525
TEAP	1.092	0.988	94	1.264	0.967	297
NaClO ₄	0.981	0.909	72	0.980	0.907	73
LiClO ₄	0.840	0.753	87	0.833	0.756	77

For the counteranions TBA⁺ and TEA⁺, delE(p) values increased with increasing sweep rates. This increase was greater at platinum than at carbon and greater for TBA⁺ than for TEA⁺. For Na⁺ and Li⁺, delE(p) values did not

change very much with variation in sweep rates. With both NaClO₄ and LiClO₄ supporting electrolytes $i(\text{pa})/i(\text{pc})$ values for the second wave were close to 1.0 at a platinum electrode. For NaClO₄, at a carbon electrode, the same result was also obtained. However, LiClO₄ supporting electrolyte at a carbon electrode gave values of $i(\text{pa})/i(\text{pc})$ which were significantly greater than 1.0. These values are given in Table 6 for different sweep rates.

Table 6. Variation of $i(\text{pa})/i(\text{pc})$ for Second Reduction of TCNE (1.00 mM) with LiClO₄ Supporting Electrolyte at a Glassy Carbon Electrode

v mV/s	$i(\text{pa})/i(\text{pc})$
50	1.29
100	1.39
200	1.41
300	1.52

The second reduction wave also gave approximately constant values for $i(\text{pc})/(v)^{\frac{1}{2}}$ at different sweep rates with Na⁺

and Li^+ counteranions. However, these values were 10-15% lower compared to those for the first wave. In the cases of TBAF and TEAP supporting electrolytes, this was also true. Further, in all cases, chronoamperometry showed that the total number of electrons transferred for the sum of the first and second reduction waves were close to 2.0 (the values obtained ranged from 1.7 to 1.9).

It has been described in Chapter 2 that variation of $\text{del}E(p)$ values with sweep rates can be used to determine heterogeneous rate constants for quasireversible electrode reactions. For this to be applicable, $\text{del}E(p)$ values should be less than about 210 mV. For this reason, heterogeneous rate constants with TBAF as supporting electrolyte at a platinum electrode could not be determined by this method. Equation (2.26) in Chapter 2 shows that the heterogeneous rate constant is related to a certain parameter Δ by

$$\Delta = ((D(O)/D(R))^{\frac{1}{2}} k_s)/(D(O)\pi v(nF/RT))^{\frac{1}{2}}$$

The values of Δ for different $\text{del}E(p)$ values have been theoretically calculated (54). These values are plotted in Figure (54).

Assuming that $D(O) \approx D(R)$ at 23°C

$$\Delta = k_s/[(2.20\text{e-}5) (\pi) v (39.206)]^{\frac{1}{2}} \quad (5.5)$$

$$k_s = 0.05505 \Delta (v)^{\frac{1}{2}} \quad (5.6)$$

The calculated values for the apparent heterogeneous rate constants for the second reduction of TCNE are given in Tables 7-9.

Table 7. Apparent Heterogeneous Rate Constants for TCNE (1.00 mM in ACN) Second Reduction at a Glassy Carbon Electrode with TBAF Supporting Electrolyte

v mV/s	$\text{del}E(p)$ mV	Δ	k_s cm/s
10	132	0.28	1.5e-3
15	168	0.20	1.3e-3
20	171	0.19	1.5e-3
25	177	0.18	1.6e-3
35	205	0.13	1.3e-3

average $(1.4 \pm 0.1)\text{e-}3$ cm/s

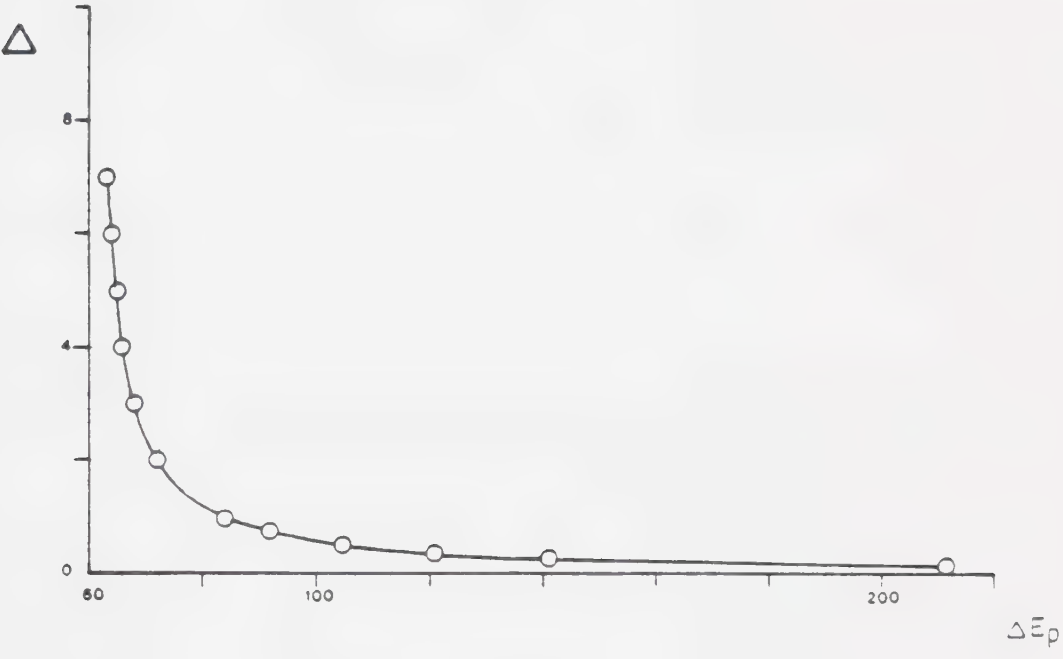


Figure 54. Plot of Δ function versus $\Delta E(p)$
Assume $\alpha = 0.5$

Table 8. Apparent Heterogeneous Rate Constants for TCNE (1.00 mM in ACN) Second Reduction at a Glassy Carbon Electrode with TEAP Supporting Electrolyte

v mV/s	$\Delta E(p)$ mV	Δ	k_s cm/s
50	84	0.98	1.2×10^{-2}
100	94	0.71	1.2×10^{-2}
200	111	0.41	1.0×10^{-2}
400	122	0.34	1.2×10^{-2}
average			$(1.1 \pm 0.1) \times 10^{-2}$ cm/s

Table 9. Apparent Heterogeneous Rate Constants for TCNE (1.00 mM in ACN) Second Reduction at a Platinum Electrode with TEAP Supporting Electrolyte

v mV/s	$\Delta E(p)$ mV	Δ	k_s cm/s
15	138	0.27	1.8×10^{-3}
20	144	0.25	1.9×10^{-3}
25	154	0.22	1.9×10^{-3}
30	184	0.17	1.6×10^{-3}
average			$(1.8 \pm 0.1) \times 10^{-3}$ cm/s

At a platinum electrode, the second reduction wave of TCNE with TBAF as supporting electrolyte showed a slow electron transfer. The method used for determination of

rate constant for quasi-reversible reactions could not be applied in this case since $\Delta E(p)$ values were too large at all sweep rates studied. Matsuda and Ayabe (180) and Nicholson (194) have shown that, for the case of irreversible charge transfer,

$$i(p) = 0.227 nF k_s C(0) \exp\left[\frac{-\alpha nF}{RT}(E(p)-E(0))\right] \quad (5.7)$$

where all the terms have their usual meaning.

However, values of $E(0)$ are not always available and Reinmuth (244) has derived a useful relationship where the current at the foot of the reduction wave ($i < 10\% i(p)$) is given by

$$i = nFAC(0) k_s \exp\left[\frac{-\alpha nF}{RT}(E-E(i))\right] \quad (5.8)$$

where $E(i)$ is the initial potential. This equation has

provided the basis for determination of rate constants for irreversible electrode reactions where $E(0)$ is unknown (62).

From equation (5.8)

$$\log i = \log(nFA C(0) k_s) - 0.4343(-\alpha nF/RT)(E-E(i)) \quad (5.9)$$

where i is in μA and $C(0)$ in mM. At $23^\circ C$

$$\log i = 4.34 + \log k_s - 17.02 \alpha (E-E(i)) \quad (5.10)$$

Therefore, if $\log i$ was plotted against $E-E(i)$, the slope would yield α . Once α is known, the value of k_s can be calculated from equation (5.10) which on rearranging gives

$$\log k_s = \log i + 17.02\alpha(E-E(i)) - 4.34. \quad (5.11)$$

This was done for the reduction of TCNE anion radical to

the dianion at a platinum electrode with TBAF as supporting electrolyte. The results are plotted in Figure 57. From the slope of the straight line plot, α was found to be 0.8. This value was substituted into equation (5.11) and k_s calculated (Table 10).

Table 10. Apparent Heterogeneous Rate Constants for the Reduction of TCNE: to TCNE= at a Platinum Electrode. Concentration of TCNE is 1.00 mM in ACN (0.10 M TBAF).

E-E(i) (Volts)	log i	log k_s	k_j cm/s
-0.06	0.75	-4.41	3.9e-5
-0.05	0.62	-4.40	4.0e-5
-0.04	0.45	-4.43	3.7e-5
-0.03	0.29	-4.46	3.5e-5
			(3.8±0.1)e-5

The value of 0.8 for α obtained from Figure 57 is in close agreement with that obtained by another method. For an irreversible electrode reaction, peak potentials and half-peak potentials depend on the sweep rate. For two different

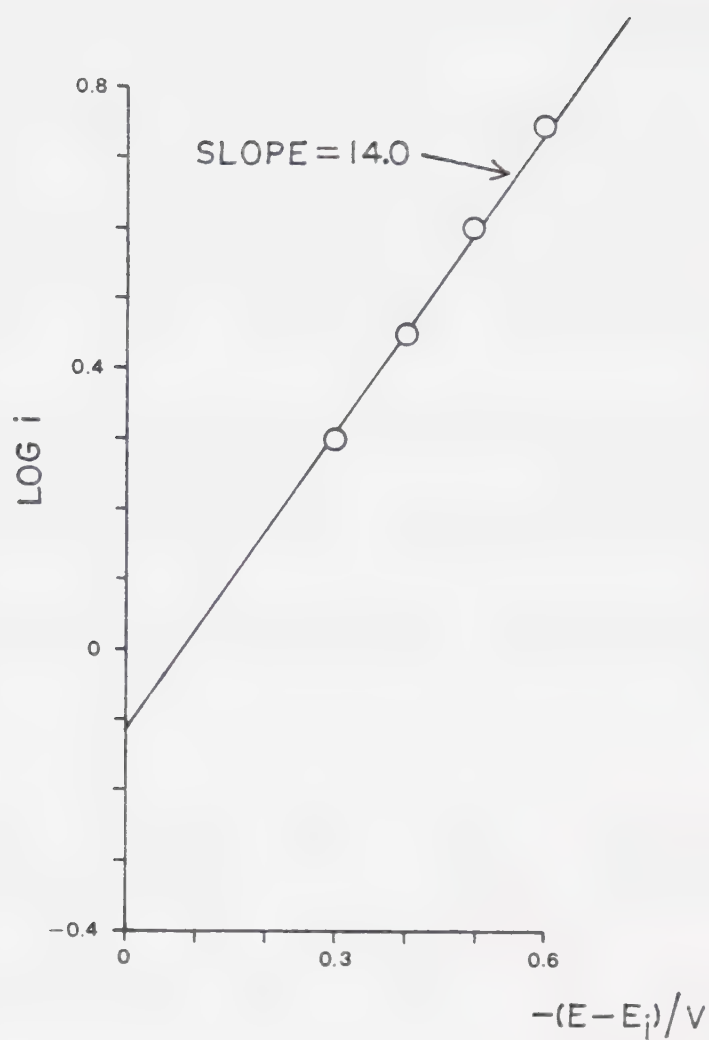


Figure 57. Plot of $\log i$ versus $E - E_i$ for the reduction of TCNE anion radical at platinum.

sweep rates, α is related to the peak potential $E(p)$, half-peak potentials $E(p/2)$ and the sweep rates v by (62)

$$\begin{aligned} (E(p/2))_2 - (E(p/2))_1 &= (E(p))_2 - (E(p))_1 \\ &= RT/nF \ln (v(1)/v(2))^{\frac{1}{2}} \end{aligned} \quad (5.12)$$

Since irreversible voltammetric waves are rather broad, the measurement of peak potentials are less accurate than half-peak potentials, and therefore $E(p/2)$ will be used.

$$(E(p/2))_2 - (E(p/2))_1 = (0.02551/\alpha) \ln (v_1/v_2) \quad (5.13)$$

The results are shown in Table 11.

Table 11. Determination of α for TCNE⁺ Reduction at a Platinum Electrode using Equation (5.13).
Concentration of TCNE is 1.00 mM ACN (0.10 M TBAF)

v mV/sec	$E(p/2)$ (Volts)	α
15	-1.374	0.71
50	-1.418	
100	-1.443	

Figure 55 shows some representative cyclic voltammograms for 1.00 mM TCNQ in acetonitrile at a glassy carbon electrode at 100 mV/sec. Peak potentials for the first and second reduction waves are given in Tables 12 and 13 respectively.

Table 12. Peak Potentials for the First Reduction of TCNQ (1.00 mM in acetonitrile) at 100 mV/sec Scan Rate

Supporting Electrolyte	Glassy Carbon			Platinum		
	E(p,c) (-V)	E(p,a) (-V)	delE(p) mV	E(p,c) (-V)	E(p,a) (-V)	delE(p) mV
TBAF	0.140	0.072	68	0.140	0.077	63
NaClO ₄	0.146	0.080	66	0.145	0.078	67
LiClO ₄	0.146	0.082	64	0.140	0.072	68

Table 13. Peak Potentials for the Second Reduction of TCNQ (1.00 mM in acetonitrile) at 100 mV/sec Scan Rate

Supporting Electrolyte	Glassy Carbon			Platinum		
	E(p,c) (-V)	E(p,a) (-V)	delE(p) mV	E(p,c) (-V)	E(p,a) (-V)	delE(p) mV
TBAF	0.691	0.627	64	0.695	0.628	70
NaClO ₄	0.659	0.597	62	0.660	0.592	68
LiClO ₄	0.551	0.490	61	0.558	0.498	60

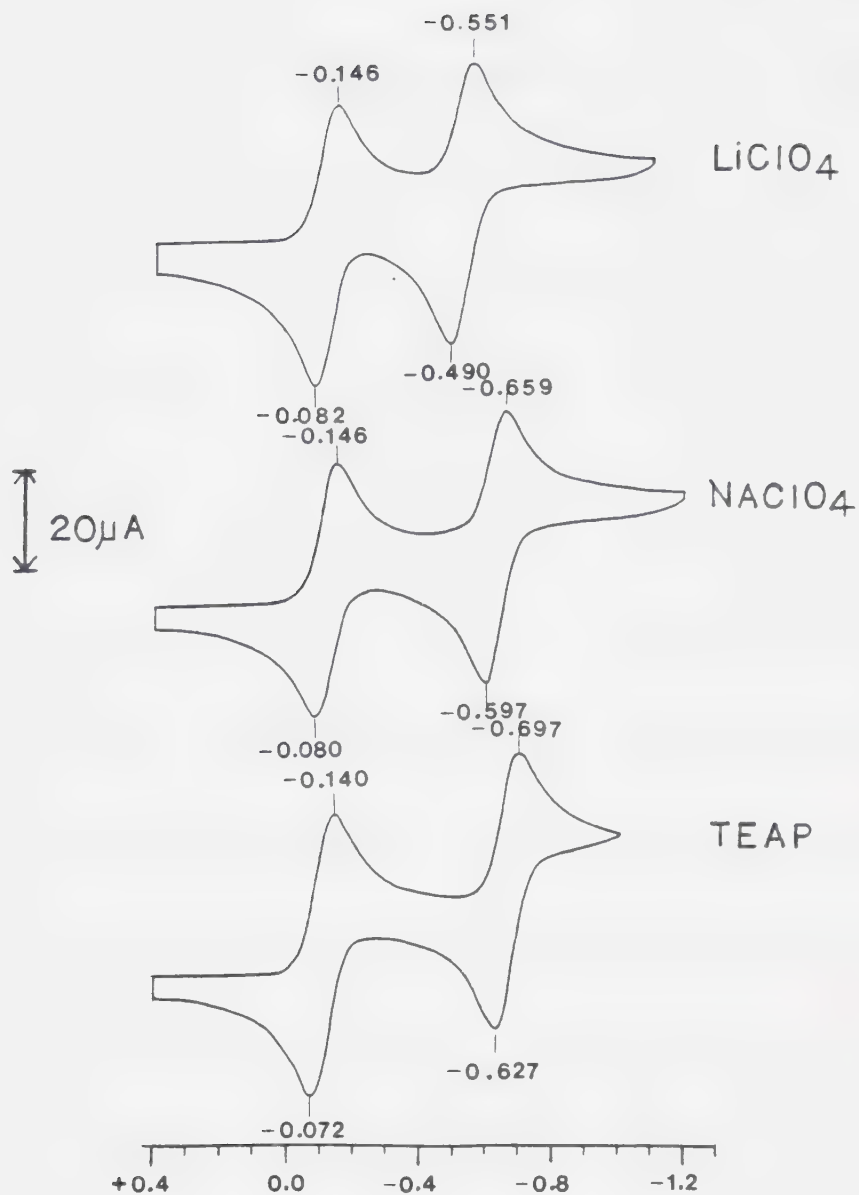


Figure 55. Cyclic voltammograms for reduction of TCNQ (1.00 mM in ACN, 0.1 M supporting electrolyte) at glassy carbon with different supporting electrolytes.

Considering the first reduction wave of TCNQ in acetonitrile, $\Delta E(p)$ values remained close to the theoretical reversible value of 59 mV at sweep rates from 25 to 500 mV/s in all cases. The ratio $i(p)/i(pc)$ was found to be 1.00 for all systems. Figure 56 shows a typical $y-t$ recording for the forward and reverse waves. Diffusion coefficients determined from chronoamperometry did not show any dependence on the supporting electrolyte used. The value obtained was $(2.00 \pm 0.06) \times 10^{-5} \text{ cm}^2/\text{s}$. The current constant $i(p)/v^{\frac{1}{2}}$ was approximately constant with sweep rate variation and has an average value of $100 \text{ } \mu\text{A}/(\text{V/s})^{\frac{1}{2}}$ for the glassy carbon and 244 for the platinum wire electrode. Malachuk's method revealed that the number of electrons transferred in the first wave was 1.0.

Similar results were obtained for the second wave. As can be seen from Table 11, $\Delta E(p)$ values were close to

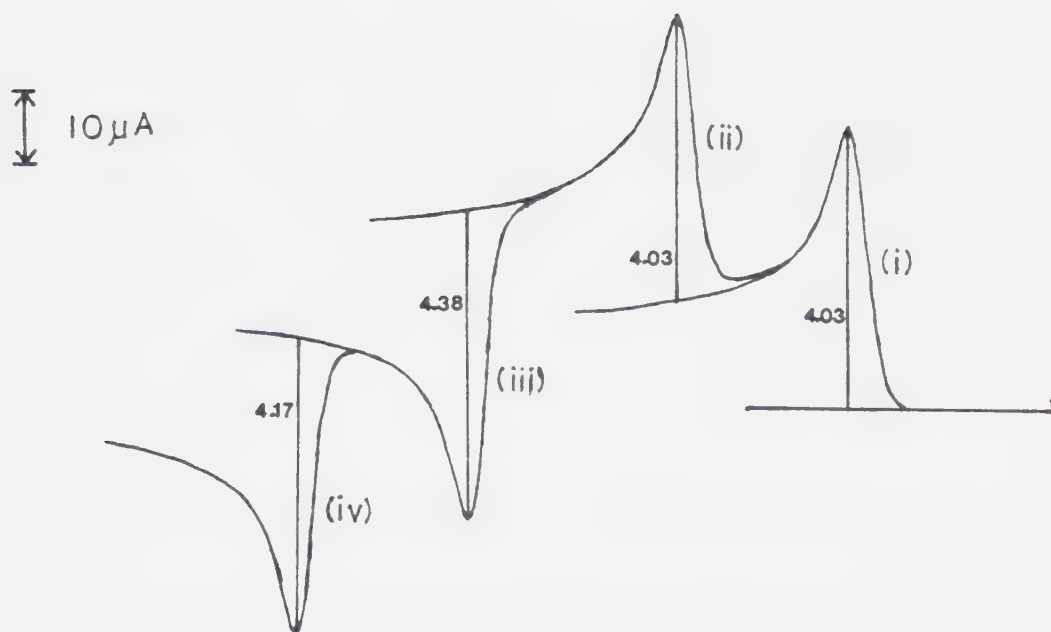


Figure 56. Cyclic voltammogram for reduction of TCNQ (1.00 mM in ACN, 0.1 M TBAF) at platinum electrode recorded in the y-t mode. Scan from +0.50 V to -1.00 V at 25 mV/s.

$$\frac{i(\text{pa})1}{i(\text{pc})1} = \frac{(iv)}{(i)} = 1.03 \quad \frac{i(\text{pa})2}{i(\text{pc})2} = \frac{(iii)}{(ii)} = 1.09$$

the reversible value in all cases. $i(\text{pa})/i(\text{pc})$ gave a value of 1.00 (see Figure 56) and $i(\text{pc})/v^{\frac{1}{2}}$ did not vary much with sweep rate. The average value obtained at the carbon electrode was 92 and at the platinum electrode $229 \text{ uA}/(\text{V/s})^{\frac{1}{2}}$. Chronoamperometry showed that the total number of electrons transferred for the first and second waves was 2.0.

The results from Tables 4 and 12 showed that the peak potentials for the first reduction wave of TCNE and TCNQ did not change significantly, with different electrode materials or counteranions. In contrast, the peak potentials of the second reduction wave changed with counteranions (Tables 5 and 13). Further, in the case of TCNE with TBA⁺ and TEA⁺, the peak potentials were more negative at platinum compared to carbon. For Na⁺ and Li⁺ this did not occur. However, with TCNQ there were no differences in peak potentials with different electrode

material. $E(p)$ values for the second reduction wave of both TCNE and TCNQ were found to shift to more positive values according to the order $TBA^+ < TEA^+ < Na^+ < Li^+$.

Plots of E_h for the second reduction wave of TCNE and TCNQ at a carbon electrode vs ionic radii of countercations are shown in Figure 58. For TCNE, E_h values with TBA^+ were not obtainable due to irreversibility of the reduction but for TEA^+ the reduction at slow sweep rates (10 mV/sec) was sufficiently close to reversibility ($\Delta E(p)$ 71 mV) for the E_h value to be known. It can be seen from Figure 58 that for TCNE, positive shift of E_h in going from TEA^+ to Na^+ countercations was 49 mV and from Na^+ to Li^+ was 77 mV. For TCNQ, where TEA^+ was not studied, positive shift of 30 mV occurred from TBA^+ to Na^+ and 80 mV from Na^+ to Li^+ .

It is well known that the presence of ion pairing of electrolytically formed negative ions with countercations causes positive shifts in the E_h values, the magnitude of

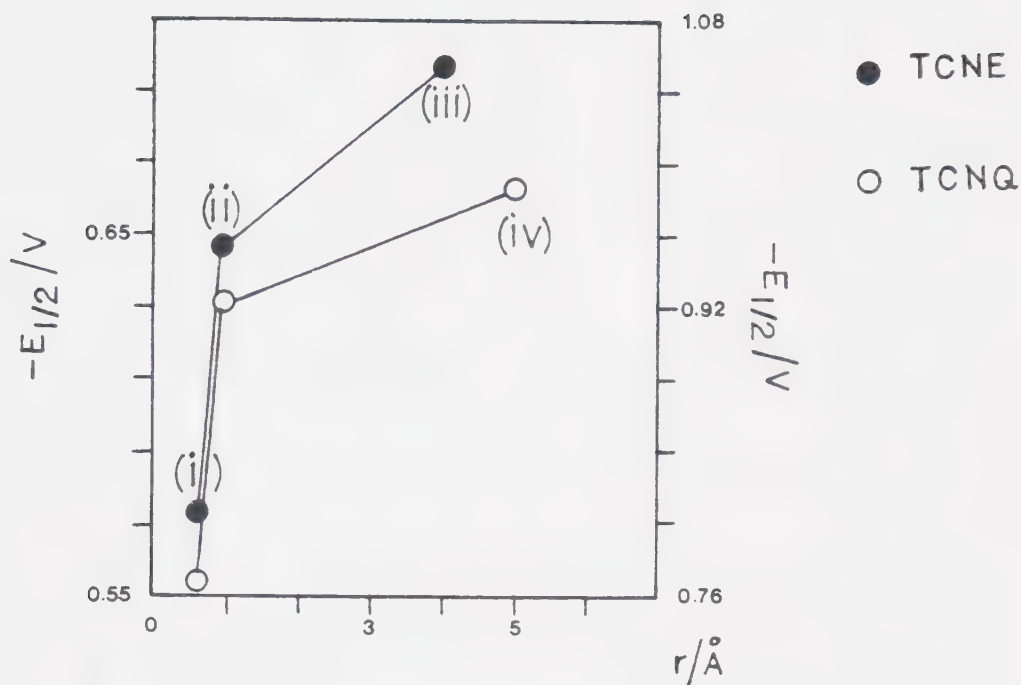


Figure 58. Plot of half-wave potential (E_h) versus ionic radii of countercations for TCNE and TCNQ second reduction wave at platinum and glassy carbon.
 i) Li^+ , ii) Na^+ , iii) TEA^+ , iv) TBA^+

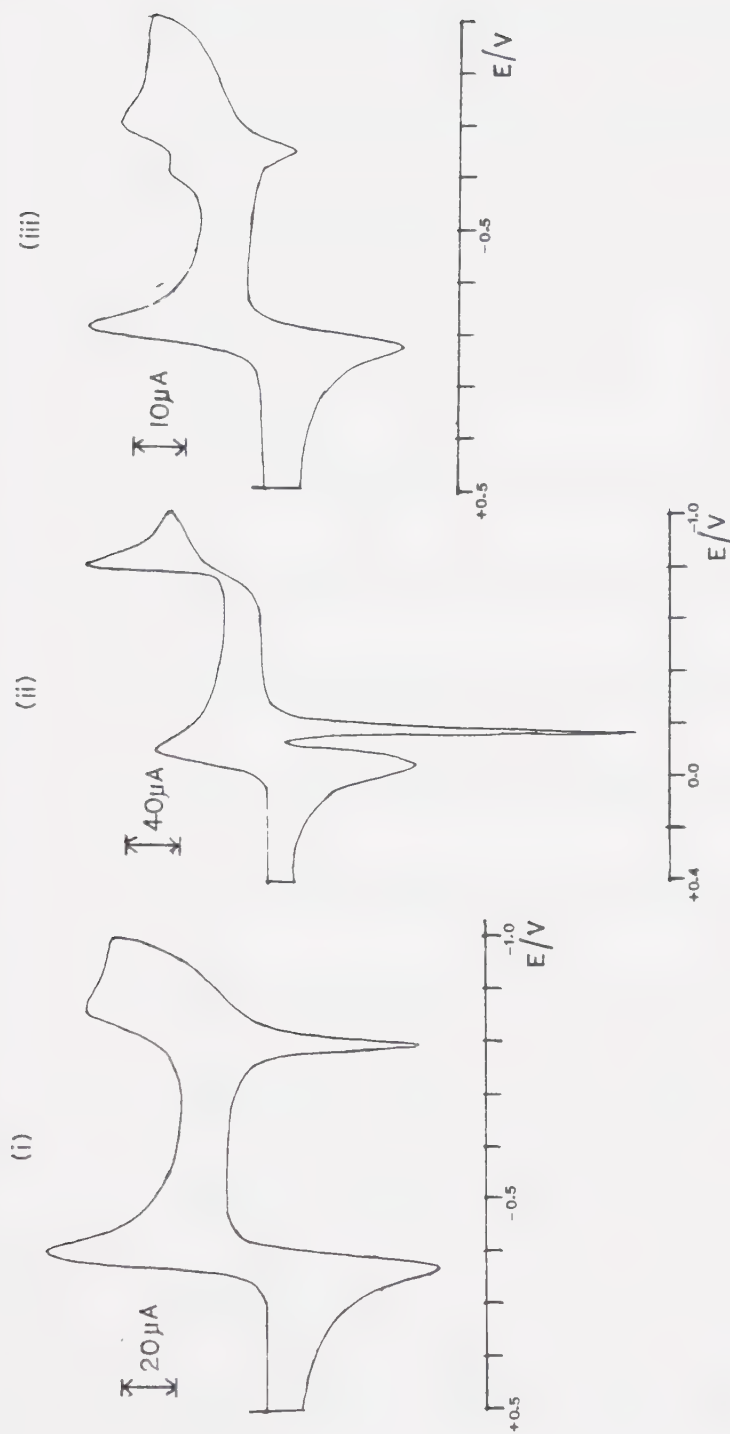


Figure 58A. Cyclic voltammogram of TCNE (1.00 M in ACN) with mixtures of supporting electrolytes.
 (i) Pt electrode 0.095 M TBAF+0.005 M LiClO₄
 (ii) Pt electrode 0.05 M TEAP+ 0.05 M LiClO₄
 (iii) Carbon electrode 0.05 M TBAF+0.05 M LiClO₄
 All at 100 mV/s.

this shift depending on the strength of ion pairing and the concentration of counteranions, where the concentration of the electroactive species is kept constant (209-212). Therefore it was decided to study the shifts in E_h as a function of concentration of counteranions. The requirements for such a study are that the reduction wave must be electrochemically reversible and the species formed stable. Further, the ionic strength should be kept constant preferably with the supporting electrolyte whose counteranion cation is assumed not to ion pair with the species of interest. In the case of TCNE, it was found that such a study could not be made since the dianion wave was irreversible with TBAF as supporting electrolyte. Further, it was observed that the reductions with mixtures of supporting electrolytes TBAF-LiClO₄, TEAClO₄-LiClO₄ gave waves which exhibited adsorption characteristics at both electrolytes (Figure 58A). As can be seen from this figure,

the reduction wave of TCNE was not affected with different mixtures of supporting electrolytes and electrode materials.

The various criteria for electrochemical reversibility as discussed earlier are still applicable. However, for mixed electrolytes, TCNE^{•-} reduction shows waves characteristic of adsorption effects. For example, with 0.095 M TBAF and

0.005 M LiClO₄ at a platinum electrode, the reverse wave is very sharp and does not show $t^{\frac{1}{2}}$ decay for diffusion

control. For 0.05 M TEAP and 0.05 M LiClO₄ at platinum, the forward wave rose sharply and the reverse wave was not

observed. Instead, a very strong sharp current transient was observed just prior to the reverse wave for the first

reduction. In the case of 0.05 M TBAF and 0.05 M LiClO₄ at carbon, a prepeak was observed for the forward wave and the

reverse wave was again quite sharp. For TCNQ, no

such problems arose. It was assumed that the TCNQ dianion did not form any ion pair with TBA⁺ and therefore the

ionic strength was kept constant at 0.10 M with appropriate additions of TBAF. This assumption was verified by reducing TCNQ at different concentrations of TBAF. The results are shown in Table 14.

Table 14. Peak Potentials for TCNQ Reduction (0.50 mM in ACN) as a Function of TBAF Concentration. Scan Rate 25 mV/s .

[TBAF] M	E(pc)1 V	E(pa)1 V	delE(p)1 mV	E(pc)2 V	E(pa)2 V	delE(p)2 mV
0.02	-0.156	-0.094	62	-0.718	-0.655	63
0.04	-0.151	-0.086	65	-0.710	-0.647	63
0.06	-0.146	-0.082	64	-0.703	-0.639	64
0.08	-0.142	-0.078	64	-0.698	-0.634	64
0.10	-0.140	-0.075	65	-0.694	-0.629	65

The calculated shifts in E_h with respect to the E_h in 0.10 M TBAF are given below.

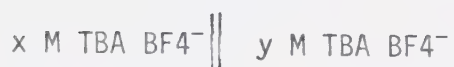
Table 15. Half Wave Potential Shifts and Calculated Junction Potentials for TCNQ Reductions as a Function of TBAF Concentration. 0.05 mM TCNQ in ACN. Scan Rate 25 mV/s

[TBAF] M	delEh(1)	delEh(2)	Ej
0.02	14	24	11
0.04	11	16	6
0.06	6	9	4
0.08	2	4	2
0.10	0	0	

However, since the reference electrode used was Ag/AgNO₃ (0.01M), 0.10 M TBAF in acetonitrile, junction potentials are expected to exist at concentrations of TBAF other than 0.10 M. These junction potentials can be estimated by making use of the Henderson equation for a 1:1 electrolyte

$$P(x)-P(y) = [(\lambda(\text{TBA}^+) - \lambda(\text{BF}_4^-))/(\lambda(\text{TBA}^+) + \lambda(\text{BF}_4^-))] \ln [(a^\pm(y))/(a^\pm(x))] \quad (5.14)$$

where the junction is given by



Since the activity coefficients for the various solutions were not known, rational activity coefficients were calculated using the extended Debye-Huckel equation

$$\log f_{\pm} = -A u^{\frac{1}{2}} / (1 + B u^{\frac{1}{2}}) \quad (5.15)$$

where f_{\pm} is the rational activity coefficient, u is the ionic strength, $A = 1.8246e6 / (\epsilon T)^{3/2}$, $B = 50.29e8 / (\epsilon T)^{\frac{1}{2}}$, ϵ being the dielectric constant. The relevant parameters for TBA⁺ and BF₄⁻ in acetonitrile, taken from the data of Coetzee and Cunningham (245) are given in the table below.

Table 16. Conductance Data for Ions of TBAF in ACN.

	$\text{cm}^2 \frac{\lambda(0)}{\Omega \text{ equiv}}$	Stokes radius (Å)
TBA ⁺	61.9	3.83
BF ₄ ⁻	120.9	1.96

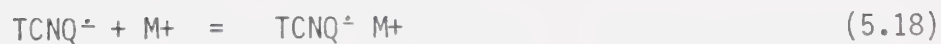
In Equation (5.15) above, the ion size parameters were taken to be the sum of the Stokes radii for the 1:1 electrolyte TBAF. Also, since the equivalent conductances were not known, ionic conductances at infinite dilution were used in equation (5.14). This is not expected to give any serious errors since only the ratio of the conductances are involved. The calculated junction potentials are given in Table 15. A similar approach to the calculation of junction potentials was used by Chauhan et al (246). Further, since the reference solution contained 0.10 M TBAF whereas the working electrode solution contained NaClO₄ and LiClO₄ up to 0.10 M, junction

potentials may be present. However this was checked experimentally and found to be negligible (< 5 mV).

For the reduction of TCNQ, the following mechanism applies:



Nagaoka and Okazaki (247) have shown that in the case where ion pairing was present for both the anion radical and the dianion.



:

:



The shift in Eh for the first reduction wave is given by

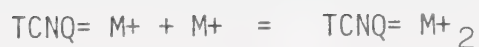
$$\Delta E_h(1) = (RT/F) \ln(1 + C_{M^+} K_{1,1} + C_{M^+}^2 K_{1,2} \dots + C_{M^+}^i K_{1,i}) \quad (5.19)$$

where the formation constant $K_{1,s}$ is given by

$$K_{1,s} = [TCNQ^{\cdot-} M_s^+] / [TCNQ^{\cdot-}] [M^+]^s \quad (5.20)$$

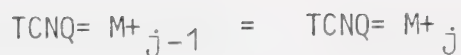
It is assumed that the concentration of the metal cation is in large excess compared to the concentration of TCNQ.

Further, for the dianion



:

:



and the shift in Eh

$$\text{delEh}(2) = (RT/F) \ln \frac{1 + C_{M^+} K_{2,1} + C_{M^+}^2 K_{2,2} + \dots + C_{M^+}^j K_{2,j}}{1 + C_{M^+} K_{1,1} + C_{M^+}^2 K_{1,2} + \dots + C_{M^+}^i K_{1,i}} \quad (5.22)$$

where

$$K_{2,t} = \frac{[\text{TCNQ} = M_t^+]}{[\text{TCNQ} =][M^+]^t} \quad (5.23)$$

Equation (5.19) predicts that a plot of $\text{delEh}(1)$ vs $\log C_{M^+}$ would give a slope of 59 mV and 118 mV at 23°C for quantitative formation of $\text{TCNQ} : M^+$ and $\text{TCNQ} : M^{2+}$. However, the behavior of $\text{delEh}(2)$ is more complicated. In the presence of only $\text{TCNQ} \rightleftharpoons M^+$, (assuming that $C_{M^+} K_{1,1} \gg 1$), a slope of 0 and 59 mV is expected for quantitative formation of $\text{TCNQ} = M^+$ and $\text{TCNQ} = M^{2+}$, respectively. In the absence of any ion pairing between TCNQ^- and M^+ then equation (5.22) reduces to

$$\text{delEh}(2) = (RT/F) \ln (1 + C_{M^+} K_{2,1} + C_{M^+}^2 K_{2,2} + \dots + C_{M^+}^j K_{2,j}) \quad (5.23A)$$

which is of the same form as equation(5.19). Therefore a similar behavior would be expected for quantitative formation of $\text{TCNQ}^- \text{M}^+$ and $\text{TCNQ}^- \text{M}_2^+$, i.e. plots of $\Delta E_h(2)$ would give 59 and 118 mV respectively.

The results obtained for TCNQ with Na^+ and Li^+ in ACN are shown in Figure 59. In all cases the concentration of TCNQ was 0.50 mM and the ionic strength was 0.10 M. The scan rate used was 25 mV/s. Both carbon and platinum electrodes gave the same results. As can be seen from Figure 59, both the plots of ΔE_h vs $\log C_{\text{M}^+}$ for Na^+ and Li^+ showed two linear sections. In the case of Na^+ the slopes were 27 and 80 mV while for Li^+ , these were 52 and 122 mV. It is clear from these results that two types of ion pairs are formed between TCNQ^- and the counter-cations, namely those with stoichiometries 1:1 and 1:2. The formation constants for both these ion pairs are calculated from the data of Figure 59 by making use of

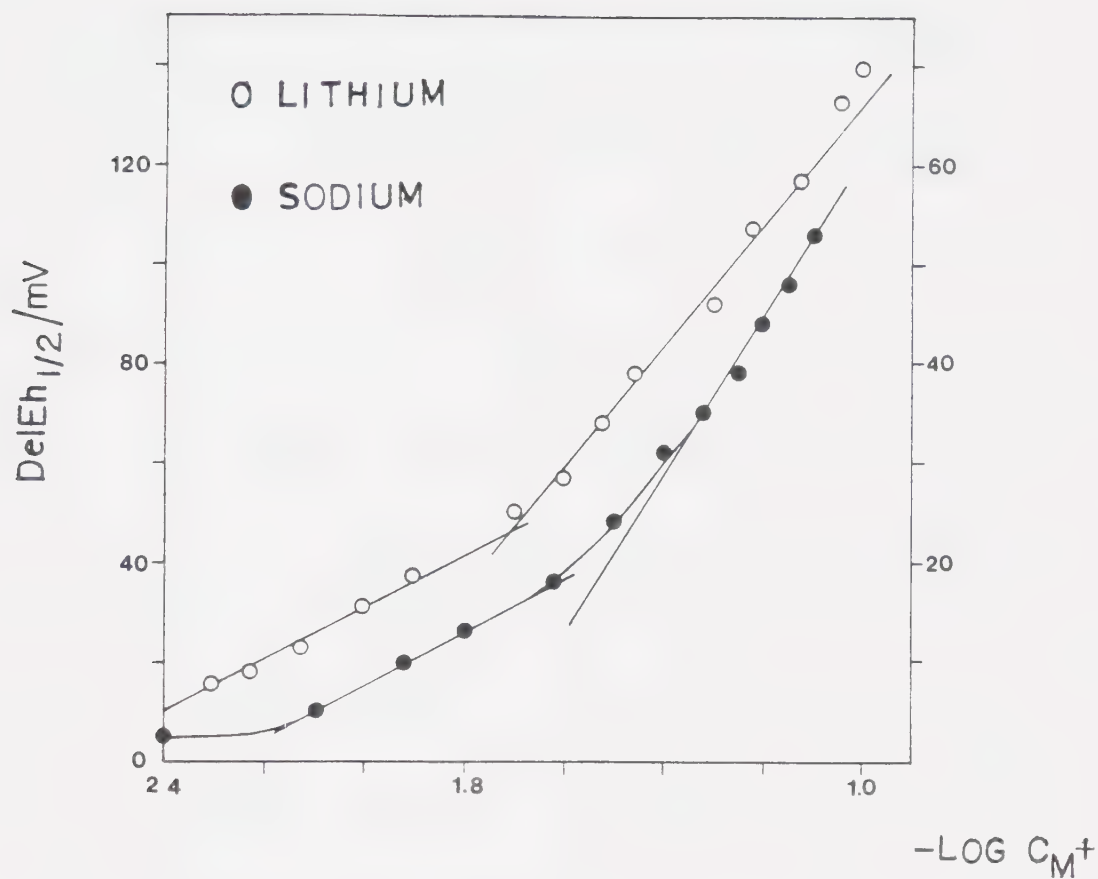


Figure 59. Plot of half-wave potential change versus the negative logarithm of metal ion concentration

equation (5.23). It is assumed that at low concentrations, only the 1:1 ion pair is formed whereas at the high concentration end both the 1:1 and 1:2 ion pairs are formed. The results of these calculations are given in Table 17.

Table 17. Formation Constants of TCNQ Ion Pairs

	Counter- cation	Stoichiometry	$K_{2,1}(M^+)$	$K_{2,2}(M^+)$
TCNQ=	Na+	1:1	33 ± 1	--
		1:2	--	394 ± 47
TCNQ=	Li+	1:1	176 ± 14	--
		1:2	--	$(1.20 \pm 0.26) \times 10^4$

As was mentioned in the introductory section of this chapter, spectroscopic techniques were used to monitor the species formed during electrolysis. Figure 60 shows the UV absorption of a solution of TCNE and TCNQ in acetonitrile. Both TCNE and TCNQ did not absorb in the visible region in acetonitrile. Further, the presence of 0.10 M TBAF or LiClO₄ did not alter the spectra of fresh solutions of TCNE or TCNQ in any way. However, if the TCNE solutions were left standing for a few days the solution containing TBAF turned yellow and showed two additional absorption maxima at 3973 Å and 4159 Å which were much weaker than the UV absorption maxima at 2610 Å and 2708 Å. The solution containing LiClO₄ did not show much color change for the same period of time. The spectrum of a solution of TCNE in water has a broad absorption maximum at 2969 Å and two weaker maxima at 3956 Å and 4125 Å (Figure 60).

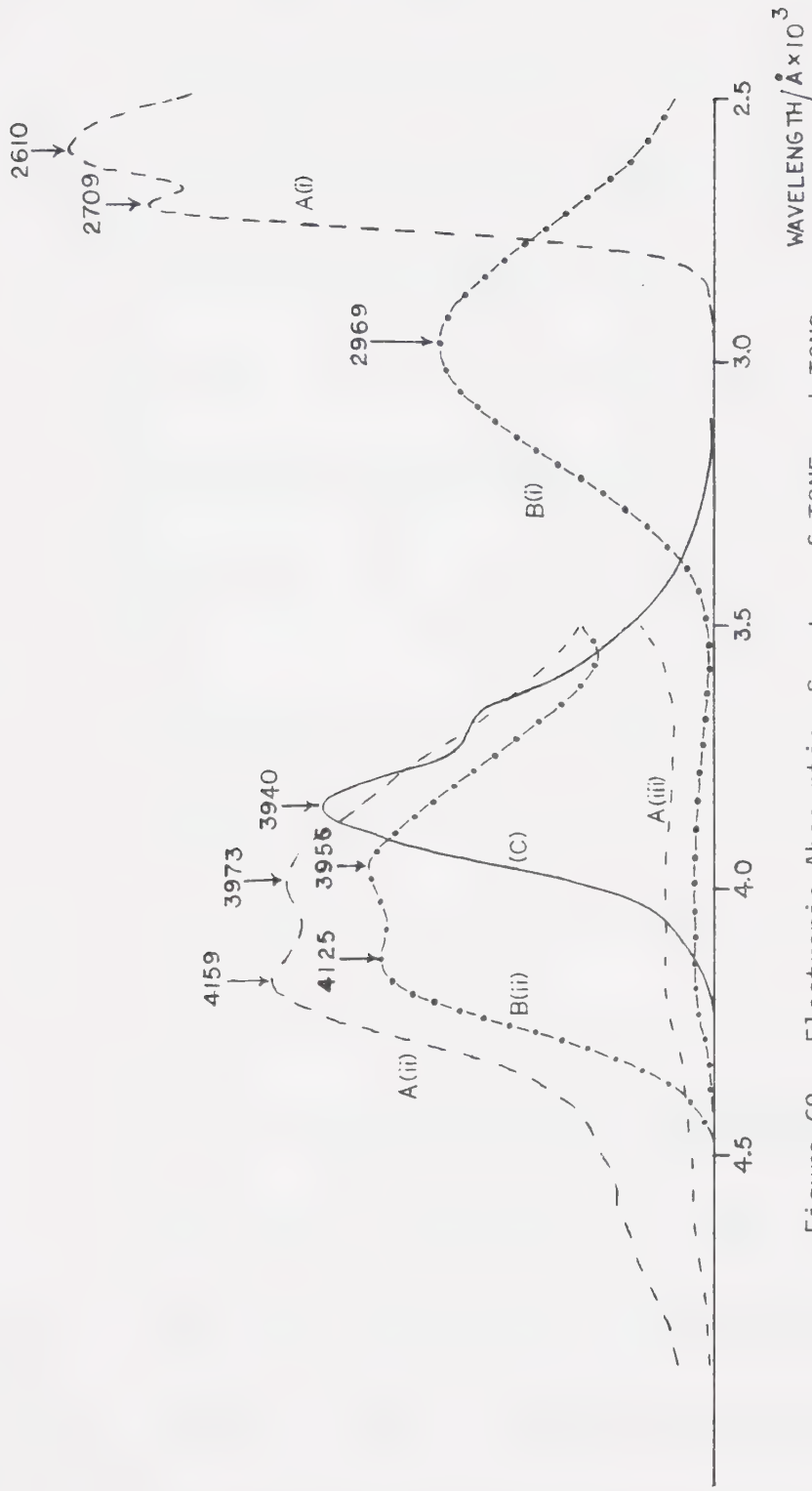


Figure 60. Electronic Absorption Spectra of TCNE and TCNQ in ACN.

- A(i) 0.50 mM TCNE in ACN fresh solution (no electrolyte, with 0.1M TBA⁺, with 0.10 M Li⁺) Path length 1 mm.
- A(ii) 10 mM TCNE in ACN (0.10M TBAF), solution five days old, pathlength 1 cm.
- A(iii) as A(ii) in 0.10M lithium perchlorate.
- B(i) as A(i), in water, no electrolyte.
- B(ii) as B(i), 10 mM, 1 cm pathlength.
- C As A(i) except TCNQ.

Figure 61 shows the MSRS spectra of TCNE and TCNQ in acetonitrile where the potential of the electrode was stepped to the diffusion controlled region of the first reduction wave. Wavelengths were scanned from 8000 Å to 2500 Å. For TCNE, the spectrum shows a broad absorption with a series of fine structure bands. The center of the absorption, which also corresponded to λ_{max} was found to be 4333 Å. This spectrum corresponded well with the spectrum obtained for the anion radical of TCNE in acetonitrile by Jeanmaire et al (138). Their spectrum showed the same feature with λ_{max} occurring at 4350 Å. In the case of TCNQ, two absorptions were obtained; a broad one in the wavelength range of 8000 to 6000 Å consisting of several peaks and a narrow one with a single peak with λ_{max} 4426 Å. For the broad absorption, λ_{max} occurred at 7349 Å. The features of this spectrum agree with those obtained by Melby et al (152) for the anion

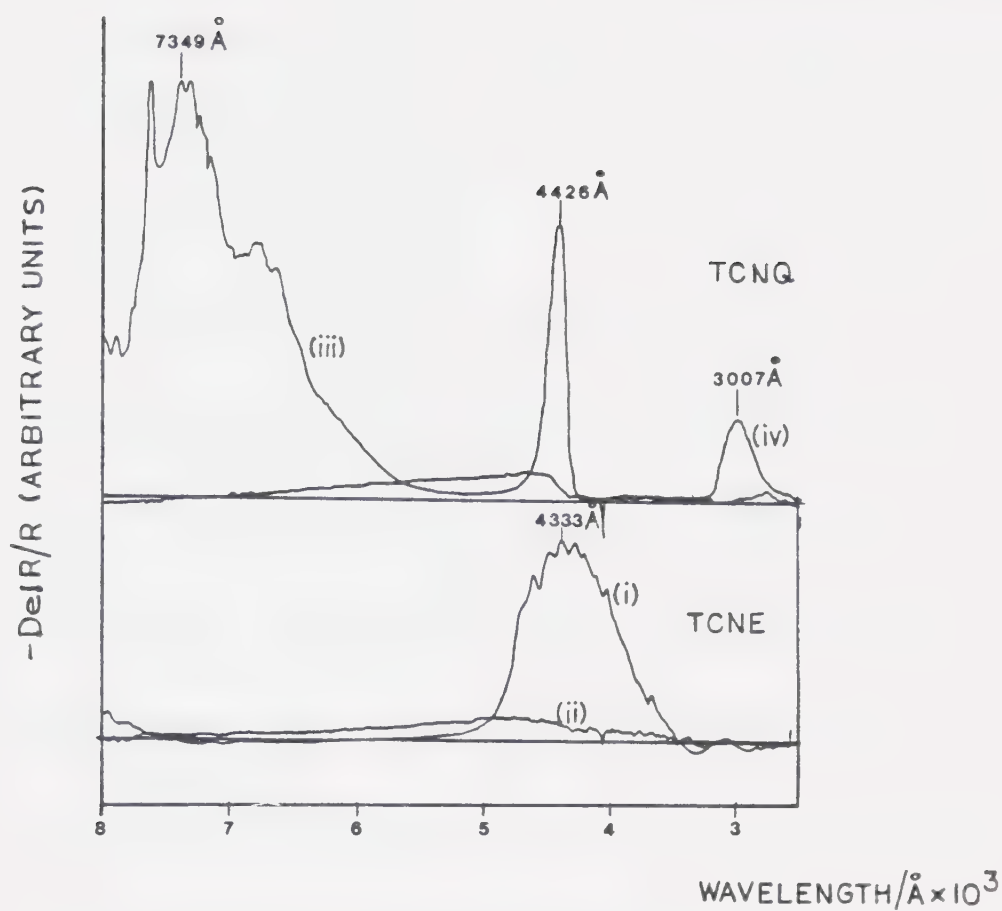


Figure 61. MSRS Spectra of anion radicals and dianions of TCNE and TCNQ in ACN (0.10 M TBAF).
 TCNE (i) Formation of $\text{TCNE}^{\cdot-}$ Potential +0.40 to -0.40 V.
 (ii) Formation of TCNE^{2-} Potential +0.40 to -2.20 V.
 TCNQ (iii) Formation of $\text{TCNQ}^{\cdot-}$ Potential +0.40 to -0.30 V.
 (iv) Formation of TCNQ^{2-} Potential +0.40 to -0.80 V.

radical in acetonitrile. These workers obtained peaks at 420, 842, 744, 760, 680 and 615 nanometers. No major differences were obtained for the spectra obtained here with different supporting electrolytes.

If the potential was stepped to the diffusion controlled region of the second wave, TCNE did not show any significant absorption peaks in the wavelength region 8000-2500 Å. TCNQ solutions had a weak absorption peak with λ max at 3007 Å (see Figure 61). Suchanski and Van Duyne (163) observed the dianion absorption in acetonitrile at 3300 Å. Again this absorption was found, in this study, to be independent of supporting electrolyte.

It was shown in Chapter 2 that the normalized reflectance is related to the integral of the current with respect to time by equation (2.38)

$$-DeIR/R = (4.606 \times 10^{-5}) / (nFA \cos \theta) \int_0^t i(t) dt$$

The integral is the total amount of the absorbing species produced and is equal to q/nFA where q is the total amount of charge passed for the time interval considered. The value of q is determined by integrating the Cottrell equation with respect to time

$$\begin{aligned} \int_0^t i \, dt &= \int_0^t (nFA(D)^{\frac{1}{2}} C) / (\pi t)^{\frac{1}{2}} \, dt \\ &= 2nFA(D\pi)^{\frac{1}{2}} C t^{\frac{1}{2}} \end{aligned} \quad (5.24)$$

Substituting,

$$-DeIR/R = \frac{4.606 \times [2nFA(D\pi)^{\frac{1}{2}} C t^{\frac{1}{2}}]}{nFA \cos \theta} \quad (5.25)$$

Therefore, if the absorbing species at the wavelength of interest is stable on the time scale of the experiment, a plot of $-DeIR/R$ vs $t^{\frac{1}{2}}$ should give a straight line through the origin.

However, if the absorbing species decay following

first order kinetics, it has been shown (198) that the first order homogeneous rate constant is given by

$$k = \frac{[A(t)]_0 - [A(t)]_k}{\int_0^t [A(t)]_k dt} \quad (5.26)$$

where $[A(t)]_0$ is the absorbance which would be obtained at time t if the absorbing species does not decay, $[A(t)]_k$ the absorbance at time t where decay occurs with first order rate constant k . The denominator in the above equation represents the area under the actual absorbance-time profile for the time interval 0 to t . Since for the small values of $\Delta \ell R/R$ which are normally obtained (1.0×10^{-3} or less), the time-dependent absorbance is directly proportional to $-\Delta \ell R/R$ (see Chapter 2), then

$$k = \frac{[-\Delta \ell R/R]_0 - [-\Delta \ell R/R]_k}{\int_0^t [-\Delta \ell R/R]_k dt} \quad (5.27)$$

Figure 62 shows the normalized reflectance-time profiles for 1.00 mM solutions of TCNE and TCNQ in acetonitrile. For these profiles, plots of $-\Delta\epsilon R/R$ vs $t^{\frac{1}{2}}$ show a straight line through the origin (Figure 63). Normalized reflectance time profiles were also obtained for TCNE and TCNQ in the presence of water (Figure 62). From these, $-\Delta\epsilon R/R$ were again plotted vs $t^{\frac{1}{2}}$, given in Figure 64. These plots now show a marked difference in that at longer times, $-\Delta\epsilon R/R$ values deviated, on the low side, from linear behavior. Calculated k values are given in Table 18.

Table 18. Apparent First Order Rate Constants for Decay of TCNE and TCNQ Anion Radicals

Compound	λ Å	$[H_2O]$ /M	k_{-1} /s
TCNE	4250	2.05	1.58
TCNQ	6450	3.64	1.20

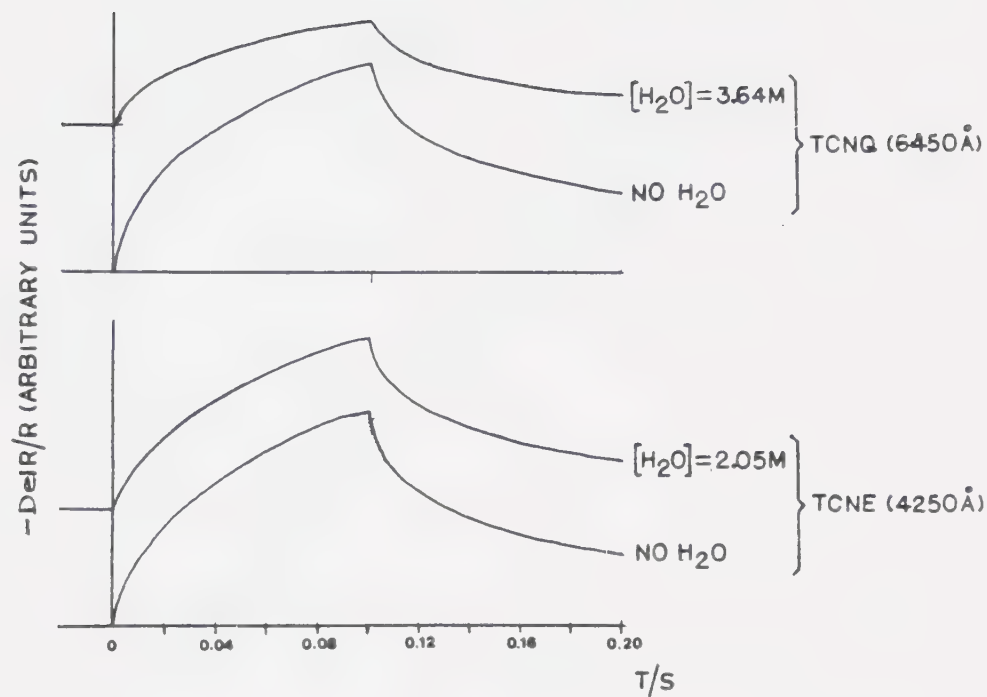


Figure 62. Normalized reflectance-time profiles for $TCNE^+$ and $TCNQ^+$, with and without water addition, in ACN (0.10 M TBAF).

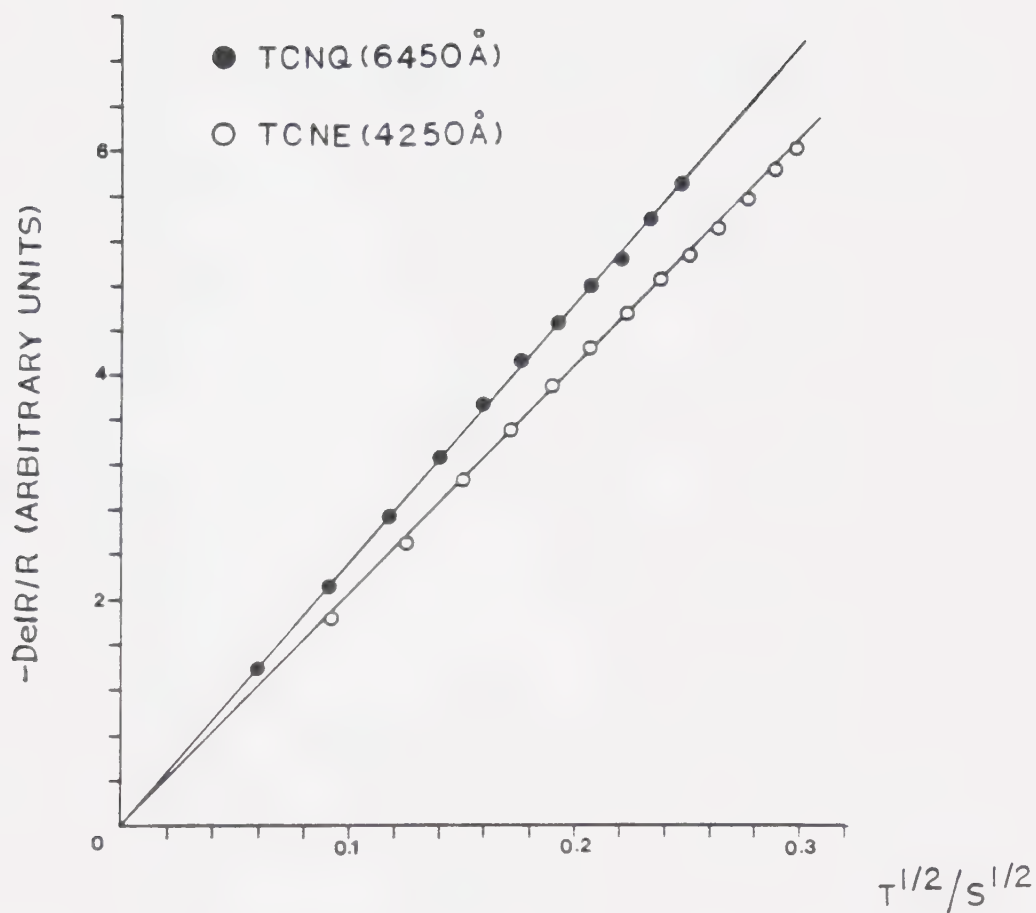


Figure 63. Plot of normalized reflectance ($-\Delta R/R$) versus square root of time for 1.00 mM solutions of anion radicals of TCNE and TCNQ.

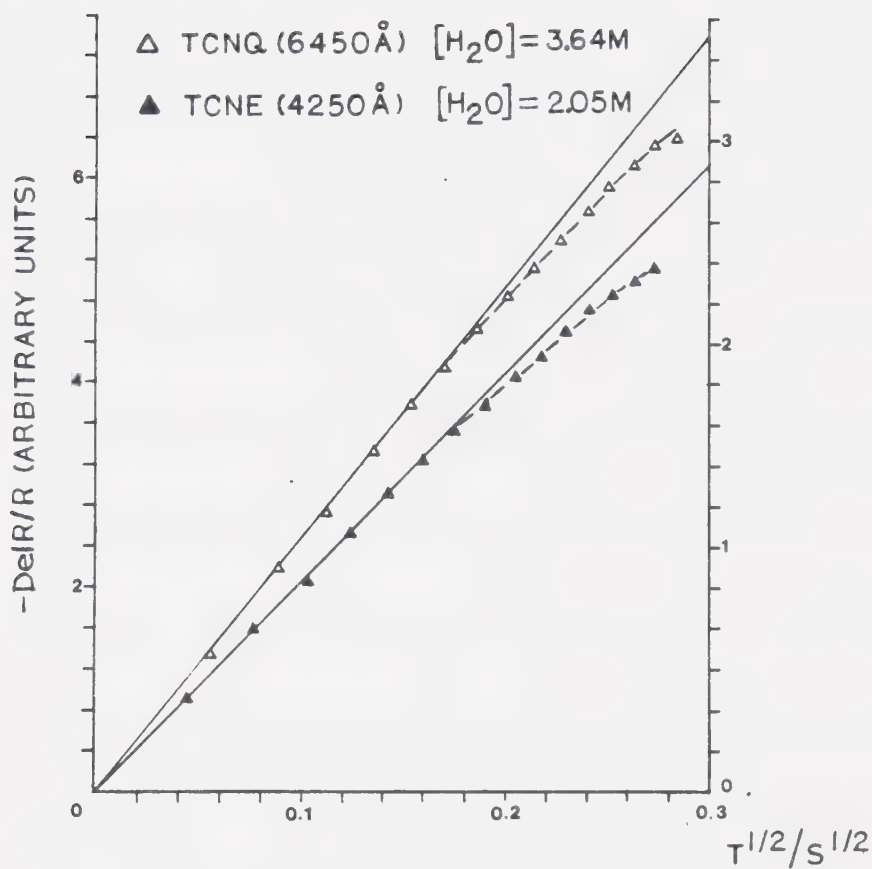


Figure 64. Plots of normalized reflectance versus square root of time for TCNE and TCNQ anion radical in ACN with water addition. Left hand scale for normalized reflectance refers to $TCNE^{\cdot-}$ and right hand scale to $TCNQ^{\cdot-}$.

5.4 Discussion

The cyclic voltammetric results gave overwhelming evidence that the first reduction of TCNE and TCNQ in acetonitrile at glassy carbon and platinum electrodes corresponded to reversible behavior: the fact that $\Delta E(p)$ values were close to the theoretical value of 59 mV and did not vary with sweep rates supports this argument. Also, $i(pa)/i(pc)$ values close to 1.0 imply that the product of the first reduction is a stable species on the time scale of the experiments. Since the slowest sweep rate was 25 mV/s, the species were stable for at least 40 s. Previous investigations have established that these products were stable for a much longer time (138,157). In both cases, the first reduction waves involved one-electron transfers. Therefore, the product formed must be the anion radicals. Diffusion coefficients obtained for TCNE ($2.20 \times 10^{-5} \text{ cm}^2/\text{sec}$) and TCNQ ($2.00 \times 10^{-5} \text{ cm}^2/\text{sec}$) were

slightly larger than those obtained by Sharp (148) who found a value of $1.91 \times 10^{-5} \text{ cm}^2/\text{s}$ for TCNE and $1.42 \times 10^{-5} \text{ cm}^2/\text{s}$ for TCNQ. $i(p)/(v)^{1/2}$ values at the planar glassy carbon electrode were constant at all sweep rates but for the platinum wire electrode, the values increased at low sweep rates. This is because, at low sweep rates, cylindrical diffusion contributions must be considered.

Peak potentials were found to be invariable with sweep rates. Also, examination of Table 4 and Table 10 reveals that different electrodes and supporting electrolytes do not affect these values. Therefore, there is negligible ion pairing between the anion radicals of TCNE and TCNQ and the counteranions in acetonitrile. The same conclusion was found for aromatic hydrocarbon anion radicals studied earlier.

For reversible reduction the peak potentials and the half peak potentials are related to polarographic E_h

values by the relation

$$E_h = E(p) + 1.11 \text{ RT/nF} \quad (5.30)$$

$$E_h = E(p/2) - 1.09 \text{ RT/nF} \quad (5.31)$$

At 23°C, and for n=1, RT/nF=0.0255 volts and

$$E_h = E(p) + 0.028. \quad (5.32)$$

or in terms of half peak potentials

$$E_h = E(p/2) - 0.028 \quad (5.33)$$

The calculated E_h values are compared relatively to literature values in Table 19.

Table 19. Comparison of E_h Values for the First Reduction Wave of TCNE and TCNQ in Acetonitrile (0.10 M LiClO₄)

Compound	E_h vs Ag/Ag ⁺ This Work	E_h vs SCE Melby et al (152)
TCNE	-0.086	+0.152
TCNQ	-0.118	+0.127

In both cases, the Eh value for TCNE is slightly more positive than that for TCNQ. This means that TCNE in acetonitrile is a slightly stronger π -acid than TCNQ. Pons et al (139) have found, using a surface sensitive FTIR technique, that in the presence of non-complexing TBAF supporting electrolyte, that a monolayer of TCNE anion radicals adsorbed flat on the surface of the platinum electrode. This was attributed to the formation of an electron-donor-acceptor complex between the platinum metal and the TCNE molecules. This behavior was absent when LiClO₄ was used as supporting electrolyte. However, this behavior was not detected in the cyclic voltammetric studies of the first reduction wave. The presence of adsorbed TCNE anion radical could affect the reversibility of the first wave. $i(p_a)/i(p_c)$ values could deviate from unity values. If the adsorption was strong, prepeaks and postpeaks could be observed. However, none of these

effects were observed. It is possible that the effect observed by Pons et al (139) was very small and since cyclic voltammetry is not as sensitive to surface species as the FTIR technique used, it was not observed in this work.

For the second reduction wave of TCNE, i.e. the reduction of the anion radical to the dianion (chronoamperometry showed that this reduction involved one electron) reversibility was only found for both platinum and carbon electrodes for Na^+ countercation. With Li^+ , platinum electrode showed reversible reduction but the increase of $i(\text{pa})/i(\text{pc})$ values was about the same as for the other case where no adsorption was present which means that the anion radical was not adsorbed. The behavior of the second wave with increase of $i(\text{pa})/i(\text{pc})$ with increase in scan rate and the absence of prepeaks or postpeaks points toward weak product adsorption as discussed by Wopschall and Shain (243). Except for this

adsorption of the dianion at carbon, the electron transfer rate for TCNE at both platinum and carbon electrodes with Na^+ and Li^+ countercations appears to be fast enough so that for the time scale of the voltammetric experiments (25 mV/s to 500 mV/s scan rates), Nernstian behavior was observed. However this cannot be said for TBA^+ and TEA^+ countercations as shown by the results for these two countercations. Not only was cation effect apparent but there was also dependence on electrode materials. With TBA^+ countercation the peak cathodic potential for the second wave at glassy carbon electrode was 335 mV more positive compared to that at platinum (Table 5). This value was 172 mV with TEA^+ countercation. Further, the apparent heterogeneous rate constants at glassy carbon with TEA^+ countercation was $(1.2 \pm 0.1) \times 10^{-2}$ cm/s compared to 1.8×10^{-3} cm/s at platinum, which was 7 times slower. The same trend was observed with TBA^+ (3.8×10^{-5} cm/s) being 37 times slower than that at glassy carbon (1.4×10^{-3} cm/s).

In addition, it was noted that the rate was faster with TEA⁺ than TBA⁺ counteranion. The large shifts in E_{pc} values, for the case of Na⁺ and Li⁺, where electrode reaction was fast points toward the existence of ion pairing. Further, the plot of E_h vs ionic radius given in Figure 58 showed that the smaller the ionic radius of the cation, the larger the positive shift. This indicates that contact ion pairs (172,210) were formed as opposed to solvent separated ion pairs. For contact ion pairs it would be expected that the strength of ion pairing increased in the order of decreasing ionic radius this being TBA⁺ < TEA⁺ < Na⁺ < Li⁺ as was shown here.

At a glassy carbon electrode, there was no evidence of adsorption of TCNE^{•-} with both electrodes and all cations, and except for the differences in heterogeneous rate constants with different counteranions points toward the ion pairing abilities of the cations. TBA⁺ is not expected to ion pair to

TCNE= to any appreciable extent as confirmed by the results obtained for TCNQ= (Table 15). Chauhan et al (246) have found that TEA+ formed weak ion pairs with nitromesitylene anion radicals in ACN and this may well occur for TCNE=. However, Na+ and Li+ ion paired strongly with TCNE= as shown by the positive shifts in E_h . Therefore strong ion pairing tends to increase the rate of electron transfer for TCNE $\dot{-}$ reduction. The present results seem to confirm the proposal by Jeanmaire et al (138): a change in geometry from planarity for TCNE $\dot{-}$ to nonplanarity for TCNE= causes irreversibility for the reduction of TCNE $\dot{-}$. Also no evidence was given in that study. In the presence of the strong ion pairing Na+ and Li+ counteranions, the irreversibility of the reduction was lifted because ion pairing tends to localize the negative charges at the ethylene carbons and therefore maintain the planarity of the dianion. For TEA+, only weak ion pairing may be present, and therefore a compromised position is reached and the rate constant is

between the two extreme cases. Huebert and Smith (2) have observed a large stereochemical effect for the reduction of the nonplanar cyclooctatetracene to its planar anion radical. The electron transfer was found to be slow for this system.

The results obtained at a platinum electrode are more difficult to explain. Certainly, the ion pairing effect is present since the TCNE^{•-} reduction showed Nernstian behavior in the presence of Na⁺ and Li⁺ but not with TEA⁺ and TBA⁺. For the latter two cations, rate constants were much slower compared to those at a glassy carbon electrode. Strong adsorption of TCNE^{•-} at platinum was not observed since this would result in postpeaks and prepeaks. Further, anion radical would show up in the first reduction wave. However, this was not so because the first wave gave Nernstian behavior in all cases. Also, adsorption of the dianion will cause the reverse peaks to occur at more positive values but this was not the case as can be seen from the data of Table 5. However,

the fact that the reduction peak potentials were more negative than those observed at carbon indicate the presence of adsorption. Also, Pons et al (139) have shown that adsorption of the anion radical of TCNE was present at platinum with TBA⁺ as counteranion. It is possible that, as was mentioned earlier, cyclic voltammetry was not sensitive enough to detect adsorption in this case and further the presence of weak adsorption would be masked by the irreversibility of the wave due to geometry change. However, the cathodic peak potential shifts at platinum compared to carbon (335 mV for TBA⁺, 172 mV for TEA⁺) appear to be rather large to be explained by weak adsorption. Therefore, the only firm conclusion which can be reached here is that geometry change caused the irreversibility of TCNE^{•-} reduction with TBA⁺ and TEA⁺ cations. The smaller rate constants found at a platinum electrode compared to a carbon electrode, together with the negative shift in cathodic peak potential, could only be

tentatively attributed to adsorption of the TCNE^{•-} assigned based on the results of Pons et al (139).

In passing, the method of the variation of $\Delta E(p)$ with scan rate used in the determination of rate constants deserves a little discussion. The Δ values for different $\Delta E(p)$ values, as calculated by Nicholson (84), assumes that the transfer coefficient α is 0.5. The error expected in the calculated rate constant with this assumption is small, approximately 5%, if the reduction is sufficiently close to Nernstian behavior; i.e. if α does not deviate too much from 0.5. This means that $\Delta E(p)$ values should be between $60/n$ and $120/n$ mV. At higher values of $\Delta E(p)$, deviations of α from 0.5 become larger. For example for $\Delta E(p)$ having a value of $200/n$ mV, an error of 20% in the determined rate constants is expected (61). However, at $\Delta E(p)$ values close to the reversible value of $59/n$ mV, small changes in $\Delta E(p)$ give rise to large variations in the values of Δ , as can be

seen from Figure 54. Therefore the best accuracy can be obtained if $\Delta E(p)$ values are kept between about 75 mV and 120 mV, if possible.

For the reduction of TCNQ, diagnostic criteria for the cyclic voltammetric technique confirms the Nernstian behavior of both the first and second wave at both electrodes and all supporting electrolytes used. These include the constancy of peak potentials at all sweep rates, the value of 1.0 obtained for $i(pa)/i(pc)$ values, and $\Delta E(p)$ values close to 59 mV for reversible one-electron waves at all sweep rates. The number of electrons transferred for the first wave was found to be approximately 2.0 for the sum of the first and second wave. This implies the formation of the anion radical and the dianion. $i(pc)/v^{\frac{1}{2}}$ value for the second wave was found about 10% lower than that for the first wave, as was the case for TCNE. This is attributed to a small decrease in diffusion coefficient for the anion radicals. The peak potentials, for

the TCNQ potentials did not show any dependence on counter-cations or electrode materials. Therefore no ion pairing was present between $\text{TCNQ}^{\cdot-}$ and TBA^+ , Na^+ , or Li^+ , the cations used in this investigation. The second reduction, $\text{TCNQ}^{\cdot-}$ to TCNQ^{2-} , gave peak potential which were dependent on countercations although not electrode material. The Eh values, from Figure 58, increased with decreasing size of ionic radius according to $\text{TBA}^+ > \text{Na}^+ > \text{Li}^+$. These large shifts with ionic radius were again attributed to the formation of contact ion pairs. For the $\text{TCNQ}^{\cdot-}$ reduction no decrease in heterogeneous rate constant was observed for TBA^+ because there was no change in planar geometry in going from $\text{TCNQ}^{\cdot-}$ to TCNQ^{2-} . The presence of the quinoid functionality assures planarity whereas the ethylenic group in TCNE could not.

In the presence of mixed electrolytes, the reduction of $\text{TCNE}^{\cdot-}$ showed adsorption effects as was mentioned earlier (Figure 58A). However, the reversible nature of TCNE reduction

was not affected. In general the adsorption characteristics are typical of product adsorption, namely the adsorption of TCNE= or its ion pairs. For example, with 0.095 M TBAF and 0.005 M LiClO₄, at a platinum electrode, the sharpness of the anodic peak is indicative of product adsorption. With 0.05 M TBAF and 0.05 M LiClO₄ at carbon a prepeak was observed for the cathodic scan as well as the sharp anodic peak. This is the criterion for strong product adsorption, as given by Wopschall and Shain (243). The change in cyclic voltammograms for TCNE with 0.05 M TEAF and 0.05 M LiClO₄ at platinum was even more dramatic. Not only was a sharp cathodic peak for TCNE^{•-} reduction observed but no reverse peak was seen. Instead a very large, sharp peak was observed just anodic of the peak for TCNE^{•-} oxidation. This is highly indicative of formation of an insoluble mixed salt of TCNE= deposited on the electrode which is not oxidized in the potential region of the simple TCNE= oxidation and therefore no oxidation current was

seen. However at far more positive potential, destruction of the insoluble film occurred giving rise to the large, sharp peak. The occurrence of this type of peak, which was much larger than that caused by usual adsorption behavior, was found by Nagaoka and Okazaki (247) for the sparingly soluble anthranthrone anion radical / Ba^{++} salt in DMF. However, in their case, the peak occurred in the region of the oxidation of anion radical.

For TCNQ, mixed electrolytes did not change the reversible behavior of both the first and second reduction. This means that variation of E_h with cation concentrations could be studied at constant ionic strength without the deleterious effect of adsorption. Initially, it was established that TBA^+ did not ion pair significantly with TCNQ^- . This was shown by the fact that E_h did not shift appreciably with TBA^+ concentration after correction for liquid junction potential. From Table 15 it can be seen that for the concentrations of TBA^+

used, the largest shift in E_h after correction for E_j was only 10 mV, certainly not much larger than experimental errors such as errors in reading and in locating $E(p/2)$ values used for obtaining E_h (about 5 mV). For the variation of E_h with metal cations Na^+ and Li^+ , the condition of the metal cations being in large excess of the TCNQ concentration for the validity of equations (5.19) and (5.22) is satisfied by keeping the TCNQ concentration at 5.00 mM or greater. Since TCNQ= did not form any ion pairs with the cations studied, only equation (5.23) applies to the present study. It was shown in Figure 59 the plots for ΔE_h vs $\log C_{M^+}$ exhibited two linear segments for both Na^+ and Li^+ . This is indicative of the formation of ion pairs with two different stoichiometries. In the case of Li^+ , the slopes of 52 and 122 mV for the two segments are very close to those of 59 and 118 mV for the theoretical quantitative formation of TCNQ=, Li^+ ion pairs with 1:1 and 1:2 stoichiometries. The formation constants were then calculated from

equation (5.23) using the data from the segment where the respective ion pair was formed. In the case of sodium the slopes for the linear segments were smaller than the theoretical values, being only 27 and 80 mV. This means that formation of the 1:1 and 1:2 ion pairs was not quantitative and therefore less strong than for Li^+ . The same method was used for calculation of the formation constants for the $\text{TCNQ}^{\cdot-}, \text{Na}^+$ ion pairs. However, in this case, care was taken to avoid points in the crossover region for the two line segments where curvature of the plot arose. Values of formation constants obtained in this manner were found to be reasonably constant for different points in the same linear segment, in all cases exhibiting a standard deviation of about 10% of the calculated values. The values for the formation constants given in Table 17 show that the strength of ion pair formation for Li^+ was about 100 times greater than that for Na^+ for both species formed.

The presence of ion pairing between $\text{TCNQ}^{\cdot-}$ and Na^+ and Li^+

cations has been confirmed by shifts in vibrational absorptions of the C=N stretch mode observed in the authors laboratory (172). The results are shown in Table 20.

Table 20. Vibrational Absorption (C=N stretch) for TCNQ: and TCNQ= with Different Supporting Electrolytes (0.10M). C=N Absorption Bands (cm⁻¹).

Species	TBAF	NaClO ₄	LiClO ₄
TCNQ:	2181.5	no change	no change
	2154.5	no change	no change
TCNQ=	2150.6	2156.4	2116.1
	2104.3	2110.1	2117.8

For TCNQ: no ion pairing was present and no shift in the absorption bands was observed. However, the TCNQ= absorption bands shifted to higher energy with increased strength of ion pairing (TBA⁺ > Na⁺ > Li⁺). This is consistent with the view that ion pairing localizes the negative charges on the dicyano carbon and reduces delocalization through the C=N bond which

tends to reduce the triple bond character.

As mentioned in the results section, freshly prepared solutions of TCNE in acetonitrile were colorless but upon standing turned yellow. If supporting electrolyte was present the color change was obvious for TBAF but not so much for LiClO₄. The fact that the solution containing TBAF showed two additional absorption peaks at 3973 Å and 4159 Å (Figure 60) offers a simple explanation since these two peaks correspond to the absorption maxima of TCNE in water at 3956 Å and 4125 Å (Figure 60). These two absorptions are probably due to the formation of weak charge-transfer complexes between water and TCNE. In the presence of LiClO₄, these absorptions were not observed because at the low concentration level of water in purified acetonitrile (probably 1-2 mM), most of the water present was tied up by Li⁺ ions, which were present at 0.1M.

The MSRS spectrum obtained when the potential was

stepped to the diffusion controlled region of the first wave corresponded to the spectra of the anion radicals of TCNE and TCNQ obtained by other workers. The dianion of TCNE did not show any absorption in the wavelength region studied (8000 \AA to 2000 \AA) whereas for TCNQ only a weak absorption was observed with λ_{max} at 3007 \AA . This is in agreement with results by other investigators (163). The determination of rate constant for the protonation of TCNE and TCNQ anion radicals is based on the assumption of first order decay of these species. Since the concentrations of water were 2.05 M and 3.64 M for TCNE (1.00 mM) and TCNQ (1.00 mM) respectively, pseudo first order conditions existed and the assumption is valid.

Sharp (148) studied the first order decay of TCNE and TCNQ anion radicals in acetonitrile by observing changes in $i(\text{pa})/i(\text{pc})$ with scan rates. No water was added to the solutions and decay was assumed to be due to trace

impurities present in the solvent. The rate constant for TCNE: decay was found to be about 20 times greater than that for TCNQ:. However, in this work, this value was found to be 2.

It is concluded that simple electrochemical techniques can be effectively utilized to study ion association reactions in solutions of high dielectric constant. Coupled with standard spectrophotometry and spectroelectrochemistry, these methods allow fast and accurate determination of stoichiometries, mechanisms, and kinetic parameters of these reactions.

LITERATURE REFERENCES

1. M.E. Peover, J.S. Powell, J. Electroanal. Chem., 20 (1969) 427.
2. B.J. Huebert, D.E. Smith, J. Electroanal. Chem., 31 (1971) 333.
3. J.P. Stradins, Electrochim. Acta, 9 (1964) 711.
4. G.J. Hoijtink in P. Delahay and C.W. Tobias, Eds., "The Electrochemical Reduction of Aromatic Hydrocarbons," in "Advances in Electrochemistry and Electrochemical Engineering," Vol. 7, Interscience, New York, 1970, p. 221.
5. V.D. Parker, J. Am. Chem. Soc., 98 (1978) 98.
6. P.H. Rieger, C.K. Fraenkel, J. Chem. Phys., 37 (1962) 2795.
7. A. Macoll, Nature, 163 (1949) 178.
8. T.J. Katz, W.H. Reinmuth, D.E. Smith, J. Am. Chem. Soc., 84 (1962) 802.
9. E. Itabashi, J. Electroanal. Chem., 36 (1972) 179.
10. W.J.M. van Tilborg, L.J.G. Dekker, C.J. Smit, Rec. Trav. Chim. Pays-Bas, 97, (1978) 321.
11. W.J.M. Van Tilborg. C.J. Smit, R.A. van Santen, Rec. Trav. Chim. Pays-Bas, 98 (1979) 526.
12. M.T. Watts, M.L. Lu, R.C. Chen, M.P. Eastman, J. Phys. Chem., 77 (1973) 2959.
13. M. Ogasawara, H. Takaoka, K. Hayashi, Bull. Chem. Soc. Japan, 46 (1973) 36.
14. Ions and Ion Pairs in Organic Reactions, M. Szwarc, Ed., Vol. 1, Interscience, New York, 1972.
15. Ions and Ion Pairs in Organic Reactions, M. Szwarc, Ed., Vol. 2, Interscience, New York, 1972.
16. B. Bockrath, L.M. Dorfman, J. Phys. Chem., 77 (1973) 2618.

17. A. Rainis, M. Szwarc, *Int. J. Chem. Kinetics*, 7 (1975) 919.
18. E.J. Panck, T.J. Rodgers, *J. Am. Chem. Soc.*, 96 (1974) 6921.
19. H.A. Laitinen, S. Wawzonek, *J. Am. Chem. Soc.*, 64 (1942) 1765.
20. S. Wawzonek, H.A. Laitinen, *J. Am. Chem. Soc.*, 64 (1942) 2365.
21. S. Wawzonek, J.W. Fan, *J. Am. Chem.* 68 (1946) 2541.
22. L.H. Chopard-dit-Jean, E. Heilbronner, *Helv. Chim. Acta*, 36 (1953) 144.
23. G.J. Hoijtink, J. van Schooten, E. de Boer, W.I. Aalsberg, *Rec. Trav. Chim. Pays-Bas*, 73 (1954) 355.
24. S. Wawzonek, E.W. Blaka, R. Berkey, M.E. Runner, *J. Electrochem. Soc.*, 102 (1955) 235.
25. A.C. Aten, C. Buthker, G.J. Hoijtink, *Trans Faraday Soc.*, 55 (1959) 324.
26. P.H. Given, M.E. Peover, *J. Chem. Soc.*, (1960) 385.
27. P.H. Given, M.E. Peover, J. Schoen, *J. Chem. Soc.*, (1958) 2674.
28. A.J. Bard, L.R. Faulkner, *Electrochemical Methods: Fundamentals and Applications*, John Wiley and Sons, New York, 1980, p. 96.
29. A.C. Aten, G.J. Hoijtink, *Advances in Polarography*, Pergamon Press, Oxford, 1961, p. 777.
30. H. Kojima, A.J. Bard, *J. Electroanal. Chem.*, 63 (1975) 117.
31. D.E.G. Austen, P.H. Given, J.E. Ingram, M.E. Peover, *Nature*, 182 (1968) 1784.
32. B.S. Jensen, V.D. Parker, *J. Am. Chem. Soc.*, 97 (1975) 5211.
33. S.V. Laszczynski, *Z Elektrochem.*, 2 (1895) 55.

34. A. Brenner, "Electrolysis in Nonaqueous Systems," in P. Delahay and C.W. Tobias, Eds., "Advances in Electrochemistry and Electrochemical Engineering," Vol. 5, Interscience, New York, 1967, p. 205.
35. R. Jasinski, High Energy Batteries, Plenum Pres, New York, 1967.
36. Lithium Batteries, The Electrochemical Society Soft-bound Series, H.V. Venkatesetty, Ed., 1981.
37. D.J. Astley, J.A. Harrison, H.R. Thirsk, Trans Faraday Soc., 64 (1968) 192.
38. R.F. Scarr, J. Electrochem. Soc., 117 (1970) 295.
39. S.G. Meibuhr, J. Electrochem. Soc., 117 (1970) 56.
40. J.N. Butler, D.R. Cogley, J.C. Synott, J. Phys. Chem., 73 (1969) 4026.
41. J.N. Butler, J. Electroanal. Chem., 14 (1967) 89.
42. B. Burrows, S. Kirkland, J. Electrochem. Soc., 115, (1968) 1164.
43. B.N. Kabanov, I.I. Astakhov, I.G. Kiseleva, Russian Chem. Rev., 34 (1965) 775.
44. J. Heyrovsky, Chem. Listy, 16 (1922) 256.
45. E.S. Peracchio, V.W. Meloche, J. Am. Chem. Soc., 60 (1938) 1770.
46. I. Zlotowsky, I.M. Kolthoff, Ind. Eng. Chem. Anal. Ed., 14 (1942) 473.
47. I. Zlotowsky, I.M. Kolthoff, J. Am. Chem. Soc., 64 (1942) 1297.
48. A.A. Vlcek, Coll. Czech. Chem. Commun., 20 (1955) 413.
49. V. Gutman, E. Nedbalek, Mh. Chem., 89 (1958) 203.
50. R.C. Larson, R.T. Iwamoto, J. Am. Chem. Soc., 82 (1960) 3239, 3526.
51. J.F. Coetzee, J.L. Hedrick, J. Physik. Chem., 67 (1963) 221.

52. V. Gutman, G. Schober, Z. Anal Chem., 171 (1959) 339.
53. G. Schober, V. Gutman, "Advances in Polarography," I.S. Longmuir, Ed., Pergamon Press, London, 1960, p. 940.
54. J.F. Coetzee, W.S. Siao, J. Inorg. Chem., 2 (1963) 14.
55. G. Schober, V. Gutman, Mh. Chem., 89 (1958) 401.
56. H.A. Laitinen, C.E. Shoemaker, J. Am. Chem. Soc., 72 (1950) 4975.
57. L.A. Knecht, I.M. Kolthoff, J. Inorg. Chem., 1 (1962) 195.
58. I.M. Kolthoff, J.F. Coetzee, J. Am. Chem. Soc., 79 (1957) 870.
59. G.H. Brown, R.A. Urfali, J. Am Chem. Soc., 80 (1958) 2113.
60. D.L. McMasters, R.B. Dunlap, J.R. Kuempel, L.W. Kreider, T.R. Shearer, Anal. Chem., 39 (1967) 103.
61. J.W. Diggle, A.J. Parker, D.A. Owensby, Aust. J. Chem., 28 (1975) 237.
62. G.J. Hills, L.M. Peter, J. Electroanal. Chem., 50 (1974) 175.
63. V. Gutmann, M. Michlmayr, G. Peychal-Heiling, Anal. Chem., 40 (1968) 619.
64. R.R. Besette, D.F. Harwood, Anal. Chim. Acta, 66 (1973) 105.
65. A. Baranski, W.R. Fawcett, J. Electroanal. Chem., 94 (1978) 237.
66. A. Baranski, W.R. Fawcett, J. Chem. Soc. Faraday Trans. 1, 78 (1982) 1279.
67. W.R. Fawcett, J.S. Jaworski, J. Chem. Soc. Faraday Trans. 1, 78 (1982) 1971.
68. H. Berthelot, Ann., 143 (1867) 98.

69. W. Schlenk, J. Appenrodt, A. Michael, A. Tahl, Ber, 47 (1914) 479.
70. W. Schlenk, J. Bergmann, Ann., 463 (1928) 91.
71. C.B. Wooster, F.B. Smith, J. Am. Chem. Soc., 53 (1931) 179.
72. N.D. Scott, J.F. Walker, V.L. Hansley, J. Am. Chem. Soc., 58 (1936) 2442.
73. A. Jeannes, R. Adams, J. Am. Chem. Soc., 59 (1937) 2608.
74. V.L. Hansley, Ind. Eng. Chem., 43 (1951) 1759.
75. D. Lipkin, D.E. Paul, J. Townshend, S.I. Weissman, Science, 117 (1953) 534.
76. T.L. Chu, S.C. Yu, J. Am. Chem. Soc., 76 (1954) 3367.
77. G.J. Hoijtink, E. de Boer, P.H. Van der Meij, W.P. Weijland, Rec. Trav. Chim. Pays-Bas 74 (1955) 277.
78. G.J. Hoijtink, E. de Boer, P.H. Van der Meij, W.P. Weijland, Rec. Trav. Chim. Pays-Bas, 75 (1956) 487.
79. G.J. Hoijtink, Rec. Trav. Chim. Pays-Bas, 74 (1955) 1525.
80. D.E. Paul, D. Lipkin, S.I. Weissman, J. Am. Chem. Soc., 78 (1956) 116.
81. P. Balk, G.J. Hoijtink, J.W.H. Schreurs. Rec. Trav. Chim. Pays-Bas, 76 (1957) 813.
82. P. Balk, S. de Bruijn, G.J. Hoijtink, Mol. Phys., 1 (1958) 151.
83. P. Balk, S. de Bruijn, G.J. Hoijtink, Rec. Trav. Chim. Pays-Bas, 76 (1957) 860.
84. G.J. Hoijtink, Rec. Trav. Chim. Pays-Bas, 76 (1957) 869.
85. G.J. Hoijtink, Rec. Trav. Chim. Pays-Bas, 76 ((1957) 885.

86. P. Balk, S. de Bruijn, G.J. Hoijtink, *Rec. Trav. Chim. Pays-Bas*, 76 (1957) 907.
87. P. Balk, S. de Bruijn, G.J. Hoijtink, *Mol. Phys.*, 2 (1957) 151.
88. J. Jagur-Grodzinski, M. Feld, S.L. Yang, M. Szwarc, *J. Phys. Chem.*, 69 (1965) 628.
89. S.I. Weissman, J. Townsend, D.E. Paul, G.E. Pake, *J. Chem. Phys.*, 21 (1953) 2227.
90. S. Winstein, E. Clippinger, A.H. Fainberg, G.C. Robinson, *J. Am. Chem. Soc.*, 76 (1954) 2597.
91. E. Grunwald, *Anal. Chem.*, 26 (1954) 1696.
92. M. Szwarc, *Carbanions, Living Polymers and Electron Transfer Processes*, Interscience, New York, 1968.
93. S. Miertus, O. Kysel, J. Danciger, *Coll. Czech. Chem. Commun.*, 45 (1980) 360.
94. R.N. Adams, *J. Electroanal. Chem.*, 8 (1964) 151.
95. P.H. Rieger, I. Bernal, W.H. Reinmuth, G.K. Fraenkel, *J. Am. Chem. Soc.*, 85 (1963) 683.
96. K.H.J. Buschow, J. Dieleman, G.. Hoijtink, *J. Chem. Phys.*, 42 (1965) 1993.
97. J. Smid in "Ions and Ion Pairs in Org. Reactions," Vol. 1, M. Szwarc Ed., Wiley-Interscience, New York 1972, p. 85.
98. A. Streitwieser, G.J. Chang, W.B. Hollyhead, J.R. Murdoch, *J. Am. Chem. Soc.*, 94 (1972) 5288.
99. A.J. Popov, *Pure Appl. Chem.*, 41 (1975) 275.
100. S. Konishi, Y. Morioka, I Nakagawa, *Chem. Phys. Lett.*, 55 (1978) 428.
101. J.C. Evans, G.Y.-S Lo, *J. Phys. Chem.*, 69 (1965) 3223.
102. B. Herold, *J. Catal. Rev.*, (1978) 17.

103. T.L. Cairns, R.A. Carboni, D.D. Coffman, V.A. Engelhardt, R.E. Heckert, E.L. Little, E.G. McGeer, B.C. McKusick, W.J. Middleton, J. Am. Chem. Soc., 80 (1957) 2340.
104. F.J. Brockman, Can. J. Chem., 33 (1955) 507.
105. T.L. Cairns, R.A. Carboni, D.D. Coffman, V.A. Engelhardt, R.E. Heckert, E.L. Little, E.G. McGeer, B.C. McKusick, W.J. Middleton, R.M. Scriber, G.W. Theobald, H.E. Weinberg, J. Am. Chem. Soc., 80 (1958) 2775.
106. W.J. Middleton, R.E. Heckert, E.L. Little, C.G. Krespan, J. Am. Chem. Soc., 80 (1958) 2378.
107. W.J. Middleton, V.A. Engelhardt, J. Am. Chem. Soc., 80 (1958) 2788.
108. W.J. Middleton, V.A. Engelhardt, J. Am. Chem. Soc., 80 (1958) 2829.
109. B.C. McKusick, R.E. Heckert, T.L. Cairns, D.D. Coffman, H.F. Mower, J. Am. Chem. Soc., 80 (1958) 2806.
110. G. Briegleb, Elektronen-Donator-Acceptor Komplexe, Springer 1961.
111. S.A. Berger, Spectrochim. Acta, 23A (1967) 2213.
112. Y. Matsunaga, Bull. Chem. Soc. Japan, 42 (1969) 2170.
113. L.E. Lyons, L.D. Palmer, Aust. J. Chem., 29 (1976) 19.
114. E.C.M. Chen, W.E. Wentworth, J. Chem. Phys., 63 (1975) 3183.
115. M.J.S. Dewar, H.S. Rzepa, J. Am. Chem. Soc., 100 (1978) 784.
116. C.E. Looney, J.R. Downing, J. Am. Chem. Soc., 80 (1958) 2840.
117. D.A. Long, W.O. George, Spectrochim. Acta, 19 (1963) 1717.
118. T. Takenaka, S. Hayashi, Bull. Chem. Soc. Japan, 37 (1964) 1216.

119. F.A. Miller, O. Sala, P. Devlin, J. Overend, E. Liipert, W. Luder, H. Moser, J. Varchmin, *Spectrochim. Acta*, 20 (1964) 1233.
120. P.A. Malachuk, *Anal. Chem.*, 41 (1969) 1493.
121. S. Pons, T. Davidson, A. Bewick, *J. Am. Chem. Soc.*, 105 (1983) 1802.
122. Y. Lida, *Bull. Chem. Soc. Japan*, 46 (1973) 423.
123. M. Itoh, *J. Am. Chem. Soc.*, 92 (1970) 886.
124. O.W. Webster, W. Mahler, R.E. Benson, *J. Am. Chem. Soc.*, 84 (1962) 3678.
125. J. Halper, W.D. Closson, H.B. Gray, *Theoret. Chim. Acta*, 4 (1966) 174.
126. M.D. Gordon, *Tetrahedron*, 36 (1980) 2113.
127. R.E. Merrifield, W.D. Phillips, *J. Am. Chem. Soc.*, 80 (1958) 2778.
128. M.E. Peover, *Trans. Faraday Soc.*, 60 (1964) 417.
129. M.E. Peover, *Trans. Faraday Soc.*, 58 (1962) 2370.
130. A.R. Lepley, C.C. Thompson, Jr., *J. Am. Chem. Soc.*, 89 (1967) 5523.
131. O. Webster, W. Mahler, R.E. Benson, *J. Org. Chem.*, 25 (1960) 1470.
132. S.I. Weissman, *J. Chem. Phys.*, 33 (1960) 626.
133. T. Sato, E. Yamada, Y. Okamura, J. Amada, K. Hata, *Bull. Chem. Soc. Japan*, 38 (1965) 1048.
134. D.F. Ilten, M. Calvin, *J. Chem. Phys.*, 42 (1965) 3760.
135. F.E. Stewart, M. Eisner, W.R. Carper, *J. Chem. Phys.*, 44 (1966) 2866.
136. F.E. Stewart, M. Eisner, *Mol. Phys.*, 12 (1967) 173.
137. R.N. Butler, J. Oakes, M.C.R. Symons, *J. Chem. Soc. A*, (1968) 1134.

138. D.L. Jeanmaire, M.R. Suchanski, R.P. Van Duyne, J. Am. Chem. Soc., 97 (1975) 1699.
139. S. Pons, S.B. Khoo, A. Bewick, M. Datta, J.J. Smith, A. S. Hinman, G. Zachmann, J.Phys. Chem., in press.
140. J.C. Moore, D. Smith, Y. Youchne, J.P. Devlin, J. Phys. Chem., 75 (1971) 325.
141. J.E. Pemberton, R.P. Buck, Appl. Spectroscopy, 35 (1981) 571.
142. M. Itoh, Bull. Chem. Soc. Japan, 45 (1972) 1947.
143. M.T. Watts, M.L. Lu, R.C. Chen, M.P. Eastman, J. Phys. Chem., (1973) 2959.
144. E. Samuel, D. Vivien, J. Livage, Inorg. Chim. Acta, 21 (1977) 179.
145. M. Ogasawara, H. Takaoka, K. Hayashi, Bull. Chem. Soc. Japan, 46 (1973) 35.
146. J.E. Bloor, B.R. Gilson, D.D. Shillady, J. Phys. Chem., 71 (1967) 1238.
147. M.L. Kaplan, R.C. Haddon, F.B. Bramwell, F. Wudl, J.H. Marshall, D.O. Cowan, S. Gronowitz, J. Phys. Chem., 84 (1980) 427.
148. M. Sharp, Electrochim. Acta, 21 (1976) 973.
149. M. Sharp, J. Electroanal. Chem., 88 (1978) 193.
150. T.L. Cairns, B.C. McKusick, Agnew. Chem., 73 (1961) 520.
151. D.S. Acker, W.R. Hertler, J. Am. Chem. Soc., 84 (1962) 3370.
152. L.R. Melby, R.T. Harder, W.R. Hertler, W. Mahler, R.E. Benson, W.E. Mochel, J. Am. Chem. Soc., 84 (1962) 3374.
153. L.B. Coleman, M.T. Cohen, D.J. Sandman, F.G. Yamagishi, A. Garito, A.J. Heeger, Solid State Commun., 12 (1973) 1125.
154. R.C. Wheland, J.L. Gilson, J. Am. Chem. Soc., 98 (1976) 3916.

155. J.T. Devreuse, R.P. Evrard, V.E. van Doren, *Highly Conducting One-Dimensional Solids*, Plenum, New York, 1979.
156. W.R. Hertler, H.D. Hartzler, D.S. Acker, R.E. Benson, *J. Am. Chem. Soc.*, 84 (1962) 3387.
157. D.L. Jeanmaire, R.P. van Duyne, *J. Am. Chem. Soc.*, 98 (1976) 4129.
158. E. Ezumi, H. Miyasaki, T. Kubota, *J. Phys. Chem.*, 74 (1970) 2397.
159. I.N. Juchnovski, I.G. Biner, *Chem. Phys. Lett.*, 12 (1971) 40.
160. R. Bozio, A. Girlando, C. Pecille, *J. Chem. Soc. Faraday Trans. 2*, 71 (1975) 1237.
161. G.R. Anderson, J.P. Devlin, *J. Phys. Chem.*, 79 (1975) 1100.
162. M.S. Khatkale, J.P. Devlin, *J. Chem. Phys.*, 70 (1979) 1851.
163. M.R. Suchanski, R.P. van Duyne, *J. Am. Chem. Soc.*, 98 (1976) 250.
164. K.K. Jespersen, *Theoret. Chim. Acta*, 47 (1978) 283.
165. M.A. Komanynsky, A.C. Wahl, *J. Phys. Chem.*, 7 (1975) 695.
166. P.H.H. Fischer, C.A. McDowell, *J. Am. Chem. Soc.*, 85 (1963) 2694.
167. P.H. Rieger, G.F. Fraenkel, *J. Chem. Phys.*, 37 (1962) 2795.
168. A.W. Addison, N.S. Dalal, Y. Huyano, S. Huizinaga, L. Weiter, *Can. J. Chem.*, 55 (1979) 4191.
169. A. Yamagishi, *Bull. Chem. Soc. Japan*, 49 (1976) 1417.
170. A. Yamagishi, M. Sakamoto, *Bull. Chem. Soc. Japan*, 47 (1974) 2152.
171. R.H. Boyd, W.D. Phillips, *J. Chem. Phys.*, 43 (1965) 2927.

172. J. Foley, private communication.
173. R.N. Adams, *Electrochemistry at Solid Electrodes*, Marcel Dekker, New York, 1969.
174. A.M. Bond, *Modern Polarographic Methods in Analytical Chemistry*, Marcel Dekker, New York 1980.
175. J.A. Plambeck, *Electroanalytical Chemistry: Basic Principles and Applications*, Wiley, New York, 1982.
176. Louis Meites, *Polarographic Techniques*, Interscience, New York, 1955.
177. G.F. Cottrell, *Z. Physik. Chem.*, 42 (1902) 385.
178. J.E.B. Randles, *Trans. Faraday Soc.*, 44 (1948) 327.
179. A. Sevcik, *Coll. Czech. Chem. Commun.*, 13 (1948) 349.
180. H. Matsuda, Y. Ayabe, *Z. Elektrochem.*, 59 (1957) 494.
181. H. Matsuda, *Z. Elektrochem.*, 61 (1957) 489.
182. Y.P. Gokhstein, *Doklady Akad. Nauk. SSSR*, 126 (1959) 598.
183. J. Koutecky, *Coll. Czech. Chem. Commun.*, 21 (1956) 433.
184. R.S. Nicholson, *Anal. Chem.*, 37 (1965) 1351.
185. P. Delahay, *J. Am. Chem. Soc.*, 75 (1953) 1190.
186. J.M. Saveant, E. Vianello, in "Advances in Polarography," I.S. Longmuir, Ed., Vol 1 Pergamon Press, New York, 1960, p. 367.
187. J.M. Saveant, E. Vianello, *Electrochim. Acta*, 8 (1963) 905.
188. J.M. Saveant, E. Vianello, *Compdt. Rend.*, 256 (1963) 2597.
189. W.H. Reinmuth, *Anal. Chem.*, 33 (1961) 1793.
190. J. Weber, *Coll. Czech. Chem. Commun.*, 24 (1959) 1770.
191. R.S. Nicholson, I. Shain, *Anal. Chem.*, 36 (1964) 706.

192. T. Kuwana, R.K. Darlington, D.W. Leedy, *Anal. Chem.*, 36 (1964) 2023.
193. S. Pons, J.S. Mattson, L.O. Winstrom, H.B. Mark, Jr., *Anal. Chem.*, 39 (1967) 685.
194. A. Bewick, K. Kunitatsu, S. Pons, *Electrochim. Acta*, 25 (1980) 465.
195. A. Bewick, A.M. Tuxford, *Symp. Faraday Soc.*, 4 (1970)
196. E. Yeager, *Surf. Sci.*, 101 (1980) 1.
197. M. Fleischmann, I.R. Hill, in "Modern Aspects of Electrochemistry," J. O'M. Bockris, B.E. Conway, Eds., Plenum Press, New York, 1983.
198. A. Bewick, J.M. Mellor, S. Pons, *Electrochim. Acta*, 25 (1980) 931.
199. N. Winograd, T. Kuwana, *J. Electroanal. Chem.*, 23 (1969) 333.
200. A.W.B. Aylmer-Kelly, A. Bewick, P.R. Cantrill, A.M. Tuxford, *Disc. Faraday Soc.*, 56 (1973) 96.
201. T. Davidson, S. Pons, A. Bewick, P.P. Schmidt, *J. Electroanal. Chem.*, 132 (1982) 329.
202. S. Pons, S.B. Khoo, *J. Am. Chem. Soc.*, 104, (1982) 3045.
203. N. Winograd, T. Kuwana, *J. Electroanal. Chem.*, 7 (1974) 1.
204. W.N. Hansen in P. Delahay and C.W. Tobias, Eds., "Advances in Electrochemistry and Electrochemical Engineering," Vol. 9, Interscience, New York, 1973 p. 1.
205. J.D.E. McIntyre in P. Delahay and C.W. Tobias, Eds., "Advances in Electrochemistry and Electrochemical Engineering," Vol. 9, Interscience, New York, 1973, p. 227.
206. J. Heyrovsky, *Chem. Listy*, 16 (1922) 256.
207. D. Ilkovic, *Collect. Czech. Chem. Commun.*, 6 (1934) 498.

- 208. D. Ilkovic, J. Chem. Phys., 35 (1938) 129.
- 209. T. Nagaoka, S. Okazaki, T. Fujinaga, J. Electroanal. Chem., 133 (1982) 89.
- 210. M.E. Peover, J.D. Davies, J. Electroanal. Chem., 6 (1963) 46.
- 211. J.S. Jaworski, M.K. Kalinowski, J. Electroanal. Chem., 76 (1977) 301.
- 212. A. Lasia, M.K. Kalinowski, J. Electroanal. Chem., 36 (1972) 511.
- 213. H. Lund, P. Iverson, in "Organic Electrochemistry," M. Baizer, Ed., Marcel Dekker, New York, 1973.
- 214. C.K. Mann, "Nonaqueous Solvents for Electrochemical Uses," in Electroanalytical Chemistry, A.J. Bard, Ed., Marcel Dekker, New York, 1969, p. 57.
- 215. H.A. Laitinen. A.J. Frank. P. Kivalo, J. Am. Chem. Soc., 75 (1953) 2865.
- 216. E. Itabashi, J. Electroanal. Chem., 36 (1972) 179.
- 217. J.E. Gordon, The Organic Chemistry of Electrolyte Solutions, Wiley Interscience, Wiley and Sons, New York, 1975, p. 216-217.
- 218. R.B. Slates, M. Szwarc, J. Phys. Chem., 69 (1965) 4124.
- 219. J. Janata, R.D. Holtby-Brown, J. Chem. Soc. Perkin II, (1973) 991.
- 220. V.D. Parker, J. Am. Chem. Soc., 98 (1978) 98.
- 221. D.L. Marille, W.G. Hodgson, J. Chem. Phys. 37(1965) 1562.
- 222. R.R. Bessette, I.W. Olver, J. Electroanal. Chem., 17 (1968) 327.
- 223. F. Jachinowicz, H.C. Wang. G. Levin. M. Szwarc, J. Phys. Chem., 82 (1978) 1371.
- 224. H.C. Wang, G. Levin, M. Szwarc, J. Am. Chem. Soc., 99 (1977) 5056.

- 225. A. Rainis, M. Szwarc, J. Am. Chem. Soc., 96 (1974) 3008.
- 226. O. Popovych, R.P.T. Tomkins, Nonaqueous Solution Chemistry, Wiley-Interscience, New York, 1981, p 27.
- 227. M.E. Peover, J.D. Davies, J. Electroanal. Chem., 6 (1963) 46.
- 228. G. Levin, C. Sutphen, M. Szwarc, J. Am. Chem. Soc., 94 (1972) 2652.
- 229. S. Arai, L.M. Dorfman, J. Chem. Phys., 41 (1964) 2190.
- 230. S. Arai, E.L. Tremba, J.R. Brandon, L.M. Dorfman, Can. J. Chem., 45 (1967) 119.
- 231. A. Rainis, M. Szwarc., Int. J. Chem. Kinetics, 7 (1975) 919.
- 232. A. Rainis, R. Tung, M. Szwarc, J. Am. Chem. Soc., 95 (1973) 659.
- 233. A. Smolucowski, Z. Phys. Chem., 92 (1917) 129.
- 234. P. Debye, Trans. Electrochem. Soc., 82 (1942) 265.
- 235. F. Gutman, A.M. Herman, A. Rambaum, J. Electrochem. Soc., 114 (1967) 325.
- 236. O.K. Kolnikov, V.M. Vozzbeunikov, Z.V. Zvonkova, V.P. Glushkova, E.E. Shapiro, Dokl. Akad. Nauk. SSSR, 189 (1969) 353.
- 237. E.P. Goodings, Endeavour, 34 (1975) 129.
- 238. M. Sharp, G. Johansson, Anal. Chim. Acta, 54 (1971) 31.
- 239. J.E. Mulvaney, R.J. Cramer, H.K. Hall, Jr., J. Polymer Sci., 21 (1983) 309.
- 240. A.R. Siedle, G.A. Candela, J.F. Finnegan, Inorg. Chim. Acta, 35 (1979) 125.
- 241. A.J. Fry, Synthetic Organic Electrochemistry, Harper and Row, New York, 1972, p. 72.
- 242. G.J. Janz, R.P.T. Tomkins, Nonaqueous Electrolyte Handbook Vol. 1, Academic Press, New York, 1972.

- 243. R.H. Wopshall, I. Shain, *Anal. Chem.*, 39 (1967) 1514.
- 244. W.H. Reinmuth, *Anal. Chem.*, 32 (1983) 139.
- 245. J.F. Coetzee, G.P. Cunningham, *J. Am. Chem. Soc.*, 87 (1965) 2529.
- 246. B.G. Chauhan, W.R. Fawcett, A. Lasia, *J. Phys. Chem.*, 81 (1977) 476.
- 247. T. Nagaoka, S. Okazaki, *J. Electroanal. Chem.*, 158 (1983) 139.

B30424